

Copyright
by
Kapil Gulati
2011

The Dissertation Committee for Kapil Gulati
certifies that this is the approved version of the following dissertation:

**Radio Frequency Interference Modeling and Mitigation
in Wireless Receivers**

Committee:

Brian L. Evans, Supervisor

Jeffrey G. Andrews

Elmira Popova

Haris Vikalo

Sriram Vishwanath

**Radio Frequency Interference Modeling and Mitigation
in Wireless Receivers**

by

Kapil Gulati, B.Tech.; M.S.E.

DISSERTATION

Presented to the Faculty of the Graduate School of
The University of Texas at Austin
in Partial Fulfillment
of the Requirements
for the Degree of

DOCTOR OF PHILOSOPHY

THE UNIVERSITY OF TEXAS AT AUSTIN

August 2011

Acknowledgments

I would like to thank, first of all, my closest friend and now lovely wife Parul. Her unconditional love and encouragement is the greatest motivation in my life. I also thank my family and friends for their constant support.

I am indebted to my advisor, Prof. Brian Evans, for his guidance and financial support throughout my graduate studies. I have great reverence for Prof. Evans, both as a researcher and as a person. I aspire to imbibe his professional ethics, diligence, and discipline. He is the best advisor I could have hoped for and has been a great influence in my life.

My graduate studies would not have been possible without the recommendations from Prof. Ratnajit Bhattacharjee, Prof. Prabin Bora, and Prof. Marius Pesavento, and I thank them for their encouragement. I am grateful to Prof. Vishal Monga, alumnus of IIT Guwahati and ESPL group, for encouraging me to join the ESPL group under Prof. Evans.

I would like to thank my committee members, Prof. Jeff Andrews, Prof. Elmira Popova, Prof. Haris Vikalo, and Prof. Sriram Vishwanath, for their constructive feedback on this dissertation. I especially thank Prof. Andrews for his in-depth feedback on the first two contributions of this dissertation, and for co-authoring the papers on the same. He has been like a technical co-advisor for this dissertation. I am greatly indebted to Dr. Radha Ganti for

mentoring me through the second contribution of this dissertation.

The problem addressed in this dissertation was first introduced to our research group by Mr. Keith Tinsley, when he was with Intel Labs, and I am indebted to him for guiding my research. I worked in close collaboration with Dr. Nageen Himayat, Mr. Kirk Skeba, Dr. Srikathyayani Srikanteswara, and Mr. Keith Tinsley at Intel Labs, and I thank them for their guidance. I am deeply grateful to Dr. David Bormann, Dr. Anthony Chun, and Mr. Kirk Skeba from Intel Labs, who not only mentored me during my internships at Intel, but have also guided me throughout my graduate studies.

Last, but not the least, I would like to thank the ESPL members: Greg Allen, Hugo Andrade, Wael Barakat, Aditya Chopra, Marcus DeYoung, Chao Jia, Jing Lin, Yousof Mortazavi, Marcel Nassar, Karl Nieman, Alex Olson, Kenneth Perrine, Hamood Rehman, Rabih Saliba, Akshaya Srivatsa, Kyle Wesson, and Ian Wong, for their camaraderie and feedback on my work. I have benefited greatly by collaborating with Aditya, Marcel, Marcus, and Yousof, on the early research that lead to this dissertation.

Radio Frequency Interference Modeling and Mitigation in Wireless Receivers

Publication No. _____

Kapil Gulati, Ph.D.

The University of Texas at Austin, 2011

Supervisor: Brian L. Evans

In wireless communication systems, receivers have generally been designed under the assumption that the additive noise in system is Gaussian. Wireless receivers, however, are affected by radio frequency interference (RFI) generated from various sources such as other wireless users, switching electronics, and computational platforms. RFI is well modeled using non-Gaussian impulsive statistics and can severely degrade the communication performance of wireless receivers designed under the assumption of additive Gaussian noise.

Methods to avoid, cancel, or reduce RFI have been an active area of research over the past three decades. In practice, RFI cannot be completely avoided or canceled at the receiver. Methods to reduce the intensity of RFI at the receiver are acceptable as long as the degradation in communication performance caused by the residual RFI is tolerable. Intensity of residual

RFI, however, is rapidly increasing as the reuse of available radio spectrum increases, sources of electromagnetic radiation increase, and the form factor of computational platform decreases. To this end, this dissertation derives the statistics of the residual RFI and utilizes them to analyze and improve the communication performance of wireless receivers.

Prior work in statistical modeling of RFI is limited by the spatial distribution of the sources of RFI considered. This dissertation derives closed-form instantaneous statistics of RFI in a broad range of interferer topologies, with applications to wireless ad hoc, cellular, local area, and femtocell networks.

This dissertation then extends the RFI statistics to include the temporal dimension. The network model adopted in this dissertation spans the extremes of temporal independence to long-term temporal dependence. The joint temporal statistics of RFI are utilized to derive closed-form expressions for various performance measures for single hop communications in decentralized wireless networks, unveiling $2\times$ potential improvement in network throughput by optimizing certain medium access control layer parameters.

Finally, the knowledge of joint temporal statistics of RFI is used to derive pre-filtering methods, amenable to real-time implementation, for mitigating the residual RFI. This dissertation uses a recently proposed non-linear measure of distance that yields improved robustness and improves the link spectral efficiency, for example, by an additional 1–6 bits/s/Hz per communication link in a decentralized wireless network.

Table of Contents

Acknowledgments	iv
Abstract	vi
List of Tables	xii
List of Figures	xv
Chapter 1. Introduction	1
1.1 Sources of RFI	3
1.1.1 Intelligent sources of RFI	3
1.1.2 Non-intelligent sources of RFI	7
1.2 RFI in Wireless Receiver: Impact and Mitigation Methods . .	8
1.3 Statistical Modeling and Mitigation of Residual RFI	12
1.4 Dissertation Summary	14
1.4.1 Thesis Statement	14
1.4.2 Summary of Contributions	15
1.5 Organization	17
1.6 Nomenclature	18
1.7 Notation	20
Chapter 2. Background	21
2.1 Introduction	21
2.2 RFI Mitigation in Wireless Receivers	22
2.2.1 Static Methods	22
2.2.2 Dynamic Methods	25
2.3 Statistical Modeling and Mitigation of RFI	29
2.3.1 Statistical Modeling of RFI	30
2.3.2 Communication Performance of Wireless Networks . . .	35

2.3.3	Receiver Design to Mitigate RFI	38
2.4	Conclusions	43
Chapter 3. Instantaneous Statistics of Co-Channel Interference in Wireless Networks		45
3.1	Introduction	45
3.1.1	Motivation and Prior Work	46
3.1.2	Contribution, Organization, and Notation	48
3.2	System Model	49
3.3	Co-Channel Interference in a Poisson Field of Interferers	52
3.3.1	Case I: Interferers distributed over the entire plane	55
3.3.2	Case II: Interferers distributed over a finite-area annular region	56
3.3.3	Case III: Interferers distributed over infinite-area annular region with guard zone	59
3.4	Co-Channel Interference in a Poisson-Poisson Cluster Field of Interferers	64
3.4.1	Case I: Cluster centers distributed over the entire plane	67
3.4.2	Case II: Cluster centers distributed over finite-area annular region	69
3.4.3	Case III: Cluster centers distributed over infinite-area annular region with guard zone	72
3.5	Summary and Discussion	75
3.6	Simulation Results	78
3.6.1	Co-channel interference in a Poisson field of interferers	81
3.6.2	Co-channel interference in a Poisson-Poisson cluster field of interferers	83
3.6.3	Comments on simulation results	84
3.7	RFI in laptop embedded wireless transceiver	85
3.8	Conclusions	88
Chapter 4. Throughput, Delay, and Reliability of Decentralized Wireless Networks with Temporal Correlation		90
4.1	Introduction	90
4.1.1	Motivation and Prior Work	91

4.1.2	Contribution, Organization, and Notation	95
4.2	System Model	96
4.2.1	Network Model I: Synchronous	98
4.2.2	Network Model II: Asynchronous	100
4.3	Joint Statistics of Interference	102
4.3.1	Network Model I	102
4.3.2	Network Model II	108
4.3.3	Joint Tail Probability of Interference Amplitude	109
4.4	Single Hop Communication Performance Analysis	113
4.4.1	Local Delay	114
4.4.2	Outage with respect to Throughput	117
4.4.3	Average Network Throughput (Network Model II)	119
4.4.4	Transmission Capacity and Throughput-Delay-Reliability (TDR) Tradeoff (Network Model II)	120
4.5	Simulation Results	121
4.5.1	Local Delay	122
4.5.2	Outage with respect to Throughput	122
4.5.3	Average Network Throughput (Network Model II)	125
4.5.4	Transmission Capacity and Throughput-Delay-Reliability (TDR) Tradeoff (Network Model II)	126
4.6	Conclusions	127
 Chapter 5. Pre-filter Design to Mitigate RFI in Wireless Re-		
ceivers		129
5.1	Introduction	129
5.1.1	Motivation and Prior Work	130
5.1.2	Contributions, Organization, and Notation	134
5.2	System Model	135
5.2.1	Baseband Model of Transmitter and Receiver	135
5.2.2	Network Interference Model	138
5.3	Joint Statistics of Interference	141
5.3.1	Joint characteristic function of $\bar{\mathbf{I}}_{k,1:n}$	142
5.3.2	Joint characteristic function of $\bar{\mathbf{I}}_{1:n}$	146

5.4	Pre-filter Design Criterion	148
5.4.1	Correntropy and Correntropy Induced Metric (CIM) . . .	149
5.4.2	Zero-Order Statistics (ZOS)	152
5.4.3	Using CIM and ZOS in pre-filter design	154
5.4.4	Lower Bound on Error Probability	156
5.5	Pre-filter Design to Mitigate RFI	156
5.5.1	Selection Pre-filter (S pre-filter)	157
5.5.2	Combination Pre-filter ($L\ell$ pre-filter) with Impulse Masking	158
5.5.3	Extensions to include temporal dependence in RFI ($L^J\ell$ pre-filter)	162
5.5.4	Computational Complexity Analysis	162
5.6	Simulation Results	163
5.6.1	Joint Statistics of Interference	164
5.6.2	Communication Performance of Pre-filter Based Receivers	165
5.7	Conclusions	170
Chapter 6. Conclusions		171
6.1	Summary	171
6.2	Future Work	175
Appendices		179
Appendix A. Statistical Properties of Symmetric Alpha Stable Random Vectors		180
Appendix B. Statistical Properties of Gaussian Mixture Random Vectors		189
Appendix C. Statistical Properties of Middleton Class A Complex Random Variables		191
Bibliography		193
Vita		216

List of Tables

1.1	Radio frequency interference (RFI) in wireless receivers: classification of sources, impact, and common mitigation methods. Acronyms ALOHA, CSMA, LCD, MAC, Wi-Fi, WiMAX are defined in Section 1.6.	11
2.1	Statistical properties of symmetric alpha stable (SAS), Middleton Class A (MCA), and Gaussian mixture (GMM) distributions, for a two-dimensional zero-centered isotropic random vector $\{\mathbf{I}^{(I)}, \mathbf{I}^{(Q)}\}$. A detailed discussion of the statistical properties of the SAS, GMM, and MCA distributions is provided in Appendix A, B, and C, respectively.	31
2.2	Summary of prior work on (i) statistical modeling of RFI, (ii) use of RFI statistics for communication performance analysis of wireless networks, and (iii) use of RFI statistics for receiver design to mitigate RFI. Prior work has been categorized by the key statistical-physical models of RFI derived in prior work. Here SAS, MCA, and GMM stand for symmetric alpha stable, Middleton Class A, and Gaussian mixture model, respectively.	44
3.1	Summary of Notation used in Chapter 3	50
3.2	Values for $\{\eta, \beta\}$ and the associated weighted mean squared error (WMSE), obtained by solving (3.31), for different values of the power pathloss exponent (γ) and using the weighting function $u(k) = e^{-k}$. Solution to (3.31) was obtained by using the <code>fminunc</code> function in <code>MATLAB</code> , which uses the BFGS quasi-Newton method [1].	62
3.3	Statistical-physical modeling of co-channel interference in a field of Poisson distributed interferers categorized by the region containing the interferers.	76
3.4	Statistical-physical modeling of co-channel interference in a field of Poisson-Poisson cluster distributed interferers categorized by the region containing the cluster centers.	77

3.5	Kullback-Leibler divergence between empirical and statistical model distribution (joint in-phase and quadrature-phase distribution) in Poisson and Poisson-Poisson cluster field of interferers for different wireless network scenarios. Here SAS, MCA, and GMM stand for symmetric alpha stable, Middleton Class A, and Gaussian mixture model, respectively. Parameter values governing the interference space for each of the scenarios are listed in caption to Figs. 3.3 through 3.8.	84
4.1	Summary of Notation used in Chapter 4	97
5.1	Summary of Notation used in Chapter 5	136
5.2	Distance cost function corresponding to L_2 norm, L_1 norm, and CIM as a distance measure in a S pre-filter.	157
5.3	Weight update factor $\frac{\partial J(e^{(I)}[n],0)}{\partial \overline{W}_{L\ell,n}^{(I)}}$ for weights corresponding to in-phase sample values using L_2 norm, L_1 norm, and CIM as a distance measure in a adaptive $L\ell$ pre-filter. Here $e[n] = x_{\text{Tx}}[n] - \overline{W}_{L\ell}^T \overline{X}_{L\ell}(n)$ is the error in the estimate of the n^{th} training sample. Weight update factor for weights corresponding to quadrature phase sample values $\frac{\partial J(e^{(Q)}[n],0)}{\partial \overline{W}_{L\ell,n}^{(Q)}}$ follow similarly with (I) replaced by (Q)	161
5.4	Comparison of computation complexity of S and $L\ell$ pre-filters (PF) of length W that use L_2 , L_1 , or CIM as a distance measure. The computations are reported per output sample in the runtime phase (RN), and per training sample in the training phase (TR). T training samples are assumed to be available in the training phase. Computational complexity is reported with respect to the number of real multiplications or inverse operations ($\times, (\cdot)^{-1}$), additions or subtractions ($+, -$), comparisons ($>, <, =$), and exponential evaluations ($e^{(\cdot)}$) required. Reported numbers are accurate only up to $O(1)$. Other $O(\frac{1}{T})$ and $O(\frac{1}{W})$ operations, such as $\log(\cdot)$ and $\sqrt{(\cdot)}$ required in certain pre-filters, are not reported.	163

6.1	Contributions of this dissertation compared to prior work in (i) statistical modeling of RFI, (ii) use of RFI statistics for network performance analysis, and (iii) use of RFI statistics for receiver design to mitigate RFI. SAS, MCA, and GMM are defined in Section 1.6. BPL/UBPL refer to the assumption of bounded/unbounded pathloss function. Unless specified, statistics are derived assuming an UBPL function. CIM and ZOS stand for correntropy induced metric and zero-order statistics, respectively.	174
-----	--	-----

List of Figures

1.1	Illustration of radio frequency interference (RFI) in dense Wi-Fi networks that is common in apartment complexes, university, and market place. Wireless receivers are affected by interference from various intelligent (co-channel and adjacent channel) and non-intelligent sources (out-of-platform and in-platform). . . .	6
2.1	Summary of commonly used techniques to mitigate RFI in wireless receivers. Under dynamic RFI mitigation methods, this dissertation proposes direct contributions in robust transceiver design and identifies potential improvement in network throughput via optimization of MAC layer channel access protocols. The acronyms CDMA, CSMA, FDMA, MAC, MUD, OFDMA, SIC, and TDMA are defined in Section 1.6.	23
3.1	Interference space and receiver location for different network topologies in a field of Poisson distributed interferers categorized by the region containing the interferers.	53
3.2	Interference space and receiver location for different network topologies in a field of Poisson-Poisson cluster distributed interferers categorized by the region containing the cluster centers.	64
3.3	Decay rates for tail probabilities of simulated co-channel interference and the symmetric alpha stable (SAS) model for <i>Case I</i> ($r_l = 0, r_h = \infty, \mathbf{B} = 5$) of <i>Poisson field of interferers</i> . The Middleton Class A and Gaussian models are not suitable in this scenario as the mean intensity $\Omega_{2A} \rightarrow \infty$	80
3.4	Decay rates for tail probabilities of simulated co-channel interference and the symmetric alpha stable (SAS), Middleton Class A (MCA), and Gaussian models for <i>Case II</i> ($r_l = 20, r_h = 40, \ R_m\ = 4, \mathbf{B} = 1400$) of <i>Poisson field of interferers</i> . MCA has the best match to the empirical (simulated) co-channel interference.	80

3.5	Decay rates for tail probabilities of simulated co-channel interference and the symmetric alpha stable (SAS), Middleton Class A (MCA), and Gaussian models for <i>Case III</i> ($r_l = 30, r_h = \infty, \ R_m\ = 4, \mathbf{B} = 2200$) of <i>Poisson field of interferers</i> . $\{\eta, \beta\} = \{2.781, -1.025\}$ for $\gamma = 4$ and $u(k) = e^{-k}$ from Table 3.2. MCA has the best match to the empirical (simulated) co-channel interference.	81
3.6	Decay rates for tail probabilities of simulated co-channel interference and the symmetric alpha stable (SAS) model for <i>Case I</i> ($R_l = 0, R_h = \infty, r_l = 0, r_h = 10, \mathbf{B} = 100$) of <i>Poisson-Poisson cluster field of interferers</i> . The Gaussian mixture and Gaussian models are not suitable in this scenario as the mean intensity $\Omega_{2A} \rightarrow \infty$	82
3.7	Decay rates for tail probabilities of simulated co-channel interference and the symmetric alpha stable (SAS), Gaussian mixture (GMM), and Gaussian models for <i>Case II</i> ($R_l = 40, R_h = 80, r_l = 0, r_h = 10, \ R_m\ = 4, \mathbf{B} = 6000$) of <i>Poisson-Poisson cluster field of interferers</i> . GMM has the best match to the empirical (simulated) co-channel interference.	82
3.8	Decay rates for tail probabilities of simulated co-channel interference and the symmetric alpha stable (SAS), Gaussian mixture (GMM), and Gaussian models for <i>Case III</i> ($R_l = 30, R_h \rightarrow \infty, r_l = 0, r_h = 10, \ R_m\ = 4, \mathbf{B} = 4000$) of <i>Poisson-Poisson cluster field of interferers</i> . $\{\eta, \beta\} = \{2.781, -1.025\}$ for $\gamma = 4$ and $u(k) = e^{-k}$ from Table 3.2. MCA has the best match to the empirical (simulated) co-channel interference.	83
3.9	Kullback-Leibler (KL) divergence of the measured distribution from the estimated Gaussian, symmetric alpha stable, Middleton Class A, and Gaussian mixture distributions. KL divergence for twenty-five measured RFI datasets is compared.	86
3.10	Tail probability of the measured and estimated Gaussian, symmetric alpha stable, Middleton Class A, and Gaussian mixture models for measurement set number 23. Gaussian mixture model provides closest fit to tail probability of measured data.	87
4.1	Network Model I: nodes emerge only at fixed time slots and transmit for a random number of time slots ($= \mathbf{L}$).	98
4.2	Network Model II: nodes can emerge at any time slot and are active for a random number of time slots ($= \mathbf{L}$).	101

4.3	Local delay in network model I with and without power control, $L_{max} = 20$ ($\bar{L} = 10$), and power pathloss exponent γ of $\{4, 6\}$. Local delay increases sublinearly as SIR threshold T required for successful detection increases, and exponentially as the power pathloss exponent increases. Channel inversion power control reduces the local delay of the network.	123
4.4	Local delay in network model II with and without power control, $L_{max} = 20$ ($\bar{L} = 10$), and power pathloss exponent γ of $\{4, 6\}$. Variations of local delay with various network parameters are similar to those observed for network model I in Fig. 4.3. . . .	123
4.5	Outage probability associated with achieving at least $s = \{1, 2, 3, 4\}$ successes in $L_{max} = 20$ time slots for network model I.	124
4.6	Outage probability associated with achieving at least $s = \{1, 2, 3, 4\}$ successes in $L_{max} = 20$ time slots for network model II.	124
4.7	Average throughput for network model II for $L_{max} = 10$, $\bar{L} = 5$, and for $\lambda = \{0.01, 0.005\}$. Average throughput decreases as the SIR detection threshold T increases. Average throughput grows sublinearly with λ	125
4.8	Transmission capacity $\text{TC}(\bar{L}, \epsilon)$ of network model II as a function of the outage constraint ϵ and delay constraint of $\bar{L} = \frac{L_{max}}{2} = \{20, 10\}$ for a SIR detection threshold T of 0.1. Transmission capacity is plotted for a truncated Poisson lifetime distribution defined in (4.56) and that obtained by optimizing over all feasible lifetime distributions.	126
5.1	Simplistic baseband model of a typical transmitter and receiver pair in the network employing single carrier, uncoded, QAM modulated transmissions.	137
5.2	Network model used to derive interference statistics. Interferers can emerge at any time slot and are active for a random number of time slots ($= \mathbf{L}$). A bounded pathloss function $l(r) = \min\{1, r^{-\frac{\gamma}{2}}\}$ is assumed, where r is the distance of interferer from the origin and $\gamma = 4$ is the power pathloss exponent.	139
5.3	Contours of $\text{CIM}(X, 0)$ in a two-dimensional sample space ($N = 2$, $X = [x_1, x_2]$) for Gaussian kernel size $\sigma_c = 1$. When X is close to the origin, $\text{CIM}(X, 0)$ behaves like L_2 norm. As X moves away from the origin, the behavior of $\text{CIM}(X, 0)$ changes from L_2 norm, to L_1 norm, and to L_0 norm when they are far apart [2].	150

5.4	Sample snapshot of a Gaussian and Gaussian mixture random process with the same zero-order statistic (ZOS) power. With the same ZOS = 0.5300, smaller variations in the Gaussian mixture random process are indistinguishable from a Gaussian process, as indicated by the dotted lines. A similar illustration is presented in [3] for a symmetric alpha stable random process. . .	153
5.5	Joint tail probability of interference amplitude over $n = 1, 2, 3$ time slots with the intensity of emerging interferers $\lambda = 0.1$. A bounded pathloss function $l(r) = \min(1, r^{-\frac{\gamma}{2}})$ is assumed, where r is the propagation distance and $\gamma = 4$ is the power pathloss exponent. The number of mixture terms N_T for each contributing component was chosen as 4, that results in a total number of mixture terms $(N_T)^{2n} = 4^2, 4^4, 4^6$ for $n = 1, 2,$ and $3,$ respectively.	165
5.6	Communication performance of correntropy induced metric (CIM) based pre-filters in the presence of the simulated network interference. Intensity of emerging interferers $\lambda = 0.0001$ results in non-Gaussian impulsive interference. Interference-to-noise ratio is fixed at 30 dB. While $L\ell$ pre-filter outperform S pre-filter, the latter provides a good tradeoff between communication performance and computational complexity in the presence of impulsive non-Gaussian interference. Both pre-filters provide around 15–20 dB improvement over conventional matched receiver at a symbol-error-rate (SER) of 10^{-3}	166
5.7	Communication performance of S pre-filters in the presence of the simulated network interference. Intensity of emerging interferers $\lambda = 0.0001$ results in non-Gaussian impulsive interference. Interference-to-noise ratio is fixed at 30 dB. CIM based S pre-filter outperforms its counterparts that use L_2 or L_1 norm as a distance measure.	167
5.8	Communication performance of $L\ell$ pre-filters in the presence of the simulated network interference. Intensity of emerging interferers $\lambda = 0.0001$ results in non-Gaussian impulsive interference. Interference-to-noise ratio is fixed at 30 dB. CIM based $L\ell$ pre-filter outperforms its counterparts that use L_2 or L_1 norm as a distance measure.	167
5.9	Communication performance of correntropy induced metric (CIM) based pre-filters in the presence of Gaussian distributed interference. Interference-to-noise ratio is fixed at 30 dB. Matched filter receiver is BER optimal in the presence of Gaussian distributed interference. At a symbol-error-rate (SER) of 10^{-3} , degradation in communication performance due to $L\ell$ and S pre-filters is approximately 0.3 dB and 1 dB, respectively. . . .	169

Chapter 1

Introduction

Performance of wired or wireless communication systems is limited by the *noise* present in the system. The term *noise* has varied meaning, connotation, and impact based on the physical phenomenon it is used to describe – from proving the existence of atoms to denoting undesired effects in electrical conductors [4, 5]. In wireless communication systems, noise is commonly used to denote the unwanted additive distortions caused by the system in conjunction to linear and other non-linear distortions to the transmitted signal. Additive noise degrades the ability of the receiver to successfully detect the information in the transmitted signal.

An unavoidable source of noise is due to the electronic circuitry at the receiver, and is termed as *circuit noise*. Impact of circuit noise on communication systems was first studied by Schottky in 1918, where he considered the impact due to two forms of circuit noise: thermal and shot noise [6]. These are the dominant sources of circuit noise and are unavoidable in any electronic circuit. Thermal noise is due to random motion of electrons inside an electrical conductor and occurs regardless of the voltage applied. Shot noise, on the other hand, is due to statistical variations in the electrical current in a

conductor as the moving charges are randomly emitted (hence the name *shot noise*) [7]. Schottky studied the impact of thermal and shot noise as they pass through the receiver and perturb the desired signal. This helped in recognizing that the fluctuations caused due to thermal noise and shot noise (under weak assumption that the rate of *shots* is greater than receiver bandwidth) are spectrally flat and the amplitude statistics follow a Gaussian distribution [6–8]. In this dissertation, circuit noise is loosely referred to as *thermal noise* and is assumed to be spectrally flat and Gaussian distributed.

To date, wireless transceivers are generally designed, and their performance analyzed, under the assumption of additive Gaussian thermal noise at the receiver. While thermal noise was the dominant noise source in early communication systems, it is no longer the case in many of the current wireless communication systems. Wireless receivers are affected by *radio frequency interference* (RFI) from various sources of electromagnetic radiation, including other wireless communication sources [9], electronic devices such as microwave ovens [10], and clocks and busses on the computational platform on which the receiver is deployed [11]. Unlike thermal noise, RFI is typically well modeled using non-Gaussian impulsive statistics. The non-Gaussian statistics of RFI can severely degrade the communication performance of wireless transceivers that are designed assuming additive Gaussian noise.

1.1 Sources of RFI

Sources of RFI can be classified in numerous ways. Based on the method in which RFI is introduced in the systems, sources are classified as either radiated or conductive sources of RFI. Conductive RFI is caused by the physical contact of conductors as opposed to radiated RFI that is picked up by the radio. Radiated RFI is the dominant source that limits the performance of typical commercial wireless communication systems [5,11]. Focusing on radiated RFI, this dissertation adopts a broad classification introduced by Middleton [12,13]. Middleton classifies the sources of RFI as either intelligent or non-intelligent based on the presence or absence of information content in source emissions, respectively [12,13].

1.1.1 Intelligent sources of RFI

Intelligent or information bearing sources of RFI primarily include other wireless communication systems. The dominant form of such interference is due to sources that transmit in the same frequency band as the signal of interest, occupying partial or the complete band, are commonly referred to as *co-channel interference* [14]. Comparatively weaker, but still significant, form of intelligent interference is due to transmissions that ideally lie adjacent to the frequency band of desired transmission. Even though such sources are designed to occupy adjacent, but non-overlapping frequencies, some of the energy leaks into neighboring frequency band due to non-linearity in the transmitter circuitry. This form of interference is commonly referred to as

adjacent channel interference [14].

Co-channel interference: Communication performance of many of the current wireless networks, such as cellular networks and wireless ad hoc networks, is limited due to co-channel interference [9, 15]. Driven by the increasing demand in user data rates, current wireless networks employ a dense spatial reuse of the available radio spectrum [16]. This results in increased co-channel interference from other active users in the network that occupy the same radio spectrum.

In addition to interfering users associated with the same network, wireless transceivers are prone to co-channel interference from users in co-existing wireless networks that occupy the same radio spectrum [17]. This is particularly true for wireless technologies, such as Wi-Fi [18], Bluetooth [19], and ZigBee (built on IEEE 802.15.4 standard [20]) [21], that work in the globally unlicensed 2.4 GHz Industrial, Scientific and Medical (ISM) radio frequency band [17, 22].

Let us consider the example of a Wi-Fi network (IEEE 802.11g) as depicted in Fig. 1.1. One of the methods to reduce RFI in 802.11g networks involves the use of the request-to-send/clear-to-send (RTS/CTS) protocol [18]. A user that wishes to transmit sends a RTS packet to the access point indicating the duration of the upcoming transmission. The access point responds by sending a CTS packet, thereby reserving the wireless medium for the duration indicated in the RTS packet. Other users in network refrain from using the wireless medium if they receive either the RTS or CTS packet. Thus, under

idealistic assumptions, users within some distance of either the access point or the active user will not interfere. However, the users beyond that guarded distance may interfere if they also wish to transmit. The aggregate RFI due to all active users outside the guard distance can be significant. Further, the network is prone to interference from users associated with other Wi-Fi networks operating in close vicinity that use the same frequency band. Such interference can be severe in dense Wi-Fi network deployments, such as universities, office buildings, and apartment complexes. Further, other wireless devices on co-existing technologies, such as a Bluetooth mouse or cordless phone, interfere with the Wi-Fi transmissions. Even though the transmit power of such devices may be relative small, close proximity to the Wi-Fi transceiver may still cause significant degradation in communication performance [22].

Adjacent channel interference: Adjacent channel interference has been a growing concern for co-located wireless transceivers working in adjacent channels, e.g., Wi-Fi and WiMAX [23] transceivers deployed on a laptop computer [24]. The spurious power that leaks into adjacent channels is controlled by strict regulations in the wireless standard by organizations such as the Federal Communications Commission (FCC) in United States [25]. Even with strict limitations, the spurious power leaking into the adjacent channel can cause significant degradation in communication performance due to close proximity – as is the case in co-located transceivers.

There is an increasing demand to integrate multiple wireless transceivers on the same platform, e.g., to have Wi-Fi and cellular connectivity on a mo-

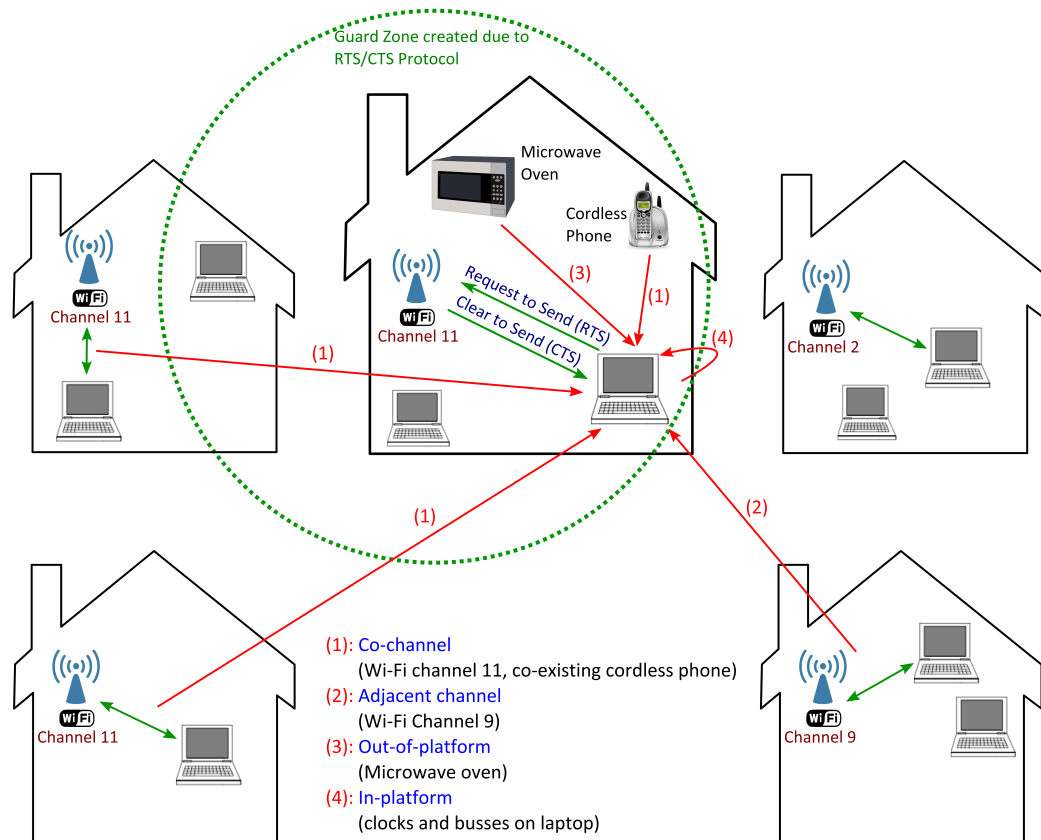


Figure 1.1: Illustration of radio frequency interference (RFI) in dense Wi-Fi networks that is common in apartment complexes, university, and market place. Wireless receivers are affected by interference from various intelligent (co-channel and adjacent channel) and non-intelligent sources (out-of-platform and in-platform).

bile phone [17]. In addition, simultaneous use of these transceivers is desired, e.g., downloading data via Wi-Fi during an ongoing voice call over the cellular link. The impact of adjacent channel interference among co-located wireless transceivers co-located on a platform, such as a laptop, is increasing as the demand for simultaneous use of multiple data transmission technologies increases and form factor of the platforms decreases.

1.1.2 Non-intelligent sources of RFI

Non-intelligent sources affect the communication performance of wireless communication systems due to unintentional electromagnetic emissions. In contrast to intelligent sources of RFI, emissions from non-intelligent sources do not bear any information. Non-intelligent sources interfering with a particular wireless transceiver embedded on a computational platform can be further classified as in-platform or out-of-platform, based on their physical location being either inside or outside of the platform, respectively.

Out-of-platform: Commercial electronic devices, such as microwave ovens, emit electromagnetic radiations due to the electronic circuitry present in them. Commercial electronic devices are required to abide by regulations (from regulatory organizations such as FCC in United States) that limit the electromagnetic interference that they can produce. FCC regulations for devices causing unintended interference, for example, specifies the limit on radiations when measured at a minimum distance of 3m [25]. The limit is generally intended to provide some protection and may still cause significant degrada-

tion in communication performance. For example, microwave ovens radiate power as high as -50 dBm at 15m in the 2.4 GHz ISM band, which is comparable to the transmit power of an access point of a Wi-Fi network [26]. Thus RFI from microwave interference is a common concern for 802.11b/g networks working in the 2.4 GHz ISM band [27].

In-platform: In-platform sources include clocks and busses in the platform on which the wireless transceiver is embedded. Because of the close proximity, RFI from in-platform sources may severely impair the wireless transceivers on the same platform [11, 28]. Moreover, there are no regulations by organization such as the FCC that limit the RFI inside the platform itself [11, 25]. For example, while a laptop computer has to abide by the RFI regulations as specified at a distance of 3m away, there is no limit on how much RFI power the LCD clock circuitry inside the laptop can generate at a distance of 3 cm where a Wi-Fi antenna is located [11]. In-platform RFI is an increasing concern in computational platforms, such as laptops and smart phones, as the number of electronic components integrated on the platform increase and form factors decrease.

1.2 RFI in Wireless Receiver: Impact and Mitigation Methods

The severity of impact caused by RFI on the communication performance of wireless transceivers can be attributed to three factors: (i) strength of the desired signal at the wireless receiver; (ii) non-impulsive statistics of RFI;

and (iii) large number of RFI sources. Regarding (i), it is common in many wireless networks for the strength of the desired signal at the receiver to be comparable to the thermal noise power [14]. Let us consider the example of a Wi-Fi network where the user is transmitting at the maximum allowable power of around 23 dBm. Assuming a simple home propagation environment (power pathloss model with an exponent of 3.5 and 40 dB loss at 1m at 2.4 GHz), the received signal strength at a moderate distance of ≈ 235 m is then around -100 dBm [14]. Typical thermal noise power in commercial Wi-Fi receivers is also around -100 dBm (generally higher) [11]. Thus the margin in wireless receivers to tolerate additional interference is low, particularly for receivers at a moderate distance away from the source. Regarding (ii), even marginal power levels of non-Gaussian interference have an adverse affect on the receiver that is designed assuming Gaussian statistics for the additive noise [29]. Regarding (iii), impact of the increasing intelligent and non-intelligent sources of RFI is evident. Even centralized networks such as cellular networks are widely acknowledged to be interference limited [30]. Further, for wireless transceivers embedded on a laptop, recent studies have demonstrated that platform RFI alone can cause up to 50% reduction in the range and throughput of the transceiver [11].

If wireless networks were designed without considering interference from other users, then a majority of the users will not be able to successfully communicate to their corresponding destinations due to network interference. In centralized wireless networks, such as cellular networks, interference can be re-

duced to a certain extent due to the ability to plan the network topology and the presence of centralized control during regular operation of the network. For example, in cellular networks, the frequency spectrum is split among various geographical cell sites such that two cells using the same fraction of the spectrum are far apart. Further, users in the same cell site are often coordinated by the basestation such that they are not active at the same time (time division multiple access, a.k.a., TDMA) or use the same frequency band (frequency division multiple access, a.k.a., FDMA or orthogonal frequency division modulation, a.k.a., OFDM). Such coordination, however, reduces the aggregate throughput of the network since the limited wireless resources are multiplexed among the users. Further, residual RFI from uncoordinated users will still be present, e.g., out-of-cell users in cellular networks.

Radio frequency planning and centralized control in wireless networks also have economic implications due to both network infrastructure layout and network operation. These factors have motivated the emergence of decentralized wireless networks such as wireless ad hoc network and femtocell network [31, 32]. In decentralized wireless networks, co-channel interference is even more severe due to the lack of any infrastructure and control in the network. At best, local coordination among the users can be enforced, for example, using medium access control (MAC) layer protocols such as carrier sense multiple access (CSMA) protocol. CSMA protocol entails the users to sense the wireless medium for ongoing transmissions, and transmit only if no ongoing transmissions are observed. This reduces the interference in the

Table 1.1: Radio frequency interference (RFI) in wireless receivers: classification of sources, impact, and common mitigation methods. Acronyms ALOHA, CSMA, LCD, MAC, Wi-Fi, WiMAX are defined in Section 1.6.

Sources of RFI	Intelligent		Non-intelligent	
	Co-channel	Adjacent Channel	Out-of-platform	In-platform
Example	Out-of-cell users in cellular networks	Users operating in adjacent frequency band, e.g., Wi-Fi and WiMAX	Microwave oven	LCD clock harmonics on a laptop
Impact increase with	Increasing user density	Close proximity of transceivers	Increasing electronic devices	Decreasing form factor of platform
Mitigation Methods	<ul style="list-style-type: none"> a. Interference alignment or cancellation b. MAC schemes such as ALOHA, CSMA 	<ul style="list-style-type: none"> a. Dedicated coordination for interference avoidance 	<ul style="list-style-type: none"> a. Shielding b. MAC schemes such as ALOHA, CSMA 	<ul style="list-style-type: none"> a. Shielding
Residual RFI due to	Uncoordinated users	Uncoordinated transceivers	Unshielded sources	Unshielded sources

network, but residual RFI is still present in abundance.

Table 1.1 lists some of the common methods to avoid, cancel, and reduce RFI classified according to the source of RFI. Residual RFI, however, is present in all cases. The intensity of the residual RFI is rapidly increasing as the reuse of available radio spectrum increases, the form factor of computational platform decreases, and the number of wireless transceivers integrated on a platform increases. To this end, this dissertation derives the statistics of the residual RFI and utilizes them to analyze and improve the communication performance of wireless receivers. A more detailed review of the common methods to mitigate RFI in wireless receivers is presented in Chapter 2.

1.3 Statistical Modeling and Mitigation of Residual RFI

Residual RFI, henceforth referred to as RFI, is unavoidable as it is caused by sources that cannot be coordinated with the desired transmissions. Motivated by the increasing strength of RFI in current wireless networks, wireless receivers should be designed to be robust to the non-Gaussian statistics of residual RFI.

Knowledge of RFI statistics can be used to design physical (PHY) layer methods and MAC layer protocols to mitigate RFI. Deriving closed-form RFI statistics that are applicable to a wide range of interference scenarios is central to the approach adopted in this dissertation. PHY layer methods to mitigate RFI include pre-filtering and detection methods which are robust to the non-Gaussian statistics of RFI. This dissertation investigates design of

pre-filtering methods based on the closed-form RFI statistics derived. Explicit design of MAC protocols to improve the communication performance of the network using the closed-form RFI statistics is not addressed in this dissertation. Rather, the focus of the dissertation is to derive closed-form expressions for various measures of communication performance using closed-form RFI statistics. Closed-form expressions for communication performance measures enable identifying the ways to improve the network performance and motivate the design of MAC protocols to achieve the same.

Prior research on statistical modeling of RFI, communication performance analysis of wireless networks, and receiver design to mitigate RFI is limited due to the following reasons:

1. **Statistical modeling of RFI:** Closed-form statistics of RFI are known only for certain spatial distributions and topologies of the interfering sources. Further, prior research lacks a unified approach towards statistical modeling and hence results in different statistics for different wireless networks. This limits the applicability of the RFI statistics when the interference scenarios deviate from the assumption made during statistical modeling.
2. **Communication performance analysis of wireless networks:** In absence of closed-form RFI statistics, much of the prior work derives bounds on the measures of communication performance. Based on the approximations used, these bounds can be relatively loose and the worst-

case performance might be significantly different from the expected performance. Lack of closed-form expressions for performance measures also limits insight into the effect of various network parameters on the performance of the wireless network. Knowledge of the relation between various network parameters and the network performance is integral to the design of channel access protocols that mitigate RFI.

3. **Receiver design to mitigate RFI:** The literature on non-linear filtering and detection methods to mitigate RFI for single carrier, single antenna receivers is rich. The optimality (with respect to communication performance measure such as bit-error-rate) of such methods, however, is limited by the assumption on the RFI statistics. Much of the prior work in receiver design is based on assumptions regarding RFI statistics that are not entirely justified or physically valid. RFI statistics dictate the optimal filter structure (such as linear or non-linear) and the distance measure to use for designing the filter.

1.4 Dissertation Summary

1.4.1 Thesis Statement

In this dissertation, I defend the following thesis statement:

For interference-limited wireless networks, deriving closed-form non-Gaussian statistics to model the tail probabilities of radio frequency interference unlocks analysis of network throughput, delay, and reliability

tradeoffs and designs of physical layer receivers to increase link spectral efficiency by several bits/s/Hz, without requiring knowledge of the number, locations, or types of interference sources.

1.4.2 Summary of Contributions

Following is the summary of the contributions of this dissertation.

- 1. Statistical Modeling of RFI:** *Instantaneous statistics of co-channel interference* are derived using statistical-physical principles for a wide range of interference scenarios. In particular, I consider co-channel interference from an annular field of Poisson or Poisson-Poisson cluster distributed interferers. Poisson and Poisson-Poisson cluster processes are commonly used to model interferer distributions in large wireless networks without and with interferer clustering, respectively. I develop a unified framework for deriving RFI statistics for various wireless network environments. The symmetric alpha stable and Gaussian mixture distributions are shown to be applicable for modeling RFI in a wide range of wireless networks, including wireless ad hoc, cellular, local area, and femtocell networks. The applicability of these distributions for modeling platform RFI is also established using measured RFI data from a laptop computer.
- 2. Communication performance analysis of wireless networks:** I demonstrate the benefit of using closed-form statistics of RFI to analyze

the communication performance of wireless networks. To illustrate this novel approach, I analyze the *throughput, delay, and reliability of decentralized wireless networks with temporal correlation*. Temporal correlation in user locations results in temporal dependence in network interference, and increases as user mobility decreases and transmission time increases. The network model adopted in this work spans the extremes of temporal independence to long-term temporal dependence in network interference. I first derive the joint temporal statistics of interference (using the framework developed for deriving instantaneous statistics) and show that they follow a multivariate symmetric alpha stable distribution. The closed-form statistics are then used to derive closed-form expressions for throughput, delay, and reliability of single hop transmissions in the network. Simulation results demonstrate gains up to $2\times$ in network throughput and reliability by optimizing the closed-form performance measures over certain parameters of the MAC layer protocol.

3. **Receiver design to mitigate RFI:** A key motivation of deriving interference statistics that are applicable to a wide range of interference scenarios is to use the statistics for designing methods to mitigate RFI at the receiver. I focus on *pre-filtering methods to mitigate temporally dependent RFI* in baseband. Pre-filtering methods require minimum redesign of conventional receivers and hence are attractive for real-time implementation. The temporal statistics of RFI, under more realistic assumptions regarding propagation of RFI in the wireless medium, are

shown to follow a multivariate Gaussian mixture distribution. The multivariate Gaussian mixture distribution motivates the use of a recently proposed non-linear measure of distance as a design criterion for pre-filtering methods. The pre-filters proposed have superior bit-error-rate performance than existing prior work and are robust to deviations in the interference statistics.

1.5 Organization

This dissertation is organized as follows. Chapter 2 presents a brief survey of previous work with their relative strengths and limitations.

Chapter 3 derives the instantaneous statistics of RFI in a field of Poisson and Poisson-Poisson cluster distributed interferers. The framework used to derive the instantaneous statistics is utilized in the subsequent chapter to extend the statistical modeling approach to include the temporal dependence in interference.

Chapter 4 characterizes the single hop communication performance of decentralized wireless networks with temporal correlation. Using the approach introduced in the previous chapter, joint temporal statistics of interference are first derived in closed-form. The temporal statistics of interference are then used to derive closed-form expressions for the throughput, delay, and reliability of single hop transmissions in the network.

Chapter 5 utilizes the RFI statistics to derive pre-filtering methods

to mitigate RFI at the receiver. The temporal statistics derived in Chapter 4 are extended using the approach used in Chapter 3 for a more realistic assumption on propagation of RFI in the wireless medium. The knowledge of the temporal RFI statistics is then utilized to propose pre-filtering methods that are amenable to implementation.

Finally, Chapter 6 summarizes the contributions of this dissertation and outlines avenues for future research.

1.6 Nomenclature

3GPP	Third Generation Partnership Project
3GPP2	: Third Generation Partnership Project 2
AWGN	: Additive White Gaussian noise
BER	: Bit-error-rate
CDMA	: Code Division Multiple Access
CSMA	: Carrier Sense Multiple Access
CSMA/CA	: Carrier Sense Multiple Access with Collision Avoidance
EMI	: Electromagnetic Interference
FDMA	: Frequency Division Multiple Access
GMM	: Gaussian mixture model
LCD	: Liquid Crystal Display
LTE	: Long Term Evolution
MAC	: Medium Access Control
MCA	: Middleton Class A

MSE	: Mean squared error
MUD	: Multiuser Detection
OFDM	: Orthogonal Frequency Division Multiplexing
OFDMA	: Orthogonal Frequency Division Multiple Access
PHY	: Physical
PPP	: Poisson Point Process
QAM	: Quadrature Amplitude Modulation
RFI	: Radio Frequency Interference
SAS	: Symmetric Alpha Stable
SC-FDMA	: Single Carrier Frequency Division Multiple Access
SER	: Symbol-error-rate
SIC	: Successive Interference Cancellation
SINR	: Signal-to-interference-plus-noise ratio
SIR	: Signal-to-interference ratio
SNR	: Signal-to-noise ratio
TDMA	: Time Division Multiple Access
Wi-Fi	: Wireless Fidelity (WLAN built on IEEE 802.11a/b/g/n standards)
WiMAX	: Worldwide Interoperability for Microwave Access (built on IEEE 802.16 standards)
WLAN	: Wireless Local Area Networks

1.7 Notation

Throughout this dissertation, random variables are represented using boldface notation and deterministic parameters are represented using non-boldface type. Following are the mathematical notations used throughout this dissertation. Further notations are introduced in the chapters as the need arises and are kept consistent between chapters.

$\mathcal{CN}(0, \sigma^2)$: Zero-mean complex normal distribution with variance σ^2
$\Im(\cdot)$: Imaginary part
$\Re(\cdot)$: Real part
$\mathbb{E}_{\mathbf{X}} \{f(\mathbf{X})\}$: Expectation of the function $f(\mathbf{X})$ with respect to \mathbf{X}
$\mathbb{P}(\cdot)$: Probability of a random event
\otimes, \oplus	: Kronecker product, sum
$\stackrel{p}{=}, \stackrel{p}{\neq}$: Equality, non-equality in probability
$ \cdot , \ \cdot\ $: Euclidean norm
$\delta(\cdot)$: Dirac delta functional
j	: $\sqrt{-1}$
$(\cdot)^T$: Vector transpose

Chapter 2

Background

2.1 Introduction

This chapter provides a literature survey of the commonly used techniques to mitigate RFI in wireless receivers. In particular, Section 2.2 discusses various RFI management techniques used in wireless networks, without which multi-user interference would severely limit the communication performance of the network. Residual RFI is always present despite of the RFI management techniques. To this end, Section 2.3.1 provides a review of the prior work on statistical modeling of residual RFI. Closed-form RFI statistics have been primarily used to design filtering and detection methods to mitigate RFI at the receiver. This dissertation also shows the benefit of using closed-form RFI statistics for communication performance analysis of wireless networks. Survey of prior work on communication performance analysis of wireless networks and using the RFI statistics for receiver design is presented in Sections 2.3.2 and 2.3.3, respectively.

2.2 RFI Mitigation in Wireless Receivers

This section reviews some of the common methods of RFI mitigation and their limitations that result in residual RFI to be present. For simplicity of exposition, methods of RFI mitigation are classified as either *static* or *dynamic* methods. Static methods encompass techniques that attempt to reduce RFI using prior knowledge of the network topology and sources of RFI. In context of wireless networks, prior knowledge of network topology restricts the applicability of these methods to centralized networks. Dynamic methods, on the contrary, encompass techniques that avoid or cancel RFI by adapting to the current state of the network, but may require coordination among users. Summary of the various static and dynamic methods of RFI mitigation is presented in Fig. 2.1.

2.2.1 Static Methods

Static methods of RFI mitigation are applied during network planning and transceiver deployment phase. In regard to isolated sources of RFI, these methods require the knowledge of the location of the RFI sources. In regard to network interference, these methods require prior knowledge of the network topology. Following are some of the commonly used static methods of RFI mitigation.

Shielding: Shielding is a common industry practice used to mitigate platform noise in wireless transceivers embedded on a platform [11]. In-platform RFI in commercial laptops, for example, is measured at various loca-

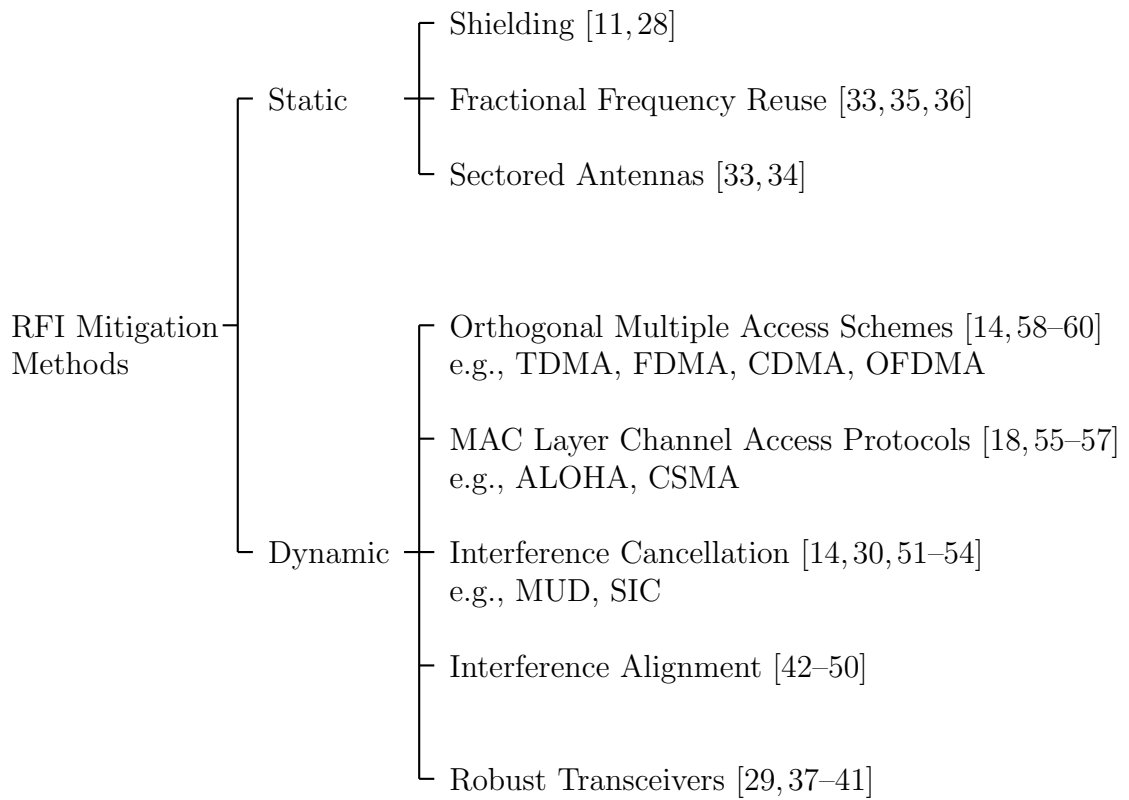


Figure 2.1: Summary of commonly used techniques to mitigate RFI in wireless receivers. Under dynamic RFI mitigation methods, this dissertation proposes direct contributions in robust transceiver design and identifies potential improvement in network throughput via optimization of MAC layer channel access protocols. The acronyms CDMA, CSMA, FDMA, MAC, MUD, OFDMA, SIC, and TDMA are defined in Section 1.6.

tions and sources of RFI are identified. Shielding from the identified sources, while expensive, may become a necessity based on the location where the transceiver is deployed [28]. Residual RFI is however always present due to unshielded sources [11].

Fractional frequency reuse: Early deployments of cellular networks reduced co-channel interference in the network through fractional frequency reuse [33, 35, 36]. In fractional frequency reuse, the available spectrum is geographically split among the cells in the network with a spatially repeating pattern. Since each cell is allocated only a fraction of the total spectrum, fractional frequency reuse results in reduced peak data rates that can be achieved. Distance between cells using the same fraction of the frequency spectrum increases as the frequency reuse fraction increases. Thus residual RFI, however restricted, will still be present.

Current and upcoming cellular standards, like the third generation partnership program (3GPP) long term evolution (LTE) Advanced [16], aim to increase the peak data rate by using the entire available spectrum in each cell. This increases the co-channel interference present in cellular networks.

Sectored antennas: It is common for cellular networks to employ sectored antennas at the basestation to reduce the interference within a cell [33]. It is common in current cellular deployments for a cell site to be partitioned into 3 sectors [34]. Partitioning a cell site into sectors helps in fractional reduction of RFI, but residual RFI is still present.

2.2.2 Dynamic Methods

Dynamic methods encompass PHY layer and MAC layer protocols to mitigate RFI.

Orthogonal multiple access schemes: Such schemes allow multiple users to simultaneously access the wireless medium by making their transmissions orthogonal to each other in some space - time, frequency, or code space. Common orthogonal multiple access schemes include time division multiple access (TDMA), frequency division multiple access (FDMA), code division multiple access (CDMA), single carrier frequency division multiple access (SC-FDMA), and orthogonal frequency division multiple access (OFDMA) [14]. Orthogonal multiple access schemes are a backbone of many centralized wireless networks, such as a cellular network. 2G cellular standards employed TDMA, the most popular 3G cellular standards employ CDMA (CDMA/TDMA hybrid in 3GPP2 Evolution-Data Optimized, a.k.a. EVDO), and the current and upcoming 4G cellular standards are using OFDMA (downlink in 3GPP-LTE, IEEE 802.16e WiMAX) and SC-FDMA (uplink in 3GPP-LTE) [58]. While TDMA, FDMA, and OFDMA require user coordination and centralized control to distribute the time or frequency resource among the users, use of CDMA physical layer has been proposed as a viable option in decentralized wireless networks. [59, 60]

Residual RFI will be present due to the following reasons. First, only a finite number of user transmissions can be made orthogonal to each other. For example, in cellular networks only a finite number of users are scheduled

at any time, and their transmissions are made orthogonal to each using orthogonal multiple access schemes. Residual RFI is present, however, due to out-of-cell users that use the same resources. Further, residual RFI may be present when the transmissions are not perfectly orthogonal. For example, CDMA physical layer with pseudo-random spreading codes do not make the simultaneous transmissions perfectly orthogonal [14].

MAC layer channel access protocols: Decentralized wireless networks, such as wireless ad hoc networks and dense Wi-Fi networks, rely on MAC layer channel access protocols such as ALOHA and carrier sense multiple access (CSMA) to reduce RFI [18, 55–57]. Schemes such as ALOHA and time/frequency hopping attempt to reduce the simultaneous user transmissions that use the same frequency spectrum and have been widely applied to reduce RFI in wireless ad hoc networks [55]. CSMA involves listening to the wireless medium and schedule a user transmission only if no ongoing transmissions are observed. Variants of CSMA, such as CSMA with collision avoidance (CSMA/CA) and CSMA/CA with RTS/CTS are used in IEEE 802.11a/b/g/n Wi-Fi networks [18].

Because the primary aim of such schemes is to reduce and not eliminate RFI, residual RFI is always present. This dissertation identifies certain parameters of the MAC protocol that can be optimized to reduce RFI in a decentralized wireless network.

Interference cancellation: The basic idea behind interference cancellation schemes is that if the interference can be successfully decoded at the

receiver, then it can be subtracted from the received signal to improve the detection performance of the desired signal [14]. Interference cancellation for cellular networks has been an active area of research since the mid-1980s, peaking in the 1990s [30]. Methods of interference cancellation include multiuser detection (MUD), successive interference cancellation (SIC) and spatial interference cancellation schemes such as Bell Labs layered space-time (BLAST) system for multi-antenna receivers [51, 52]. Interference cancellation schemes in decentralized wireless networks are an active area of current research [53, 54].

The goal of interference cancellation schemes is to cancel out dominant interferers, and residual RFI will be present due to other users whose individual power is not that significant at the receiver. Cumulative RFI from users that are not canceled at the receiver may still be strong to cause significant degradation in communication performance.

Interference alignment: Interference alignment is a relatively new technique that is a subject of current research. Interference alignment is a linear precoding technique that attempts to align interfering signals in time, frequency, or space. It was first introduced in [42] as a coding technique in two-user multi-input multi-output (MIMO) interference channel where it was shown to achieve rates higher than MIMO interference cancellation techniques. Explicit formulation of interference alignment was later done in [43]. The key idea of interference alignment is that users coordinate their transmissions, using linear precoding, such that the interference signal lies in a reduced dimensional subspace at each receiver. The importance of this technique is the result

that in a network with K transmit-receiver pairs, an interference alignment strategy will result in a sum throughput of $\frac{K}{2} \log(SNR) + o(K \log(SNR))$. This is a significant improvement (K times) over orthogonal multiple access techniques where the sum throughput is $\frac{1}{2} \log(SNR) + o(K \log(SNR))$, and is somewhat surprising at first [43]. The assumption in achieving these gains is that each transmitter and receiver has a global knowledge of all interfering links in the network [43]. Thus a lot of feedback and coordination is required among the users to achieve these gains.

Interference alignment has received a lot of attention in the last couple of years. Methods for interference alignment in cellular network [44], wireless ad hoc networks [45,46], cognitive networks [47], and MIMO wireless networks [48] have been studied in recent past. The feasibility of interference alignment techniques in practice, due to limited capacity and accuracy in the feedback channels, has also been studied [49,50]. Delay introduced in the system for exchanging the global channel states is also an important concern.

Interference alignment methods require coordination among user pairs. Thus such methods can be used in practice to align only certain users, e.g., a limited number of neighboring basestations in cellular networks to reduce inter-cell interference [44]. Residual interference will still be present due to uncoordinated users and imperfect interference alignment due to limited accuracy in the global channel state information available at the transmitter and receivers.

Robust Transceivers: Treating interference as noise at the receiver,

communication performance of wireless transceivers in the presence of RFI can be improved by using better modulation schemes, error-correction-codes, and receiver pre-filtering methods [29, 37–41]. Such methods do not attempt to avoid, reduce, or cancel RFI, but rather try to improve the communication performance given that RFI is present. Motivated by the increasing RFI in wireless networks, designing robust transceivers in conjunction to other methods to avoid, reduce, or cancel RFI are being investigated to suppress the residual RFI. Using the accurate statistics of residual RFI to analyze and design wireless receivers overlaps directly with the approach adopted in this dissertation.

2.3 Statistical Modeling and Mitigation of RFI

Communication performance of point-to-point communication links, and wireless networks as a whole, is affected by the residual RFI present due to various sources. Knowledge of closed-form RFI statistics can be used to design both PHY layer and MAC layer techniques with improved communication performance. Closed-form statistics of RFI are however known in only a few interference scenarios. *This is the key limitation in prior work that is addressed in this dissertation.* Further, this dissertation shows the benefit of using closed-form RFI statistics for communication performance analysis of wireless networks and designing receivers to mitigate RFI. The following subsections review the prior work on statistical modeling of RFI, communication performance analysis of wireless networks, and receiver design to mitigate RFI.

2.3.1 Statistical Modeling of RFI

Statistical techniques used in modeling RFI include empirical and statistical-physical methods. Empirical approaches fit a mathematical model to received signals, without regard to the physical generation mechanisms behind the interference. Statistical-physical models, on the other hand, model interference based on the physical principles that govern the generation and propagation of the interference-causing emissions. Statistical-physical models are thus more widely applicable than empirical models [12, 13]. The key statistical-physical models derived in prior work include symmetric alpha stable and Middleton Class A distributions. In this dissertation, the Gaussian mixture distribution is also derived using statistical-physical principles. Table 2.1 presents a brief introduction to these distributions, including the distribution parameters, for a two-dimensional zero-centered isotropic random vector $\{\mathbf{I}^{(I)}, \mathbf{I}^{(Q)}\}$. A detailed discussion of the statistical properties of the symmetric alpha stable, Gaussian mixture, and Middleton Class A distributions is provided in Appendix A, B, and C, respectively.

Statistics of RFI are affected by the following key factors [12, 13, 61]:

- (i) Duration and frequency bandwidth of typical interferer emissions relative to the receiver bandwidth.
- (ii) Spatial or spatio-temporal distribution of interferers.
- (iii) Spatial region over which the interferers are distributed.

Table 2.1: Statistical properties of symmetric alpha stable (SAS), Middleton Class A (MCA), and Gaussian mixture (GMM) distributions, for a two-dimensional zero-centered isotropic random vector $\{\mathbf{I}^{(I)}, \mathbf{I}^{(Q)}\}$. A detailed discussion of the statistical properties of the SAS, GMM, and MCA distributions is provided in Appendix A, B, and C, respectively.

Statistical Model	Distribution Characteristics		
SAS	Characteristic function: $\Phi_{\mathbf{I}^{(I)}, \mathbf{I}^{(Q)}}(\omega_I, \omega_Q) = e^{-\sigma \sqrt{\omega_I^2 + \omega_Q^2} ^\alpha}$ Closed-form PDF do not exist, except for $\alpha = 2$ (Gaussian) and $\alpha = 1$ (Cauchy).		
	Parameter	Description	Range
	α	Characteristic exponent (indicates impulsiveness)	$[0, 2]$
	σ	Dispersion (analogous to variance)	$(0, \infty)$
MCA	PDF: $f_{\mathbf{I}^{(I)}, \mathbf{I}^{(Q)}}(i^{(I)}, i^{(Q)}) = e^{-A} \delta(i^{(I)}, i^{(Q)}) + \sum_{m=1}^{\infty} \frac{e^{-A} A^m}{m!} e^{-\frac{(i^{(I)})^2 + (i^{(Q)})^2}{\frac{2m\Omega_{2A}}{A}}}$ Particular form of Gaussian mixture distribution The above form is without the additive Gaussian component		
	Parameter	Description	Range
	A	Overlap index (indicates impulsiveness)	$(0, \infty)$
	Ω_{2A}	Mean intensity	$(0, \infty)$
	PDF: $f_{\mathbf{I}^{(I)}, \mathbf{I}^{(Q)}}(i^{(I)}, i^{(Q)}) = p_0 \delta(i^{(I)}, i^{(Q)}) + \sum_{l=1}^{\infty} p_l \frac{1}{\sigma_l \sqrt{2\pi}} e^{-\frac{(i^{(I)})^2 + (i^{(Q)})^2}{2\sigma_l^2}}$		
GMM	Parameter	Description	Range
	p_l	Mixture probabilities such that $\sum_{l=0}^{\infty} p_l = 1$	$[0, 1]$
	σ_l^2	Variance of individual Gaussian components	$(0, \infty)$

- (iv) Propagation characteristics of the wireless medium including pathloss and fading.

Following is a review of prior work on statistical modeling of RFI with respect to these factors.

Regarding (i), the duration and frequency bandwidth of the interferer emissions, with respect to the receiver bandwidth, affects the response at the receiver front end. Interferers with typical duration of emission much greater than the reciprocal of the receiver bandwidth are referred to as narrowband interferers, as they do not cause any transients (ringing effect) in the receiver [12]. Much of the prior work assumes a field of narrowband interferers to model both intelligent and non-intelligent sources of RFI in the environment. This is a reasonable assumption since it precludes only certain non-intelligent sources of RFI that have very short duration of electromagnetic emissions.

Regarding (ii) and (iii), much of the prior work on statistical modeling of RFI assumes the interferers to be distributed according to a homogeneous Poisson point process over the entire plane [62–69]. The instantaneous statistics of RFI in a homogeneous Poisson field of interferers distributed over the entire plane have been shown to follow a symmetric alpha stable distribution [70–72]. When the interferers are distributed according to a homogeneous Poisson point process over a finite area region with a guard zone around the receiver, then the RFI has been shown to follow a Middleton Class A distribution [12, 13]. Extensions for joint temporal statistics of RFI when the Poisson

point process has temporal correlation have been limited [71–73].

The knowledge of closed-form RFI statistics, along with certain desirable properties of the Poisson point process, renders the assumption of Poisson distributed interferers over the entire plane analytically tractable for modeling interference in wireless networks [63, 67, 68]. The validity of Poisson assumption has been argued for decentralized networks, such as wireless sensor and ad hoc networks, where the user locations are spatially random to a great extent. For example, in wireless mobile ad hoc networks, this assumption is justified by arguing that the users move independently from each other resulting in complete spatial randomness [31, 74–76].

While the assumption of Poisson interferer filed may be accurate for certain interferer environments (e.g., co-channel interference in wireless sensor networks), it fails to capture certain important characteristics such as interferer clustering and guard zone creation in wireless networks [32, 57, 60, 64, 66, 75, 77]. Other spatial distributions have also been studied in the literature to some extent [68, 75, 78]. Closed form amplitude statistics of the interference, however, are not known for most spatial distributions and topologies of the interferers [64, 66, 75, 79].

Regarding (iv), in addition to the assumption of spatially Poisson distributed user locations, deriving closed-form RFI statistics requires additional assumptions on the fading and pathloss function. For example, the symmetric alpha stable distribution is derived assuming an unbounded pathloss function of the form $r^{-\frac{\gamma}{2}}$, where r is the propagation distance and

γ is the power pathloss exponent [70–72]. Unbounded pathloss function, however, is not realistic because it suggests that the received power is greater than the transmitted power when $r < 1$ [61]. Further, the Middleton Class A model is exact only under the assumption of Rayleigh distributed amplitude of the received signal (that has experienced fading), and is a good approximation of the tail probabilities otherwise [12, 13].

To address the aforementioned limitations in prior work, Chapter 3 derives closed-form instantaneous statistics of RFI in a field of Poisson and Poisson-Poisson clustered distributed interferers assuming an unbounded pathloss model. Further, by considering the interferers distributed over a parametric annular region, interference statistics are derived for finite- and infinite area interference region with and without a guard zone around the receiver. When exact statistics cannot be derived in closed-form, this dissertation attempts to derive approximate closed-form expressions that accurately model the tail probability of RFI. The motivation of accurately modeling tail probability arises from the fact that the communication performance measures (such as outage probability and bit-error-rates) depend on tail probability of RFI, particularly in the low outage regime.

In addition to symmetric alpha stable and Middleton Class A distributions derived in prior work, Chapter 3 establishes the applicability of the Gaussian mixture distribution in accurately modeling the RFI statistics in a wide range of interference scenarios. Further, the framework used to derive the instantaneous statistics in Chapter 3 is exploited to derive closed-form joint

interference statistics of RFI in temporally correlated Poisson field of interferers, for both unbounded and bounded pathloss function in Chapter 4 and Chapter 5, respectively.

2.3.2 Communication Performance of Wireless Networks

Capacity is the fundamental limit on communication performance of a network. The capacity of wireless networks is a cross layer design issue and depends on varied factors such as the properties of the physical layer, MAC layer protocol, and spatio-temporal traffic patterns. For a network of n nodes, the unicast capacity region of the network has a dimensionality of $n(n - 1)$ since each node can potentially communicate with all other nodes. Characterizing the multidimensional capacity region of ad hoc networks is an open problem in information theory [31, 80]. In the seminal paper [9], the authors proposed the capacity analysis of random and arbitrary networks with asymptotically large number of nodes. With n nodes randomly located on a unit-area disk, and grouped into source-destination pairs randomly, [9] shows that the per-node throughput capacity is $\Theta\left(\frac{1}{\sqrt{n \log n}}\right)$. In [81], the authors show using percolation theory that a per-node throughput capacity of $\Theta\left(\frac{1}{\sqrt{n}}\right)$ is achievable in networks with randomly located nodes - improving the result in [9] by a factor of $\sqrt{\log n}$. If the node locations and traffic patterns are chosen optimally, then the *transport capacity* defined as the bit-meters that can be achieved for each node over a given time interval was shown to be $\Theta\left(\frac{1}{\sqrt{n}}\right)$ [9]. While many publications suggest more optimistic throughput scaling [82, 83] in

special cases (such as with node mobility [83]), it is widely agreed that a per-node throughput of $\Theta\left(\frac{1}{\sqrt{n}}\right)$ can be achieved using nearest-neighbor routing in ad hoc networks [9, 81, 84, 85].

While transport capacity provides a high-level insight on how different network scenarios (including routing and node placement) may affect the scaling law, the results are typically asymptotic scaling laws with little [86] or no information about the constant multiplier. This restricts comparing different networks and studying capacity tradeoffs in network design choices (such as physical layer properties and MAC protocols). This has motivated computing the achievable rate regions for different network architectures including assumptions on node distribution and MAC protocol [87, 88]. In [87], the authors defined the *transmission capacity* of a network as the number of successful transmissions taking place in the network per unit area, subject to a constraint on the network outage probability [87]. Transmission capacity framework has been widely used in the literature to characterize the effect of various physical layer techniques and MAC layer protocols in ad hoc networks, such as successive interference cancellation [53], guard zone based scheduling [56, 60], and multiple antennas [89, 90]. While much of the prior work considers the nodes to be Poisson distributed, there has been notable work done to characterize transmission capacity in networks with non-Poisson distributed nodes [79]. While transmission capacity was initially defined for single-hop communication in the networks, extensions for multi-hop communication performance have also been investigated [84, 91].

Exact closed-form expressions of single-hop communication measures such as outage probability and transmission capacity have been derived in closed-form only under the assumptions of unbounded pathloss model and that the interferers are distributed according to Poisson point process over the entire plane [63, 68, 76]. Exact expressions can be derived since RFI is known to follow a symmetric alpha stable distribution in this case [76]. Further, even though RFI statistics are known to follow a Middleton Class A distribution in a Poisson field of interferers distributed over an annular region around the receiver, Middleton Class A distribution has not been used for communication performance analysis of wireless networks [74]. Poisson field of interferers distributed over an annular region around the receiver serves as a good model for local area networks, such as local Wi-Fi hotspots.

For network models where closed-form RFI statistics are not known, much of the prior work resorts to deriving bounds on the measures of communication performance [76, 91]. Further, single-hop communication performance measures such as outage probability and transmission capacity have been defined and analyzed under the assumption of temporal independence in user locations [76]. User locations, however, may exhibit temporal correlation due to limited user mobility and increased time duration of typical transmissions in the network. Recently, the local delay of decentralized wireless networks was derived for the extremes of temporal independence and complete temporal correlation in user locations [92–95]. Local delay is defined as the average number of time slots required for a typical single-hop communication link to

be successful in the network [92]. To address the aforementioned limitations in prior work, Chapter 4 derives closed-form expressions for throughput, local delay, and reliability (throughput outage probability) of single-hop transmissions in a decentralized wireless network with temporal correlation. The definition of transmission capacity of single-hop transmissions is extended to account for temporal correlation in user locations such that it captures the throughput-delay-reliability tradeoff of single hop transmissions. Closed-form communication performance measures and the extended definition of transmission capacity enables identifying MAC parameters that can be optimized to improve the throughput and reliability of the network.

2.3.3 Receiver Design to Mitigate RFI

Prior work has demonstrated significant gains in communication performance by designing filtering and detection methods at the receiver to mitigate RFI [29, 37, 40, 96–99]. Two common approaches for designing filtering or detection methods at the receiver to mitigate RFI are (a) exploiting the exact statistics of the RFI and deriving bit-error-rate (BER) optimal filtering and detection methods [29, 37, 40], and (b) designing the receivers based on “robust statistics” which are resilient to the general impulsive nature of RFI [100–103]. Exploiting exact statistics of the RFI is useful in deriving receiver structures that are optimal with respect to the chosen communication performance measure (such as BER). The robustness of the receiver, however, is not guaranteed if the statistics of observed RFI deviate from those assumed

while designing the receiver [37]. Further, such methods require estimation of parameters governing the RFI distribution at the receiver - which adds to the computational complexity. On the other hand, designing receivers based on the general impulsive nature of RFI may yield limited improvement in communication performance. The improvement depends on the extent of the knowledge of RFI statistics exploited. This motivates designing receivers that are closely bound to RFI statistics and are yet robust to deviations in RFI statistics, and do not require estimation of parameters that govern the RFI distribution.

Designing receivers using interference statistics can be divided into pre-filtering and detection techniques. Detection techniques refer to deriving the optimum decision criterion based on Bayesian or maximum *a posteriori* inference, and may require significant redesign of the receiver [29,37]. Pre-filtering methods, on the contrary, introduce a filtering stage prior to the conventional receiver structure [29,97]. While pre-filtering methods may not be optimal with respect to the communication performance measure considered, they present a tradeoff in improvement of communication performance vs. implementation complexity of the receiver structure. Motivated by the minimal redesign of conventional receivers required, this dissertation focuses on developing pre-filtering methods to mitigate RFI.

Statistics of RFI affects the design of per-filters with regard to the following factors: (i) filter structure, and (ii) the distance measure used for deriving filter parameters. Knowledge of the optimum filter structure and dis-

tance measure for a certain RFI distribution (zero-centered and symmetric) is related directly to the knowledge of closed-form maximum likelihood (ML) estimate of a constant signal in presence of RFI. For example, the ML estimate of a constant signal in zero-mean Gaussian distributed RFI is the mean of the observed samples, and minimizes the mean squared error (MSE) from the observed samples [101]. This leads to the optimality of a linear filter structure and MSE (L_2 -norm) as the distance measure in the presence of Gaussian distributed noise. Similarly, for Laplacian distributed RFI, the median pre-filter and absolute deviation (L_1 -norm) distance measure is optimal [101].

As discussed in Section 2.3.1, prior work has shown the applicability of symmetric alpha stable and Middleton Class A distributions for modeling RFI in certain network environments. Further, this dissertation shows the applicability of the Gaussian mixture distribution in modeling RFI in a wide variety of wireless networks. Middleton Class A distribution is a particular form of the Gaussian mixture distribution. Symmetric alpha stable model is derived assuming an unbounded pathloss function, and is not realistic [70–72]. Further, inclusion of thermal noise in the design of receivers is difficult since the sum of symmetric alpha stable and Gaussian random variables is no longer symmetric alpha stable distributed [13]. Gaussian mixture models, on the contrary, can be motivated by physical constraints and can easily be extended to include the background thermal noise component [13, 104]. Following is a summary of prior work in pre-filter design categorized based on the distribution of RFI.

Symmetric Alpha Stable: There is a rich literature on receiver design in the presence of symmetric alpha stable interference, including both pre-filtering [101, 105–107] and detection methods [37, 108, 109]. Prior work has shown the optimality of the Myriad pre-filter in the presence of symmetric alpha stable distribution in the context of removing impulsive noise from images. The robustness of Myriad pre-filters to general impulsive nature of RFI has also been argued [105–107].

Gaussian Mixture Model (includes Middleton Class A): Knowledge of the optimum pre-filter structure or distance measure for Gaussian mixture distribution (which includes Middleton Class A distribution) is not known in prior work. Nonetheless, many pre-filters and detection methods have been proposed for both Middleton Class A noise and Gaussian mixture noise [38, 97, 100–102, 110–113]. Much of the prior work, however, use the Gaussian mixture (or Middleton Class A) distribution to analyze the performance of a receiver, rather than designing the pre-filter based on the Gaussian mixture statistics. Minimum mean squared error (MMSE) based pre-filtering methods in the presence of Gaussian mixture noise were studied in [112, 113]. BER optimality of these pre-filtering methods [112, 113], however, is not guaranteed since the MMSE criterion is BER optimal only if the noise is Gaussian distributed. Extension of pre-filtering methods to the case when RFI is temporally dependent have been limited.

In addition to symmetric alpha stable, Middleton Class A, and Gaussian mixture distributions, many other distributions have been used to model

the impulsive nature of RFI. Some of the common distributions used for analysis and design RFI mitigation methods include Generalized Gaussian distribution [114], Laplacian distribution [115], and mixture of Laplacian and Gaussian distribution [116].

Common pre-filtering structures assumed in prior work include memoryless clipping and/or blanking non-linearities [97, 102], order statistics filtering methods [101], and polynomial filters based on Volterra series [117]. Pre-filtering structures such as the memoryless clipping and/or blanking non-linearity [97, 114], myriad pre-filter [107], and median pre-filter [118] belong to a general class of M-estimation based pre-filters [100]. Bit-error-rate optimality or the design of filter parameters (e.g., threshold for clipping or blanking) using RFI statistics, however, is not accurately established [97].

Common distance measures used for design of pre-filters or other detection methods in the presence of RFI include higher order statistical distance [119, 120], fractional lower order norms [108], zero order statistics [3], error entropy [121], and correntropy [2]. Motivating the distance measure used, along with the pre-filter structure, for the particular form of RFI statistics is a limitation in prior work.

To address the aforementioned limitations in prior work, Chapter 5 first motivates the use of multivariate Gaussian mixture distribution to model the temporal statistics of RFI. Order statistic filters are then proposed that use correntropy as a distance measure and zero-order-statistics of RFI to scale the correntropy induced metric space. The use of correntropy and zero-order-

statistics is justified for the given RFI statistics.

2.4 Conclusions

In this chapter, a survey of prior work on RFI management in wireless receivers was presented. No single technique of RFI management can completely eliminate RFI. The residual RFI is treated as noise at the receiver. Limitations in prior work on statistical modeling and mitigation of the residual RFI in wireless receivers were identified. Table 2.2 summarizes the prior work on statistical modeling and mitigation of the residual RFI in wireless receivers. This dissertation builds on the prior work on statistical modeling and mitigation of the residual RFI. Chapter 3 derives closed-form RFI statistics in a wide range of interference scenarios. Chapter 4 shows the benefit in the novel approach of deriving communication performance measures using the amplitude statistics of RFI. Throughput, delay, and reliability of decentralized wireless networks are analyzed as an illustration of the approach. Results demonstrate potential improvement in the throughput and reliability of the networks - thereby motivating design of MAC layer protocols to achieve the same. Chapter 5 designs pre-filters at the PHY layer using the knowledge of RFI statistics for improved communication performance in the presence of RFI.

Table 2.2: Summary of prior work on (i) statistical modeling of RFI, (ii) use of RFI statistics for communication performance analysis of wireless networks, and (iii) use of RFI statistics for receiver design to mitigate RFI. Prior work has been categorized by the key statistical-physical models of RFI derived in prior work. Here SAS, MCA, and GMM stand for symmetric alpha stable, Middleton Class A, and Gaussian mixture model, respectively.

	RFI Statistics	SAS	MCA	GMM
Statistical Modeling of RFI	Key Prior Work	[70–72]	[12, 13]	- ^a
	Interferer distribution	Poisson	Poisson	- ^a
	Space containing interferers	Entire Plane	Finite Area	- ^a
	Bounded pathloss	No	Yes	- ^a
Network Performance Analysis	Key Prior Work	[63, 68, 76]	- ^b	- ^b
	Networks with temporal correlation	Limited ^c	No	No
Receiver Design to Mitigate RFI	Key Prior Work	[37, 101, 105–109]	[29, 40, 96]	[38, 102, 110–113]
	L ₂ norm exists	No	Yes	Yes
	Can include Thermal noise	No	Yes	Yes
	Optimal pre-filter structure	Myriad ^d	Unknown	Unknown
	Optimal distance measure	LD ^{d e}	Unknown	Unknown

^aApplicability of Gaussian mixture distribution to model RFI is not shown in prior work using statistical-physical principles.

^bNot used for communication performance analysis of wireless networks

^cOnly extremes of full temporal correlation studied in [92–94]

^dExact optimality in case of Cauchy distribution, i.e., when $\alpha = 1$ [107].

^eLogarithmic Deviation

Chapter 3

Instantaneous Statistics of Co-Channel Interference in Wireless Networks

3.1 Introduction

Current and future wireless communication systems require higher spectral usage due to increasing demand in user data rates. One of the principal techniques for efficient spectral usage is to implement a dense spatial reuse of the available radio spectrum. This causes severe co-channel interference, which limits the communication system performance. Chapter 2 highlighted the benefit of using closed-form interference statistics to analyze and improve the communication performance of wireless networks. As reviewed in Section 2.3.1, closed-form statistics of co-channel interference are known only in a few interference scenarios. In this chapter, I derive the instantaneous statistics of co-channel interference with applicability to a wide range of interference scenarios that is common in many wireless networks. Applicability of statistical distributions derived in modeling in-platform RFI obtained from a laptop embedded wireless receiver is also established using empirical methods. The contents of this chapter are close to that of the papers [99, 104, 122, 123].

3.1.1 Motivation and Prior Work

Co-channel interference statistics in wireless networks are affected by the following key factors: (i) the spatial distribution of interferers, (ii) the spatial region over which the interferers are distributed, and (iii) propagation characteristics including the power pathloss exponent and fading. Regarding (i), the distribution of active interferers in large random wireless networks is generally assumed to be a homogeneous spatial Poisson point process [62–64, 67, 68]. While this assumption may be valid for certain wireless networks (e.g. wireless sensor and ad hoc networks), it may be common for interfering users to cluster in space due to geographical factors (e.g. gathering places or femtocell networks [32, 124]), or medium access control (MAC) layer protocols [68, 77]. Regarding (ii), the spatial region containing the interferers is commonly assumed to be an infinite plane [62–64, 67]. Many wireless networks, however, employ contention-based MAC protocols (e.g. carrier sense multiple access and multiple access with collision avoidance) or other local coordination techniques to limit the interference, thereby creating a guard zone around the receiver (e.g. in wireless ad hoc networks [60] and in dense Wi-Fi networks [18, 68]). Guard zones around the receiver can also occur due to scheduling-based MAC protocols, such as in cellular networks in which the users in the same cell site are orthogonal to each other and all interfering users are outside the cell site in which the receiver is located. Further, receivers in many wireless networks may experience interference from finite-area regions (e.g. interference from a cell site in cellular networks with reuse factor greater than one) [65]. This mo-

tivates characterizing the interference statistics in Poisson and Poisson-Poisson clustered interferers distributed over a parametric annular region. For each of the interferer distributions, the finite- and infinite- area with and without a guard zone around the receiver can then be studied as particular cases of the parametric annular interference region.

Statistical-physical modeling of co-channel interference in random Poisson interference fields has been extensively studied in literature [65, 70–72, 122, 123]. In [70], it was shown that interference from a homogeneous Poisson field of interferers distributed over the entire plane can be modeled using the symmetric alpha stable distribution [125]. This result was later extended to include channel randomness [71] and second-order statistics capturing the temporal dependence [72]. Recently, the authors in [65] investigated extensions for a finite-area field and derived the interference moments. Closed form approximations to the interference distribution, however, were not investigated.

Other key statistical-physical models for co-channel interference in random Poisson interference fields include Middleton Class A, B, and C models [13]. Middleton models are useful because they characterize a wider range of physical conditions, including narrowband and broadband interference emissions, transients at the receiver, and background thermal noise [12, 13]. Middleton models, however, have not been widely used to characterize co-channel interference in wireless network environments.

Statistical-physical modeling of co-channel interference in random Poisson clustered interference fields was recently studied in [75]. The focus of the

work was to characterize the network performance (outage probability and transmission capacity) and the interferer clusters were assumed to be distributed over the entire plane. Closed form interference statistics, however, were not derived.

The problem considered in this chapter is also closely related to the problem of deriving the amplitude distribution of shot noise processes [7]. Co-channel interference in a planar network of nodes distributed according to any point process can be modeled as a generalized shot noise process [7, 126]. The shot noise process is studied in detail in [7] and existence of generalized shot noise process for any point process was shown in [126]. Properties of the shot noise processes, such as characteristic function for power-law shot noise process [127], are commonly used to evaluate bounds on outage probabilities in wireless networks [124, 128]. To the best of my knowledge, closed form expression of the amplitude distribution for shot noise process are not known for the interferer topologies considered in this chapter.

3.1.2 Contribution, Organization, and Notation

In this chapter, I derive the interference statistics of co-channel interference from a field of Poisson and Poisson-Poisson clustered distributed interferers. Further, for each of the interferer distributions, the statistics are derived for interferers or interferer clusters distributed over (i) the entire plane, (ii) finite-area annular region, and (iii) infinite-area annular region with a guard zone around the desired receiver. One of the key contributions of this chapter

is to develop a unified framework to derive the co-channel interference statistics in different wireless network environments and establish the applicability of the symmetric alpha stable and Gaussian mixture model (with Middleton Class A model as a particular form). Analytical constraints on the system model parameters for which these distributions accurately model the statistical properties of the interference are also derived. When exact statistics cannot be derived in closed form, I focus on accurately modeling the tail probability of the interference distribution.

The chapter is organized as follows. Section 3.2 discusses the system model. Section 3.3 derives the interference statistics for interferers distributed according to a homogeneous spatial Poisson point process. Section 3.4 derives the interference statistics for a interferers distributed according to a homogeneous spatial Poisson-Poisson clustered process. Section 3.5 summarizes the interference models derived in this chapter. Section 3.6 presents results from numerical simulations. Section 3.7 presents results from empirical fitting of measured in-platform RFI data to the statistical models derived. Appendices A, B, and C contains a brief discussion on the statistical properties of the interference models derived in the chapter. Table 3.1 summarizes the notation used in this chapter.

3.2 System Model

At each sampling time instant n , the locations of the active interferers are assumed to be distributed according to a homogeneous spatial point process

Table 3.1: Summary of Notation used in Chapter 3

Symbol	Description
$\Pi = \{\mathbf{R}_i\}$	point process of active interferers
\mathbf{K}	(random) number of active interferers
Γ	region containing interferers
R_m	receiver location
$\mathbf{r} = \ \mathbf{R} - R_m\ $	(random) distance of interferer from receiver
$\mathbf{X} = \mathbf{B}e^{j\phi}$	amplitude and phase of interferer emissions
$\gamma > 2$	power pathloss exponent
$\mathbf{g} = \mathbf{h}e^{j\theta}$	amplitude and phase of narrowband fading
$\mathbf{I} = \mathbf{I}^{(I)} + j\mathbf{I}^{(Q)}$	(complex) sum interference at receiver
$\bar{\mathbf{I}} \triangleq \{\mathbf{I}^{(I)}, \mathbf{I}^{(Q)}\}$	inphase and quadrature phase components
$\bar{\omega} = [\omega^{(I)}, \omega^{(Q)}]^T$	frequency variables for characteristic function of $\bar{\mathbf{I}}$
$ \bar{\omega} , \bar{\omega}_\phi$	$\triangleq \sqrt{(\omega^{(I)})^2 + (\omega^{(Q)})^2}, \triangleq -\tan^{-1}(\omega^{(Q)}/\omega^{(I)})$
$\Phi_{\bar{\mathbf{I}}}(\bar{\omega}), \Psi_{\bar{\mathbf{I}}}(\bar{\omega})$	joint characteristic, log-characteristic function of $\bar{\mathbf{I}}$
$\Lambda(\bar{\omega})$	$= O(\bar{\omega} ^4)$ as $ \bar{\omega} \rightarrow 0$ correction term given by (3.20)
λ	intensity of Π for a Poisson interferer field
λ_c	intensity of Poisson process for cluster centers
λ_f	intensity of Poisson process for interferers in a cluster
r_l, r_h	inner, outer radii of annular interferer region
R_l, R_h	inner, outer radii of annular region with cluster centers
α, σ	parameters of symmetric alpha stable model
A, Ω_{2A}	parameters of Middleton Class A model
p_l, σ_l^2	parameters of Gaussian mixture model, $l \geq 0$

$\Pi = \{\mathbf{R}_1, \mathbf{R}_2, \dots\}$ over the space Γ , where \mathbf{R}_i are the random locations of the interferers. This model is sufficient to capture both the emerging interferers, whose contributions arrive at the receiver for the first time at the time instant n , and interferers that first emerged at some prior sampling time instant $m < n$ but are still active until the sample time n [72].

The baseband model for the sum interference \mathbf{I} at any time instant can then be represented as

$$\mathbf{I} = \sum_{i=1}^{\mathbf{K}} \mathbf{r}_i^{-\frac{\gamma}{2}} \mathbf{g}_i \mathbf{X}_i \quad (3.1)$$

where \mathbf{K} is the random number of active interferers at that time instant, i is the interferer index, $\mathbf{r}_i = \|\mathbf{R}_i - R_m\|$ are the random distances of active interferers from the receiver, γ is the power pathloss exponent, \mathbf{g}_i is the independent and identically distributed (*i.i.d.*) random fast fading experienced by each interferer emission, and \mathbf{X}_i are the random interferer emissions.

All potential interferers are assumed to have *i.i.d.* symmetric narrow-band emissions of the form [12]

$$\mathbf{X}_i = \mathbf{B}_i e^{j\phi_i} = \mathbf{B}_i \cos(\phi_i) + j\mathbf{B}_i \sin(\phi_i) \quad (3.2)$$

where \mathbf{B}_i is the *i.i.d.* envelope, and ϕ_i is the *i.i.d.* random phase of the emissions. Further, emerging times of the interferers are assumed to be uniformly distributed between the sampling times at the receiver. Thus the phase ϕ_i of the emissions at the sampling instants can be assumed to be uniformly distributed on $[0, 2\pi]$. The assumption of *i.i.d.* emissions is valid for wireless communication networks without power control and may not be true for

modeling interference from diverse types of interferers with unequal transmit power (e.g. base stations and mobile users).

The fast fading experienced by the interferer emissions is also assumed to be narrowband of the form

$$\mathbf{g}_i = \mathbf{h}_i e^{j\theta_i} \quad (3.3)$$

where \mathbf{h}_i is the random amplitude scaling and θ_i is the random phase variation due to fading. The in-phase and quadrature-phase components of the emissions are assumed to experience uncorrelated fading and thus θ_i is uniformly distributed on $[0, 2\pi]$. The sum interference can be expressed as

$$\mathbf{I} = \sum_{i=1}^{\mathbf{K}} \mathbf{r}_i^{-\frac{\gamma}{2}} \mathbf{h}_i \mathbf{B}_i \cos(\phi_i + \theta_i) + j \sum_{i=1}^{\mathbf{K}} \mathbf{r}_i^{-\frac{\gamma}{2}} \mathbf{h}_i \mathbf{B}_i \sin(\phi_i + \theta_i) \quad (3.4)$$

3.3 Co-Channel Interference in a Poisson Field of Interferers

Consider a scenario, as shown in Fig. 3.1, in which the spatial point process Π in (3.1) is a homogeneous spatial Poisson point process with intensity λ and the interferers are distributed over the space $\Gamma(r_l, r_h)$. The parametric interference space is defined as

$$\Gamma(r_l, r_h) = \{x \in \mathbb{R}^2 : r_l \leq \|x\| \leq r_h\}. \quad (3.5)$$

From (3.4), the joint characteristic function of the in-phase and quadrature-phase components of the sum interference $\mathbf{I} = \mathbf{I}^{(I)} + j\mathbf{I}^{(Q)}$ can be expressed

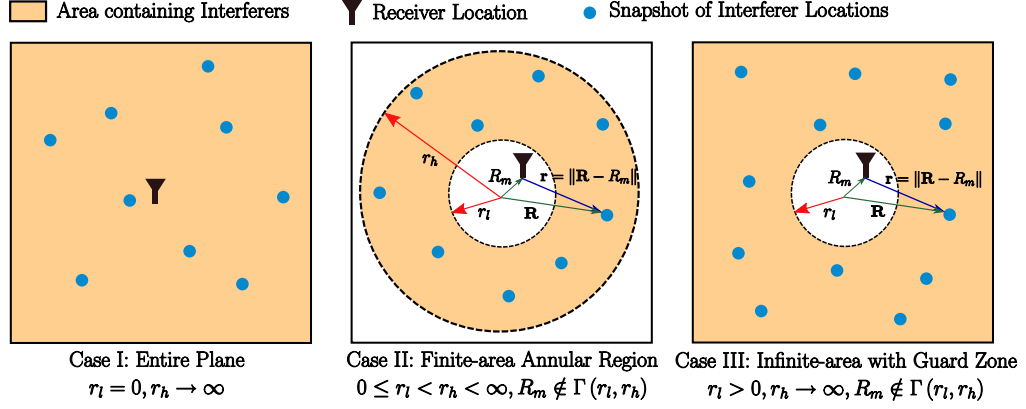


Figure 3.1: Interference space and receiver location for different network topologies in a field of Poisson distributed interferers categorized by the region containing the interferers.

as

$$\Phi_{\mathbf{I}^{(I)}, \mathbf{I}^{(Q)}}(\omega^{(I)}, \omega^{(Q)}) = \mathbb{E}_{\mathbf{I}^{(I)}, \mathbf{I}^{(Q)}} \left\{ e^{j\omega^{(I)} \mathbf{I}^{(I)} + j\omega^{(Q)} \mathbf{I}^{(Q)}} \right\} \quad (3.6)$$

$$= \mathbb{E} \left\{ e^{j \sum_{i=1}^K \mathbf{r}_i^{-\frac{\gamma}{2}} \mathbf{h}_i \mathbf{B}_i (\omega^{(I)} \cos(\phi_i + \theta_i) + \omega^{(Q)} \sin(\phi_i + \theta_i))} \right\} \quad (3.7)$$

$$= \mathbb{E} \left\{ e^{j|\bar{\omega}| \sum_{i=1}^K \mathbf{r}_i^{-\frac{\gamma}{2}} \mathbf{h}_i \mathbf{B}_i \cos(\phi_i + \theta_i + \bar{\omega}_\phi)} \right\} \quad (3.8)$$

$$= \sum_{k=0}^{\infty} \mathbb{E} \left\{ e^{j|\bar{\omega}| \sum_{i=1}^k \mathbf{r}_i^{-\frac{\gamma}{2}} \mathbf{h}_i \mathbf{B}_i \cos(\phi_i + \theta_i + \bar{\omega}_\phi)} \mid k \text{ in } \Gamma(r_l, r_h) \right\} \mathbb{P}(k \text{ in } \Gamma(r_l, r_h)) \quad (3.9)$$

where $\bar{\omega} = [\omega^{(I)}, \omega^{(Q)}]^T$, $|\bar{\omega}| = \sqrt{(\omega^{(I)})^2 + (\omega^{(Q)})^2}$, and $\bar{\omega}_\phi = -\tan^{-1} \left(\frac{\omega^{(Q)}}{\omega^{(I)}} \right)$.

The expectation in (3.9) is with respect to the set of random variables $\{\mathbf{r}_i, \mathbf{h}_i, \mathbf{B}_i, \phi_i, \theta_i\}$.

Conditioned on the number of interferers present in the space $\Gamma(r_l, r_h)$, the interferer locations are mutually independent and uniformly distributed

across this space [125]. Henceforth, the conditioning on the number of interferers is removed from the expectation by noting that the interferers are uniformly distributed over $\Gamma(r_l, r_h)$. Further, in the absence of power control, the interferer emissions can be assumed to be *i.i.d.*. The characteristic function can then be expressed as

$$\Phi_{\bar{\mathbf{Y}}}(\bar{\omega}) = \sum_{k=0}^{\infty} \left[\mathbb{E} \left\{ e^{j|\bar{\omega}|\mathbf{r}^{-\frac{\gamma}{2}} \mathbf{hB} \cos(\phi + \theta + \bar{\omega}\phi)} \right\} \right]^k \frac{[\lambda\pi (r_h^2 - r_l^2)]^k e^{-\lambda\pi(r_h^2 - r_l^2)}}{k!} \quad (3.10)$$

$$= e^{\lambda\pi(r_h^2 - r_l^2) \left(\mathbb{E} \left\{ e^{j|\bar{\omega}|\mathbf{r}^{-\frac{\gamma}{2}} \mathbf{hB} \cos(\phi + \theta + \bar{\omega}\phi)} \right\} - 1 \right)} \quad (3.11)$$

where $\bar{\mathbf{Y}}$ is the set $\{\mathbf{I}^{(I)}, \mathbf{I}^{(Q)}\}$. By taking the logarithm of $\Phi_{\bar{\mathbf{Y}}}(\bar{\omega})$, the log-characteristic function is

$$\psi_{\bar{\mathbf{Y}}}(\bar{\omega}) \triangleq \log \Phi_{\bar{\mathbf{Y}}}(\bar{\omega}) = \lambda\pi (r_h^2 - r_l^2) \left(\mathbb{E} \left\{ e^{j|\bar{\omega}|\mathbf{r}^{-\frac{\gamma}{2}} \mathbf{hB} \cos(\phi + \theta + \bar{\omega}\phi)} \right\} - 1 \right). \quad (3.12)$$

By using the identity

$$e^{ja \cos(\phi)} = \sum_{k=0}^{\infty} j^k \epsilon_k J_k(a) \cos(k\phi) \quad (3.13)$$

where $\epsilon_0 = 1$, $\epsilon_k = 2$ for $k \geq 1$, and $J_k(\cdot)$ denotes the Bessel function of order k , the log-characteristic function can be expressed as

$$\psi_{\bar{\mathbf{Y}}}(\bar{\omega}) = \lambda\pi (r_h^2 - r_l^2) \left(\mathbb{E} \left\{ \sum_{k=0}^{\infty} j^k \epsilon_k J_k \left(|\bar{\omega}|\mathbf{r}^{-\frac{\gamma}{2}} \mathbf{hB} \right) \cos(k(\phi + \theta + \bar{\omega}\phi)) \right\} - 1 \right). \quad (3.14)$$

Since ϕ and θ are uniformly distributed on $[0, 2\pi]$, $\mathbb{E}_{\phi, \theta} \{ \cos(k(\phi + \theta + \bar{\omega}\phi)) \} = 0$ for $k \geq 1$, and (3.14) reduces to

$$\psi_{\bar{\mathbf{Y}}}(\bar{\omega}) = \lambda\pi (r_h^2 - r_l^2) \left(\mathbb{E}_{\mathbf{r}, \mathbf{h}, \mathbf{B}} \left\{ J_0 \left(|\bar{\omega}|\mathbf{r}^{-\frac{\gamma}{2}} \mathbf{hB} \right) \right\} - 1 \right). \quad (3.15)$$

The log-characteristic function derived in (3.15) holds in general for narrow-band interferers distributed over the parametric space $\Gamma(r_l, r_h)$, governed by the parameters r_h and r_l and the receiver location R_m . The receiver location R_m affects the expectation in (3.15). The following three cases are now considered and the log-characteristic function is further simplified.

3.3.1 Case I: Interferers distributed over the entire plane ($r_l = 0, r_h \rightarrow \infty$)

Consider a wireless network, as shown in Fig. 3.1, where the interfering sources are distributed according to a spatial Poisson point process over the entire plane. Note that $\|R_m\|$ can be assumed to be zero without any loss in generality of the result. This scenario corresponds to a decentralized network in which nodes do not employ any contention-based MAC protocol, and has been widely studied [63, 70–72, 108, 122, 123]. Lets consider the interference space $\Gamma(0, r_h)$ and take the limit on the log-characteristic function as $r_h \rightarrow \infty$ [63, 70]. Recall that the expectation in (3.15) is conditioned such that the interferer locations are uniformly distributed over $\Gamma(r_l, r_h)$. The distance of each interferer from the receiver thus follows the distribution

$$f_{\mathbf{r}|\mathbf{K}}(r|K) = \begin{cases} \frac{2r}{r_h^2} & \text{if } 0 \leq r \leq r_h, \\ 0 & \text{otherwise.} \end{cases}$$

Expanding the expectation in (3.15) gives

$$\psi_{\bar{\mathbf{Y}}}(\bar{\omega}) = \lim_{r_h \rightarrow \infty} \lambda \pi r_h^2 \left(\int_0^{r_h} \mathbb{E}_{\mathbf{h}, \mathbf{B}} \left\{ J_0 \left(|\bar{\omega}| r^{-\frac{\gamma}{2}} \mathbf{h} \mathbf{B} \right) \right\} \frac{2r}{r_h^2} dr - 1 \right). \quad (3.16)$$

Integrating the above by parts, noting that $\lim_{r_h \rightarrow \infty} \mathbb{E}_{\mathbf{h}, \mathbf{B}} \left\{ r_h^2 \left(J_0 \left(|\bar{\omega}| r_h^{-\frac{\gamma}{2}} \mathbf{h} \mathbf{B} \right) - 1 \right) \right\} = 0$ for $\gamma > 2$, and $\frac{d}{dx} J_0(x) = -J_1(x)$, gives

$$\psi_{\mathbf{Y}}(\bar{\omega}) = -|\bar{\omega}|^{\frac{4}{\gamma}} \lambda \pi \mathbb{E}_{\mathbf{h}, \mathbf{B}} \left\{ \mathbf{h}^{\frac{4}{\gamma}} \mathbf{B}^{\frac{4}{\gamma}} \right\} \int_0^{\infty} \frac{J_1(x)}{x^{\frac{4}{\gamma}}} dx. \quad (3.17)$$

Equation (3.17) is the log-characteristic function of a two-dimensional isotropic symmetric alpha stable distribution centered at zero such that

$$\psi_{\mathbf{I}^{(I)}, \mathbf{I}^{(Q)}}(\omega^{(I)}, \omega^{(Q)}) = -\sigma \left| \sqrt{(\omega^{(I)})^2 + (\omega^{(Q)})^2} \right|^{\alpha} \quad (3.18)$$

where $\alpha = \frac{4}{\gamma}$ is the characteristic exponent, and $\sigma = \lambda \pi \mathbb{E}_{\mathbf{h}, \mathbf{B}} \left\{ \mathbf{h}^{\alpha} \mathbf{B}^{\alpha} \right\} \int_0^{\infty} \frac{J_1(x)}{x^{\alpha}} dx$ is the dispersion parameter of the symmetric alpha stable distribution [125].

Here, $0 < \alpha < 2$ and $\sigma > 0$. Hence, the sum interference in a Poisson field of interferers distributed over the entire plane follows a symmetric alpha stable distribution.

3.3.2 Case II: Interferers distributed over a finite-area annular region ($0 \leq r_l < r_h < \infty$, $R_m \notin \Gamma(r_l, r_h)$)

Consider a wireless network, as shown in Fig. 3.1, where the interferers are distributed over a finite-area annular region. When $r_l > 0$ and $\|R_m\| < r_l$, this corresponds to a scenario where all the interferers are outside a guard zone around the receiver and within a maximum distance ($r_h < \infty$) beyond which they do not generate significant interference. When $\|R_m\| > r_h$, this corresponds to a scenario where the interferers are distributed over a finite-area circular or annular region with the receiver exterior to this region. The

former scenario is applicable for wireless networks with contention-based or scheduling-based MAC protocols creating a guard zone around the receiver (e.g. cellular networks with reuse factor of one and ad hoc networks with guard zones [60]). The latter scenario is useful in characterizing the interference from a hotspot (e.g. interferers localized in space around a cafe) and in cellular networks with reuse factor greater than one. In cellular networks with reuse factor greater than one, the interferers are distributed within a regular pattern of isolated cell sites and the sum interference is thus a sum of the interference from these isolated finite-area cell sites.

In [12], Middleton proposed an approximation of the log-characteristic function for $|\bar{\omega}|$ in the neighborhood of zero. From Fourier analysis, the behavior of the characteristic function for $|\bar{\omega}|$ in the neighborhood of zero governs the tail probability of the random envelope. The proposed approximation is based on the following identity [12]:

$$\mathbb{E}_{\mathbf{r}, \mathbf{h}, \mathbf{B}} \left\{ J_0 \left(|\bar{\omega}| \mathbf{r}^{-\frac{\gamma}{2}} \mathbf{h} \mathbf{B} \right) \right\} = e^{-\frac{|\bar{\omega}|^2 \mathbb{E}_{\mathbf{r}, \mathbf{h}, \mathbf{B}} \{ \mathbf{r}^{-\gamma} \mathbf{h}^2 \mathbf{B}^2 \}}{4}} (1 + \mathbf{\Lambda}(|\bar{\omega}|)) \quad (3.19)$$

where $\mathbf{\Lambda}(|\bar{\omega}|)$ indicates a correction term with the lowest exponent in $|\bar{\omega}|$ of four and is given by

$$\mathbf{\Lambda}(|\bar{\omega}|) = \sum_{k=2}^{\infty} \frac{(\mathbb{E}_{\mathbf{Z}} \{ \mathbf{Z} \})^k |\bar{\omega}|^{2k}}{2^{2k} k!} \mathbb{E}_{\mathbf{Z}} \left\{ {}_1F_1 \left(-k; 1; \frac{\mathbf{Z}}{\mathbb{E}_{\mathbf{Z}} \{ \mathbf{Z} \}} \right) \right\} \quad (3.20)$$

where the random variable $\mathbf{Z} = \mathbf{r}^{-\gamma} \mathbf{h}^2 \mathbf{B}^2$, and ${}_1F_1(a; b; x)$ is the confluent hypergeometric function of the first kind, such that $\mathbf{\Lambda}(|\bar{\omega}|) = O(|\bar{\omega}|^4)$ as $|\bar{\omega}| \rightarrow 0$.

Using this identity, and approximating $\Lambda(|\bar{\omega}|) \ll 1$ for $|\bar{\omega}|$ in the neighborhood of zero, the log-characteristic function in (3.15) can be expressed as

$$\psi_{\bar{\mathbf{Y}}}(\bar{\omega}) \approx \lambda\pi (r_h^2 - r_l^2) \left(e^{-\frac{|\bar{\omega}|^2 \mathbb{E}_{\mathbf{r}, \mathbf{h}, \mathbf{B}} \{ \mathbf{r}^{-\gamma} \mathbf{h}^2 \mathbf{B}^2 \}}{4}} - 1 \right). \quad (3.21)$$

Equation (3.21) is the log-characteristic function of a Middleton Class A distribution such that

$$\psi_{\mathbf{I}^{(I)}, \mathbf{I}^{(Q)}}(\omega^{(I)}, \omega^{(Q)}) = A \left(e^{-\frac{((\omega^{(I)})^2 + (\omega^{(Q)})^2) \Omega_{2A}}{2A}} - 1 \right) \quad (3.22)$$

where $A = \lambda\pi (r_h^2 - r_l^2)$ is the overlap index that indicates the amount of impulsiveness of the interference, and $\Omega_{2A} = \frac{A \times \mathbb{E}_{\mathbf{r}, \mathbf{h}, \mathbf{B}} \{ \mathbf{r}^{-\gamma} \mathbf{h}^2 \mathbf{B}^2 \}}{2}$ is the mean intensity of the interference [13]. Hence, the co-channel interference from a field of Poisson distributed interferers over the finite-area space $\Gamma(r_l, r_h)$ with $R_m \notin \Gamma(r_l, r_h)$ follows the Middleton Class A distribution. It should be emphasized that the correspondence to the Middleton Class A distribution is particularly valid for modeling the tail probabilities.

The approximation in (3.19) and the subsequent interference model in (3.22) is valid for $R_m \notin \Gamma(r_l, r_h)$, since $\Omega_{2A} \rightarrow \infty$ as $\|R_m\| \rightarrow r_l$ or as $\|R_m\| \rightarrow r_h$. This is unlike *Case I* in Section 3.3.1 where the interference was modeled for $r_l = 0$. This is the key difference between the symmetric alpha stable and Middleton Class A models for interference.

Next, I quantify the range of the system model parameters over which the Middleton Class A model provides an accurate approximation to the co-channel interference in this scenario. From (3.19), a first-order measure of the

accuracy of the approximation can be expressed by comparing the coefficient of $|\bar{\omega}|^4$ term in $e^{-\frac{|\bar{\omega}|^2 \mathbb{E}_{\mathbf{r}, \mathbf{h}, \mathbf{B}} \{ \mathbf{r}^{-\gamma} \mathbf{h}^2 \mathbf{B}^2 \}}{4}}$ against the coefficient of $|\bar{\omega}|^4$ in the correction term $\Lambda(|\bar{\omega}|)$. Using the fact that

$${}_1F_1(-2; 1; x) = \frac{1}{2}(x^2 - 4x + 2), \quad (3.23)$$

the coefficient of $|\bar{\omega}|^4$ in the correction term (i.e., c_4) can be expressed as

$$c_4 = \frac{\mathbb{E}_{\mathbf{Z}} \{ \mathbf{Z}^2 \} - 2 [\mathbb{E}_{\mathbf{Z}} \{ \mathbf{Z} \}]^2}{128}. \quad (3.24)$$

Thus, the Middleton Class A model provides a good approximation when the system parameters, such as r_h, r_l, R_m , and γ , satisfy

$$\left| \frac{\mathbb{E}_{\mathbf{Z}} \{ \mathbf{Z}^2 \} - 2 [\mathbb{E}_{\mathbf{Z}} \{ \mathbf{Z} \}]^2}{128} \right| \ll \frac{[\mathbb{E}_{\mathbf{Z}} \{ \mathbf{Z} \}]^2}{32} \quad (3.25)$$

$$\Rightarrow \left| \frac{\mathbb{E}_{\mathbf{r}, \mathbf{h}, \mathbf{B}} \{ \mathbf{r}^{-2\gamma} \mathbf{h}^4 \mathbf{B}^4 \}}{4 \times [\mathbb{E}_{\mathbf{r}, \mathbf{h}, \mathbf{B}} \{ \mathbf{r}^{-\gamma} \mathbf{h}^2 \mathbf{B}^2 \}]^2} - \frac{1}{2} \right| \ll 1. \quad (3.26)$$

To provide some intuition about the above result, for a non-random \mathbf{h} and \mathbf{B} , the condition is satisfied when $\|R_m\| \ll r_l$ and $\frac{r_l}{r_h}$ is greater than a fraction that depends on γ and R_m , or when $\|R_m\| \gg r_h$. The conditions $\|R_m\| \ll r_l$ and $\|R_m\| \gg r_h$ ensure that the interferers are not close to the receiver and a lower bound on $\frac{r_l}{r_h}$ ensures that r_h is not very large compared to r_l when $\|R_m\| < r_l$.

3.3.3 Case III: Interferers distributed over infinite-area annular region with guard zone ($r_l > 0, r_h \rightarrow \infty$, and $\|R_m\| < r_l$)

Consider a wireless network, as shown in Fig. 3.1, where the interfering sources are distributed according to a spatial Poisson point process on the

entire plane, except within a guard zone around the receiver. The applicability of *Case II* for guard zone scenarios was limited to finite-area fields and does provide a good approximation for a wide range of system parameters. In this subsection, the interference region is allowed to have infinite area and is thereby more applicable to large random wireless networks with guard zones [60]. Lets consider the interference space $\Gamma(r_l, r_h)$ and take the limit on the log-characteristic function as $r_h \rightarrow \infty$. Conditioned on the number of interferers in $\Gamma(r_l, r_h)$, the interferer locations are mutually independent and uniformly distributed in the space $\Gamma(r_l, r_h)$. Thus as $r_h \rightarrow \infty$, with high probability, the distance of an interferer from receiver located at R_m can be approximated as $\mathbf{r} = \|\mathbf{R} - R_m\| \approx \|\mathbf{R}\|$, particularly for $\|R_m\| \ll r_l$. The distance of each interferer from the receiver thus follows the distribution

$$f_{\mathbf{r}|\mathbf{K}}(r|K) = \begin{cases} \frac{2r}{r_h^2 - r_l^2} & \text{if } r_l \leq r \leq r_h, \\ 0 & \text{otherwise.} \end{cases}$$

Expanding the expectation in (3.15) gives

$$\psi_{\overline{\mathbf{Y}}}(\overline{\omega}) = \lim_{r_h \rightarrow \infty} \lambda\pi(r_h^2 - r_l^2) \left(\int_{r_l}^{r_h} \mathbb{E}_{\mathbf{h}, \mathbf{B}} \left\{ J_0 \left(|\overline{\omega}| r^{-\frac{\gamma}{2}} \mathbf{hB} \right) \right\} \frac{2r}{r_h^2 - r_l^2} dr - 1 \right). \quad (3.27)$$

Integrating the above by parts, reordering terms, and noting that

$$\lim_{r_h \rightarrow \infty} \lambda\pi r_h^2 (\mathbb{E}_{\mathbf{h}, \mathbf{B}} \left\{ J_0 \left(|\overline{\omega}| r_h^{-\frac{\gamma}{2}} \mathbf{hB} \right) \right\} - 1) = 0 \text{ for } \gamma > 2, \text{ gives}$$

$$\begin{aligned} \psi_{\overline{\mathbf{Y}}}(\overline{\omega}) &= -\lambda\pi r_l^2 \left(\mathbb{E}_{\mathbf{h}, \mathbf{B}} \left\{ J_0 \left(|\overline{\omega}| r_l^{-\frac{\gamma}{2}} \mathbf{hB} \right) \right\} - 1 \right) \\ &\quad - \lim_{r_h \rightarrow \infty} \lambda\pi \int_{r_l}^{r_h} \frac{\partial}{\partial r} \left(\mathbb{E}_{\mathbf{h}, \mathbf{B}} \left\{ J_0 \left(|\overline{\omega}| r^{-\frac{\gamma}{2}} \mathbf{hB} \right) \right\} \right) r^2 dr. \quad (3.28) \end{aligned}$$

Invoking the identity (3.19), and approximating $\Lambda(|\bar{\omega}|) \ll 1$ for $|\bar{\omega}|$ in the neighborhood of zero, the log-characteristic function can be expressed as

$$\begin{aligned} \psi_{\bar{\mathbf{Y}}}(\bar{\omega}) \approx & -\lambda\pi r_l^2 \left(e^{-\frac{|\bar{\omega}|^2 r_l^{-\gamma} \mathbb{E}_{\mathbf{h}, \mathbf{B}}\{\mathbf{h}^2 \mathbf{B}^2\}}{4}} - 1 \right) \\ & - \lim_{r_h \rightarrow \infty} \lambda\pi \int_{r_l}^{r_h} \frac{\partial}{\partial r} \left(e^{-\frac{|\bar{\omega}|^2 r^{-\gamma} \mathbb{E}_{\mathbf{h}, \mathbf{B}}\{\mathbf{h}^2 \mathbf{B}^2\}}{4}} \right) r^2 dr. \end{aligned} \quad (3.29)$$

Note that unlike (3.19), the approximation in (3.29) involves a non-random r . Using Taylor series expansion of e^x , the log-characteristic function reduces to

$$\psi_{\bar{\mathbf{Y}}}(\bar{\omega}) = \lambda\pi r_l^2 \left[\sum_{k=1}^{\infty} \frac{(-1)^k |\bar{\omega}|^{2k}}{4^k k!} (\mathbb{E}\{\mathbf{h}^2 \mathbf{B}^2\})^k r_l^{-\gamma k} \frac{2}{k\gamma - 2} \right] \quad (3.30)$$

valid for $\gamma > 2$. The $\frac{2}{k\gamma-2}$ multiplicative factor inside the summation prevents the log-characteristic function to be expressed in closed form. I thus approximate the function $\frac{2}{k\gamma-2}$ as $\eta e^{\beta k}$ for $k \geq 1$. The parameters η and β are chosen to minimize the weighted mean squared error (WMSE)

$$\{\eta, \beta\} = \arg \min_{\eta, \beta} \sum_{k=1}^{\infty} \left(\frac{2}{k\gamma - 2} - \eta e^{\beta k} \right)^2 u(k) \quad (3.31)$$

where $u(k)$ are the weights. The weights should be chosen such that penalty of error is large when k is small, since it affects the coefficients of terms with lower order exponents of $|\bar{\omega}|$. Equation (3.31) is an unconstrained nonlinear optimization problem and can be solved efficiently using numerical techniques such as quasi-Newton methods [1]. Quasi-Newton methods have superlinear convergence and require $O(\ln(|\ln(\epsilon)|))$ number of iterations and $O(d^2 \ln(|\ln(\epsilon)|))$ algebraic computational effort, where d is the dimensionality of the problem and ϵ is the maximum permissible error tolerance in the result. Table 3.2

Table 3.2: Values for $\{\eta, \beta\}$ and the associated weighted mean squared error (WMSE), obtained by solving (3.31), for different values of the power pathloss exponent (γ) and using the weighting function $u(k) = e^{-k}$. Solution to (3.31) was obtained by using the `fminunc` function in `MATLAB`, which uses the BFGS quasi-Newton method [1].

γ	$\{\eta, \beta\}$	WMSE
2.5	$\{22.818, -1.741\}$	4.32×10^{-3}
3.0	$\{7.484, -1.321\}$	1.84×10^{-3}
3.5	$\{4.132, -1.132\}$	9.81×10^{-4}
4.0	$\{2.781, -1.025\}$	5.96×10^{-4}
4.5	$\{2.073, -0.954\}$	3.96×10^{-4}
5.0	$\{1.645, -0.905\}$	2.80×10^{-4}

lists the values for $\{\eta, \beta\}$ and the associated WMSE for certain values of γ , using the weights $u(k) = e^{-k}$. By approximating $\frac{2}{k\gamma-2}$ as $\eta e^{\beta k}$ for $k \geq 1$, the log-characteristic exponent can be expressed as

$$\psi_{\mathbf{Y}}(\bar{\omega}) \approx \lambda \pi r_l^2 \eta \left(e^{-\frac{|\bar{\omega}|^2 r_l^{-\gamma} e^{\beta} \mathbb{E}_{\mathbf{h}, \mathbf{B}} \{\mathbf{h}^2 \mathbf{B}^2\}}{4}} - 1 \right). \quad (3.32)$$

Equation (3.32) is the log-characteristic function of a Middleton Class A distribution such that

$$\psi_{\mathbf{I}^{(I)}, \mathbf{I}^{(Q)}}(\omega^{(I)}, \omega^{(Q)}) = A \left(e^{-\frac{((\omega^{(I)})^2 + (\omega^{(Q)})^2) \Omega_{2A}}{2A}} - 1 \right) \quad (3.33)$$

where $A = \lambda \pi r_l^2 \eta$ is the overlap index that indicates the impulsiveness of the interference, and $\Omega_{2A} = \frac{A \times r_l^{-\gamma} e^{\beta} \mathbb{E}_{\mathbf{h}, \mathbf{B}} \{\mathbf{h}^2 \mathbf{B}^2\}}{2}$ is the mean intensity of the interference [13].

The functional form of $\eta e^{\beta k}$ to approximate $\frac{2}{k\gamma-2}$ for $k \geq 1$ was chosen since, a) it provides a good approximation and enables the log-characteristic function to be expressed in closed form, and b) provides two parameters $\{\eta, \beta\}$

such that η affects only the impulsive index A , while β affects only the variance $\sigma_m^2 = \frac{m}{A}\Omega_{2A}$ of individual components of the Gaussian mixture form of Middleton Class A model.

Similar to *Case II*, a first-order measure of accuracy of the approximation can be expressed by comparing the coefficient of $|\bar{\omega}|^4$ term in the true log-characteristic function (3.28) against the the coefficient of $|\bar{\omega}|^4$ term in the approximated log-characteristic function (3.32). The two approximations involved are using $\eta e^{\beta k}$ to approximate the function $\frac{2}{k\gamma-2}$ for $k \geq 1$, and approximating $\mathbf{\Lambda}(|\bar{\omega}|) \ll 1$ for $|\bar{\omega}|$ close to zero. Note that the lowest order term affected by the former approximation is the coefficient of $|\bar{\omega}|^2$ term. The approximation error is assumed to be negligible due to the optimization in (3.31). Using (3.19) and (3.20), the coefficient of $|\bar{\omega}|^4$ term in the true log-characteristic function (3.32) is

$$\lambda\pi r_l^{-2\gamma+2} \left(\frac{\mathbb{E}\{\mathbf{Z}^2\} + 2[\mathbb{E}\{\mathbf{Z}\}]^2}{128} \right) \left(\frac{2}{2\gamma-2} \right)$$

where $\mathbf{Z} = \mathbf{h}^2\mathbf{B}^2$. Comparing with the coefficient of $|\bar{\omega}|^4$ term in (3.32), the Middleton Class A distribution provides a good approximation to co-channel interference statistics in this scenario when

$$\left| \left(\frac{[\mathbb{E}\{\mathbf{Z}\}]^2}{64} \right) \left(\frac{2}{2\gamma-2} - 2\eta e^{2\beta} \right) + \left(\frac{\mathbb{E}\{\mathbf{Z}^2\}}{128} \right) \left(\frac{2}{2\gamma-2} \right) \right| \ll \left| \frac{[\mathbb{E}\{\mathbf{Z}\}]^2}{32} \eta e^{2\beta} \right|. \quad (3.34)$$

Note that if $\eta e^{2\beta} = \frac{2}{2\gamma-2}$, then the above condition is same as the one obtained for *Case II* in (3.25), with the exception that $\mathbf{Z} = \mathbf{h}^2\mathbf{B}^2$ in this case. The above

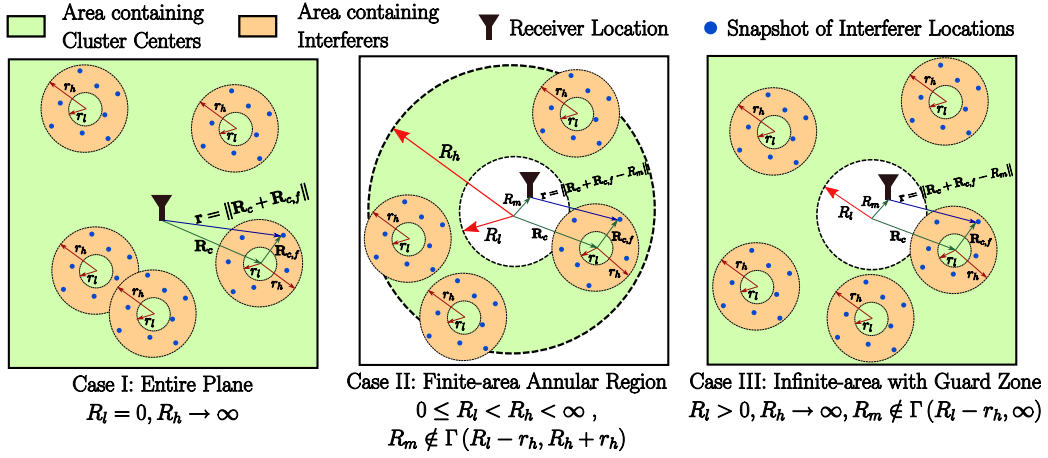


Figure 3.2: Interference space and receiver location for different network topologies in a field of Poisson-Poisson cluster distributed interferers categorized by the region containing the cluster centers.

condition is independent of the parameter r_l that governs the interference space and is valid when the variance of $\mathbf{h}^2\mathbf{B}^2$ is low when compared to $[\mathbb{E}\{\mathbf{h}^2\mathbf{B}^2\}]^2$. The above condition does not capture the error due to the approximation $\mathbf{r} = \|\mathbf{R} - R_m\| \approx \mathbf{R}$, which is true with high probability in this scenario and is particularly valid for $\|R_m\| \ll r_l$.

3.4 Co-Channel Interference in a Poisson-Poisson Cluster Field of Interferers

Consider a scenario, as shown in Fig. 3.2, where the interferers are clustered in space. The center of the clusters are assumed to distributed according to a spatial Poisson point process Π_c with intensity λ_c over the space $\Gamma(R_l, R_h)$. For each cluster center $\mathbf{R}_c \in \Pi_c$, interferers are assumed to be distributed according to an independent spatial Poisson process $\Pi_{c,f}$ with intensity λ_f over

the space $\Gamma(r_l, r_h)$ around the center \mathbf{R}_c . The point process Π in (3.1) is then a homogeneous spatial Poisson-Poisson cluster process such that

$$\Pi = \bigcup_{\mathbf{R}_c \in \Pi_c} \bigcup_{\mathbf{R}_{c,f} \in \Pi_{c,f}} \{\mathbf{R}_c + \mathbf{R}_{c,f}\}. \quad (3.35)$$

Note that the cluster centers are themselves not included. The parametric interference space $\Gamma(\cdot, \cdot)$ is defined in (3.5). When $r_l = 0$, Π is a Matern cluster process [129].

The joint characteristic function of the in-phase and quadrature-phase components of the sum interference $\mathbf{I} = \mathbf{I}^{(I)} + j\mathbf{I}^{(Q)}$ can be expressed as

$$\begin{aligned} & \Phi_{\mathbf{I}^{(I)}, \mathbf{I}^{(Q)}}(\omega^{(I)}, \omega^{(Q)}) \\ &= \mathbb{E}_{\mathbf{I}^{(I)}, \mathbf{I}^{(Q)}} \left\{ e^{j\omega^{(I)}\mathbf{I}^{(I)} + j\omega^{(Q)}\mathbf{I}^{(Q)}} \right\} \end{aligned} \quad (3.36)$$

$$= \mathbb{E} \left\{ e^{j|\bar{\omega}| \sum_{i=1}^{\mathbf{K}_c} \sum_{m=1}^{\mathbf{K}_{c,f}} \mathbf{r}_{i,m}^{-\frac{\gamma}{2}} \mathbf{h}_{i,m} \mathbf{B}_{i,m} \cos(\phi_{i,m} + \theta_{i,m} + \bar{\omega}_\phi)} \right\} \quad (3.37)$$

$$\begin{aligned} &= \sum_{k_c=0}^{\infty} \mathbb{E} \left\{ e^{j|\bar{\omega}| \sum_{i=1}^{k_c} \sum_{m=1}^{\mathbf{K}_{c,f}} \mathbf{r}_{i,m}^{-\frac{\gamma}{2}} \mathbf{h}_{i,m} \mathbf{B}_{i,m} \cos(\phi_{i,m} + \theta_{i,m} + \bar{\omega}_\phi)} \mid k_c \text{ in } \Gamma(R_l, R_h) \right\} \\ & \quad \times \mathbb{P}(k_c \text{ in } \Gamma(R_l, R_h)) \end{aligned} \quad (3.38)$$

where \mathbf{K}_c is the random number of active clusters, $\mathbf{K}_{c,f}$ is the random number of active interferers per cluster, $\bar{\omega} = [\omega^{(I)}, \omega^{(Q)}]^T$, $|\bar{\omega}| = \sqrt{(\omega^{(I)})^2 + (\omega^{(Q)})^2}$, and $\bar{\omega}_\phi = -\tan^{-1}\left(\frac{\omega^{(Q)}}{\omega^{(I)}}\right)$. The expectation in (3.38) is with respect to the set of random variables $\{\mathbf{K}_{c,f}, \mathbf{r}_{i,m}, \mathbf{h}_{i,m}, \mathbf{B}_{i,m}, \phi_{i,m}, \theta_{i,m}\}$. The indexing $(\cdot)_{i,m}$ denotes the m^{th} active interferer in the i^{th} cluster.

Conditioned on the number of clusters present in the space $\Gamma(R_l, R_h)$, location of the cluster centers (\mathbf{R}_c) are mutually independent and uniformly

distributed over this space [125]. Further, in the absence of power control, the sum interference from each cluster can be assumed to be *i.i.d.*, such that

$$\Phi_{\bar{\mathbf{Y}}}(\bar{\omega}) = \sum_{k_c=0}^{\infty} \left[\mathbb{E} \left\{ e^{j|\bar{\omega}| \sum_{m=0}^{\mathbf{K}_{c,f}} \mathbf{r}_m^{-\frac{\gamma}{2}} \mathbf{h}_m \mathbf{B}_m \cos(\phi_m + \theta_m + \bar{\omega}_\phi)} \right\} \right]^{k_c} \times \frac{[\lambda_c \pi (R_h^2 - R_l^2)]^{k_c} e^{-\lambda_c \pi (R_h^2 - R_l^2)}}{k_c!} \quad (3.39)$$

$$= e^{A_c \left(\mathbb{E} \left\{ e^{j|\bar{\omega}| \sum_{m=0}^{\mathbf{K}_{c,f}} \mathbf{r}_m^{-\frac{\gamma}{2}} \mathbf{h}_m \mathbf{B}_m \cos(\phi_m + \theta_m + \bar{\omega}_\phi)} \right\} - 1 \right)} \quad (3.40)$$

where $\bar{\mathbf{Y}}$ is the set $\{\mathbf{I}^{(I)}, \mathbf{I}^{(Q)}\}$, and $A_c = \lambda_c \pi (R_h^2 - R_l^2)$. The expectation in (3.40) is with respect to the set of random variables $\{\mathbf{R}_c, \mathbf{K}_{c,f}, \mathbf{R}_{c,m}, \mathbf{h}_m, \mathbf{B}_m, \phi_m, \theta_m\}$. By taking the logarithm of $\Phi_{\bar{\mathbf{Y}}}(\bar{\omega})$, the log-characteristic function is

$$\psi_{\bar{\mathbf{Y}}}(\bar{\omega}) = A_c \left(\mathbb{E} \left\{ e^{j|\bar{\omega}| \sum_{m=0}^{\mathbf{K}_{c,f}} \mathbf{r}_m^{-\frac{\gamma}{2}} \mathbf{h}_m \mathbf{B}_m \cos(\phi_m + \theta_m + \bar{\omega}_\phi)} \right\} - 1 \right). \quad (3.41)$$

The above equation can be expressed in the form

$$\psi_{\bar{\mathbf{Y}}}(\bar{\omega}) = A_c \left(\mathbb{E}_{\mathbf{R}_c} \left\{ \mathbb{E}_{\mathbf{I}_{c,f}} \left\{ e^{j|\bar{\omega}| \mathbf{I}_{c,f}} \right\} \right\} - 1 \right) \quad (3.42)$$

where $\mathbf{I}_{c,f}$ is the sum interference from an interferer cluster and is a function of the set of random variables $\{\mathbf{K}_{c,f}, \mathbf{R}_{c,m}, \mathbf{h}_m, \mathbf{B}_m, \phi_m, \theta_m\}$, similar to (3.8). Thus $\mathbf{I}_{c,f}$ is the sum interference from a field of Poisson distributed interferers over the interference space $\Gamma(r_l, r_h)$ around the cluster center \mathbf{R}_c . Using (3.15), the log-characteristic function can then be expressed as

$$\psi_{\bar{\mathbf{Y}}}(\bar{\omega}) = A_c \left[\mathbb{E}_{\mathbf{R}_c} \left\{ e^{A_f \left(\mathbb{E}_{\mathbf{R}_{c,f}, \mathbf{h}, \mathbf{B}} \left\{ J_0(|\bar{\omega}| \mathbf{r}^{-\frac{\gamma}{2}} \mathbf{h} \mathbf{B}) \right\} - 1 \right)} \right\} - 1 \right] \quad (3.43)$$

where $A_f = \lambda_f \pi (r_h^2 - r_l^2)$, $\mathbf{r} = \|\mathbf{R}_c + \mathbf{R}_{c,f} - \mathbf{R}_m\|$, \mathbf{R}_c is uniformly distributed in $\Gamma(R_l, R_h)$, and $\mathbf{R}_{c,f}$ is uniformly distributed in $\Gamma(r_l, r_h)$.

The log-characteristic function derived in (3.43) holds in general for a Poisson-Poisson clustered field of narrowband interferers, where the cluster centers are distributed over the parametric space $\Gamma(R_l, R_h)$ and the interferers are distributed over the parametric space $\Gamma(r_l, r_h)$ around each cluster center. The receiver location R_m affects the inner expectation in (3.43). I now consider the same three cases, categorized by the region containing the cluster centers, and further simplify the log-characteristic function.

3.4.1 Case I: Cluster centers distributed over the entire plane ($R_l = 0, R_h \rightarrow \infty$)

Consider a wireless network scenario, as shown in Fig. 3.2, where the center of interferer clusters are distributed according to a homogeneous spatial Poisson point process over the entire plane. Similar to *Case I* for a Poisson field of interferers, $\|R_m\|$ can be assumed to be zero without any loss in generality of the result. Conditioned on the number of clusters in $\Gamma(0, R_h)$, the distance of each cluster center from the origin follows the distribution

$$f_{\mathbf{R}_c|\mathbf{K}_c}(R_c|K_c) = \begin{cases} \frac{2R_c}{R_h^2} & \text{if } 0 \leq R_c \leq R_h, \\ 0 & \text{otherwise.} \end{cases}$$

Thus as $R_h \rightarrow \infty$, with high probability, the distance of an interferer from the receiver can be approximated as $\mathbf{r} = \|\mathbf{R}_c + \mathbf{R}_{c,f}\| \approx \|\mathbf{R}_c\|$. Expanding the expectation over \mathbf{R}_c in (3.43) and using the Taylor series expansion of e^x gives

$$\psi_{\bar{\mathbf{Y}}}(\bar{\omega}) = \lim_{R_h \rightarrow \infty} A_c \left[\int_0^{R_h} e^{A_f \left(\mathbb{E} \left\{ J_0 \left(|\bar{\omega}| R_c^{-\frac{\gamma}{2}} \mathbf{hB} \right) \right\}^{-1} \right) \frac{2R_c}{R_h^2} dR_c - 1 \right]$$

$$\begin{aligned}
&= e^{-A_f} \sum_{k=0}^{\infty} \frac{A_f^k}{k!} \left[\lim_{R_h \rightarrow \infty} A_c \left(\int_0^{R_h} \left(\mathbb{E} \left\{ J_0 \left(|\bar{\omega}| R_c^{-\frac{\gamma}{2}} \mathbf{hB} \right) \right\} \right)^k \frac{2R_c}{R_h^2} dR_c - 1 \right) \right] \\
&= e^{-A_f} \sum_{k=0}^{\infty} \frac{A_f^k}{k!} \Upsilon
\end{aligned} \tag{3.44}$$

where

$$\Upsilon = \lim_{R_h \rightarrow \infty} A_c \left(\int_0^{R_h} \left(\mathbb{E} \left\{ J_0 \left(|\bar{\omega}| R_c^{-\frac{\gamma}{2}} \mathbf{hB} \right) \right\} \right)^k \frac{2R_c}{R_h^2} dR_c - 1 \right). \tag{3.45}$$

Integrating the above by parts, reordering terms, and noting that

$$\lim_{R_h \rightarrow \infty} A_c \left[\left(\mathbb{E} \left\{ J_0 \left(|\bar{\omega}| R_h^{-\frac{\gamma}{2}} \mathbf{hB} \right) \right\} \right)^k - 1 \right] = 0 \text{ for } \gamma > 2, \text{ gives}$$

$$\Upsilon = \lim_{R_h \rightarrow \infty} -\lambda_c \pi \int_0^{R_h} \frac{\partial}{\partial R_c} \left[\left(\mathbb{E} \left\{ J_0 \left(|\bar{\omega}| R_c^{-\frac{\gamma}{2}} \mathbf{hB} \right) \right\} \right)^k \right] R_c^2 dR_c. \tag{3.46}$$

Invoking the identity (3.19), and approximating $\Lambda(|\bar{\omega}|) \ll 1$ for $|\bar{\omega}|$ close to zero, gives

$$\left[\mathbb{E} \left\{ J_0 \left(|\bar{\omega}| R_c^{-\frac{\gamma}{2}} \mathbf{hB} \right) \right\} \right]^k = e^{-\frac{|\bar{\omega}|^2 k R_c^{-\gamma} \mathbb{E} \{ \mathbf{h}^2 \mathbf{B}^2 \}}{4}} (1 + \Lambda(|\bar{\omega}|))^k \tag{3.47}$$

$$\approx \mathbb{E} \left\{ J_0 \left(|\bar{\omega}| \sqrt{k} R_c^{-\frac{\gamma}{2}} \mathbf{hB} \right) \right\}. \tag{3.48}$$

Substituting (3.48) in (3.46), and noting that $\frac{d}{dx} J_0(x) = -J_1(x)$, gives

$$\Upsilon = -|\bar{\omega}|^{\frac{4}{\gamma}} \lambda_c \pi \left(\sqrt{k} \right)^{\frac{4}{\gamma}} \mathbb{E}_{\mathbf{h}, \mathbf{B}} \left\{ \mathbf{h}^{\frac{4}{\gamma}} \mathbf{B}^{\frac{4}{\gamma}} \right\} \int_0^{\infty} \frac{J_1(x)}{x^{\frac{4}{\gamma}}} dx. \tag{3.49}$$

Using (3.49), the log-characteristic function in (3.44) reduces to

$$\psi_{\bar{\mathbf{Y}}}(\bar{\omega}) = -|\bar{\omega}|^{\frac{4}{\gamma}} \left[\left(\lambda_c \pi \mathbb{E}_{\mathbf{h}, \mathbf{B}} \left\{ \mathbf{h}^{\frac{4}{\gamma}} \mathbf{B}^{\frac{4}{\gamma}} \right\} \int_0^{\infty} \frac{J_1(x)}{x^{\frac{4}{\gamma}}} dx \right) \sum_{k=0}^{\infty} \frac{e^{-A_f} A_f^k \left(\sqrt{k} \right)^{\frac{4}{\gamma}}}{k!} \right]. \tag{3.50}$$

Equation (3.50) is the log-characteristic function of a two-dimensional isotropic symmetric alpha stable distribution centered at zero such that

$$\psi_{\mathbf{I}^{(I)}, \mathbf{I}^{(Q)}}(\omega^{(I)}, \omega^{(Q)}) = -\sigma \left| \sqrt{(\omega^{(I)})^2 + (\omega^{(Q)})^2} \right|^\alpha \quad (3.51)$$

where $\alpha = \frac{4}{\gamma}$ is the characteristic exponent ($0 < \alpha < 2$), and $\sigma = \left[\left(\lambda_c \pi \mathbb{E}_{\mathbf{h}, \mathbf{B}} \{ \mathbf{h}^\alpha \mathbf{B}^\alpha \} \int_0^\infty \frac{J_1(x)}{x^\alpha} dx \right) \sum_{k=0}^\infty \frac{e^{-A_f} A_f^k (\sqrt{k})^\alpha}{k!} \right]$ is the dispersion parameter ($\sigma > 0$) of the symmetric alpha stable distribution [125]. Hence, when the center of interferer clusters are distributed according to a spatial Poisson process on the entire plane, the co-channel interference follows a symmetric alpha stable distribution. Note that unlike *Case I* for a Poisson field of interferers, the symmetric alpha stable distribution is not an exact model due to approximation in (3.48), but accurately models the tail probability of the interference.

3.4.2 Case II: Cluster centers distributed over finite-area annular region ($0 \leq R_l < R_h < \infty$, and $R_m \notin \Gamma(R_l - r_h, R_h + r_h)$)

Consider a wireless network scenario, as shown in Fig. 3.2, where the cluster centers are distributed over a finite-area annular region. The receiver location is such that it does not belong to the space of active interferers ($R_m \notin \Gamma(R_l - r_h, R_h + r_h)$). Similar to *Case II* for a Poisson field of interferers, this scenario is useful in characterizing interference from a finite-area annular field when the receiver is located interior to the region with a guard zone (when $\|R_m\| < R_l - r_h$) or at a point exterior to the region (when $\|R_m\| > R_h + r_h$).

Using the identity (3.19), the log-characteristic function in (3.43) can

be expressed as

$$\psi_{\bar{\mathbf{Y}}}(\bar{\omega}) = A_c \left[\mathbb{E}_{\mathbf{R}_c} \left\{ \exp \left(A_f \left(e^{\frac{-|\bar{\omega}|^2 \mathbb{E}_{\mathbf{R}_c, f, \mathbf{h}, \mathbf{B}} \{ \mathbf{r}^{-\gamma} \mathbf{h}^2 \mathbf{B}^2 \}}{4}} (1 + \mathbf{\Lambda}(|\bar{\omega}|)) - 1 \right) \right) \right\} - 1 \right] \quad (3.52)$$

where $\mathbf{\Lambda}(|\bar{\omega}|)$ is the correction term given by (3.20). For notational simplicity, let $\mathbf{F} = \mathbb{E}_{\mathbf{R}_c, f, \mathbf{h}, \mathbf{B}} \{ \mathbf{r}^{-\gamma} \mathbf{h}^2 \mathbf{B}^2 \}$. \mathbf{F} is then a function of the random variable \mathbf{R}_c . Approximating $\mathbf{\Lambda}(|\bar{\omega}|) \ll 1$ for $|\bar{\omega}|$ in the neighborhood of zero, and using the Taylor series expansion of e^x , the log-characteristic function reduces to

$$\psi_{\bar{\mathbf{Y}}}(\bar{\omega}) \approx A_c \left[\mathbb{E}_{\mathbf{R}_c} \left\{ e^{-A_f} \sum_{k=0}^{\infty} \frac{A_f^k}{k!} e^{\frac{-k|\bar{\omega}|^2 \mathbf{F}}{4}} \right\} - 1 \right] \quad (3.53)$$

$$= A_c \left[e^{-A_f} \sum_{l=0}^{\infty} \frac{(-1)^l |\bar{\omega}|^{2l} \mathbb{E}_{\mathbf{R}_c} \{ \mathbf{F}^l \}}{4^l l!} \sum_{k=0}^{\infty} \frac{A_f^k k^l}{k!} - 1 \right]. \quad (3.54)$$

To express the log-characteristic function in closed form, I approximate $\mathbb{E}_{\mathbf{R}_c} \{ \mathbf{F}^l \} \approx (\mathbb{E}_{\mathbf{R}_c} \{ \mathbf{F} \})^l$. This approximation holds with equality for $l = 0, 1$ and hence does not affect the coefficient of $|\bar{\omega}|^2$ term. The coefficient of the lowest order term affected by this approximation is the $|\bar{\omega}|^4$ term. Thus the log-characteristic function is not severely affected by this approximation for $|\bar{\omega}|$ in the neighborhood of zero, which is desired for accurately modeling the tail probability, and can be expressed as

$$\psi_{\bar{\mathbf{Y}}}(\bar{\omega}) \approx A_c \left[\exp \left(A_f \left(e^{\frac{-|\bar{\omega}|^2 \mathbb{E}_{\mathbf{R}_c} \{ \mathbf{F} \}}{4}} - 1 \right) \right) - 1 \right]. \quad (3.55)$$

Using the log-characteristic function, and using the Taylor series expansion from e^x , the characteristic function can be expressed as

$$\Phi_{\bar{\mathbf{Y}}}(\bar{\omega}) = e^{-A_c} \sum_{l=0}^{\infty} \frac{A_f^l}{l!} \left(\sum_{k=0}^{\infty} \frac{A_c^k k^l e^{-k A_f}}{k!} \right) e^{\frac{-l|\bar{\omega}|^2 \mathbb{E}_{\mathbf{R}_c} \{ \mathbf{F} \}}{4}}. \quad (3.56)$$

Equation (3.56) is the characteristic function of a two-dimensional isotropic Gaussian mixture model such that

$$\Phi_{\mathbf{I}^{(I)}, \mathbf{I}^{(Q)}}(\omega^{(I)}, \omega^{(Q)}) = \sum_{l=0}^{\infty} p_l e^{-\frac{((\omega^{(I)})^2 + (\omega^{(Q)})^2) \sigma_l^2}{2}} \quad (3.57)$$

where $p_l = \frac{e^{-A_c A_f^l}}{l!} \left(\sum_{k=0}^{\infty} \frac{A_c^k k^l e^{-k A_f}}{k!} \right)$ are the mixture probabilities, and $\sigma_l^2 = \frac{l \times \mathbb{E}_{\mathbf{R}_c, \mathbf{R}_{c,f}, \mathbf{h}, \mathbf{B}} \{ \mathbf{r}^{-\gamma} \mathbf{h}^2 \mathbf{B}^2 \}}{2}$ are the variance of the individual Gaussian components, for $l \geq 0$.

The two approximations involved in expressing the true log-characteristic function (3.52) as (3.55) are approximating $\mathbf{\Lambda}(|\bar{\omega}|) \ll 1$ for $|\bar{\omega}|$ in the neighborhood of zero, and expressing $\mathbb{E}_{\mathbf{R}_c} \{ \mathbf{F}^l \}$ as $(\mathbb{E}_{\mathbf{R}_c} \{ \mathbf{F} \})^l$. Using (3.20), the coefficient of $|\bar{\omega}|^4$ term in the true log-characteristic function (3.52) can be expressed as

$$A_c e^{-A_f} \left[\frac{\mathbb{E}_{\mathbf{R}_c} \{ \mathbf{F}^2 \}}{32} \sum_{k=0}^{\infty} \frac{k^2 A_f^k}{k!} + \mathbb{E}_{\mathbf{R}_c} \{ \mathbf{c}_4 \} \sum_{k=0}^{\infty} \frac{k A_f^k}{k!} \right]$$

where $\mathbf{c}_4 = \frac{\mathbb{E}_{\mathbf{R}_{c,f}, \mathbf{h}, \mathbf{B}} \{ \mathbf{r}^{-2\gamma} \mathbf{h}^4 \mathbf{B}^4 \} - 2(\mathbb{E}_{\mathbf{R}_{c,f}, \mathbf{h}, \mathbf{B}} \{ \mathbf{r}^{-\gamma} \mathbf{h}^2 \mathbf{B}^2 \})^2}{128}$, and $\mathbf{F} = \mathbb{E}_{\mathbf{R}_{c,f}, \mathbf{h}, \mathbf{B}} \{ \mathbf{r}^{-\gamma} \mathbf{h}^2 \mathbf{B}^2 \}$.

Comparing with the coefficient of the $|\bar{\omega}|^4$ term in the approximated log-characteristic function (3.55), the Gaussian mixture distribution provides a good approximation to the interference statistics in this scenario when

$$\left| \frac{Var(\mathbf{F})}{32} \sum_{k=0}^{\infty} \frac{k^2 A_f^k}{k!} + \mathbb{E}_{\mathbf{R}_c} \{ \mathbf{c}_4 \} \sum_{k=0}^{\infty} \frac{k A_f^k}{k!} \right| \ll \left| \frac{(\mathbb{E}_{\mathbf{R}_c} \{ \mathbf{F} \})^2}{32} \sum_{k=0}^{\infty} \frac{k^2 A_f^k}{k!} \right| \quad (3.58)$$

where $Var(\mathbf{F}) = \mathbb{E}_{\mathbf{R}_c} \{ \mathbf{F}^2 \} - (\mathbb{E}_{\mathbf{R}_c} \{ \mathbf{F} \})^2$. Intuitively, the above condition is satisfied when the interferers are not close to the receiver (i.e., $\|R_m\| \ll R_l - r_h$ or $\|R_m\| \gg R_h + r_h$) and R_h is not very high compared to R_l when $\|R_m\| < R_l - r_h$.

3.4.3 Case III: Cluster centers distributed over infinite-area annular region with guard zone ($R_l > 0, R_h \rightarrow \infty$, and $\|R_m\| < R_l - r_h$)

Consider a wireless network, as shown in Fig. 3.2, where the center of interferer clusters are distributed according to a homogeneous spatial Poisson point process over the entire plane, except within a guard zone around the receiver. Analogous to *Case III* for a Poisson field of interferers, the distance of each cluster center from the origin follows the distribution

$$f_{\mathbf{R}_c|\mathbf{K}_c}(R_c|K_c) = \begin{cases} \frac{2R_c}{R_h^2 - R_l^2} & \text{if } R_l \leq R_c \leq R_h, \\ 0 & \text{otherwise.} \end{cases}$$

Thus as $R_h \rightarrow \infty$, with high probability, the distance of an interferer from receiver located at R_m can be approximated as $\mathbf{r} = \|\mathbf{R}_c + \mathbf{R}_{c,f} - R_m\| \approx \|\mathbf{R}_c\|$, particularly for $R_m \ll R_l - r_h$. Analogous to *Case I*, on expanding the expectation over \mathbf{R}_c in (3.43) and using the Taylor series expansion for e^x gives

$$\psi_{\mathbf{Y}}(\bar{\omega}) = \lim_{R_h \rightarrow \infty} A_c \left[\int_{R_l}^{R_h} e^{A_f \left(\mathbb{E} \left\{ J_0 \left(|\bar{\omega}| R_c^{-\frac{\gamma}{2}} \mathbf{hB} \right) \right\} - 1 \right)} \frac{2R_c}{R_h^2 - R_l^2} dR_c - 1 \right] \quad (3.59)$$

$$= e^{-A_f} \sum_{k=0}^{\infty} \frac{A_f^k}{k!} \Upsilon \quad (3.60)$$

where

$$\Upsilon = \lim_{R_h \rightarrow \infty} A_c \left(\int_{R_l}^{R_h} \left(\mathbb{E} \left\{ J_0 \left(|\bar{\omega}| R_c^{-\frac{\gamma}{2}} \mathbf{hB} \right) \right\} \right)^k \frac{2R_c}{R_h^2 - R_l^2} dR_c - 1 \right). \quad (3.61)$$

Integrating the above by parts, reordering terms, and noting that

$\lim_{R_h \rightarrow \infty} \lambda_c \pi R_h^2 \left[\left(\mathbb{E} \left\{ J_0 \left(|\bar{\omega}| R_h^{-\frac{\gamma}{2}} \mathbf{hB} \right) \right\} \right)^k - 1 \right] = 0$ for $\gamma > 2$, gives

$$\Upsilon = -\lambda_c \pi R_l^2 \left(\left(\mathbb{E}_{\mathbf{h}, \mathbf{B}} \left\{ J_0 \left(|\bar{\omega}| R_l^{-\frac{\gamma}{2}} \mathbf{hB} \right) \right\} \right)^k - 1 \right) -$$

$$\lim_{R_h \rightarrow \infty} \lambda_c \pi \int_{R_l}^{R_h} \frac{\partial}{\partial R_c} \left[\left(\mathbb{E}_{\mathbf{h}, \mathbf{B}} \left\{ J_0 \left(|\bar{\omega}| R_c^{-\frac{\gamma}{2}} \mathbf{h} \mathbf{B} \right) \right\} \right)^k \right] R_c^2 dR_c. \quad (3.62)$$

Invoking the identity (3.19), approximating $\mathbf{\Lambda}(|\bar{\omega}|) \ll 1$ for $|\bar{\omega}|$ in the neighborhood of zero, and using the Taylor series expansion of e^x , gives

$$\Upsilon \approx \lambda_c \pi R_l^2 \left[\sum_{m=1}^{\infty} \frac{(-1)^m |\bar{\omega}|^{2m} k^m}{4^m m!} \left(\mathbb{E} \{ \mathbf{h}^2 \mathbf{B}^2 \} \right)^m R_l^{-\gamma m} \frac{2}{\gamma m - 2} \right]. \quad (3.63)$$

Similar to *Case III* for Poisson field of interferers, the $\frac{2}{\gamma m - 2}$ multiplicative factor inside the summation prevents Υ , and hence the log-characteristic function, to be expressed in closed form. I thus approximate the function $\frac{2}{\gamma m - 2}$ as $\eta e^{\beta m}$ for $m \geq 1$, where $\{\eta, \beta\}$ are chosen to minimize a weighted mean squared error (WMSE) criterion as discussed in Section 3.3.3. Using this approximation, (3.63) reduces to

$$\Upsilon \approx \lambda_c \pi R_l^2 \eta \left(e^{\frac{-l|\bar{\omega}|^2 R_l^{-\gamma} e^{\beta \mathbb{E} \{ \mathbf{h}^2 \mathbf{B}^2 \}}}{4}} - 1 \right) \quad (3.64)$$

Substituting the above equation in (3.60), the log-characteristic function can be expressed as

$$\psi_{\bar{\mathbf{Y}}}(\bar{\omega}) = \lambda_c \pi R_l^2 \eta \left[\exp \left(A_f \left(e^{\frac{-l|\bar{\omega}|^2 R_l^{-\gamma} e^{\beta \mathbb{E} \{ \mathbf{h}^2 \mathbf{B}^2 \}}}{4}} - 1 \right) \right) - 1 \right]. \quad (3.65)$$

Using the log-characteristic function, and the Taylor series expansion for e^x , the characteristic function can be expressed as

$$\Phi_{\bar{\mathbf{Y}}}(\bar{\omega}) = e^{-\lambda_c \pi R_l^2 \eta} \sum_{l=0}^{\infty} \left[\frac{A_f^l}{l!} \left(\sum_{k=0}^{\infty} \frac{(\lambda_c \pi R_l^2 \eta)^k k^l e^{-k A_f}}{k!} \right) e^{\frac{-l|\bar{\omega}|^2 R_l^{-\gamma} e^{\beta \mathbb{E} \{ \mathbf{h}^2 \mathbf{B}^2 \}}}{4}} \right]. \quad (3.66)$$

Equation (3.66) is the characteristic function of a two-dimensional isotropic Gaussian mixture model such that

$$\Phi_{\mathbf{I}^{(I)}, \mathbf{I}^{(Q)}}(\omega^{(I)}, \omega^{(Q)}) = \sum_{l=0}^{\infty} p_l e^{-\frac{((\omega^{(I)})^2 + (\omega^{(Q)})^2) \sigma_l^2}{2}} \quad (3.67)$$

where $p_l = \frac{e^{-\lambda_c \pi R_l^2 \eta} A_f^l}{l!} \left(\sum_{k=0}^{\infty} \frac{(\lambda_c \pi R_l^2 \eta)^k k^l e^{-k A_f}}{k!} \right)$ are the mixture probabilities, and $\sigma_l^2 = \frac{l \times R_l^{-\gamma} e^{\beta} \mathbb{E}_{\mathbf{h}, \mathbf{B}} \{\mathbf{h}^2 \mathbf{B}^2\}}{2}$ are the variance of the individual Gaussian components, for $l \geq 0$.

Using (3.62), (3.19), and (3.20), the coefficient of $|\bar{\omega}|^4$ term in the true log-characteristic function (3.60) can be expressed as

$$\lambda_c \pi R_l^{-2\gamma+2} e^{-A_f} \left[\frac{(\mathbb{E}\{\mathbf{Z}\})^2}{32} \sum_{k=0}^{\infty} \frac{k^2 A_f^k}{k!} + c_4 \sum_{k=0}^{\infty} \frac{k A_f^k}{k!} \right] \left(\frac{2}{2\gamma-2} \right). \quad (3.68)$$

where $\mathbf{Z} = \mathbf{h}^2 \mathbf{B}^2$ and $c_4 = \frac{\mathbb{E}\{\mathbf{Z}^2\} - 2(\mathbb{E}\{\mathbf{Z}\})^2}{128}$. Comparing with the coefficient of $|\bar{\omega}|^4$ term in the approximated log-characteristic function (3.66), the Gaussian mixture distribution provides a good approximation to the interference statistics in this scenario when

$$\left| \frac{(\mathbb{E}\{\mathbf{Z}\})^2}{32} \left(\frac{2}{2\gamma-2} - \eta e^{2\beta} \right) \sum_{k=0}^{\infty} \frac{k^2 A_f^k}{k!} + \frac{2c_4}{(2\gamma-2)} \sum_{k=0}^{\infty} \frac{k A_f^k}{k!} \right| \ll \left| \frac{(\mathbb{E}\{\mathbf{Z}\})^2}{32} \eta e^{2\beta} \sum_{k=0}^{\infty} \frac{k^2 A_f^k}{k!} \right|. \quad (3.69)$$

Analogous to *Case III* for a Poisson field of interferers, the above condition is independent of the parameter R_l that governs the interference space and is satisfied when the variance of the random variable $\mathbf{h}^2 \mathbf{B}^2$ is low when compared to $[\mathbb{E}\{\mathbf{h}^2 \mathbf{B}^2\}]^2$. Note that the above condition does not capture the error due

to the approximation $\mathbf{r} = \|\mathbf{R}_c + \mathbf{R}_{c,f} - R_m\| \approx \mathbf{R}_c$, which is true with high probability and is particularly valid for $\|R_m\| \ll R_l - r_h$.

3.5 Summary and Discussion

Tables 3.3 and 3.4 summarize the key results derived in this chapter for a field of Poisson and Poisson-Poisson cluster distributed interferers, respectively. The following observations are made.

1. **Narrowband emissions from interferers:** The narrowband form of the interfering emissions is truly attributed to the narrowband filtering done at the receiver. Hence the interferer emissions can have a higher bandwidth than the receiver, as long as the transients caused due to interferer emissions at the receiver can be ignored [13]. From [13], the analysis and results presented in this chapter are valid as long as the duration of the interfering emissions (T_I) is much greater than the reciprocal of the receiver bandwidth (Δf_R), i.e., $T_I \gg \frac{1}{\Delta f_R}$.
2. **Extensions for finite-area interference fields with arbitrary shape:** The finite-area cases are studied for Poisson and Poisson-Poisson clustered field of interferers in Sections 3.3.2 and 3.4.2, respectively. For a finite-area interference Γ with arbitrary shape, $\mathbb{P}\{k \text{ in } \Gamma\} = \lambda|\Gamma|$, where $|\Gamma|$ denotes the area of the space Γ in (3.9) and (3.38). The remaining analysis does not change since the expectation over the random variable \mathbf{r} is not expanded for finite-area cases. Hence it can be readily shown

Table 3.3: Statistical-physical modeling of co-channel interference in a field of Poisson distributed interferers categorized by the region containing the interferers.

Poisson field of Interferers		
Wireless Scenario	Example Wireless Network	Statistical Model
Case I: Entire Plane ($r_l = 0, r_h \rightarrow \infty$)	Sensor or Ad hoc networks	Symmetric Alpha Stable Parameters: $\alpha = \frac{4}{\gamma}$ $\sigma = \lambda \pi \mathbb{E}_{\mathbf{h}, \mathbf{B}} \{ \mathbf{h}^\alpha \mathbf{B}^\alpha \} \int_0^\infty \frac{J_1(x)}{x^\alpha} dx$ Models exact statistics
Case II: Finite-area Annular Region ($0 \leq r_l < r_h < \infty$, and $R_m \notin \Gamma(r_l, r_h)$)	a. Cellular networks (out-of-cell interference) b. Interference from a hotspot (e.g. cafe)	Middleton Class A Parameters: $A = \lambda \pi (r_h^2 - r_l^2)$ $\Omega_{2A} = \frac{A \times \mathbb{E}_{\mathbf{r}, \mathbf{h}, \mathbf{B}} \{ \mathbf{r}^{-\gamma} \mathbf{h}^2 \cdot \mathbf{B}^2 \}}{2}$ where $\mathbf{r} = \ \mathbf{R} - R_m\ $. Models tail probability when (3.26) is met.
Case III: Infinite-area with Guard Zone ($r_l > 0, r_h \rightarrow \infty$, and $\ R_m\ < r_l$)	a. Cellular networks (out-of-cell interference) b. Decentralized networks with contention-based MAC protocols c. Dense WiFi networks	Middleton Class A Parameters: $A = \lambda \pi r_l^2 \eta$ $\Omega_{2A} = \frac{A \times r_l^{-\gamma} e^{\beta} \mathbb{E}_{\mathbf{h}, \mathbf{B}} \{ \mathbf{h}^2 \cdot \mathbf{B}^2 \}}{2}$ where $\{\eta, \beta\}$ are obtained from (3.31). Models tail probability when (3.34) is met.

Table 3.4: Statistical-physical modeling of co-channel interference in a field of Poisson-Poisson cluster distributed interferers categorized by the region containing the cluster centers.

Poisson-Poisson Cluster field of Interferers			
Wireless Scenario	Scenario	Example Wireless Network	Statistical Model
Case I: Entire Plane ($R_l = 0, R_h \rightarrow \infty$)		a. Two-tier femtocell networks (femtocell interference) b. Sensor or ad hoc networks with geographical or MAC induced clustering	Symmetric Alpha Stable Parameters: $\alpha = \frac{4}{\gamma}$ $\sigma = \left[\lambda_c \pi \mathbb{E}_{\mathbf{h}, \mathbf{B}} \{ \mathbf{h}^\alpha \mathbf{B}^\alpha \} \int_0^\infty \frac{J_1(x)}{x^\alpha} dx \right]$ $\times \sum_{k=0}^{\infty} \frac{e^{-A_f} A_f^k (\sqrt{k})^\alpha}{k!}$ where $A_f = \lambda_f \pi (r_h^2 - r_l^2)$. Models tail probability.
Case II: Finite-area Annular Region ($0 \leq R_l < R_h < \infty$, and $R_m \notin \Gamma(R_l - r_h, R_h + r_h)$)		a. Cellular networks (out-of-cell interference) with user clustering b. Interference from region with multiple (random) hotspots (e.g. market place, university)	Gaussian Mixture Model Parameters: $p_l = \frac{e^{-A_c} A_f^l}{l!} \left(\sum_{k=0}^{\infty} \frac{A_c^k k^l e^{-k A_f}}{k!} \right)$ $\sigma_l^2 = \frac{l \times \mathbb{E}_{\mathbf{R}_c, \mathbf{R}_{c,f}, \mathbf{h}, \mathbf{B}} \{ \mathbf{r}^{-\gamma} \mathbf{h}^2 \mathbf{B}^2 \}}{2}$ where $A_c = \lambda_c \pi (R_h^2 - R_l^2)$, $A_f = \lambda_f \pi (r_h^2 - r_l^2)$, and $\mathbf{r} = \ \mathbf{R}_c + \mathbf{R}_{c,f} - R_m\ $. Models tail probability when (3.58) is met.
Case III: Infinite-area with Guard Zone ($R_l > 0, R_h \rightarrow \infty$, and $\ R_m\ < R_l - r_h$)		a. Two-tier femtocell networks (out-of-cell femtocell interference) b. Cellular networks (out-of-cell interference) with user clustering	Gaussian Mixture Model Parameters: $p_l = \frac{e^{-\lambda_c \pi R_l^2 \eta} A_f^l}{l!} \sum_{k=0}^{\infty} \frac{(\lambda_c \pi R_l^2 \eta)^k k^l e^{-k A_f}}{k!}$ $\sigma_l^2 = \frac{l \times R_l^{-\gamma} e^{\beta} \mathbb{E}_{\mathbf{h}, \mathbf{B}} \{ \mathbf{h}^2 \mathbf{B}^2 \}}{2}$ where $A_f = \lambda_f \pi (r_h^2 - r_l^2)$, $\{\eta, \beta\}$ are obtained from (3.31). Models tail probability when (3.69) is met.

that Middleton Class A and the Gaussian mixture models are still applicable for interference spaces with arbitrary shape using the following changes in the parameters. The overlap index for Middleton Class A is expressed more generally as $A = \lambda|\Gamma|$ for finite-area field of Poisson distributed interferers. For finite-area field of Poisson-Poisson cluster distributed interferers, the parameters $A_f = \lambda_f|\Gamma_f|$ and $A_c = \lambda_c|\Gamma_c|$, where Γ_c is the space in which the cluster centers are distributed and Γ_f is the space in which the interferers are distributed around each cluster center.

3.6 Simulation Results

Using the physical model discussed in Section 3.2, I apply Monte-Carlo numerical techniques to simulate the co-channel interference observed at the receiver in various wireless network environments based on (3.1). At each sample instant, the location of the active interferers is generated as a realization of a spatial Poisson or Poisson-Poisson cluster point process. Parameter values governing the interference space and the receiver location change according to the wireless network model under consideration. It should be noted that parameters denoting distance are treated as dimensionless quantities as this does not influence the statistics of the resultant interference.

System model parameters used in the numerical simulations are

$$\gamma = 4, \mathbf{h} \sim \text{Rayleigh} \left(\frac{1}{\sqrt{2}} \right), \lambda = 10^{-4}, \lambda_c = 10^{-4}, \lambda_f = 10^{-3}.$$

The amplitude of the interferer emissions, \mathbf{B} , was chosen as a constant for a particular wireless environment such that the tail probability, $\mathbb{P}(\|\mathbf{I}\| > y)$, at an interference threshold of $y = 7$, is of the order of 10^{-4} . The probability distribution of co-channel interference is empirically estimated from 500000 time samples of the received interference using kernel smoothed density estimators [130].

Accuracy of the statistical models is established by comparing the empirical and interference model tail probabilities. I compare the asymptotic decay rates of the tail probabilities given by

$$\rho(y) = -\frac{\log(\mathbb{P}(\|\mathbf{I}\| > y))}{y} \quad (3.70)$$

where $\rho(y)$ is the asymptotic decay rate at interference amplitude y . The decay rate is the rate at which the tail probability asymptotically approaches zero. The decay rates are a useful measure to compare the extreme value statistics of different statistical models with respect to the empirically estimated distribution.

Accuracy of fit of the statistical models is also quantified using the Kullback-Leibler divergence (KLD) measure [131], where a KLD of zero indicates an exact match of the densities. Lower KLD, however, does not imply correspondence in tail probabilities since the KLD is the relative error between two distribution functions over their entire support. Thus, even though a statistical model has a low KLD with respect to the empirical distribution, it may be an inaccurate model for modeling extreme statistics.

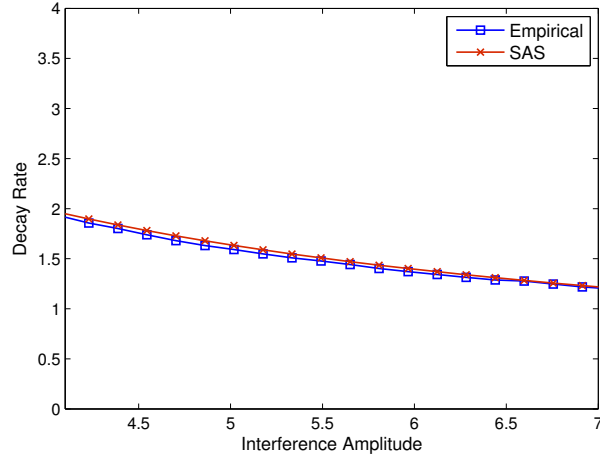


Figure 3.3: Decay rates for tail probabilities of simulated co-channel interference and the symmetric alpha stable (SAS) model for *Case I* ($r_l = 0, r_h = \infty, \mathbf{B} = 5$) of *Poisson field of interferers*. The Middleton Class A and Gaussian models are not suitable in this scenario as the mean intensity $\Omega_{2A} \rightarrow \infty$.

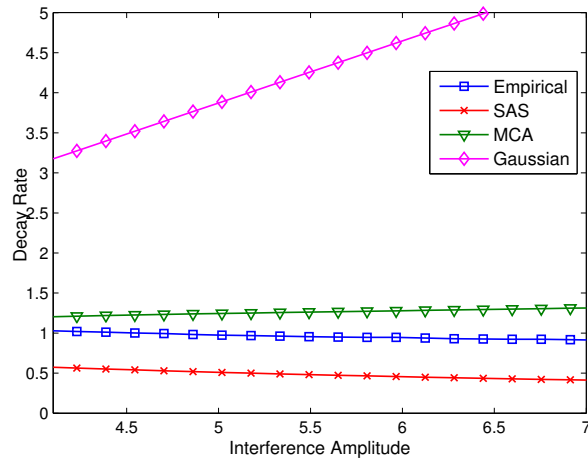


Figure 3.4: Decay rates for tail probabilities of simulated co-channel interference and the symmetric alpha stable (SAS), Middleton Class A (MCA), and Gaussian models for *Case II* ($r_l = 20, r_h = 40, \|R_m\| = 4, \mathbf{B} = 1400$) of *Poisson field of interferers*. MCA has the best match to the empirical (simulated) co-channel interference.

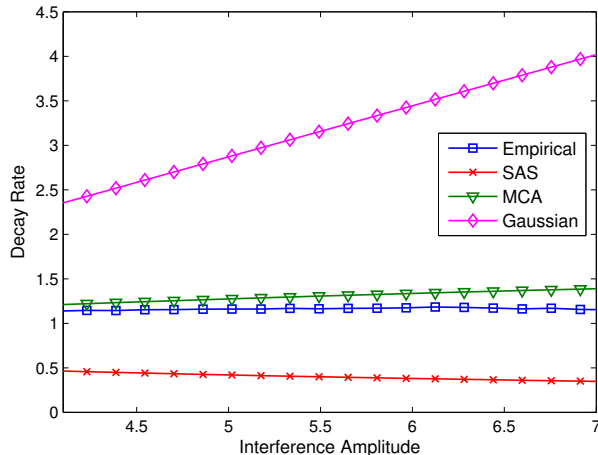


Figure 3.5: Decay rates for tail probabilities of simulated co-channel interference and the symmetric alpha stable (SAS), Middleton Class A (MCA), and Gaussian models for *Case III* ($r_l = 30, r_h = \infty, \|R_m\| = 4, \mathbf{B} = 2200$) of *Poisson field of interferers*. $\{\eta, \beta\} = \{2.781, -1.025\}$ for $\gamma = 4$ and $u(k) = e^{-k}$ from Table 3.2. MCA has the best match to the empirical (simulated) co-channel interference.

3.6.1 Co-channel interference in a Poisson field of interferers

Figs. 3.3, 3.4, and 3.5 show the decay rates of the empirical distribution compared with the statistical models for *Case I*, *Case II*, and *Case III* (see Fig. 3.1), respectively. In each scenario, the empirical distribution is compared against the symmetric alpha stable and the Middleton Class A distribution with appropriate parameters (see Table 3.3), and a Gaussian distribution with equal variance.

For a Poisson field of interferers, the results demonstrate that the tail probabilities of the co-channel interference in *Case I* are well modeled using a symmetric alpha distribution, while the Middleton Class A distribution provides a good fit to the tail probabilities in *Case II* and *Case III*.

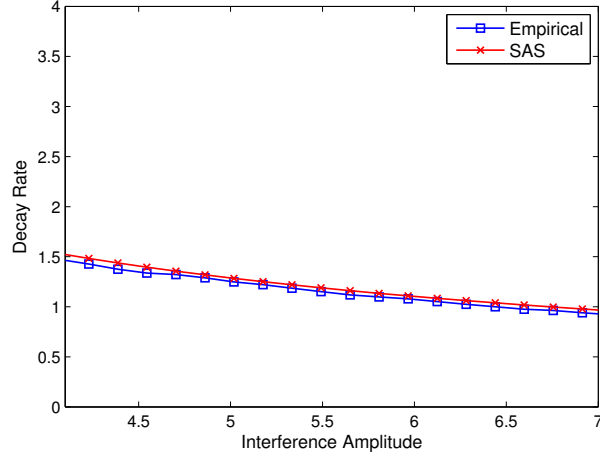


Figure 3.6: Decay rates for tail probabilities of simulated co-channel interference and the symmetric alpha stable (SAS) model for *Case I* ($R_l = 0, R_h = \infty, r_l = 0, r_h = 10, \mathbf{B} = 100$) of *Poisson-Poisson cluster field of interferers*. The Gaussian mixture and Gaussian models are not suitable in this scenario as the mean intensity $\Omega_{2A} \rightarrow \infty$.

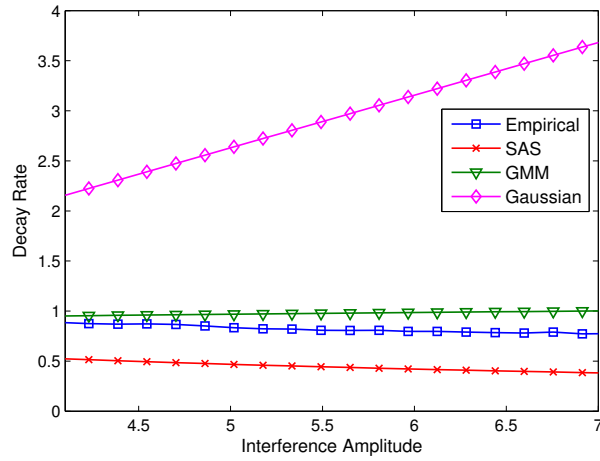


Figure 3.7: Decay rates for tail probabilities of simulated co-channel interference and the symmetric alpha stable (SAS), Gaussian mixture (GMM), and Gaussian models for *Case II* ($R_l = 40, R_h = 80, r_l = 0, r_h = 10, \|R_m\| = 4, \mathbf{B} = 6000$) of *Poisson-Poisson cluster field of interferers*. GMM has the best match to the empirical (simulated) co-channel interference.

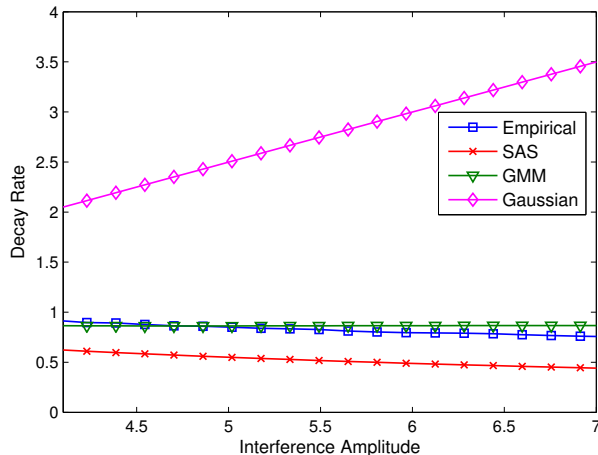


Figure 3.8: Decay rates for tail probabilities of simulated co-channel interference and the symmetric alpha stable (SAS), Gaussian mixture (GMM), and Gaussian models for *Case III* ($R_l = 30, R_h \rightarrow \infty, r_l = 0, r_h = 10, \|R_m\| = 4, \mathbf{B} = 4000$) of *Poisson-Poisson cluster field of interferers*. $\{\eta, \beta\} = \{2.781, -1.025\}$ for $\gamma = 4$ and $u(k) = e^{-k}$ from Table 3.2. MCA has the best match to the empirical (simulated) co-channel interference.

3.6.2 Co-channel interference in a Poisson-Poisson cluster field of interferers

Figs. 3.6, 3.7, and 3.8 show the decay rates of the empirical distribution compared with the statistical models for *Case I*, *Case II*, and *Case III* (see Fig. 3.2), respectively. In each scenario, the empirical distribution is compared against the symmetric alpha stable and the Gaussian mixture distribution with appropriate parameters (see Table 3.4). Further, the empirical distribution of co-channel interference is compared to a Gaussian distribution with equal variance for all scenarios.

For a Poisson-Poisson clustered field of interferers, the results demonstrate that the tail probabilities of the co-channel interference in *Case I* are

Table 3.5: Kullback-Leibler divergence between empirical and statistical model distribution (joint in-phase and quadrature-phase distribution) in Poisson and Poisson-Poisson cluster field of interferers for different wireless network scenarios. Here SAS, MCA, and GMM stand for symmetric alpha stable, Middleton Class A, and Gaussian mixture model, respectively. Parameter values governing the interference space for each of the scenarios are listed in caption to Figs. 3.3 through 3.8.

Poisson Field of Interferers			
Wireless Scenario	SAS	MCA	Gaussian
Case I	0.0154	–	–
Case II	0.0953	0.0141	0.2275
Case III	0.1594	0.8869	0.2246
Poisson-Poisson Cluster Field of Interferers			
Wireless Scenario	SAS	GMM	Gaussian
Case I	0.1656	–	–
Case II	0.1243	0.0182	0.2789
Case III	0.3309	3.2177	0.6234

well modeled using a symmetric alpha distribution, while the Gaussian mixture distribution provides a good fit to the tail probabilities in *Case II* and *Case III*.

3.6.3 Comments on simulation results

In all of the network models discussed above, the statistics of co-channel interference are not modeled well by the Gaussian distribution. The Gaussian distribution decays far too quickly to accurately model the impulsive nature of co-channel interference.

For *Case II* of Poisson and Poisson-Poisson cluster distributed interferers, accuracy of the Middleton Class A and the Gaussian mixture models in approximating the tail probability of co-channel interference depends on the

interference space based on (3.26) and (3.58), respectively. The results shown in Figs. 3.4 and 3.7 are when these conditions are met with moderate accuracy. For example, the Middleton Class A and the Gaussian mixture models provides a much closer approximation to the simulated tail probabilities for $\|R_m\| = 0$, with the remaining parameters held constant.

For *Case III*, even though the Middleton Class A and the Gaussian mixture models closely approximate the tail probability of the simulated interference (see Figs. 3.5 and 3.8), Table 3.5 shows that the KL-divergence from the empirical distribution is significantly higher than the other statistical models. This is because the approximations used for accurately modeling the tail probabilities may introduce significant mismatch in approximated distribution for near-zero amplitudes (discrete probability mass of e^{-A} and $e^{-A_c(1-e^{-A_f})}$ at zero amplitude in this case for Poisson and Poisson-Poisson clustered interferers, respectively).

3.7 RFI in laptop embedded wireless transceiver

Measurements of RFI from a computation platform collected using a 20GSPS scope were obtained from Intel Corporation. Twenty-five sets of measurement data were recorded in different configuration of the computation platform (i.e., different subsystems active). No further information was provided. The first 50000 samples in each measurement dataset were fitted to the Gaussian, symmetric alpha stable, Middleton Class A, and Gaussian mixture models. For Gaussian mixture distribution, 10 mixture terms were assumed. Fig. 3.9 shows the Kullback-Leibler (KL) divergence of the probability distri-

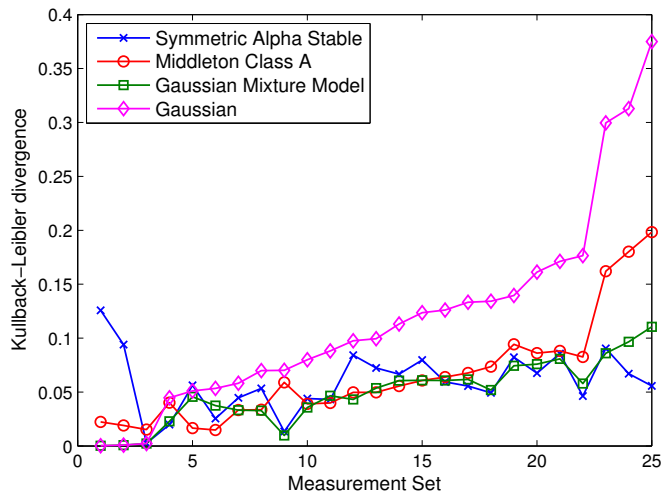


Figure 3.9: Kullback-Leibler (KL) divergence of the measured distribution from the estimated Gaussian, symmetric alpha stable, Middleton Class A, and Gaussian mixture distributions. KL divergence for twenty-five measured RFI datasets is compared.

bution of the estimated statistical models from the empirical density of the measured data. The empirical probability density of the measured data was estimated using kernel smoothing density estimators [130]. The measurement sets have been sorted to have increasing KL divergence from the estimated Gaussian model, i.e. increasing impulsiveness of the noise samples.

Fig. 3.9 suggests that the Gaussian mixture model, symmetric alpha stable model, and also the Middleton Class A model in some cases, provide a good approximation to the empirical distribution in varying scenarios. KL divergence, however, may not be an accurate measure to quantify the fit of the statistical models to the measured data. Recall that the emphasis in this chapter is to accurately model the tail probabilities of the RFI, as the tail probabilities govern the BER performance of the wireless receivers. Since KL

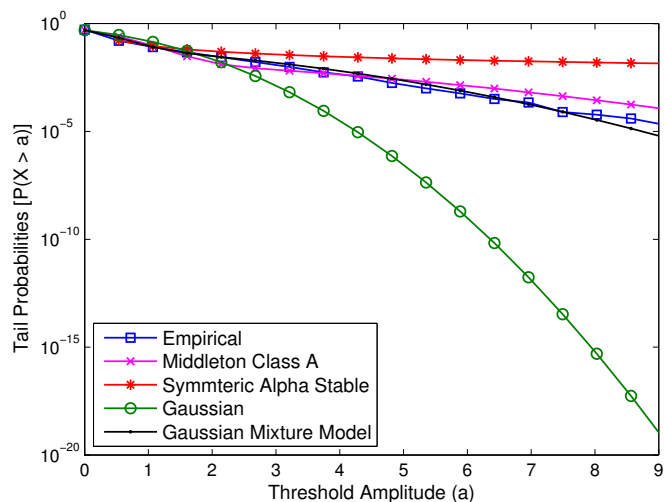


Figure 3.10: Tail probability of the measured and estimated Gaussian, symmetric alpha stable, Middleton Class A, and Gaussian mixture models for measurement set number 23. Gaussian mixture model provides closest fit to tail probability of measured data.

divergence finds the relative error between two distributions on their entire support, a lower KL divergence does not imply a match in the tail probability of distributions.

Consider the measurement set number 23 in Fig. 3.9. Comparing the KL divergence, it seems that both Gaussian mixture and symmetric alpha stable models provide a good fit to measured density. Fig. 3.10, however, shows that the tail probability of the measured data closely matches the estimated Gaussian mixture model tails and is significantly apart from the tails estimated by the symmetric alpha stable model. Further, the Gaussian mixture model was observed to be robust to the number of mixture terms and the number of samples used for empirical fitting. This motivates the design of wireless receivers under the assumption of Gaussian mixture distributed interference.

3.8 Conclusions

The results presented in this chapter are applicable to a wide variety of wireless network topologies, including user clustering, contention-based and contention-free MAC protocols, and finite-area interference regions. Tables 3.3 and 3.4 list some of the example wireless networks for which the results are applicable. Knowledge of closed form amplitude statistics of co-channel interference can be used to analyze and improve the communication performance of wireless networks, including both PHY layer algorithms and MAC layer protocols. This is illustrated in Chapters 4 and 5 using the framework introduced in this chapter.

Chapter 4 shows the benefit of closed-form interference statistics in analyzing the communication performance of a decentralized wireless network. The network model therein extends the *Case I* of Poisson field of interferers to include temporal correlation in interferer locations. The joint statistics of interference is then derived using the framework introduced in this chapter. The joint interferer statistics are used to derive closed-form expressions for various measures of communication performance of the network. The results of Chapter 4 are used to motivate the design of MAC layer protocols to mitigate interference in wireless networks.

Chapter 5 uses the knowledge of interference statistics to derive pre-filtering techniques at the PHY layer to improve the BER performance of wireless receivers in the presence of non-Gaussian interference. While this chapter, and the next chapter, assumes an unbounded pathloss function to

derive interference statistics, Chapter 5 assumes a bounded pathloss function in addition to including temporal dependence in user locations. Using the framework developed in this chapter, closed-form joint statistics of interference are derived. The joint interference statistics are used to motivate the design of pre-filtering methods.

Chapter 4

Throughput, Delay, and Reliability of Decentralized Wireless Networks with Temporal Correlation

4.1 Introduction

As indicated in Chapter 2, prior work on communication performance analysis of wireless networks has been limited by the knowledge of closed-form statistics of interference in the network [63, 68, 76]. In the absence of closed-form interference statistics, much of the prior work resorts to deriving bounds on the measures of communication performance [76, 91]. In Chapter 3, I developed a framework to derive closed-form instantaneous statistics of interference in a wide range of wireless networks. In this chapter, I utilize the framework to first derive joint temporal statistics of interference in a decentralized wireless network. The joint interference statistics are then used to study the throughput, delay, and reliability of single hop transmissions in a decentralized wireless network. Communication performance measures such as local delay, throughput outage probability, and average network throughput are derived in closed-form in the low outage regime. The closed-form expressions of communication performance measure unveil $2\times$ potential improvement in network throughput by optimizing certain MAC layer parameters.

4.1.1 Motivation and Prior Work

Characterizing the communication performance of single hop transmissions from a transmitter to its next hop receiver is a fundamental step towards understanding the end-to-end performance of multihop wireless networks. Over the last decade, significant research has been done towards analyzing the single hop communication performance in a decentralized wireless network, such as a wireless ad hoc network, under the assumption that user locations at any given time instant follow a spatial Poisson point process (PPP) [63, 68]. Key measures of communication performance include outage probability [63], transmission capacity [76], and local delay [92, 94]. Such measures are affected not only by the user locations at any given time instant, but also the correlation in user locations over time [132]. Much of the prior work assumes either no dependence or complete correlation in the user locations over time [92, 94]. This captures only the extremes of either no mobility and infinitely backlogged user queues (complete correlation), or highly mobile users and/or short user queues (little or no correlation). In most realistic settings, however, there is some mobility or traffic bursts that play out over a significantly slower time scale than contention and channel access. It is therefore important to study the throughput, delay, and reliability of single hop transmissions when there is nontrivial correlation in the transmitter locations. The network model adopted in this chapter spans the extremes of temporal independence to long-term temporal dependence in interference, capturing random mobility and random queue size of users in the network.

Temporal correlation in user locations, and hence temporal dependence in interference, depends on user mobility and the typical duration of user transmissions. The effect of mobility on the local delay of wireless ad hoc networks was recently studied in [92, 94] for static and highly mobile ad hoc networks. Local delay was defined as the mean time required for a successful transmission from a transmitter to its next hop receiver. In [92, 94], the network was assumed to have an infinite backlog and thus the users attempt to transmit at all time instants. In static networks, the users are assumed to have no mobility, and hence the user locations are fully correlated over time. In a highly mobile network, on the other hand, the user mobility may be sufficient to make the user locations nearly independent over adjacent contention time slots. Static and highly mobile network models also have an equivalent interpretation in terms of classification with respect to the duration of user transmissions. Complete correlation in user locations over time is a result of no mobility and when the users intend to transmit at all time instants. Temporal independence in user locations, on the contrary, may occur when the typical user is highly mobile and/or the duration of user transmissions is small. Thus static and highly mobile network models are two extremes, in which user locations are either independent or fully correlated over time.

In this chapter, I model a wider spectrum of temporal dependence in interference that may exist in a decentralized wireless network. Although the system model is described with respect to the duration of user transmissions, it can also be interpreted with respect to the varying user mobility. A user

may start a transmission at any time, termed as the *emerging time*, and the transmissions lasts for a random duration, termed as the *lifetime*. Distribution of the random lifetime of users can be deduced from typical data transfer characteristics in the network. Thus at any given time, users that transmit include those whose transmissions are ongoing from some time in the past, and users that just started transmitting. Hence the temporal dependence in the interference increases as the lifetime of a typical user increases. The static and highly mobile network models are included as special cases in this network model by appropriately choosing the lifetime distribution and constraints on the emerging time of users. Although I assume a channel access probability of one, the results can be readily extended to include a ALOHA type MAC layer protocol in conjunction to the network model adopted in this chapter [55, 68].

This chapter adopts a novel approach to derive the single hop communication performance measures in closed-form. Much of the prior work formulates the system model as an abstraction of transmit and receive power, uses tools from stochastic geometry, and attempts to express the measures of communication performance in terms of the Laplace transform of interference [63, 67, 68]. The performance measures can typically be derived in closed-form only under the assumption of Rayleigh fading. Further, to the best of my judgment, using prior methods to derive closed-form expressions for the performance measures considered in this chapter is hard. In contrast, I formulate the problem as an abstraction of amplitude and phase of the interfering and desired signals, and express the performance measures in terms

of the joint tail probability of the interference. The joint tail probabilities are arrived at by first deriving the joint characteristic function of interference in a known statistical form. Advantage of this approach is that closed-form expressions can be derived with ease and do not require stringent assumptions on the fading random variable [104]. The disadvantage of this approach is that our results are mathematically exact only in the low outage probability regime. Low outage regime is assumed to derive a closed-form expression for the joint tail probability, and also the joint characteristic function for non-Rayleigh fading. However, the results match closely in simulations even when the outage probability is fairly high.

As shown in Chapter 3, interference at any given time instant follows the symmetric alpha stable distribution under the assumptions of power-law pathloss function and PPP distributed user locations [64, 70–72, 104, 127]. Further, the second-order joint temporal statistics of interference have been shown to follow a two-dimensional symmetric alpha stable distribution [72]. To the best of my knowledge, closed-form joint temporal statistics of interference of higher order, required for deriving the single hop communication performance measures, are not known in general [72].

The mathematical problem in hand closely resembles analyzing end-to-end outages in multi-hop wireless ad hoc networks, where spatial and temporal dependence in interference affects the performance of successive hops [91]. Relevant prior work includes [84, 91, 133]. To the best of my knowledge, the results presented in this chapter cannot be derived directly from the prior work

in multi-hop networks - key difference being the network model governing the temporal dependence.

4.1.2 Contribution, Organization, and Notation

I derive the closed-form joint characteristic function of interference over multiple time instants in a decentralized wireless network with temporally correlated user locations. The joint characteristic function of interference is shown to follow the multivariate symmetric alpha stable distribution. The joint characteristic function is exact when the amplitude of the faded interferer emissions are Rayleigh distributed, and closely characterizes the tail probability of interference otherwise in the low outage regime. Using properties of the multivariate symmetric alpha stable distribution, I provide new theorems for expressing the joint tail probability of interference in closed-form. The closed-form expressions of tail probability enable us to derive the following single hop communication performance measures: (i) local delay, (ii) throughput outage probability, (iii) average network throughput, and (iv) transmission capacity. Transmission capacity for single hop transmissions was first defined for temporally independent user locations as the maximum allowable density of transmitting users satisfying an outage probability constraint [76, 87]. In this chapter, I extend the definition of transmission capacity to account for temporal dependence and show that it captures the throughput-delay-reliability tradeoff of single hop transmissions. Using the extended definition, I demonstrate up to $2\times$ gain in network throughput and reliability by optimizing over

the lifetime distribution - which motivates designing MAC protocols to incorporate the effect of temporal correlation.

The chapter is organized as follows. Section 4.2 discusses the system model. Section 4.3 derives joint interference statistics, including characteristic function and tail probability, of interference for the two network models discussed in the system model. Section 4.4 uses the results on tail probability to derive various single hop communication performance measures. Section 4.5 presents the numerical simulation results. Appendix A contains a brief overview of statistical properties of symmetric alpha stable vectors and proofs for the new theorems used in the chapter. Table 4.1 summarizes the notation used in this chapter.

4.2 System Model

Time is assumed to be slotted with respect to the duration required for one physical packet transmission. The locations of transmitters, also referred to as nodes, are modeled using a spatial point process. A node is said to *emerge* at a particular time slot if it first starts to transmit at that time slot. All nodes transmitting at a given time slot are referred to as *active* nodes at that time slot. Thus at each time slot n , the set of active nodes is a union over the sets of nodes that first emerged at a slot $m \leq n$ and are still active at the time slot n . Emerging nodes at any time slot m are assumed to be spatially distributed according to a homogeneous PPP $\Pi^{(m)} = \left\{ \left(\mathbf{R}_i^{(m)}, \mathbf{L}_i^{(m)} \right), i \geq 1 \right\}$ with intensity $\lambda^{(m)}$. Here $\mathbf{R}_i^{(m)}$ is the random location of the node i that

Table 4.1: Summary of Notation used in Chapter 4

Symbol	Description
$\Pi^{(m)}$	Poisson point process of emerging nodes at time slot m
$\lambda^{(m)}$	intensity of $\Pi^{(m)}$
$\Xi_n(\Xi_{k,n})$	point process of nodes active at time slot n (that emerged at time slot k)
$\mathbf{R}, \mathbf{R}^{(m)}$	(random) location of a node in space
$\mathbf{L}, \mathbf{L}^{(m)}$	(random) time slots a node transmits (i.e., lifetime)
γ	power pathloss exponent ($\gamma > 2$)
$\mathbf{X} = \mathbf{B}e^{j\phi}$	amplitude and phase of interferer emissions
$\mathbf{g} = \mathbf{h}e^{j\theta}$	amplitude and phase of narrowband fading
$\mathbf{I}_n(\mathbf{I}_{k,n})$	interference at time slot n (due to nodes that emerged at time slot k)
$\bar{\mathbf{I}}_{k,1:n}$	$\triangleq \{ \mathbf{I}_{k,1}^{(I)}, \mathbf{I}_{k,1}^{(Q)}, \dots, \mathbf{I}_{k,n}^{(I)}, \mathbf{I}_{k,n}^{(Q)} \}$, $\mathbf{I}_{k,m} = \mathbf{I}_{k,m}^{(I)} + j\mathbf{I}_{k,m}^{(Q)}$
$\bar{\omega}_{1:n}$	$\triangleq \{ \omega_1^{(I)}, \omega_1^{(Q)}, \dots, \omega_n^{(I)}, \omega_n^{(Q)} \}$ frequency variables
$\Phi_{\bar{\mathbf{I}}}(\bar{\omega}_{1:n})$	characteristic function of $\bar{\mathbf{I}}$, where $\bar{\mathbf{I}} = \bar{\mathbf{I}}_{k,n}$ or $\bar{\mathbf{I}}_n$
$\psi_{\bar{\mathbf{I}}}(\bar{\omega}_{1:n})$	log-characteristic function of $\bar{\mathbf{I}}$, where $\bar{\mathbf{I}} = \bar{\mathbf{I}}_{k,n}$ or $\bar{\mathbf{I}}_n$
Δ	(random) number of consecutive failed transmissions
D	distance between a transmitter-receiver pair
T	signal-to-interference ratio threshold for successful detection
S_d	unit sphere in d dimensions
α	characteristic exponent of symmetric alpha stable vector, $\alpha = 4/\gamma$
$\bar{\Gamma}$	spectral measure of symmetric alpha stable vector
σ	dispersion of an isotropic symmetric alpha stable vector
$\mathcal{F}_{\mathbf{L}}(n), K(\alpha)$	constants defined in (4.33) and (4.39), respectively

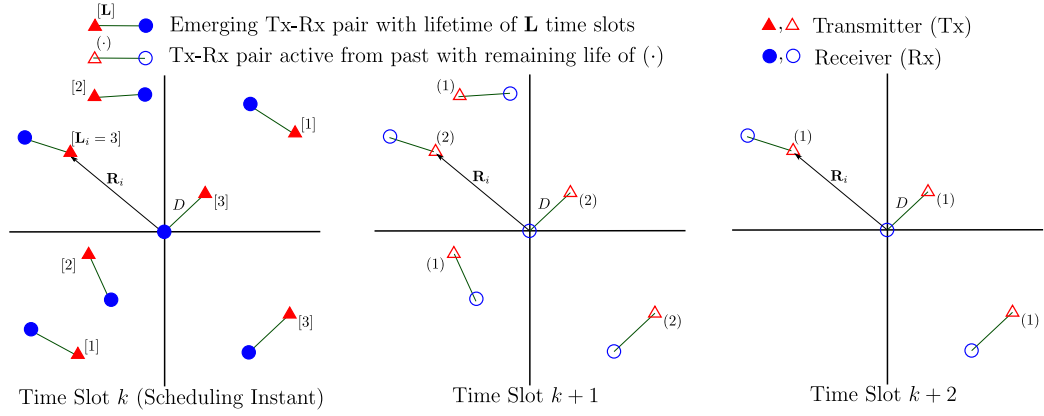


Figure 4.1: Network Model I: nodes emerge only at fixed time slots and transmit for a random number of time slots ($= \mathbf{L}$).

first emerged at time m , and $\mathbf{L}_i^{(m)} \geq 1$ is the random number of time slots (lifetime) it intends to be active. The node i disappears after $\mathbf{L}_i^{(m)}$ time slots after its emergence at time slot m . Each node of the point process represents an active transmitter and is assumed to be associated with a distinct receiver at a distance D in a random direction. Extension to include randomness in D is straightforward [76]. A node may intend to transmit single or multiple packets in its lifetime, and may not be successful due to packet errors. Two network models are considered - network model I represents a synchronous network where nodes emerge only at fixed time slots, while network model II represents an asynchronous network where nodes may emerge at any time slot.

4.2.1 Network Model I: Synchronous

Consider a network, as depicted in Fig. 4.1, in which the nodes can start transmitting only at fixed time slots, referred to as MAC scheduling instants.

The MAC scheduling instants are spaced apart by $L_{max} + 1$ time slots such that all nodes complete their transmission prior to the next scheduling instant. For analysis of such a network, just one MAC scheduling cycle is considered. Thus the interference can be modeled by assuming that nodes emerge only at the time slot k with $\lambda^{(k)} = \lambda$, $\lambda^{(m)} = 0$ for $m \neq k$, and $\mathbb{P}(\mathbf{L}^{(k)} \leq L_{max}) = 1$ for all nodes. Further, without loss of generality, $k = 1$ could be chosen for analysis of the network. However, k is kept as a variable so that it can be used as a building block for network model II.

The point process of active nodes at any time slot $n \geq k$ is then a subset of the point process $\mathbf{\Pi}^{(k)}$, such that $\mathbf{\Xi}_{k,n} = \left\{ \mathbf{R} : (\mathbf{R}, \mathbf{L}) \in \mathbf{\Pi}^{(k)}, \mathbf{L} \geq n - k + 1 \right\}$. For $n < k$, $\mathbf{\Xi}_{k,n}$ is an empty set since no nodes have yet emerged. Since the underlying node distribution follows a PPP, by Slivnyak's theorem and the random translation invariance property of PPP, a typical transmit node can be added to the point process such that its associated receiver lies on the origin without affecting the node distribution. Note that the active node distribution at any given time instant $n \geq k$ is still a PPP with intensity $\lambda \mathbb{P}(\mathbf{L} \geq n - k + 1)$. The node distribution, however, is correlated across time slots. Complete temporal correlation is a special case of network model I with $\mathbf{L} \xrightarrow{P} \infty$.

The sum interference $\mathbf{I}_{k,n}$ observed at the typical receiver located at the origin at the time slot n due to the nodes that emerged at time slot k can

then be represented as

$$\mathbf{I}_{k,n} = \sum_{\mathbf{R}_i \in \Xi_{k,n}} \mathbf{r}_i^{-\frac{\gamma}{2}} \mathbf{h}_i(n) \mathbf{B}_i(n) (\cos(\phi_i(n) + \theta_i(n)) + j \sin(\phi_i(n) + \theta_i(n))). \quad (4.1)$$

where i is the interferer index, $\mathbf{r}_i = \|\mathbf{R}_i\|$ are the random distances of active interferers from the receiver, γ is the power pathloss exponent, $\mathbf{B}_i(n)e^{j\phi_i(n)}$ are the narrowband interferer emissions from interferer i at time slot n , and $\mathbf{h}_i(n)e^{j\theta_i(n)}$ is the narrowband fading experienced by the interferer emissions. Random variables $\mathbf{B}_i(n), \mathbf{h}_i(n), \phi_i(n), \theta_i(n)$ are each assumed to be *i.i.d.* for each interferer i and time slot n . Assuming the actual emerging time of the interferers to be uniformly distributed between two time slots, $\phi_i(n)$ and $\theta_i(n)$ can be assumed to be uniformly distributed on $[0, 2\pi]$. The rationale behind the narrowband assumption of user emissions and fast fading is discussed in Chapter 3.

The signal-to-interference ratio (SIR) at the typical receiver at time slot n in the presence of interferers that first emerged at time slot k can be expressed as

$$\text{SIR}_{k,n} = \frac{\|D^{-\frac{\gamma}{2}} \mathbf{h}_0(n) \mathbf{B}_0(n) e^{j(\phi_0(n) + \theta_0(n))}\|^2}{\|\mathbf{I}_{k,n}\|^2} = \frac{D^{-\gamma} \mathbf{h}_0^2(n) \mathbf{B}_0^2(n)}{\|\mathbf{I}_{k,n}\|^2} \quad (4.2)$$

where $\mathbf{B}_0(n)e^{j(\phi_0(n))}$ is the random emission and $\mathbf{h}_0(n)e^{j(\theta_0(n))}$ is random fading at time slot n corresponding to the desired transmitter-receiver pair.

4.2.2 Network Model II: Asynchronous

Model II, as depicted in Fig. 4.2, extends the network model I by removing the assumption of globally synchronized MAC scheduling instants. This

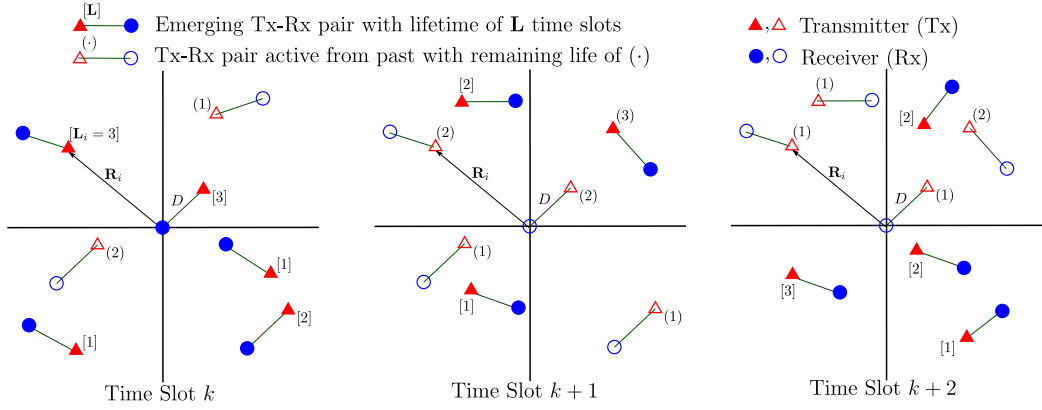


Figure 4.2: Network Model II: nodes can emerge at any time slot and are active for a random number of time slots ($= \mathbf{L}$).

represents a more dynamic and fully decentralized wireless network where the nodes can emerge at any time slot and stay active for random number of slots. The point process for the emerging nodes $\mathbf{\Pi}^{(m)}$ is assumed to be independent and identical over the time slots m with $\lambda^{(m)} = \lambda, \forall m$. The point process of active nodes $\mathbf{\Xi}_n$ is thus a stationary process.

The point process of active nodes at time slot n can then be represented as union over the active node point process for network model I, given as $\mathbf{\Xi}_n = \bigcup_{k=-\infty}^n \mathbf{\Xi}_{k,n}$. Using Slivnyak's theorem, stationarity of the point process, and the random translation invariance property of PPP, a typical node can be added to the point process of active nodes such that its associated receiver lies on the origin without affecting the node distribution. Note that the active node distribution at any given time instant n is still a PPP with intensity $\lambda \sum_{k=-\infty}^n \mathbb{P}(\mathbf{L} \geq n - k + 1) = \lambda \mathbb{E}\{\mathbf{L}\}$. Similar to model I, the node distribution is correlated across time slots unless $\mathbb{P}(\mathbf{L}^{(k)} = 1) = 1$ for all nodes and time

slots k .

Since $\Xi_n = \bigcup_{k=-\infty}^n \Xi_{k,n}$, the sum interference at the typical receiver located at the origin from all active interfering nodes at time slot n can be expressed as

$$\mathbf{I}_n = \sum_{k=-\infty}^n \mathbf{I}_{k,n} \quad (4.3)$$

$$= \sum_{k=-\infty}^n \left[\sum_{\mathbf{R}_i \in \Xi_{k,n}} \mathbf{r}_i^{-\frac{\gamma}{2}} \mathbf{h}_i(n) \mathbf{B}_i(n) (\cos(\phi_i(n) + \theta_i(n)) + j \sin(\phi_i(n) + \theta_i(n))) \right]. \quad (4.4)$$

The signal-to-interference ratio (SIR) at the typical receiver at time slot n can be expressed as

$$\text{SIR}_n = \frac{\|D^{-\frac{\gamma}{2}} \mathbf{h}_0(n) \mathbf{B}_0(n) e^{j(\phi_0(n) + \theta_0(n))}\|^2}{\|\mathbf{I}_n\|^2} = \frac{D^{-\gamma} \mathbf{h}_0^2(n) \mathbf{B}_0^2(n)}{\|\mathbf{I}_n\|^2}. \quad (4.5)$$

4.3 Joint Statistics of Interference

In this section, I derive the joint temporal statistics of interference for network models I and II. The properties of the joint temporal statistics of interference are then used to derive closed-form expressions for the joint tail probability of interference over time. The joint tail probability enable us to derive closed-form expressions for various network performance measures.

4.3.1 Network Model I

Let $\bar{\mathbf{I}}_{k,1:n} = \{\mathbf{I}_{k,1}^{(I)}, \mathbf{I}_{k,1}^{(Q)}, \mathbf{I}_{k,2}^{(I)}, \mathbf{I}_{k,2}^{(Q)}, \dots, \mathbf{I}_{k,n}^{(I)}, \mathbf{I}_{k,n}^{(Q)}\}$ denote the vector of in-phase and quadrature phase components on the interference at time slots 1

through n due to nodes that emerged at time instant k , where $\mathbf{I}_{k,n}$ is given by (4.1). Further, let $\bar{\omega}_{1:n} = \{\omega_1^{(I)}, \omega_1^{(Q)}, \omega_2^{(I)}, \omega_2^{(Q)}, \dots, \omega_n^{(I)}, \omega_n^{(Q)}\}$ denote the vector of frequency variables. To derive the joint statistics, I first consider the nodes distributed over disc of radius R , denoted as $b(0, R)$, and take the limit on the joint distribution as $R \rightarrow \infty$. Using (4.1), the joint characteristic function of $\bar{\mathbf{I}}_{k,1:n}$ can be expressed as

$$\begin{aligned} & \Phi_{\bar{\mathbf{I}}_{k,1:n}}(\bar{\omega}_{1:n}) \\ &= \mathbb{E} \left\{ e^{j \sum_{m=1}^n (\omega_m^{(I)} \mathbf{I}_{k,m}^{(I)} + \omega_m^{(Q)} \mathbf{I}_{k,m}^{(Q)})} \right\} \end{aligned} \quad (4.6)$$

$$= \mathbb{E} \left\{ e^{j \sum_{m=1}^n |\omega_m| \sum_{\mathbf{R}_i \in \Xi_{k,m}} \mathbf{r}_i^{-\frac{\gamma}{2}} \mathbf{h}_i(m) \mathbf{B}_i(m) \cos(\phi_i(m) + \theta_i(m) + \phi_{\omega_m})} \right\} \quad (4.7)$$

$$= \mathbb{E} \left\{ e^{j \sum_{m=1}^n |\omega_m| \sum_{(\mathbf{R}_i, \mathbf{L}_i) \in \Pi^{(k)}} \mathbf{r}_i^{-\frac{\gamma}{2}} \mathbf{h}_i(m) \mathbf{B}_i(m) \cos(\phi_i(m) + \theta_i(m) + \phi_{\omega_m}) \mathbf{1}(\mathbf{L}_i \geq m - k + 1 > 0)} \right\} \quad (4.8)$$

$$= e^{\lambda \pi R^2 \left(-1 + \mathbb{E} \left\{ e^{j \sum_{m=1}^n |\omega_m| \mathbf{r}^{-\frac{\gamma}{2}} \mathbf{h}(m) \mathbf{B}(m) \cos(\phi(m) + \theta(m) + \phi_{\omega_m}) \mathbf{1}(\mathbf{L} \geq m - k + 1 > 0)} \right\} \right)}. \quad (4.9)$$

where $|\omega_m| = \sqrt{(\omega_m^{(I)})^2 + (\omega_m^{(Q)})^2}$, $\phi_{\omega_m} = \tan^{-1} \left(\frac{\omega_m^{(Q)}}{\omega_m^{(I)}} \right)$, $\mathbf{1}(\cdot)$ is the indicator function, and the expectation in (4.9) is with respect to the set of random variables $\{\mathbf{r}, \mathbf{L}, \mathbf{h}(m), \mathbf{B}(m), \phi(m), \theta(m)\}$. Equation (4.8) holds since $\Xi_{k,m} = \{\mathbf{R} : (\mathbf{R}, \mathbf{L}) \in \Pi^{(k)}, \mathbf{L} \geq m - k + 1\}$ for $m \geq k$, and is an empty set for $m < k$. Equation (4.9) is derived using the probability generating functional (PGFL) of a homogeneous PPP [63] and holds since the node emissions, node lifetime, and fading are each assumed to be *i.i.d.* across time slots and nodes. Note that the expectation in (4.9) is conditioned such that the node locations are uniformly distributed over $b(0, R)$ [63, 104]. The distance of each node from

the typical receiver at the origin thus follows the distribution

$$f_{\mathbf{r}}(r) = \begin{cases} \frac{2r}{R^2} & \text{if } 0 \leq r \leq R, \\ 0 & \text{otherwise.} \end{cases}$$

Using the identity

$$e^{ja \cos(\phi)} = \sum_{l=0}^{\infty} j^l \epsilon_l J_l(a) \cos(l\phi) \quad (4.10)$$

where $\epsilon_0 = 1$, $\epsilon_l = 2$ for $l \geq 1$, and $J_l(\cdot)$ denotes the Bessel function of order l , the log-characteristic function $\psi_{\bar{\mathbf{I}}_{k,1:n}}(\bar{\omega}_{1:n}) \triangleq \log \Phi_{\bar{\mathbf{I}}_{k,1:n}}(\bar{\omega}_{1:n})$ can be expressed as

$$\begin{aligned} & \psi_{\bar{\mathbf{I}}_{k,1:n}}(\bar{\omega}_{1:n}) \\ &= \lambda \pi R^2 \left[-1 + \mathbb{E} \left\{ \prod_{m=1}^n \left(\sum_{l=0}^{\infty} j^l \epsilon_l J_l \left(|\omega_m| \mathbf{r}^{-\frac{\gamma}{2}} \mathbf{h}(m) \mathbf{B}(m) \mathbf{1}(\mathbf{L} \geq m - k + 1 > 0) \right) \right. \right. \right. \\ & \quad \left. \left. \left. \times \cos \left(l \left(\phi(m) + \boldsymbol{\theta}(m) + \phi_{\omega_m} \right) \right) \right) \right\} \right] \quad (4.11) \end{aligned}$$

$$= \lambda \pi R^2 \left[-1 + \mathbb{E} \left\{ \prod_{m=1}^n J_0 \left(|\omega_m| \mathbf{r}^{-\frac{\gamma}{2}} \mathbf{h}(m) \mathbf{B}(m) \mathbf{1}(\mathbf{L} \geq m - k + 1 > 0) \right) \right\} \right] \quad (4.12)$$

$$= \lambda \pi R^2 \left[\sum_{s=1}^n \bar{F}_{\mathbf{L}}^{(k,n)}(s) \left(-1 + \mathbb{E} \left\{ \prod_{m=\max(1,k)}^s J_0 \left(|\omega_m| \mathbf{r}^{-\frac{\gamma}{2}} \mathbf{h}(m) \mathbf{B}(m) \right) \right\} \right) \right] \quad (4.13)$$

where

$$\bar{F}_{\mathbf{L}}^{(k,n)}(s) = \begin{cases} 0 & s < k, \\ \mathbb{P}(\mathbf{L} = s - k + 1) & k \leq s < n, \\ \mathbb{P}(\mathbf{L} \geq s - k + 1) & s = n. \end{cases} \quad (4.14)$$

The expectation in (4.11) is with respect to the set of random variables $\{\mathbf{r}, \mathbf{L}, \mathbf{h}(m), \mathbf{B}(m), \phi(m), \boldsymbol{\theta}(m)\}$. Equation (4.12) involves expanding the expectation over $\phi(m)$ and $\boldsymbol{\theta}(m)$, where $\phi(m), \boldsymbol{\theta}(m)$ are mutually independent

and uniformly distributed in $[0, 2\pi]$ and *i.i.d.* across time slots m , and noting that $\mathbb{E}_{\phi(m), \theta(m)} \{\cos(l(\phi(m) + \theta(m) + \phi_{\omega_m}))\} = 0$ for $l \geq 1$ for all time slots m . Equation (4.13) is derived by expanding the expectation over lifetime random variable \mathbf{L} . The expectation in (4.13) is thus with respect to the set of random variables $\{\mathbf{r}, \mathbf{h}(m), \mathbf{B}(m)\}$. To further simplify (4.13), I express it as

$$\psi_{\bar{\mathbf{I}}_{k,1:n}}(\bar{\omega}_{1:n}) = \lambda\pi \left[\sum_{s=1}^n \bar{F}_{\mathbf{L}}^{(k,n)}(s) \Upsilon_{(k,s)}(\bar{\omega}_{1:n}) \right] \quad (4.15)$$

where for any parameters $\{k, s\}$,

$$\Upsilon_{(k,s)}(\bar{\omega}_{1:n}) = \lim_{R \rightarrow \infty} R^2 \left(-1 + \mathbb{E} \left\{ \prod_{m=\max(1,k)}^s J_0 \left(|\omega_m| r^{-\frac{\gamma}{2}} \mathbf{h}(m) \mathbf{B}(m) \right) \right\} \right) \quad (4.16)$$

$$= \lim_{R \rightarrow \infty} R^2 \left(-1 + \int_0^R \prod_{m=\max(1,k)}^s \mathbb{E}_{\mathbf{h}, \mathbf{B}} \left\{ J_0 \left(|\omega_m| r^{-\frac{\gamma}{2}} \mathbf{h} \mathbf{B} \right) \right\} \frac{2r}{R^2} dr \right) \quad (4.17)$$

$$= - \int_0^{\infty} \frac{\partial}{\partial r} \left(\prod_{m=\max(1,k)}^s \mathbb{E}_{\mathbf{h}, \mathbf{B}} \left\{ J_0 \left(|\omega_m| r^{-\frac{\gamma}{2}} \mathbf{h} \mathbf{B} \right) \right\} \right) r^2 dr. \quad (4.18)$$

Equation (4.17) is derived by expanding the expectation over \mathbf{r} in (4.16) and noting that $\mathbf{h}(m)$ and $\mathbf{B}(m)$ are each *i.i.d.* across time slots m . Equation (4.18) involves integrating (4.17) by parts and noting that $\lim_{R \rightarrow \infty} R^2 \left(-1 + \prod_{m=\max(1,k)}^s \mathbb{E}_{\mathbf{h}, \mathbf{B}} \left\{ J_0 \left(|\omega_m| R^{-\frac{\gamma}{2}} \mathbf{h} \mathbf{B} \right) \right\} \right) = 0$ for $\gamma > 2$.

Exact evaluation of (4.18) is possible for $s = \max(1, k)$, i.e., when only one $J_0(\cdot)$ term exists, which arises in deriving the instantaneous statistics of interference and reduces to an isotropic alpha stable form $(\propto |\omega_s|^{\frac{4}{\gamma}})$ [70,

104]. Similar reduction with exact equality, however, does not seem to be possible for terms involving product of Bessel functions. I thus propose an approximation of the log-characteristic function for $|\omega_m|, m = 1, \dots, n$ in the neighborhood of zero based on an identity proposed by Middleton [12]. From Fourier analysis, the behavior of the characteristic function for $|\omega_m|, m = 1, \dots, n$ in the neighborhood of zero governs the joint tail probability of the random envelope at time instants 1 through n . The proposed approximation is based on the following identity [12]:

$$\mathbb{E}_{\mathbf{h}, \mathbf{B}} \left\{ J_0 \left(|\omega_m| r^{-\frac{\gamma}{2}} \mathbf{h} \mathbf{B} \right) \right\} = e^{-\frac{|\omega_m|^2 r^{-\gamma} \mathbb{E}_{\mathbf{h}, \mathbf{B}} \{ \mathbf{h}^2 \mathbf{B}^2 \}}{4}} (1 + \Lambda(|\omega_m|)) \quad (4.19)$$

where $\Lambda(|\omega_m|)$ indicates a correction term with the lowest exponent in $|\omega_m|$ of four and is given by

$$\Lambda(|\omega_m|) = \sum_{k=2}^{\infty} \frac{(\mathbb{E}_{\mathbf{Z}} \{ \mathbf{Z} \})^k |\omega_m|^{2k} r^{-k\gamma}}{2^{2k} k!} \mathbb{E}_{\mathbf{Z}} \left\{ {}_1F_1 \left(-k; 1; \frac{\mathbf{Z}}{\mathbb{E}_{\mathbf{Z}} \{ \mathbf{Z} \}} \right) \right\} \quad (4.20)$$

where the random variable $\mathbf{Z} = \mathbf{h}^2 \mathbf{B}^2$, and ${}_1F_1(a; b; x)$ is the confluent hypergeometric function of the first kind. Also $\Lambda(|\omega_m|) = O(|\omega_m|^4)$ as $|\omega_m| \rightarrow 0$.

Using this identity, and approximating $\Lambda(|\omega_m|) \ll 1$ for $|\omega_m|, m = 1, \dots, n$ in the neighborhood of zero, (4.18) reduces to

$$\Upsilon_{(k,s)}(\bar{\omega}_{1:n}) \approx - \int_0^{\infty} \frac{\partial}{\partial r} \left(e^{-\frac{\left(\sum_{m=\max(1,k)}^s |\omega_m|^2 \right) r^{-\gamma} \mathbb{E}_{\mathbf{h}, \mathbf{B}} \{ \mathbf{h}^2 \mathbf{B}^2 \}}{4}} \right) r^2 dr \quad (4.21)$$

$$= - \left[\left(\sum_{m=\max(1,k)}^s |\omega_m|^2 \right) \frac{\mathbb{E}_{\mathbf{h}, \mathbf{B}} \{ \mathbf{h}^2 \mathbf{B}^2 \}}{4} \right]^{\frac{2}{\gamma}} \Gamma \left(1 - \frac{2}{\gamma} \right) \quad (4.22)$$

where $\Gamma(\cdot)$ denotes the Gamma function. When \mathbf{hB} is Rayleigh distributed, e.g., for constant amplitude modulated transmissions in Rayleigh fading environment, then $\mathbf{\Lambda}(|\omega_m|) = 0$ and the expression in (4.21) is exact. Substituting (4.22) in (4.15), the log-characteristic function can be expressed as

$$\psi_{\bar{\mathbf{I}}_{k,1:n}}(\bar{\omega}_{1:n}) = -\bar{\sigma} \left[\sum_{s=1}^n \bar{F}_{\mathbf{L}}^{(k,n)}(s) \left(\sqrt{\sum_{m=\max(1,k)}^s |\omega_m|^2} \right)^{\frac{4}{\gamma}} \right] \quad (4.23)$$

where $\bar{\sigma} = \lambda\pi \left(\frac{\mathbb{E}_{\mathbf{h},\mathbf{B}}\{\mathbf{h}^2\mathbf{B}^2\}}{4} \right)^{\frac{2}{\gamma}} \Gamma\left(1 - \frac{2}{\gamma}\right)$ and $\bar{F}_{\mathbf{L}}^{(k,n)}(\cdot)$ is defined in (4.14). Equation (4.23) is the log-characteristic function of a $2n$ -dimensional symmetric alpha stable vector with characteristic exponent $\alpha = \frac{4}{\gamma}$. To gain some intuition in the form of the joint log-characteristic function, let us consider the following example.

Example: Using (4.23), the joint log-characteristic function of interference at time slots 1 through 3 ($n = 3$) for cases when the interfering nodes first emerged at time slots $k = 0, 1$, and 2 are

$$\begin{aligned} \psi_{\bar{\mathbf{I}}_{0,1:3}} &= -\bar{\sigma} \left[\mathbb{P}(\mathbf{L}=2) \left(\sqrt{|\omega_1|^2} \right)^\alpha + \mathbb{P}(\mathbf{L}=3) \left(\sqrt{|\omega_1|^2 + |\omega_2|^2} \right)^\alpha \right. \\ &\quad \left. + \mathbb{P}(\mathbf{L} \geq 4) \left(\sqrt{|\omega_1|^2 + |\omega_2|^2 + |\omega_3|^2} \right)^\alpha \right], \\ \psi_{\bar{\mathbf{I}}_{1,1:3}} &= -\bar{\sigma} \left[\mathbb{P}(\mathbf{L}=1) \left(\sqrt{|\omega_1|^2} \right)^\alpha + \mathbb{P}(\mathbf{L}=2) \left(\sqrt{|\omega_1|^2 + |\omega_2|^2} \right)^\alpha \right. \\ &\quad \left. + \mathbb{P}(\mathbf{L} \geq 3) \left(\sqrt{|\omega_1|^2 + |\omega_2|^2 + |\omega_3|^2} \right)^\alpha \right], \\ \psi_{\bar{\mathbf{I}}_{2,1:3}} &= -\bar{\sigma} \left[\mathbb{P}(\mathbf{L}=1) \left(\sqrt{|\omega_2|^2} \right)^\alpha + \mathbb{P}(\mathbf{L} \geq 2) \left(\sqrt{|\omega_2|^2 + |\omega_3|^2} \right)^\alpha \right]. \end{aligned}$$

The parameter λ embedded inside $\bar{\sigma}$ along with the probability on the random variable \mathbf{L} forms a pre-multiplier to the terms $\left(\sqrt{\sum_m |\omega_m|^2}\right)^\alpha$ representing the density of users that affect the interference only at the time slots involved. Thus the pre-multiplier to $\left(\sqrt{|\omega_1|^2 + |\omega_2|^2}\right)^\alpha$ represents the density of users that affect the interference at time slots 1 and 2 only, which is $\lambda\mathbb{P}(\mathbf{L} = 2)$ if nodes emerged at time slot 1, $\lambda\mathbb{P}(\mathbf{L} = 3)$ if nodes emerged at time slot 0, and 0 if nodes emerged only at time slot 2.

4.3.2 Network Model II

Let $\bar{\mathbf{I}}_{1:n} = \{\mathbf{I}_1^{(I)}, \mathbf{I}_1^{(Q)}, \mathbf{I}_2^{(I)}, \mathbf{I}_2^{(Q)}, \dots, \mathbf{I}_n^{(I)}, \mathbf{I}_n^{(Q)}\}$ denote the vector of in-phase and quadrature phase components on the interference at time slots 1 through n due to nodes that emerged anytime until slot n . Using (4.4) and noting that the underlying Poisson process of emerging nodes at any time slots k are mutually independent for all k , the joint log-characteristic function of $\bar{\mathbf{I}}_{1:n}$ can be expressed as

$$\psi_{\bar{\mathbf{I}}_{1:n}}(\bar{\omega}_{1:n}) = \sum_{k=-\infty}^n \psi_{\bar{\mathbf{I}}_{k,1:n}}(\bar{\omega}_{1:n}). \quad (4.24)$$

Substituting (4.23) in (4.24), the log-characteristic function can be expanded as

$$\begin{aligned} \psi_{\bar{\mathbf{I}}_{1:n}}(\bar{\omega}_{1:n}) = & \\ & - \bar{\sigma} \left[\mathbb{P}(\mathbf{L} \geq 1) \left(\left(\sqrt{|\omega_1|^2}\right)^\alpha + \left(\sqrt{|\omega_n|^2}\right)^\alpha \right) + \mathbb{P}(\mathbf{L} = 1) \left(\sum_{l=2}^{n-1} \left(\sqrt{|\omega_l|^2}\right)^\alpha \right) \right. \\ & \left. + \mathbb{P}(\mathbf{L} \geq 2) \left(\left(\sqrt{|\omega_1|^2 + |\omega_2|^2}\right)^\alpha + \left(\sqrt{|\omega_{n-1}|^2 + |\omega_n|^2}\right)^\alpha \right) \right] \end{aligned}$$

$$\begin{aligned}
& + \mathbb{P}(\mathbf{L} = 2) \left(\sum_{l=2}^{n-2} \left(\sqrt{|\omega_l|^2 + |\omega_{l+1}|^2} \right)^\alpha \right) \\
& + \vdots \\
& + \mathbb{P}(\mathbf{L} \geq n-1) \left(\left(\sqrt{|\omega_1|^2 + \dots + |\omega_{n-1}|^2} \right)^\alpha + \left(\sqrt{|\omega_2|^2 + \dots + |\omega_n|^2} \right)^\alpha \right) \\
& + (\mathbb{P}(\mathbf{L} \geq n) + \mathbb{P}(\mathbf{L} \geq n+1) + \dots) \left(\sqrt{|\omega_1|^2 + |\omega_2|^2 + \dots + |\omega_n|^2} \right)^\alpha \Big]
\end{aligned} \tag{4.25}$$

where $\bar{\sigma} = \lambda\pi \left(\frac{\mathbb{E}_{\mathbf{h}, \mathbf{B}} \{ \mathbf{h}^2 \mathbf{B}^2 \}}{4} \right)^{\frac{2}{\gamma}} \Gamma \left(1 - \frac{2}{\gamma} \right)$. Equation (4.25) is the log-characteristic function of a $2n$ -dimensional symmetric alpha stable vector with characteristic exponent $\alpha = \frac{4}{\gamma}$. Analogous to network model I, further intuition can be gained by viewing the pre-multiplicative factor of each of $\left(\sqrt{\sum_m |\omega_m|^2} \right)^\alpha$ as the density of users that affect the interference only at the time slots involved.

4.3.3 Joint Tail Probability of Interference Amplitude

Closed-form expressions for the joint interference tails of the following form are required:

$$\mathbb{P}(\Delta > n) = \mathbb{P}(\|\mathbf{I}_1\| > \beta_1, \|\mathbf{I}_2\| > \beta_2, \dots, \|\mathbf{I}_n\| > \beta_n). \tag{4.26}$$

For simplicity in exposition, non-random thresholds β_i are assumed in this subsection. Recall that for analysis of network model I, $k = 1$ can be assumed without loss of generality. Hence, I use \mathbf{I}_n to denote the interference at time slot n for both the network models.

For both the network models, the joint characteristic function of interference at time slots 1 through n was shown to follow a $2n$ -dimensional sym-

metric alpha stable distribution. Even though the joint characteristic function of interference are derived in a known form, expressing the joint tail probability in closed-form turns out to be nontrivial. Referring to (4.23) and (4.25), the log-characteristic function is a sum of many $\left(\sqrt{\sum_m |\omega_m|^2}\right)^\alpha$ terms. To the best of my knowledge, no direct result is available in the literature to aid the derivation of (4.26) in closed-form for this specific form of joint characteristic function. To this end, I provide certain useful theorems regarding the tail probability of symmetric alpha stable vectors with the same mathematical form as (4.23) and (4.25).

I now briefly describe the steps required to derive the joint tail probability in closed-form using the results proved in Appendix A. Theorem A.5 is the key underlying theorem, and expresses the tail probability of the form (4.26) in terms of the symmetric alpha stable spectral measure in an integral form. The spectral measure, along with the characteristic exponent α , completely characterize the statistics of a symmetric alpha stable vector (see Theorem A.1). Further, for the log-characteristic function of the form (4.23) and (4.25), the spectral measure $\bar{\Gamma}$ on the $2n$ -dimensional unit sphere S_{2n} can be represented as a sum of independent measures

$$\bar{\Gamma} = \bar{\Gamma}_0 + \sum_{k=1}^{|\mathcal{X}|} \bar{\Gamma}_k \delta \left(\bigcup_{j \in \mathcal{X}(k)} \{s_{2j-1}, s_{2j}\} \right), \quad (4.27)$$

where \mathcal{X} is an arbitrary collection of non-empty proper subsets of $\{1, 2, \dots, n\}$, $|\mathcal{X}|$ denotes the cardinality of \mathcal{X} , $\mathcal{X}(k)$ denotes the k^{th} set contained in \mathcal{X} , $\delta(\dots)$ denotes the multi-dimensional dirac delta functional, $s \in S_{2n}$, $\bar{\Gamma}_0$ is a

spectral measure distributed over the unit sphere S_{2n} , and $\bar{\Gamma}_k$ is a spectral measure distributed over the unit sphere $S_{2(n-|\mathcal{X}(k)|)}$ formed from the dimensions $\cup_{j=1, \dots, 2n; j \notin \mathcal{X}(k)} \{2j-1, 2j\}$.

Example: From (4.25), the joint log-characteristic function for interference at time slots 1 through 3 ($n = 3$) for network model II can be represented as

$$\begin{aligned} \psi_{\bar{\mathbf{I}}_{1:3}}(\bar{\omega}_{1:3}) &= -\bar{\sigma} \left[\mathbb{P}(\mathbf{L} \geq 1) \left(\left(\sqrt{|\omega_1|^2} \right)^\alpha + \left(\sqrt{|\omega_3|^2} \right)^\alpha \right) + \mathbb{P}(\mathbf{L} = 1) \left(\sqrt{|\omega_2|^2} \right)^\alpha \right. \\ &\quad + \mathbb{P}(\mathbf{L} \geq 2) \left(\left(\sqrt{|\omega_1|^2 + |\omega_2|^2} \right)^\alpha + \left(\sqrt{|\omega_2|^2 + |\omega_3|^2} \right)^\alpha \right) \\ &\quad \left. + (\mathbb{P}(\mathbf{L} \geq 3) + \mathbb{P}(\mathbf{L} \geq 4) + \dots) \left(\sqrt{|\omega_1|^2 + |\omega_2|^2 + |\omega_3|^2} \right)^\alpha \right]. \end{aligned} \quad (4.28)$$

Using Theorem A.2, the spectral measure $\bar{\Gamma}$ of $\bar{\mathbf{I}}_{1:3}$ on the unit sphere S_6 can then be expressed as

$$\begin{aligned} \bar{\Gamma} &= \bar{\Gamma}_0 + \bar{\Gamma}_1 \delta(s_1, s_2) + \bar{\Gamma}_2 \delta(s_5, s_6) + \bar{\Gamma}_3 \delta(s_1, s_2, s_3, s_4) + \bar{\Gamma}_4 \delta(s_3, s_4, s_5, s_6) \\ &\quad + \bar{\Gamma}_5 \delta(s_1, s_2, s_5, s_6) \end{aligned} \quad (4.29)$$

where $\bar{\Gamma}_0$ is uniformly distributed over unit sphere S_6 . $\bar{\Gamma}_1$ and $\bar{\Gamma}_2$ are uniformly distributed over S_4 formed from the dimensions $\{3, 4, 5, 6\}$ and $\{1, 2, 3, 4\}$, respectively. $\bar{\Gamma}_3$, $\bar{\Gamma}_4$, and $\bar{\Gamma}_5$ are uniformly distributed over S_2 formed from the dimensions $\{5, 6\}$, $\{1, 2\}$, and $\{3, 4\}$, respectively. Here $\bar{\Gamma}_1 \delta(s_1, s_2)$ leads to the term $\left(\sqrt{|\omega_2|^2 + |\omega_3|^2} \right)^\alpha$, $\bar{\Gamma}_3 \delta(s_1, s_2, s_3, s_4)$ leads to the term $\left(\sqrt{|\omega_3|^2} \right)^\alpha$, and so on, in the log-characteristic function. Further, spectral measure (4.29) corresponds to $\mathcal{X} = \{\{1\}, \{3\}, \{1, 2\}, \{2, 3\}, \{1, 3\}\}$ when expressed as (4.27).

For symmetric alpha stable vectors with a spectral measure of the form (4.27), Corollary A.6 proves that the joint tail probability of the form (4.26) depends on the measure $\bar{\Gamma}_0$ alone. In other words, the joint tails depend only on the $\left(\sqrt{|\omega_1|^2 + \dots + |\omega_n|^2}\right)^\alpha$ term in the log-characteristic function when $\beta_1, \dots, \beta_n \rightarrow \infty$ with the same rate. Further, since the spectral measure $\bar{\Gamma}_0$ is uniformly distributed over unit sphere, it implies that the tails are equivalent to the tails of an isotropic symmetric alpha stable vector with spectral measure $\bar{\Gamma}_0$ (see Theorem A.2). For an isotropic symmetric alpha stable vector, Corollary A.3 derives the tail probability in closed-form.

Formalizing the aforementioned proof outline, if $\beta_i = \beta\eta_i$ for $0 < \eta_i < \infty$, then

$$\begin{aligned} & \lim_{\beta \rightarrow \infty} \left(\sqrt{\sum_{i=1}^n \beta_i^2} \right)^\alpha \mathbb{P}(\Delta > n) \\ &= \lim_{\beta \rightarrow \infty} \left(\sqrt{\sum_{i=1}^n \beta_i^2} \right)^\alpha \mathbb{P}(\|\mathbf{I}_1\| > \beta_1, \|\mathbf{I}_2\| > \beta_2, \dots, \|\mathbf{I}_n\| > \beta_n) \quad (4.30) \\ &= \lim_{\beta \rightarrow \infty} \left(\sqrt{\sum_{i=1}^n \beta_i^2} \right)^\alpha \mathbb{P}\left(\sqrt{\mathbf{Y}_1^2 + \mathbf{Y}_2^2} > \beta_1, \dots, \sqrt{\mathbf{Y}_{2n-1}^2 + \mathbf{Y}_{2n}^2} > \beta_n\right) \end{aligned}$$

$$= 2^\alpha \bar{\sigma} \mathcal{F}_{\mathbf{L}}(n) C_{\frac{\alpha}{2}} \cos\left(\frac{\pi\alpha}{4}\right) \Gamma\left(1 + \frac{\alpha}{2}\right) \quad (4.32)$$

where

$$\mathcal{F}_{\mathbf{L}}(n) = \begin{cases} \mathbb{P}(\mathbf{L} \geq n) & \text{for network model I,} \\ \sum_{k=n}^{\infty} \mathbb{P}(\mathbf{L} \geq k) & \text{for network model II,} \end{cases} \quad (4.33)$$

$C_{\frac{\alpha}{2}}$ is given by (A.5), and $\{\mathbf{Y}_1, \dots, \mathbf{Y}_{2n}\}$ is an isotropic symmetric alpha

stable vector with characteristic exponent α and dispersion parameter $\bar{\sigma}\mathcal{F}_{\mathbf{L}}(n)$. Equation (4.31) follows from Corollary A.6, Theorem A.2, and noting that the spectral measure of $\bar{\mathbf{I}}_{1:n}$ for both the network models is of the form (4.29) with $\bar{\Gamma}_0$ uniformly distributed over S_{2n} . Equation (4.32) follows from Corollary A.3, and the log-characteristic functions of network models I and II given by (4.23) and (4.25), respectively. Thus for β_1, \dots, β_n large,

$$\mathbb{P}(\Delta > n) \approx \left(\sqrt{\sum_{i=1}^n \beta_i^2} \right)^{-\alpha} 2^\alpha \bar{\sigma}\mathcal{F}_{\mathbf{L}}(n) C_{\frac{\alpha}{2}} \cos\left(\frac{\pi\alpha}{4}\right) \Gamma\left(1 + \frac{\alpha}{2}\right). \quad (4.34)$$

Intuitively, the joint tail probability is dominated by the term $\left(\sqrt{|\omega_1|^2 + \dots + |\omega_n|^2} \right)^\alpha$ in the log-characteristic function since this term corresponds to the contribution by the nodes that are active at all time slots 1 through n . The event that the interference amplitude is high at all time slots 1 through n is more likely to be due to the nodes that were active at all time slots, rather than due to nodes that were active in only some of those time slots.

4.4 Single Hop Communication Performance Analysis

In this section, the closed-form expression for the joint tail probability of interference is used to derive the following measures of communication performance for single hop transmissions: local delay, throughput outage probability, average network throughput, and transmission capacity. The closed-form tail probability expressions yield simple algebraic form for these measures, providing insight into the effect of various network parameters on communication

performance of the network. For both the network models, I assume the performance of the network is interference limited and the thermal noise present at the receiver can be ignored in comparison to interference.

4.4.1 Local Delay

Local delay (LD) of the network is defined as the expected number of time slots a typical node requires for a successful transmission to its receiver. In other words, the local delay is one more than the expected number of successive failed transmission attempts ($\mathbb{E}\{\Delta\}$) of a typical node. Noting that a node is active for a maximum of L_{max} time slots, the local delay of the network can be expressed as

$$\text{LD} = 1 + \mathbb{E}\{\Delta\} \quad (4.35)$$

$$= 1 + \sum_{n=1}^{L_{max}} \mathbb{P}(\text{SIR}_1 < T, \text{SIR}_2 < T, \dots, \text{SIR}_n < T) \quad (4.36)$$

$$= 1 + \sum_{n=1}^{L_{max}} \mathbb{P}(\|\mathbf{I}_1\| > \beta_1, \|\mathbf{I}_2\| > \beta_2, \dots, \|\mathbf{I}_n\| > \beta_n) \quad (4.37)$$

where $\beta_n^2 = T^{-1}D^{-\gamma}\mathbf{h}_0^2(n)\mathbf{B}_0^2(n)$, and T is the SIR threshold required for successful detection. I assume that $T \ll 1$ which will be valid for spread spectrum physical layer where T^{-1} is proportional to the spreading gain. Thus the local delay can be expressed as the joint tail probability of interference. For $T \ll 1$, β_n is large and thus by using (4.34) gives

$$\text{LD} \approx 1 + T^{\frac{\alpha}{2}}D^2\lambda K(\alpha) (\mathbb{E}\{\mathbf{h}^2\mathbf{B}^2\})^{\frac{\alpha}{2}} \sum_{n=1}^{L_{max}} \left[\mathbb{E} \left\{ \left(\sum_{k=1}^n \mathbf{h}_0^2(k)\mathbf{B}_0^2(k) \right)^{-\frac{\alpha}{2}} \right\} \mathcal{F}_{\mathbf{L}}(n) \right] \quad (4.38)$$

where

$$K(\alpha) = \pi C_{\frac{\alpha}{2}} \cos\left(\frac{\pi\alpha}{4}\right) \Gamma\left(1 - \frac{\alpha}{2}\right) \Gamma\left(1 + \frac{\alpha}{2}\right). \quad (4.39)$$

Equation (4.38) expresses the local delay for network models I and II in closed-form. The impact of various system parameters on the local delay can now be studied.

User density: The intensity (λ) of the PPP has a linear effect on the local delay of the network.

Power pathloss exponent: Recall that the power pathloss exponent (γ) is related to the characteristic exponent as $\alpha = \frac{4}{\gamma}$. To gain insight into the effect of α on the local delay, let us consider $\mathbb{E}(\Delta)$ for a non-random fading ($\mathbf{h}, \mathbf{h}_0(k)$) and non-random emission amplitudes ($\mathbf{B}, \mathbf{B}_0(k)$). The RHS of (4.38) becomes $T^{\frac{\alpha}{2}} D^2 \lambda K(\alpha) \sum_{n=1}^{L_{max}} n^{-\frac{\alpha}{2}} \mathcal{F}_{\mathbf{L}}(n)$. The factor $K(\alpha)$ does not vary significantly over the meaningful range of pathloss exponent ($2 < \gamma \leq 8$). Since this chapter considers $T \ll 1$, increasing γ (or equivalently decreasing α) increases the local delay $\mathbb{E}(\Delta)$ exponentially. Intuitively, this happens because an interferer close to the desired receiver becomes even more dominant as compared to the desired signal if γ is large.

SIR threshold: Since $\alpha < 2$, local delay scales sublinearly ($T^{\frac{\alpha}{2}}$) with the SIR threshold (T).

Fading: To study the effect of fading, consider non-random emission amplitudes ($\mathbf{B}, \mathbf{B}_0(k)$). Exact evaluation of (4.38) can be done for Rayleigh

fading with parameter $1/\sqrt{2}$ (i.e., $\mathbf{h}_0^2(k) \sim \exp(1)$), giving

$$\text{LD} = 1 + T^{\frac{\alpha}{2}} D^2 \lambda K(\alpha) \sum_{n=1}^{L_{max}} \frac{\Gamma(n - \frac{\alpha}{2})}{(n-1)!} \mathcal{F}_{\mathbf{L}}(n) \quad (\text{Rayleigh Fading}) \quad (4.40)$$

where the factor $\frac{\Gamma(n - \frac{\alpha}{2})}{(n-1)!}$ is approximately equal to $n^{-\frac{\alpha}{2}}$. Further, for any fading and interferer emission distributions, local delay can be lower bounded by using the Jensen's inequality and recalling that $\mathbf{h}_0^2(k)\mathbf{B}_0^2(k)$ are mutually *i.i.d.* for all k , given as

$$\text{LD} \geq 1 + T^{\frac{\alpha}{2}} D^2 \lambda K(\alpha) (\mathbb{E} \{\mathbf{h}^2 \mathbf{B}^2\})^{\frac{\alpha}{2}} \sum_{n=1}^{L_{max}} \left[\left(\mathbb{E} \left\{ \sum_{k=1}^n \mathbf{h}_0^2(k) \mathbf{B}_0^2(k) \right\} \right)^{-\frac{\alpha}{2}} \mathcal{F}_{\mathbf{L}}(n) \right] \quad (4.41)$$

$$= 1 + T^{\frac{\alpha}{2}} D^2 \lambda K(\alpha) \frac{(\mathbb{E} \{\mathbf{h}^2 \mathbf{B}^2\})^{\frac{\alpha}{2}}}{\mathbb{E} \{\mathbf{h}_0^\alpha \mathbf{B}_0^\alpha\}} \sum_{n=1}^{L_{max}} n^{-\frac{\alpha}{2}} \mathcal{F}_{\mathbf{L}}(n). \quad (4.42)$$

Equality in (4.42) is attained, for example, when $\mathbf{h}_0^2(k)\mathbf{B}_0^2(k)$ does not vary with k . Such a situation can occur when the desired node employs channel inversion power control by adapting its instantaneous transmission power $\mathbf{B}_0^2(k)$ to combat the variations due to channel fading $\mathbf{h}_0^2(k)$. Using (4.42), it can be concluded that channel inversion power control reduces the local delay of the network.

Lifetime probability: From (4.38) it can be concluded that the local delay increases as $\mathbb{E}(\mathbf{L})$ increases. This is also intuitively clear as increasing the mean lifetime of nodes causes more interference in the network. Further the static and highly network models studied in prior work [92, 94] can be analyzed as particular cases of the network models I and II.

- (a) Network model I with $\mathbf{L} \xrightarrow{p} \infty$: This would represent a static network with no node mobility, where given a particular instantiation of the PPP, the node actively transmit for a large number of time slots. Here $L_{max} \rightarrow \infty$, $\mathcal{F}_{\mathbf{L}}(n) = 1 \forall n$ from (4.33). Thus the local delay is

$$\text{LD} \geq 1 + T^{\frac{\alpha}{2}} D^2 \lambda K(\alpha) \sum_{n=1}^{\infty} n^{-\frac{\alpha}{2}} \rightarrow \infty \quad (4.43)$$

since $\alpha < 2$. This is the same result as [92, 94] for the Poisson bipolar model with medium access probability of 1 in slotted-ALOHA MAC protocol.

- (b) Network model II with $\mathbf{L} \stackrel{p}{=} 1$: This would represent a highly mobile network, where the location of active nodes at each time slot is an independent instantiation of the PPP. Here $L_{max} = 1$, $\mathcal{F}_{\mathbf{L}}(1) = 1$, and $\mathcal{F}_{\mathbf{L}}(n) = 0$ for $n \geq 2$ from (4.33). The local delay for such a network can be expressed as

$$\text{LD} = 1 + T^{\frac{\alpha}{2}} D^2 \lambda K(\alpha) \frac{(\mathbb{E} \{\mathbf{h}^2 \mathbf{B}^2\})^{\frac{\alpha}{2}}}{\mathbb{E} \{\mathbf{h}_0^\alpha \mathbf{B}_0^\alpha\}} \geq 1 + T^{\frac{\alpha}{2}} D^2 \lambda K(\alpha) \quad (4.44)$$

which is asymptotically ($T \ll 1$) same as the result in [92] for the Poisson bipolar model with Rayleigh fading and medium access probability of 1 in slotted-ALOHA MAC protocol.

4.4.2 Outage with respect to Throughput

Let $\mathbf{S}(n)$ denote the number of successful transmissions in n consecutive time slots. Then the outage probability associated with achieving at least s

successful transmissions in n time slots is

$$\begin{aligned}
& \mathbb{P}(\mathbf{S}(n) < s) \\
&= \mathbb{P}\left(\bigcup_{1 \leq i_1 \leq \dots \leq i_{n-s+1} \leq n} \text{SIR}_{i_1} < T, \dots, \text{SIR}_{i_{n-s+1}} < T\right) \quad (4.45) \\
&= \sum_{k=n-s+1}^n (-1)^{k-(n-s+1)} \binom{k-1}{n-s} \sum_{1 \leq i_1 \leq \dots \leq i_k \leq n} \mathbb{P}(\|\mathbf{I}_{i_1}\| > \beta_{i_1}, \dots, \|\mathbf{I}_{i_k}\| > \beta_{i_k}) \quad (4.46)
\end{aligned}$$

for $1 \leq s \leq n$, where $\beta_i = \beta \eta_i$, $\beta^2 = T^{-1} D^{-\gamma}$, and $\eta_i^2 = \mathbf{h}_0^2(i) \mathbf{B}_0^2(i)$. Now for $I = \{i_1, \dots, i_k\}$,

$$\begin{aligned}
& \lim_{\beta \rightarrow \infty} \left(\sqrt{\sum_{l \in I} \beta_l^2} \right)^\alpha \mathbb{P}(\|\mathbf{I}_{i_1}\| > \beta_{i_1}, \dots, \|\mathbf{I}_{i_k}\| > \beta_{i_k}) \\
&= 2^\alpha \bar{\sigma} \mathcal{M}_{\mathbf{L}}(i_1, i_k) C_{\frac{\alpha}{2}} \cos\left(\frac{\pi\alpha}{4}\right) \Gamma\left(1 + \frac{\alpha}{2}\right) \quad (4.47)
\end{aligned}$$

where

$$\mathcal{M}_{\mathbf{L}}(i, j) = \begin{cases} \mathcal{F}_{\mathbf{L}}(j) & \text{for network model I,} \\ \mathcal{F}_{\mathbf{L}}(j - i + 1) & \text{for network model II} \end{cases} \quad (4.48)$$

can be derived using (4.34) and noting that the log-characteristic function for $\{\mathbf{I}_{i_1}^{(I)}, \mathbf{I}_{i_1}^{(Q)} \dots, \mathbf{I}_{i_k}^{(I)}, \mathbf{I}_{i_k}^{(Q)}\}$ is of the form (4.23) or (4.25) for network models I and II, respectively, with $|\omega_m|$ set to zero for $m \notin I$. Using (4.46) and (4.47), for β large

$$\begin{aligned}
& \mathbb{P}(\mathbf{S}(n) < s) \approx T^{\frac{\alpha}{2}} D^2 \lambda K(\alpha) (\mathbb{E}\{\mathbf{h}^2 \mathbf{B}^2\})^{\frac{\alpha}{2}} \sum_{k=n-s+1}^n (-1)^{k-(n-s+1)} \binom{k-1}{n-s} \\
& \quad \times \sum_{1 \leq i_1 \leq \dots \leq i_k \leq n} \mathbb{E}\left\{ \left(\sum_{l \in I} \mathbf{h}_0^2(l) \mathbf{B}_0^2(l) \right)^{-\frac{\alpha}{2}} \right\} \mathcal{M}_{\mathbf{L}}(i_1, i_k) \quad (4.49)
\end{aligned}$$

$$\begin{aligned}
&= T^{\frac{\alpha}{2}} D^2 \lambda K(\alpha) (\mathbb{E} \{ \mathbf{h}^2 \mathbf{B}^2 \})^{\frac{\alpha}{2}} \sum_{k=n-s+1}^n (-1)^{k-(n-s+1)} \binom{k-1}{n-s} \\
&\quad \times \mathbb{E} \left\{ \left(\sum_{l=1}^k \mathbf{h}_0^2(l) \mathbf{B}_0^2(l) \right)^{-\frac{\alpha}{2}} \right\} \sum_{d=k}^n \mathcal{N}(n, k, d) \mathcal{F}_{\mathbf{L}}(d) \quad (4.50)
\end{aligned}$$

where

$$\mathcal{N}(n, k, d) = \begin{cases} \begin{cases} n & \text{for } k = 1, \\ (n-d+1) \binom{d-2}{k-2} & \text{for } k \geq 2, \end{cases} & \text{for network model I,} \\ \binom{d-1}{k-1} & \text{for network model II.} \end{cases} \quad (4.51)$$

Trends similar to the local delay can be observed for $\mathbb{P}(\mathbf{S}(n) < s)$ as a function of various network parameters. Further, if a node is active for n consecutive time slots, the expected number of successes during those n time slots is given as

$$\mathbb{E} \{ \mathbf{S}(n) \} = n - \sum_{s=1}^n \mathbb{P}(\mathbf{S}(n) < s). \quad (4.52)$$

Using $\mathbb{P}(\mathbf{S}(n) < s)$ and $\mathbb{E} \{ \mathbf{S}(n) \}$, the throughput performance of the network is analyzed in the following subsections for network model II.

4.4.3 Average Network Throughput (Network Model II)

I focus on network model II since the underlying point process of active nodes is statistically invariant across time slots in this case. Recall that at any give time slot, there are $\lambda \mathbb{E} \{ \mathbf{L} \}$ active nodes per unit area on average. Now consider a typical node in the network that is active for l consecutive time slots with probability $\mathbb{P}(\mathbf{L} = l)$. Assume that for each successful transmission, the typical node is able to communicate at $\log_2(1 + T)$ bits/Hz, i.e., the Shannon

rate. In l time slots, the typical node is expected to have $\mathbb{E}\{\mathbf{S}(l)\}$ successful transmissions, or an expected successful transmission rate of $\frac{\mathbb{E}\{\mathbf{S}(l)\}}{l} \log_2(1+T)$ bps/Hz. Averaging this rate over the lifetime distribution of a typical node, the average network throughput can be expressed as

$$\mathbf{c}^{\text{av}} = \lambda \mathbb{E}\{\mathbf{L}\} \log_2(1+T) \mathbb{E}_{\mathbf{L}} \left\{ \frac{\mathbb{E}\{\mathbf{S}(\mathbf{L})\}}{\mathbf{L}} \right\} \quad \text{bps/Hz/area.} \quad (4.53)$$

4.4.4 Transmission Capacity and Throughput-Delay-Reliability (TDR) Tradeoff (Network Model II)

The average throughput of the network discussed in the last subsection does not capture the quality-of-service constraints which may be required in most networks. Motivated by the approach used in [84, 91], I define the transmission capacity of the network and show that it captures the TDR tradeoff.

For single hop transmissions, delay can be interpreted as the number of time slots a typical node has to be active to achieve a desired throughput with a certain reliability. Thus $\mathbb{E}\{\mathbf{L}\}$ is considered to be the delay for single hop transmissions. This definition also enables us to study the TDR tradeoff of the network for different probability mass functions of the time slots that a node is active, $p_{\mathbf{L}}(l)$ for $l \in \{1, \dots, L_{max}\}$, given a delay constraint $\mathbb{E}\{\mathbf{L}\} = \bar{L}$. Further, given an outage constraint of ϵ , let us define

$$s^*(l, \epsilon) = \max \{s : \mathbb{P}(\mathbf{S}(l) < s) \leq \epsilon\} \quad (4.54)$$

as the maximum number of successful transmissions in l time slots that can be achieved with reliability $(1 - \epsilon)$. Hence a successful transmission rate of

$\mathbb{E}_{\mathbf{L}} \left\{ \frac{s^*(\mathbf{L}, \epsilon)}{\mathbf{L}} \right\} \log_2(1 + T)$ bps/Hz can be achieved with reliability of $(1 - \epsilon)$ for each user. I define the transmission capacity of the network as

$$\text{TC}(\bar{L}, \epsilon) \triangleq \max_{\substack{p_{\mathbf{L}}(l), l \in \{1, \dots, L_{max}\}, \\ \mathbb{E}\{\mathbf{L}\} = \bar{L}}} \lambda \bar{L} \log_2(1 + T) \mathbb{E}_{\mathbf{L}} \left\{ \frac{s^*(\mathbf{L}, \epsilon)}{\mathbf{L}} \right\} (1 - \epsilon) \quad \text{bps/Hz/area.} \quad (4.55)$$

Thus transmission capacity captures the TDR tradeoff, where the successful throughput of $\text{TC}(\bar{L}, \epsilon)$ bps/Hz/area can be achieved in a network with reliability constraint of $(1 - \epsilon)$ and delay constraint $\mathbb{E}\{\mathbf{L}\} = \bar{L}$. For a given (\bar{L}, ϵ) pair, $\text{TC}(\bar{L}, \epsilon)$ can be evaluated using numerical optimization of (4.55) over feasible lifetime distributions. Further, for a given distribution of \mathbf{L} , closed-form expression for $\mathbb{P}(\mathbf{S}(n) < s)$ in (4.50) enables direct numerical evaluation of (4.55), without requiring any Monte Carlo simulations of the network.

4.5 Simulation Results

Using the physical model discussed in Section 4.2, I apply Monte Carlo numerical techniques to simulate the dynamics of network models I and II. A typical link is simulated by generating the desired transmission link in the presence of network interference using (4.1) and (4.4) for network models I and II, respectively. The empirical performance measures are then compared against the closed-form expressions for the corresponding measures derived in this chapter. Even though the chapter assumes that T^{-1} is large for deriving closed-form expressions, simulations reveal that the results are almost exact for considerably small values of T^{-1} of around 10 – 20.

Unless mentioned otherwise, the network model parameters used in numerical simulations are:

$$\gamma = 4, \lambda = 0.01, \mathbf{h} \sim \text{Rayleigh} \left(\frac{1}{\sqrt{2}} \right), \mathbf{B} = 5,$$

and the lifetime (\mathbf{L}) of a typical node is assumed to follow a truncated Poisson distribution given as

$$\mathbf{L} \sim \frac{\frac{\bar{L}^l}{l!}}{\sum_{l=1}^{L_{max}} \frac{\bar{L}^l}{l!}} \quad l = 1, \dots, L_{max}, \quad (4.56)$$

where L_{max} and \bar{L} are the maximum and the average number of time slots a node is active, respectively. In simulations, \bar{L} is chosen to be $\frac{L_{max}}{2}$.

4.5.1 Local Delay

Figs. 4.3 and 4.4 compare the empirical and estimated local delay of the network for network models I and II, respectively, as a function of the inverse of the SIR threshold (T^{-1}) required for successful detection. Variation of local delay with various network parameters discussed in Section 4.4.1 can also be observed in Figs. 4.3 and 4.4. Note that transmit power control is implemented by adapting the instantaneous transmission power $\mathbf{B}_0^2(k)$ to the channel fading conditions $\mathbf{h}_0^2(k)$ over time slots k , such that $\mathbf{h}_0^2(k)\mathbf{B}_0^2(k) = \mathbf{B}^2 = 25$.

4.5.2 Outage with respect to Throughput

Figs. 4.5 and 4.6 compare the empirical and estimated probability throughput outage probability for network models I and II, respectively, as

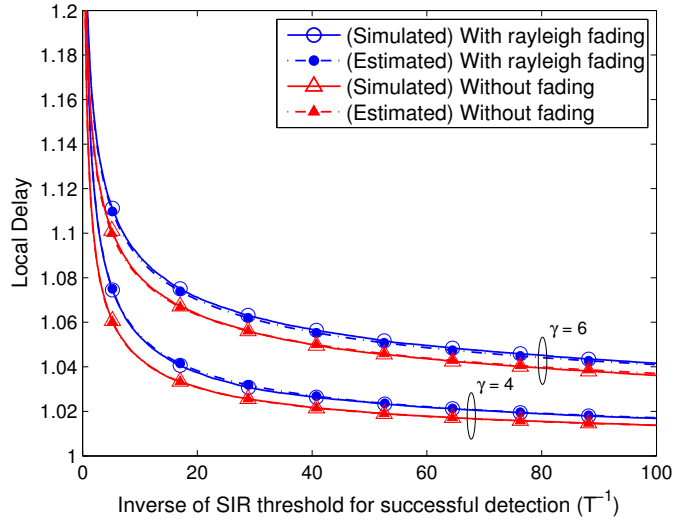


Figure 4.3: Local delay in network model I with and without power control, $L_{max} = 20$ ($\bar{L} = 10$), and power pathloss exponent γ of $\{4, 6\}$. Local delay increases sublinearly as SIR threshold T required for successful detection increases, and exponentially as the power pathloss exponent increases. Channel inversion power control reduces the local delay of the network.

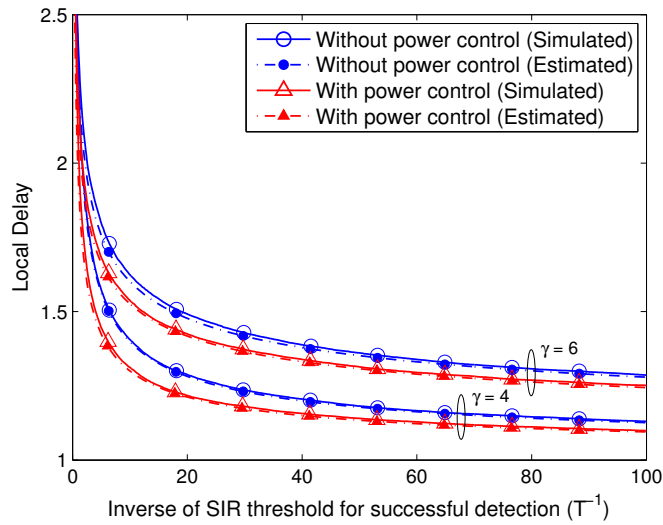


Figure 4.4: Local delay in network model II with and without power control, $L_{max} = 20$ ($\bar{L} = 10$), and power pathloss exponent γ of $\{4, 6\}$. Variations of local delay with various network parameters are similar to those observed for network model I in Fig. 4.3.

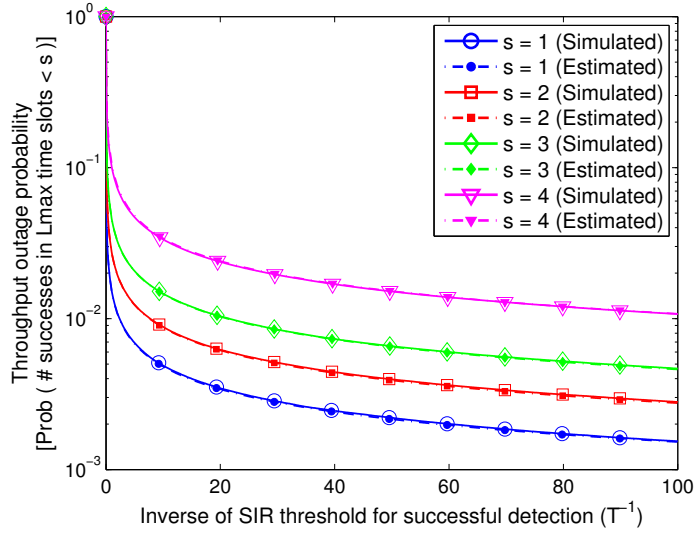


Figure 4.5: Outage probability associated with achieving at least $s = \{1, 2, 3, 4\}$ successes in $L_{max} = 20$ time slots for network model I.

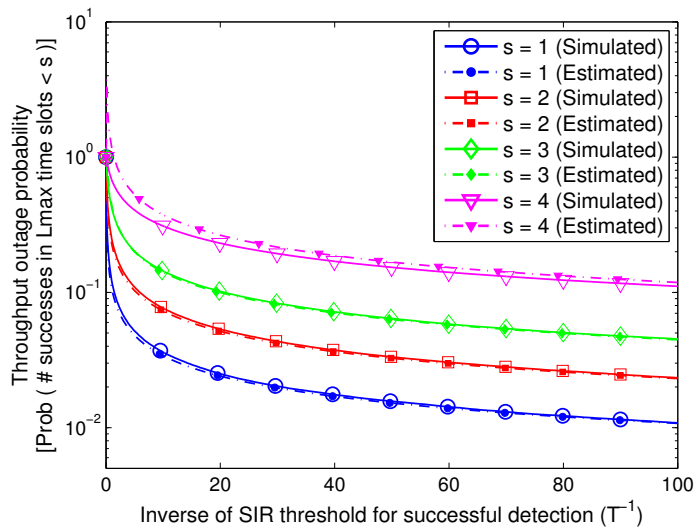


Figure 4.6: Outage probability associated with achieving at least $s = \{1, 2, 3, 4\}$ successes in $L_{max} = 20$ time slots for network model II.

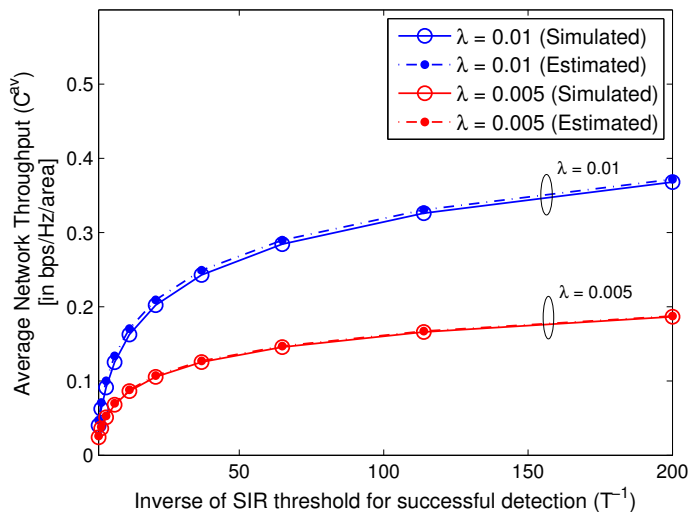


Figure 4.7: Average throughput for network model II for $L_{max} = 10$, $\bar{L} = 5$, and for $\lambda = \{0.01, 0.005\}$. Average throughput decreases as the SIR detection threshold T increases. Average throughput grows sublinearly with λ .

a function of the inverse of the SIR threshold T^{-1} . Note that $\mathbb{P}(\mathbf{S}(L_{max}) < 1)$ ($s = 1$ in Figs. 4.5 and 4.6) corresponds to the probability of outage in all L_{max} time slots, and is equivalent to the joint tail probability of interference over L_{max} time slots ($\mathbb{P}(\Delta > L_{max})$). Hence Figs. 4.5 and 4.6 also serve as a verification of the result on joint tail probability of interference derived in (4.34).

4.5.3 Average Network Throughput (Network Model II)

Fig. 4.7 compares the simulated and estimated average network throughput as a function of T^{-1} for $\lambda = \{0.01, 0.005\}$. Increasing λ results in a increased spatial density of transmissions, but also increases interference at any receiver. Thus the average throughput grows sublinearly with λ .

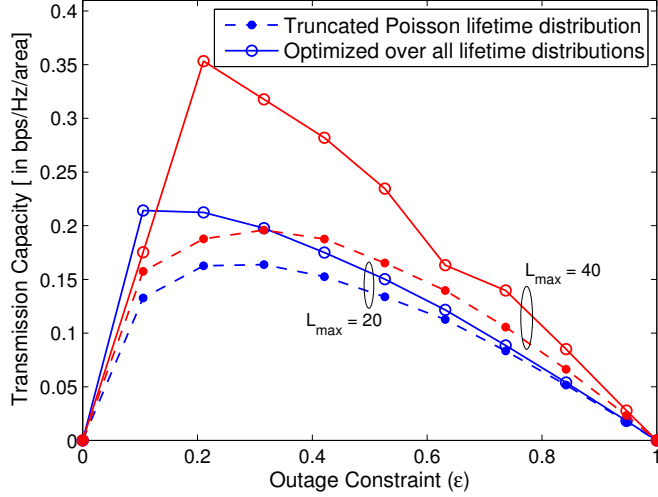


Figure 4.8: Transmission capacity $TC(\bar{L}, \epsilon)$ of network model II as a function of the outage constraint ϵ and delay constraint of $\bar{L} = \frac{L_{max}}{2} = \{20, 10\}$ for a SIR detection threshold T of 0.1. Transmission capacity is plotted for a truncated Poisson lifetime distribution defined in (4.56) and that obtained by optimizing over all feasible lifetime distributions.

4.5.4 Transmission Capacity and Throughput-Delay-Reliability (TDR) Tradeoff (Network Model II)

The transmission capacity $TC(\bar{L}, \epsilon)$ for network model II in (4.55) captures the TDR tradeoff of single hop transmissions. Fig. 4.8 compares the transmission capacity of the network as a function of the outage constraint ϵ . Further the transmission capacity is plotted for the lifetime distribution defined in (4.56) and that obtained by optimizing over all lifetime distributions that satisfy the delay constraint (as expressed in (4.55)). The optimization problem in (4.55) is solved numerically using the `fmincon` function in MATLAB using the active-set algorithm [1]. Following observations can be made regarding the TDR tradeoff of the network from Fig. 4.8.

- When higher outages are tolerable, increasing \bar{L} increases the transmission capacity of the network since the spatial density of users transmitting at any time slot ($= \lambda\bar{L}$) increases more than the loss suffered due to increased interference. When outages are constrained to be low ($\epsilon < 0.1$ in Fig. 4.8), increasing \bar{L} decreases the transmission capacity as interference becomes a limiting factor.
- Optimizing over all feasible lifetime distributions not only increases the peak throughput, but also improves the reliability at which the peak throughput is achieved. Gains in throughput and reliability increase with the increasing \bar{L} . This motivates the design of MAC strategies that achieve the optimal lifetime distribution for improved communication performance of the network.

4.6 Conclusions

The chapter utilized the approximate temporal statistics of interference amplitude to derive network performance measures in simple algebraic form. This approach deviates from the mathematical techniques commonly used in literature for analyzing various network performance measures. While not shown in the chapter, using such common methods to derive measures such as local delay for the network model assumed in this chapter yields rather intractable results, providing minimal insight into the effect of various network parameters on the communication performance. The closed-form expression for various network performance measures, along with the extended definition

of transmission capacity of the network, unveils a potential gain of $2\times$ in network throughput and improved reliability by optimizing over the lifetime distribution.

The results derived in this chapter can be easily extended to include a slotted-ALOHA channel access protocol [55] in conjunction with the network model assumed in the chapter. The analytical form of the results remain the same, with $\mathcal{F}_{\mathbf{L}}(n)$ replaced with $p^n \mathcal{F}_{\mathbf{L}}(n)$, where p is the channel access probability. Further, for a pathloss function of the form $\min(1, r^{-\frac{\alpha}{2}})$, the statistics of interference can be derived using similar steps used in this chapter and shown to follow the multivariate Gaussian mixture distribution [104]. Extensions to networks with contention based MAC protocols, however, appears nontrivial – but approximations may be proposed based on Poisson assumption with a Guard zone, that results in multivariate Gaussian mixture distributed interference [60, 104].

Chapter 5 extends the network model II introduced in this chapter to include a bounded constraint on the pathloss function. Joint temporal statistics of interference are shown to follow a multivariate Gaussian mixture distribution. Chapter 5 utilizes the knowledge of closed-form temporal statistics to design pre-filtering methods to mitigate interference at the receiver.

Chapter 5

Pre-filter Design to Mitigate RFI in Wireless Receivers

5.1 Introduction

Wireless receivers are typically designed assuming additive Gaussian distributed thermal noise in the system. Chapters 1 and 2 emphasized the presence of residual RFI in wireless networks that affects the communication performance of wireless receivers. Chapter 3 derived closed-form instantaneous statistics of residual RFI in a wide variety of wireless networks and showed that RFI follows non-Gaussian impulsive statistics. Chapter 4 extended the RFI statistics for a decentralized wireless network to include temporal dependence in RFI assuming an unbounded pathloss function to model the decay of transmit power with distance. The closed-form temporal statistics were utilized to analyze the throughput, delay, and reliability of single-hop transmissions in a decentralized wireless network. In this chapter, I first use the framework developed in Chapter 3 to derive temporal statistics of RFI in a decentralized wireless network assuming a more realistic bounded pathloss function. The knowledge of the RFI statistics is used to design non-parametric pre-filters to mitigate the residual RFI at the receiver.

5.1.1 Motivation and Prior Work

The increase in the intensity of residual RFI in wireless networks motivates the design of wireless transceivers that are robust to the non-Gaussian statistics of RFI. At the wireless receiver, this translates to deriving accurate statistics of residual RFI and using Bayesian or maximum *a posteriori* inference as a detection criterion. Based on the statistics of RFI, the optimal detection rule may not lead to a receiver structure that is amenable to real-time implementation. In this chapter, I focus on pre-filtering methods to mitigate RFI since they require minimal redesign of conventional receivers that are designed under the assumption of additive Gaussian noise in the system. Pre-filters are placed prior to the conventional receiver with the purpose of removing any outliers in the received samples that may severely affect the communication performance of conventional receivers.

Pre-filters can be classified as parametric or non-parametric. Parametric pre-filters are designed assuming a particular statistical distribution of RFI and require estimation of the parameters that characterize the RFI distribution. Non-parametric pre-filters, on the other hand, may use the knowledge of RFI statistics to choose a design criterion (such as distance measure), but do not require the estimation of any distribution parameters. In most cases, the computational advantage of non-parametric pre-filters that do not require parameter estimation outweighs the incremental improvement in communication performance of parametric pre-filters that utilize the exact RFI distribution. Further, the communication performance of parametric pre-filters may degrade

considerably when the statistics of observed RFI deviates significantly from the statistics assumed during pre-filter design. Non-parametric pre-filters, on the other hand, may be designed to be robust to variations in RFI statistics. This motivates the design of non-parametric pre-filters to mitigate RFI using knowledge of RFI statistics that are applicable to a wide range of interference scenarios, and are yet robust to deviations in RFI statistics.

In this chapter, I assume that a wireless receiver is affected by RFI from a spatial Poisson field of interferers with temporally correlated user locations. As shown in Chapter 4, such a model captures the dynamics of user locations in a decentralized wireless network. Under the assumption of an unbounded pathloss function $l(r) = r^{-\frac{\gamma}{2}}$, where r is the propagation distance and γ is the power pathloss exponent, Chapter 4 shows that the joint temporal statistics of interference follow a multivariate symmetric alpha stable distribution. The assumption of an unbounded pathloss function, however, is not realistic because it suggests that the received interference power is greater than the transmit power when $r < 1$. In this chapter, I assume a bounded pathloss function of the form $l(r) = \min(1, r^{-\frac{\gamma}{2}})$. To the best of my knowledge, closed-form instantaneous or temporal statistics of RFI under the assumption of bounded pathloss function for the network model considered in this chapter is not known. Using the framework developed in Chapters 3 and 4, this chapter shows that the joint temporal statistics of interference follows a multivariate Gaussian mixture distribution under the assumption of a bounded pathloss function. Gaussian mixture distribution is also robust to deviations from the assumptions made

in the network model, e.g., Poisson field of interferers, and has been shown to be applicable in a wide range of interference scenarios in Chapter 3. This motivates the design of pre-filters assuming a multidimensional Gaussian mixture distribution for temporal RFI.

The statistics of RFI affects the design and analysis of pre-filters with respect to the following factors: (i) pre-filter structure, (ii) distance measure, and (iii) lower bound on BER performance. Following is a review of prior work with respect to these factors.

Pre-filter structure: To the best of my knowledge, the optimal pre-filter structure for BER performance in the presence of temporally dependent Gaussian mixture distributed RFI is not known. Pre-filter comprising of a memoryless non-linearity has been shown to be locally optimal when the signal-to-interference ratio is low [134, 135]. Locally optimal non-linearity comprises of a derivative of the RFI distribution function evaluated at the received sample point, and hence requires the estimation of parameters that govern the RFI distribution. Further, a locally optimal non-linearity may exhibit significant degradation in communication performance compared to optimal Bayesian detection at moderate-to-high signal-to-interference ratios [99]. Other non-linearities commonly used to mitigate non-Gaussian RFI include clipping, blanking, and clipping/blanking [97]. While such non-linearities are computationally attractive, their selection and design (clipping and/or blanking thresholds) is rather ad hoc [97].

Mean squared error (MSE) optimal filtering signals in the presence of

additive Gaussian mixture interference was studied in [110–113]. MSE optimal filters for Gaussian mixture interference are composed of a bank of Gaussian optimal filters (Kalman [110, 111], Weiner [112], or Gaussian particle filters [113] based on the statistical assumptions on the signal) whose outputs are combined in a non-linear manner. BER optimality of these pre-filtering methods [110–113], however, is not guaranteed since the minimum MSE criterion is BER optimal only if the noise is Gaussian distributed.

Distance measure: For a given pre-filter structure, the RFI statistics govern the distance measure to be used to design or adapt the pre-filter. To the best of my knowledge, a distance measure that leads to BER optimal design in the presence of Gaussian mixture interference is not known. In this chapter, I propose the use of *correntropy induced metric* (CIM) as a distance measure [2]. The CIM between two points behaves like L_2 norm when the points are close, L_1 as they move apart, and L_0 norm when they are far apart. Varying behavior of the CIM space provides robustness against non-Gaussian RFI [2, 136]. The region of L_2 , L_1 , or L_0 norm like behavior is controlled by a parameter σ_c . The choice of the σ_c is thus central to the applicability and robustness of CIM in non-Gaussian RFI. Prior work has been limited in choosing an appropriate σ_c based on the statistics of the non-Gaussian RFI [137, 138].

In this chapter, I propose to use *zero-order statistics* (ZOS) of the observed Gaussian or non-Gaussian RFI to control the CIM space. ZOS framework was recently proposed as a measure of power of highly impulsive non-Gaussian signals [3]. Unlike L_2 norm as a measure of power, ZOS is resilient to the im-

pulsive nature of the signal and hence provides a fair estimate of power in non-Gaussian environments [3, 101]. This motivates the use of ZOS to scale CIM space according to the signal and non-Gaussian RFI power in the system.

Lower bound of BER: Numerical analysis of an accurate lower bound on BER performance of pre-filter based receivers in the presence of temporally dependent Gaussian mixture distributed RFI is mathematically intractable [139]. Intuitively, BER optimality of the pre-filter can be linked to the ability of a pre-filter to remove the “impulsive component” of RFI from the received samples, such that only the residual “Gaussian part” of RFI is present as a part of the pre-filter output. Here “Gaussian part” of interference is used to represent small variations in the interference that are indistinguishable from a Gaussian distributed random variable with certain power.

5.1.2 Contributions, Organization, and Notation

I derive the joint characteristic function of RFI over multiple time instants in a Poisson field of interferers with temporally correlated interferer locations assuming a bounded pathloss function. The joint characteristic function of RFI is shown to follow a multivariate Gaussian mixture distribution. The knowledge of RFI statistics is used to design pre-filter based receivers that mitigate RFI. While focus is on selection (S) and combination ($L\ell$) pre-filters, a robust framework is proposed that can be used to design a wide range of pre-filters to mitigate non-Gaussian RFI. The robust framework is based on using CIM as a distance measure, and use of ZOS of non-Gaussian RFI to scale

the CIM space. An approximate lower bound on communication performance of pre-filter based receivers is also proposed using the ZOS framework. Tradeoff in communication performance vs. computational complexity of S and $L\ell$ pre-filters designed using L_2 norm, L_1 norm, and CIM as a distance measure is also presented.

The chapter is organized as follows. Section 5.2 discusses the system model. Section 5.3 derives joint temporal statistics of RFI for the network model discussed in the system model. Section 5.4 uses the particular form of RFI statistics derived to motivate the pre-filter design criterion, including a review of CIM and ZOS. Section 5.5 designs the S and $L\ell$ pre-filters using CIM and ZOS based framework. Section 5.6 presents results from numerical simulations. Appendix B contains a brief overview of statistical properties of multivariate Gaussian mixture distributions that are used in the chapter. Table 5.1 summarizes the notation used in this chapter.

5.2 System Model

The following subsection describes the baseband model of transmitter and pre-filter based receiver in the presence of RFI. The network model used to derive RFI statistics is described next.

5.2.1 Baseband Model of Transmitter and Receiver

Fig. 5.1 shows a simplistic baseband model of a typical transmitter and receiver pair in the network. For illustration of pre-filter design and commu-

Table 5.1: Summary of Notation used in Chapter 5

Symbol	Description
$\Pi^{(m)}$	Poisson point process of emerging nodes at time slot m
λ	intensity of $\Pi^{(m)}$
$\Xi_n(\Xi_{k,n})$	point process of nodes active at time slot n (that emerged at time slot k)
$\mathbf{R}, \mathbf{R}^{(m)}$	(random) location of a node in space
$\mathbf{L}, \mathbf{L}^{(m)}$	(random) time slots a node transmits (i.e., lifetime)
γ	power pathloss exponent ($\gamma > 2$)
$\mathbf{X} = \mathbf{B}e^{j\phi}$	amplitude and phase of interferer emissions
$\mathbf{g} = \mathbf{h}e^{j\theta}$	amplitude and phase of narrowband fading
$\mathbf{I}_n(\mathbf{I}_{k,n})$	interference at time slot n (due to nodes that emerged at time slot k)
$\bar{\mathbf{I}}_{k,1:n}$	$\triangleq \{\mathbf{I}_{k,1}^{(I)}, \mathbf{I}_{k,1}^{(Q)}, \dots, \mathbf{I}_{k,n}^{(I)}, \mathbf{I}_{k,n}^{(Q)}\}$, $\mathbf{I}_{k,m} = \mathbf{I}_{k,m}^{(I)} + j\mathbf{I}_{k,m}^{(Q)}$
$\bar{\omega}_{1:n}$	$\triangleq \{\omega_1^{(I)}, \omega_1^{(Q)}, \dots, \omega_n^{(I)}, \omega_n^{(Q)}\}$ frequency variables
$\Phi_{\bar{\mathbf{I}}}(\bar{\omega}_{1:n})$	characteristic function of $\bar{\mathbf{I}}$, where $\bar{\mathbf{I}} = \bar{\mathbf{I}}_{k,n}$ or $\bar{\mathbf{I}}_n$
$\psi_{\bar{\mathbf{I}}}(\bar{\omega}_{1:n})$	log-characteristic function of $\bar{\mathbf{I}}$, where $\bar{\mathbf{I}} = \bar{\mathbf{I}}_{k,n}$ or $\bar{\mathbf{I}}_n$
η, β	obtained from solving (5.15) as shown in Table 3.2
N_T	number of mixture terms per Gaussian component in multivariate Gaussian mixture distribution
$p_i, \sigma_m^2(i)$	mixture probability, variances of Gaussian mixture distribution
C_g	exponential of Euler constant (≈ 1.78)
W	window size of pre-filter
T	number of training symbols
σ_c	size of the Gaussian kernel $\kappa_{\sigma_c}(\cdot, \cdot)$
$\mathbf{M}_{\text{Thres}}$	threshold used for impulse masking in $L\ell$ pre-filter
$\alpha_1, \alpha_2, \alpha_3, \alpha_4$	flexible parameters used in σ_c and $\mathbf{M}_{\text{thres}}$, with suggested values $\alpha_2 \approx 2, \alpha_3 \approx \frac{1}{0.6}, \alpha_4 \approx 2$ (α_1 depends on transmit waveform)
$\bar{W}_{L\ell}$	weight vector of $L\ell$ pre-filter
μ, ϵ	step size, perturbation factor used for adaptive weight update in (5.50) and (5.51)

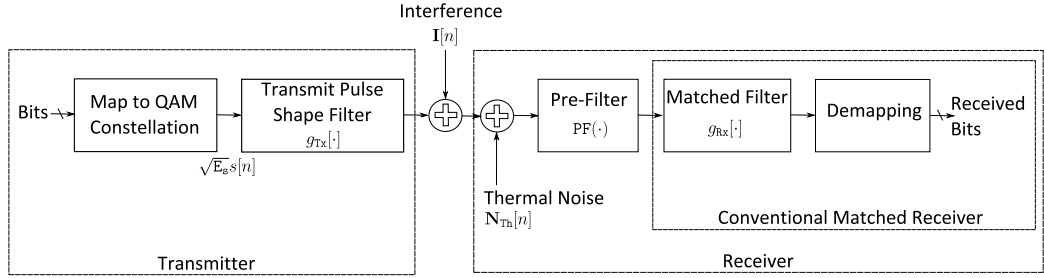


Figure 5.1: Simplistic baseband model of a typical transmitter and receiver pair in the network employing single carrier, uncoded, QAM modulated transmissions.

nication performance analysis, single carrier uncoded transmissions in an additive noise and interference channel is considered. The pre-filters proposed in this chapter are applicable to any practical communication system (e.g., with coding, multi-carrier modulation, random fading, channels with memory).

The discrete time received signal can be expressed as

$$x[n] = \sum_k \sqrt{E_s} s[k] g_{Tx} \left[n - k \frac{T_s}{T_d} \right] + \mathbf{I}[n] + \mathbf{N}_{Th}[n] \quad (5.1)$$

where $x[\cdot]$ is the received sequence of samples, $s[\cdot]$ is the sequence of complex M-QAM modulated symbols, E_s is the received signal energy, $g_{Tx}[\cdot]$ is the transmit pulse shaping filter, T_d is the sampling time period, T_s is the symbol time period, $\mathbf{I}[\cdot]$ is the random interference, and $\mathbf{N}_{Th}[\cdot]$ is the random thermal noise at the receiver. The random thermal noise is assumed to follow a zero mean complex Gaussian distribution with variance σ_{Th}^2 .

The received samples $x[\cdot]$ are pre-filtered before passing them into a receive filter $g_{Rx}[\cdot]$ that is matched to the transmit filter. The aim of the pre-filter is to remove the distortions caused due to the interference $\mathbf{I}[\cdot]$. Accurate

statistical modeling of the interference is thus required for pre-filter design. The following subsection describes the network model assumed to derive the statistics of interference at the receiver. While the baseband model assumed for pre-filter design is simplistic, the interference statistics are designed assuming more general and physically realistic assumptions of any general narrowband emissions which suffer pathloss and narrowband fading before reception at the receiver. Temporal dependence in interference is also captured.

5.2.2 Network Interference Model

This chapter adopts the *Network Model II* introduced in Section 4.2 of Chapter 4 to model interference experienced by a typical receiver in the network and is summarized here for convenience (see Fig. 5.2). While Chapter 4 assumes an unbounded pathloss function, this chapter assumes a more realistic bounded pathloss function.

Time is assumed to be slotted to represent sampling time instants. The locations of interferers, also referred to as nodes, are modeled using a spatial point process. A node is said to *emerge* at a particular time slot if it first starts to transmit at that time slot. All nodes transmitting at a given time slot are referred to as *active* nodes at that time slot. Thus at each time slot n , the set of active nodes is a union over the sets of nodes that first emerged at a slot $m \leq n$ and are still active at the time slot n . Emerging nodes at any time slot m are assumed to be spatially distributed according to a homogeneous PPP $\mathbf{\Pi}^{(m)} = \left\{ \left(\mathbf{R}_i^{(m)}, \mathbf{L}_i^{(m)} \right), i \geq 1 \right\}$ with intensity λ . Here $\mathbf{R}_i^{(m)}$ is the random

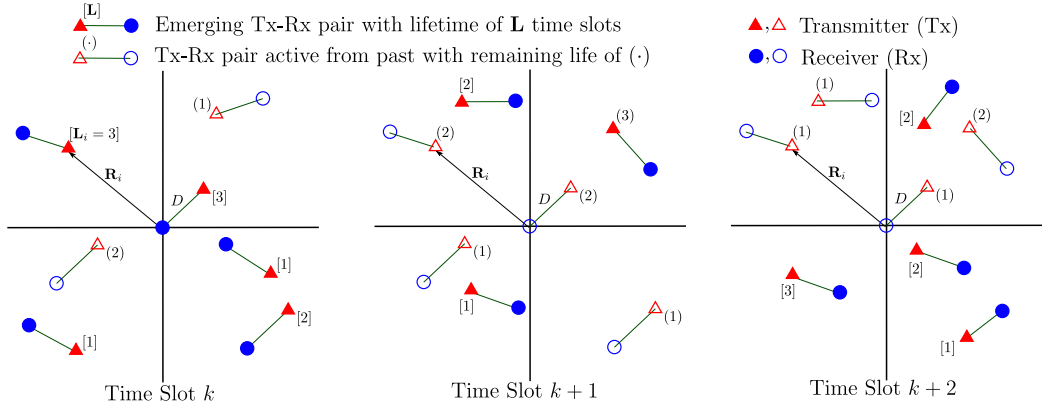


Figure 5.2: Network model used to derive interference statistics. Interferers can emerge at any time slot and are active for a random number of time slots ($= \mathbf{L}$). A bounded pathloss function $l(r) = \min\{1, r^{-\frac{\gamma}{2}}\}$ is assumed, where r is the distance of interferer from the origin and $\gamma = 4$ is the power pathloss exponent.

location of the node i that first emerged at time m , and $\mathbf{L}_i^{(m)} \geq 1$ is the random number of time slots (lifetime) it intends to be active. The node i disappears after $\mathbf{L}_i^{(m)}$ time slots after its emergence at time slot m .

The point process of active nodes at time slot n can then be represented as $\Xi_n = \bigcup_{k=-\infty}^n \Xi_{k,n}$, where $\Xi_{k,n} = \left\{ \mathbf{R} : (\mathbf{R}, \mathbf{L}) \in \Pi^{(k)}, \mathbf{L} \geq n - k + 1 \right\}$ is the set of interferers that first emerged at time slot k and are still active at time n . Note that for $n < k$, $\Xi_{k,n}$ is an empty set. The interference at any time slot n can then be represented as

$$\mathbf{I}_n = \sum_{k=-\infty}^n \mathbf{I}_{k,n} \quad (5.2)$$

$$= \sum_{k=-\infty}^n \left[\sum_{\mathbf{R}_i \in \Xi_{k,n}} l(\mathbf{r}_i) \mathbf{h}_i(n) \mathbf{B}_i(n) (\cos(\phi_i(n) + \theta_i(n)) + j \sin(\phi_i(n) + \theta_i(n))) \right]. \quad (5.3)$$

where $\mathbf{I}_{k,n}$ is the sum interference at time slot n due to interferers that first

emerged at time slot k , i is the interferer index, $\mathbf{r}_i = \|\mathbf{R}_i\|$ are the random distances of active interferers from the receiver, $\mathbf{B}_i(n)e^{j\phi_i(n)}$ are the narrowband interferer emissions from interferer i at time slot n , $\mathbf{h}_i(n)e^{j\theta_i(n)}$ is the narrowband fading experienced by the interferer emissions, and $l(\cdot)$ is the pathloss function. Random variables $\mathbf{B}_i(n), \mathbf{h}_i(n), \phi_i(n), \theta_i(n)$ are each assumed to be *i.i.d.* for every interferer i and time slot n . Assuming the actual emerging time of the interferers to be uniformly distributed between two sampling instants, $\phi_i(n)$ and $\theta_i(n)$ can be assumed to be uniformly distributed on $[0, 2\pi]$. A bounded pathloss function $l(\mathbf{r}_i) = \min\left(1, \mathbf{r}_i^{-\frac{\gamma}{2}}\right)$ is assumed to model the decay in transmit signal power with distance, where γ is the power pathloss exponent. This is a more realistic pathloss model as compared to an unbounded pathloss function $l(\mathbf{r}_i) = \mathbf{r}_i^{-\frac{\gamma}{2}}$ assumed in Chapters 3 and 4.

For the unbounded pathloss function $l(\mathbf{r}_i) = \mathbf{r}_i^{-\frac{\gamma}{2}}$, the joint interference statistics of interference was shown to follow a multivariate symmetric alpha stable distribution in Chapter 4. Deriving closed-form joint interference statistics for a bounded pathloss function $l(\mathbf{r}_i) = \min\left(1, \mathbf{r}_i^{-\frac{\gamma}{2}}\right)$, however, is more involved. The mathematical steps required for deriving the joint interference statistics with a pathloss function $l(\mathbf{r}_i) = \min\left(1, \mathbf{r}_i^{-\frac{\gamma}{2}}\right)$ are similar to deriving the statistics of interference in the presence of guard zone around the receiver. This is because the $\min\left(1, \mathbf{r}_i^{-\frac{\gamma}{2}}\right)$ function creates an artificial guard zone around the receiver, where all interferers that are at a distance $\mathbf{r} < 1$, can be interpreted to be “pushed out” to unit circle around the receiver. The two problems, however, are not equivalent since a physical guard zone around

the receiver implies that the interferers that lie within the unit circle do not contribute to the sum interference at all. Nonetheless, the similarity in mathematical formulation enables us to utilize the mathematical approach used in Chapter 3 to derive closed-form interference statistics in the presence of a guard zone around the receiver.

5.3 Joint Statistics of Interference

In this section, I derive the joint temporal statistics of interference for network model discussed in section 5.2.2. Let $\bar{\mathbf{I}}_{k,1:n} = \{\mathbf{I}_{k,1}^{(I)}, \mathbf{I}_{k,1}^{(Q)}, \dots, \mathbf{I}_{k,n}^{(I)}, \mathbf{I}_{k,n}^{(Q)}\}$ denote the vector of in-phase and quadrature phase components on the interference at time slots 1 through n due to nodes that emerged at time instant k . Similarly, let $\bar{\mathbf{I}}_{1:n} = \{\mathbf{I}_1^{(I)}, \mathbf{I}_1^{(Q)}, \dots, \mathbf{I}_n^{(I)}, \mathbf{I}_n^{(Q)}\}$ denote the vector of in-phase and quadrature phase components on the interference at time slots 1 through n due to nodes that emerged anytime until slot n . Further, let $\bar{\omega}_{1:n} = \{\omega_1^{(I)}, \omega_1^{(Q)}, \dots, \omega_n^{(I)}, \omega_n^{(Q)}\}$ denote the vector of frequency variables. To derive the joint statistics, I consider the nodes distributed over disc of radius R , denoted as $b(0, R)$, and take the limit on the joint distribution as $R \rightarrow \infty$. Using (5.3) and noting that the underlying Poisson process of emerging nodes at any time slot k is mutually independent for all k , the joint characteristic function of $\bar{\mathbf{I}}_{1:n}$ can be expressed as

$$\Phi_{\bar{\mathbf{I}}_{1:n}}(\bar{\omega}_{1:n}) = \prod_{k=-\infty}^n \Phi_{\bar{\mathbf{I}}_{k,1:n}}(\bar{\omega}_{1:n}) \quad (5.4)$$

where $\Phi_{\bar{\mathbf{I}}_{k,1:n}}(\bar{\omega}_{1:n})$ is the joint characteristic function of $\bar{\mathbf{I}}_{k,1:n}$. Equivalently, the joint log-characteristic function of $\psi_{\bar{\mathbf{I}}_{1:n}}(\bar{\omega}_{1:n}) \triangleq \log \Phi_{\bar{\mathbf{I}}_{1:n}}(\bar{\omega}_{1:n})$ can be expressed as

$$\psi_{\bar{\mathbf{I}}_{1:n}}(\bar{\omega}_{1:n}) = \sum_{k=-\infty}^n \psi_{\bar{\mathbf{I}}_{k,1:n}}(\bar{\omega}_{1:n}) \quad (5.5)$$

I first derive the joint characteristic function of $\bar{\mathbf{I}}_{k,1:n}$, and use (5.4) and (5.5) to express the joint characteristic and log-characteristic functions of $\bar{\mathbf{I}}_{1:n}$, respectively.

5.3.1 Joint characteristic function of $\bar{\mathbf{I}}_{k,1:n}$

Using (5.3), the joint log-characteristic function of $\bar{\mathbf{I}}_{k,1:n}$ is given as

$$\psi_{\bar{\mathbf{I}}_{k,1:n}}(\bar{\omega}_{1:n}) = \log \left(\mathbb{E} \left\{ e^{j \sum_{m=1}^n (\omega_m^{(I)} \mathbf{I}_{k,m}^{(I)} + \omega_m^{(Q)} \mathbf{I}_{k,m}^{(Q)})} \right\} \right) \quad (5.6)$$

$$= \lambda \pi \sum_{s=1}^n \bar{F}_{\mathbf{L}}^{(k,n)}(s) \Upsilon_{(k,s)}(\bar{\omega}_{1:n}) \quad (5.7)$$

where for $\gamma > 2$ and any parameters $\{k, s\}$

$$\Upsilon_{(k,s)}(\bar{\omega}_{1:n}) = - \int_0^{\infty} \frac{\partial}{\partial r} \left(\prod_{m=\max(1,k)}^s \mathbb{E}_{\mathbf{h}, \mathbf{B}} \{ J_0(|\omega_m| l(r) \mathbf{h} \mathbf{B}) \} \right) r^2 dr. \quad (5.8)$$

Here $|\omega_m| = \sqrt{(\omega_m^{(I)})^2 + (\omega_m^{(Q)})^2}$, and

$$\bar{F}_{\mathbf{L}}^{(k,n)}(s) = \begin{cases} 0 & s < k, \\ \mathbb{P}(\mathbf{L} = s - k + 1) & k \leq s < n, \\ \mathbb{P}(\mathbf{L} \geq s - k + 1) & s = n. \end{cases} \quad (5.9)$$

Equation (5.7) is obtained using simplifications identical to those used in (4.7) through (4.18) with the pathloss function $\mathbf{r}^{-\frac{\gamma}{2}}$ replaced with a general pathloss

function $l(\mathbf{r})$, and are not repeated here for brevity. The expectation in (5.8) is conditioned such that the node locations are uniformly distributed over $b(0, R)$ [63, 104]. The distance of each node from the typical receiver at the origin thus follows the distribution

$$f_{\mathbf{r}}(r) = \begin{cases} \frac{2r}{R^2} & \text{if } 0 \leq r \leq R, \\ 0 & \text{otherwise.} \end{cases}$$

To the best of my knowledge, exact evaluation of (5.8) for any general distribution of the random variable $\mathbf{h}\mathbf{B}$ is not possible when $s > \max(1, k)$. Under the assumption that $\mathbb{E}_{\mathbf{h}, \mathbf{B}}(\mathbf{h}^2 \mathbf{B}^2)$ is finite, I invoke an identity proposed by Middleton to further simplify (5.8) [12]. The identity, reproduced here for readability, shows that

$$\mathbb{E}_{\mathbf{h}, \mathbf{B}} \{J_0(|\omega_m| l(r) \mathbf{h}\mathbf{B})\} = e^{-\frac{|\omega_m|^2 l(r)^2 \mathbb{E}_{\mathbf{h}, \mathbf{B}}\{\mathbf{h}^2 \mathbf{B}^2\}}{4}} (1 + \Lambda(|\omega_m|)) \quad (5.10)$$

where $\Lambda(|\omega_m|)$ indicates a correction term with the lowest exponent in $|\omega_m|$ of four and is given by

$$\Lambda(|\omega_m|) = \sum_{k=2}^{\infty} \frac{(\mathbb{E}_{\mathbf{Z}}\{\mathbf{Z}\})^k |\omega_m|^{2k} (l(r))^{2k}}{2^{2k} k!} \mathbb{E}_{\mathbf{Z}} \left\{ {}_1F_1 \left(-k; 1; \frac{\mathbf{Z}}{\mathbb{E}_{\mathbf{Z}}\{\mathbf{Z}\}} \right) \right\} \quad (5.11)$$

where the random variable $\mathbf{Z} = \mathbf{h}^2 \mathbf{B}^2$, and ${}_1F_1(a; b; x)$ is the confluent hypergeometric function of the first kind. Also $\Lambda(|\omega_m|) = O(|\omega_m|^4)$ as $|\omega_m| \rightarrow 0$.

Using this identity, and approximating $\Lambda(|\omega_m|) \ll 1$ for $|\omega_m|, m = 1, \dots, n$ in the neighborhood of zero, (5.8) reduces to

$$\Upsilon_{(k,s)}(\bar{\omega}_{1:n})$$

$$\approx - \int_0^{\infty} \frac{\partial}{\partial r} \left(e^{-\frac{\left(\sum_{m=\max(1,k)}^s |\omega_m|^2\right) (l(r))^2 \mathbb{E}_{\mathbf{h}, \mathbf{B}} \{\mathbf{h}^2 \mathbf{B}^2\}}{4}} \right) r^2 dr \quad (5.12)$$

$$= - \sum_{k=1}^{\infty} \frac{\left(- \left(\sum_{m=\max(1,k)}^s |\omega_m|^2 \right) \mathbb{E}_{\mathbf{h}, \mathbf{B}} \{\mathbf{h}^2 \mathbf{B}^2\} \right)^k}{4^k k!} 2k \int_0^{\infty} (l(r))^{2k-1} r^2 \left(\frac{\partial l(r)}{\partial r} \right) dr \quad (5.13)$$

$$= \sum_{k=1}^{\infty} \frac{\left(- \left(\sum_{m=\max(1,k)}^s |\omega_m|^2 \right) \mathbb{E}_{\mathbf{h}, \mathbf{B}} \{\mathbf{h}^2 \mathbf{B}^2\} \right)^k}{4^k k!} \frac{k\gamma}{k\gamma - 2} \quad (5.14)$$

where (5.14) is derived for $l(r) = \min(1, r^{-\frac{\gamma}{2}})$. When $\mathbf{h}\mathbf{B}$ is Rayleigh distributed, e.g., for constant amplitude modulated transmissions in Rayleigh fading environment, then $\mathbf{\Lambda}(|\omega_m|) = 0$ and the expression in (5.14) is exact.

The multiplicative factor $\frac{k\gamma}{k\gamma-2}$ in (5.14) prevents the log-characteristic function to be expressed in closed-form. Similar to the approach used in Chapter 3 (in Section 3.3.3), I approximate $\frac{k\gamma}{k\gamma-2}$ as $1 + \eta e^{\beta k}$. The parameters η and β are chosen to minimize the weighted mean squared error (WMSE)

$$\{\eta, \beta\} = \arg \min_{\eta, \beta} \sum_{k=1}^{\infty} \left(\frac{k\gamma}{k\gamma - 2} - (1 + \eta e^{\beta k}) \right)^2 u(k) \quad (5.15)$$

where $u(k)$ are the weights. Note that the optimization problem (5.15) is the same as (3.31). Table 3.2 lists the values for $\{\eta, \beta\}$ and the associated WMSE for certain values of γ , using the weights $u(k) = e^{-k}$. By approximating $\frac{k\gamma}{k\gamma-2}$ as $1 + \eta e^{\beta k}$ for $k \geq 1$, (5.14) can be expressed as

$$\Upsilon_{(k,s)}(\bar{\omega}_{1:n}) = -(1 + \eta)$$

$$+ e^{-\frac{\left(\sum_{m=\max(1,k)}^s |\omega_m|^2\right) \mathbb{E}_{\mathbf{h}, \mathbf{B}} \{\mathbf{h}^2 \mathbf{B}^2\}}{4}} + \eta e^{-\frac{\left(\sum_{m=\max(1,k)}^s |\omega_m|^2\right) \mathbb{E}_{\mathbf{h}, \mathbf{B}} \{\mathbf{h}^2 \mathbf{B}^2\} e^\beta}{4}}. \quad (5.16)$$

Using (5.7) and (5.16), the log-characteristic function of $\bar{\mathbf{I}}_{k,1:n}$ can be expressed as

$$\begin{aligned} \psi_{\bar{\mathbf{I}}_{k,1:n}}(\bar{\omega}_{1:n}) &= \lambda \pi \left[- \sum_{s=1}^n \bar{F}_{\mathbf{L}}^{(k,n)}(s) (1 + \eta) \right. \\ &\quad \left. + \sum_{s=1}^n \bar{F}_{\mathbf{L}}^{(k,n)}(s) \left(e^{-\frac{\left(\sum_{m=\max(1,k)}^s |\omega_m|^2\right) \mathbb{E}_{\mathbf{h}, \mathbf{B}} \{\mathbf{h}^2 \mathbf{B}^2\}}{4}} + \eta e^{-\frac{\left(\sum_{m=\max(1,k)}^s |\omega_m|^2\right) \mathbb{E}_{\mathbf{h}, \mathbf{B}} \{\mathbf{h}^2 \mathbf{B}^2\} e^\beta}{4}} \right) \right] \end{aligned} \quad (5.17)$$

Equation (5.17) corresponds to a log-characteristic function of a multivariate Gaussian mixture distribution. The joint characteristic function, if expressed directly using (5.17), involves many summations and is omitted for now. Concise expression for the joint characteristic function of $\bar{\mathbf{I}}_{1:n}$ is tackled in the next subsection.

Example: To illustrate the particular form of the joint characteristic function of $\bar{\mathbf{I}}_{k,1:n}$, let us consider an example when $k = 1$ and $n = 2$, i.e., the joint characteristic function of interference at time slots 1 and 2 due to interferers that first emerged at time slot 1. Using (5.17), the joint characteristic function can be expressed as

$$\begin{aligned} \Phi_{\bar{\mathbf{I}}_{1,1:2}}(\bar{\omega}_{1:2}) &= e^{-\lambda \pi (1 + \eta) (\bar{F}_{\mathbf{L}}^{(1,2)}(1) + \bar{F}_{\mathbf{L}}^{(1,2)}(2))} \sum_{k_1=0}^{\infty} \sum_{k_2=0}^{\infty} \sum_{k_3=0}^{\infty} \sum_{k_4=0}^{\infty} \frac{\left(\lambda \pi \bar{F}_{\mathbf{L}}^{(1,2)}(1) \right)^{k_1+k_2} \eta^{k_2}}{k_1! k_2!} \\ &\quad \times \frac{\left(\lambda \pi \bar{F}_{\mathbf{L}}^{(1,2)}(2) \right)^{k_3+k_4} \eta^{k_4}}{k_3! k_4!} e^{-\frac{|\bar{\omega}_1|^2 \mathbb{E} \{\mathbf{h}^2 \mathbf{B}^2\} (k_1+k_2 e^\beta + k_3+k_4 e^\beta)}{4}} e^{-\frac{|\bar{\omega}_2|^2 \mathbb{E} \{\mathbf{h}^2 \mathbf{B}^2\} (k_3+k_4 e^\beta)}{4}}. \end{aligned} \quad (5.18)$$

5.3.2 Joint characteristic function of $\bar{\mathbf{I}}_{1:n}$

Using (5.5) and (5.17), the joint log-characteristic function of $\bar{\mathbf{I}}_{1:n}$ can be expressed as

$$\begin{aligned} \psi_{\bar{\mathbf{I}}_{1:n}}(\bar{\omega}_{1:n}) &= \lambda\pi \sum_{k=-\infty}^n \left[- \sum_{s=1}^n \bar{F}_{\mathbf{L}}^{(k,n)}(s)(1+\eta) \right. \\ &\left. + \sum_{s=1}^n \bar{F}_{\mathbf{L}}^{(k,n)}(s) \left(e^{-\frac{\left(\sum_{m=\max(1,k)}^s |\omega_m|^2\right) \mathbb{E}_{\mathbf{h},\mathbf{B}}\{\mathbf{h}^2\mathbf{B}^2\}}{4}} + \eta e^{-\frac{\left(\sum_{m=\max(1,k)}^s |\omega_m|^2\right) \mathbb{E}_{\mathbf{h},\mathbf{B}}\{\mathbf{h}^2\mathbf{B}^2\} e^\beta}{4}} \right) \right] \end{aligned} \quad (5.19)$$

Since (5.19) is a sum of log-characteristic functions of independent multivariate Gaussian mixture distributed random vectors, $\bar{\mathbf{I}}_{1:n}$ follows a multivariate Gaussian mixture distribution. Combining terms in (5.19), the log-characteristic function can be expressed as

$$\begin{aligned} \psi_{\bar{\mathbf{I}}_{1:n}}(\bar{\omega}_{1:n}) &= -(1+\eta) \sum_{i_1=1}^n \sum_{i_2=i_1}^n N(i_1, i_2) \\ &+ \sum_{i_1=1}^n \sum_{i_2=i_1}^n N(i_1, i_2) \left(e^{-\frac{\sum_{m=i_1}^{i_2} |\omega_m|^2 \mathbb{E}_{\mathbf{h},\mathbf{B}}\{\mathbf{h}^2\mathbf{B}^2\}}{4}} + \eta e^{-\frac{\sum_{m=i_1}^{i_2} |\omega_m|^2 \mathbb{E}_{\mathbf{h},\mathbf{B}}\{\mathbf{h}^2\mathbf{B}^2\} e^\beta}{4}} \right) \end{aligned} \quad (5.20)$$

where

$$N(i_1, i_2) = \lambda\pi \begin{bmatrix} \mathbb{P}(\mathbf{L} \geq 1) & \mathbb{P}(\mathbf{L} \geq 2) & \mathbb{P}(\mathbf{L} \geq 3) & \cdots & \mathbb{P}(\mathbf{L} \geq n-1) & \sum_{k=n}^{\infty} \mathbb{P}(\mathbf{L} \geq k) \\ 0 & \mathbb{P}(\mathbf{L}=1) & \mathbb{P}(\mathbf{L}=2) & \cdots & \mathbb{P}(\mathbf{L}=n-2) & \mathbb{P}(\mathbf{L} \geq n-1) \\ 0 & 0 & \mathbb{P}(\mathbf{L}=1) & \cdots & \mathbb{P}(\mathbf{L}=n-3) & \mathbb{P}(\mathbf{L} \geq n-2) \\ \vdots & \vdots & \ddots & \ddots & \vdots & \vdots \\ 0 & 0 & 0 & \cdots & \mathbb{P}(\mathbf{L}=1) & \mathbb{P}(\mathbf{L} \geq 2) \\ 0 & 0 & 0 & \cdots & 0 & \mathbb{P}(\mathbf{L} \geq 1) \end{bmatrix}. \quad (5.21)$$

Intuition into the above expression can be gained by recognizing that $N(i_1, i_2)$ contributes to the joint log-characteristic function in the dimensions corresponding to $\{\omega_{i_1}^{(I)}, \omega_{i_1}^{(Q)}, \dots, \omega_{i_2}^{(I)}, \omega_{i_2}^{(Q)}\}$. Thus $N(i_1, i_2)/\pi$ is the density of interferers that first emerged at time slot i_1 (or before when $i_1 = 1$, that corresponds to the first row) and are active exactly until time slot i_2 (or beyond for $i_2 = n$, that corresponds to the last column).

Each exponential term in the log-characteristic function leads to a Gaussian mixture series expression in the joint characteristic function. Using (5.20), and truncating each of the Gaussian mixture series summation to N_T terms, the joint characteristic function can be expressed in a more concise and familiar form of a multivariate Gaussian mixture distribution as

$$\Phi_{\bar{\mathbf{I}}_{1:n}}(\bar{\omega}_{1:n}) \approx e^{-(1+\eta) \sum_{i_1=1}^n \sum_{i_2=i_1}^n N(i_1, i_2)} \sum_{i=1}^{(N_T)^{2n!}} \bar{p}(i) e^{-\sum_{m=1}^n \frac{|\omega_m|^2 \bar{\sigma}_m^2(i)}{2}} \quad (5.22)$$

where $\bar{p} = \bigotimes_{i_1=1}^n \left(\bigotimes_{i_2=i_1}^n k_{i_1, i_2} \right)$ is a $(N_T)^{2n!} \times 1$ length vector of mixture probabilities. Here $k_{i_1, i_2} = k_{i_1, i_2}^{(1)} \bigotimes k_{i_1, i_2}^{(2)}$, and for $i_2 \geq i_1$,

$$k_{i_1, i_2}^{(1)}, k_{i_1, i_2}^{(2)} = e^{-(1+\eta) \sum_{i_1=1}^n \sum_{i_2=i_1}^n N(i_1, i_2)} \times \left\{ \left[\begin{array}{c} \frac{(N(i_1, i_2))^0}{0!} \\ \vdots \\ \frac{(N(i_1, i_2))^{N_T-1}}{(N_T-1)!} \end{array} \right], \left[\begin{array}{c} \frac{(\eta N(i_1, i_2))^0}{0!} \\ \vdots \\ \frac{(\eta N(i_1, i_2))^{N_T-1}}{(N_T-1)!} \end{array} \right] \right\}. \quad (5.23)$$

Similarly $\bar{\sigma}_m^2 = \bigoplus_{i_1=1}^n \left(\bigoplus_{i_2=i_1}^n t_{i_1, i_2}^{(m)} \right)$ are a $(N_T)^{2n!} \times 1$ length vector of mixture variances corresponding to the m^{th} component in the joint distribution. Here

$t_{i_1, i_2}^{(m)} = t_{i_1, i_2}^{(m,1)} \oplus t_{i_1, i_2}^{(m,2)}$, and

$$t_{i_1, i_2}^{(m,1)}, t_{i_1, i_2}^{(m,2)} = \frac{\mathbb{E}_{\mathbf{h}, \mathbf{B}} \{\mathbf{h}^2 \mathbf{B}^2\}}{2} \times \begin{cases} \left[\begin{array}{c} 0 \\ \vdots \\ N_T - 1 \end{array} \right], \left[\begin{array}{c} e^\beta \times 0 \\ \vdots \\ e^\beta \times (N_T - 1) \end{array} \right] & \text{if } i_1 \leq m \leq i_2, \\ \left[\begin{array}{c} 0 \\ \vdots \\ 0 \end{array} \right], \left[\begin{array}{c} 0 \\ \vdots \\ 0 \end{array} \right] & \text{otherwise .} \end{cases} \quad (5.24)$$

Note that $\bar{\sigma}_m$ corresponds to the vector of mixture variances for the interference observed at the m time slot. The condition $i_1 \leq m \leq i_2$ in (5.24) can thus be explained as follows. For a interferer to contribute to the m^{th} time slot, it should emerge at a time slot prior to m (i.e., $i_1 \leq m$) and remain active until at least the m^{th} time slot (i.e., $i_2 \geq m$).

Expressing the joint characteristic function of $\bar{\mathbf{I}}_{1:n}$ as (5.22) is helpful in recognizing the multivariate Gaussian mixture form and also enables quick simulation of the joint tail probability of interference. The approximation in (5.22) can be made arbitrarily accurate by increasing N_T .

5.4 Pre-filter Design Criterion

In the last section, the joint temporal statistics of interference under realistic assumptions are shown to follow a multivariate Gaussian mixture distribution. Gaussian mixture distribution is also robust to capture any deviations from the assumptions made in the network model, e.g., Poisson field

of interferers. This motivates the design of pre-filters with the knowledge that the interference observed over consecutive sampling instants follow a multi-dimensional Gaussian mixture distribution. In particular, the following characteristics of interference can be noted. The in-phase and quadrature phase components of interference at any sampling instant are dependent, but uncorrelated. Further, the interference is temporally dependent, but uncorrelated.

The characteristics of interference statistics affects the design and analysis of pre-filtering methods to mitigate RFI. The following subsections review some basic properties of CIM and ZOS that motivate their use in analysis and design of pre-filters.

5.4.1 Correntropy and Correntropy Induced Metric (CIM)

The correntropy of two scalar random variables \mathbf{X} and \mathbf{Y} using a Gaussian kernel function is defined as [2, 138]

$$v(\mathbf{X}, \mathbf{Y}) = \mathbb{E} \{ \kappa_{\sigma_c}(\mathbf{X} - \mathbf{Y}) \} \quad (5.25)$$

$$= \frac{1}{\sqrt{2\pi}\sigma_c} \mathbb{E} \left\{ \exp \left(-\frac{\|\mathbf{X} - \mathbf{Y}\|^2}{2\sigma_c^2} \right) \right\} \quad (5.26)$$

$$= \frac{1}{\sqrt{2\pi}\sigma_c} \sum_{k=0}^{\infty} \frac{(-1)^k}{(2\sigma_c^2)^k k!} \mathbb{E} \{ (\mathbf{X} - \mathbf{Y})^{2k} \} \quad (5.27)$$

where $\kappa_{\sigma_c}(\cdot, \cdot)$ is a Gaussian kernel of size σ_c given as

$$\kappa_{\sigma_c}(X - Y) = \frac{1}{\sqrt{2\pi}\sigma_c} \exp \left(-\frac{\|X - Y\|^2}{2\sigma_c^2} \right). \quad (5.28)$$

Thus correntropy is a similarity measure between scalar random variables \mathbf{X} and \mathbf{Y} that contains all even order moments of $\mathbf{X} - \mathbf{Y}$. The kernel size σ_c in

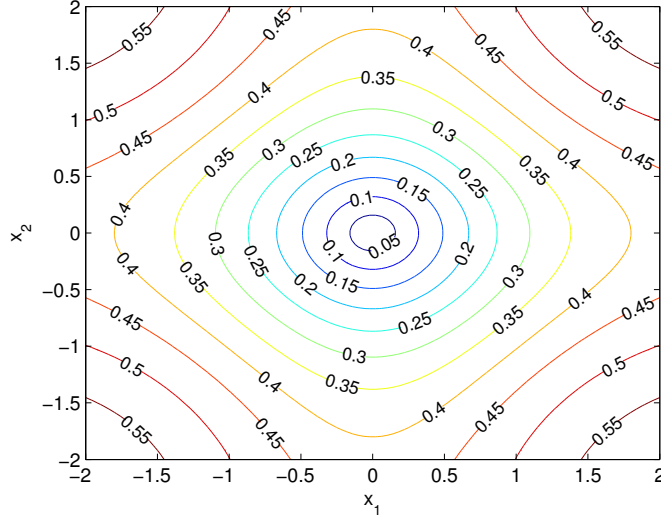


Figure 5.3: Contours of $\text{CIM}(X, 0)$ in a two-dimensional sample space ($N = 2, X = [x_1, x_2]$) for Gaussian kernel size $\sigma_c = 1$. When X is close to the origin, $\text{CIM}(X, 0)$ behaves like L_2 norm. As X moves away from the origin, the behavior of $\text{CIM}(X, 0)$ changes from L_2 norm, to L_1 norm, and to L_0 norm when they are far apart [2].

(5.27) controls the contribution of the higher order moments of $\mathbf{X} - \mathbf{Y}$ with respect to the second moment. Increasing σ_c decreases the contribution of higher order moments and the second order moment dominates. Note that $V(\mathbf{X}, \mathbf{Y})$ is symmetric, positive, and bounded in $\left[0, \frac{1}{\sqrt{2\pi\sigma_c}}\right]$.

When the joint probability density function of $\{\mathbf{X}, \mathbf{Y}\}$ is not known and only finite number of sample instantiations of $\{X, Y\} = \{(x_i, y_i), i = 1, \dots, N\}$ are available, a sample estimate of the correntropy can be expressed as [2]

$$\hat{v}(X, Y) = \frac{1}{N\sqrt{2\pi\sigma_c}} \sum_{i=1}^N \exp\left(-\frac{\|x_i - y_i\|^2}{2\sigma_c^2}\right) \quad (5.29)$$

Correntropy, as a sample estimator, induces a metric space in the sample space and is named as the Correntropy induced metric CIM [2]. However,

CIM is not homogeneous and thus does not induce a norm on the sample space. For N -dimensional vectors $\{X, Y\} = \{(x_i, y_i), i = 1, \dots, N\}$, CIM is defined as

$$\text{CIM}(X, Y) = \sqrt{\frac{1}{\sqrt{2\pi}\sigma_c} - \hat{v}(X, Y)}. \quad (5.30)$$

CIM is bounded in $\left[0, \sqrt{\frac{1}{\sqrt{2\pi}\sigma_c}}\right]$. Fig. 5.3 plots the contours of $\text{CIM}(X, 0)$ in a two-dimensional sample space ($N = 2$) for Gaussian kernel size $\sigma_c = 1$. It can be observed from Fig. 5.3 that CIM behaves like L_2 norm when the two vectors are close, L_1 norm as they move apart, and L_0 norm when they are far apart. As the two vectors grow apart, L_0 norm behavior makes the metric insensitive to the distance. This property of CIM with a Gaussian kernel can thus be exploited for rejection of outliers. For example, in selection filters, the contribution of an outlier in the CIM space is the same to all potential output points and thus does not affect the selection filter output. The kernel size σ_c controls the extend of range over which CIM behaves likes L_2, L_1 , or L_0 norm. The choice of kernel size is hence critical to use CIM to reject outliers.

CIM is also closely related to M-estimation, thus further establishing the robust behavior of CIM to outliers [136]. M-estimation is a generalized maximum likelihood method proposed by Huber to estimate the parameter set Θ from error observations $e[\cdot]$ under the cost function $\min_{\Theta} \sum_{i=1}^N \rho(e[i]|\Theta)$. Here $\rho(\cdot)$ is a differential function that satisfies $\rho(e[i]) \geq 0$, $\rho(e[i]) = 0$, $\rho(e[i]) = \rho(-e[i])$, and $\rho(e[i]) > \rho(e[j])$ for $|e[i]| > |e[j]|$. When $\rho(e[i]) = (e[i])^2$, this corresponds to mean squared error minimization. Defining $\rho(e[i]) = \frac{1}{\sqrt{2\pi}\sigma_c} \left(1 - \exp\left(-\frac{(e[i])^2}{2\sigma_c^2}\right)\right)$, all the aforementioned properties of $\rho(\cdot)$ are sat-

ified, and the M-estimation can be written as

$$\min_{\Theta} \sum_{i=1}^N \rho(e[i]|\Theta) = \min_{\Theta} \sum_{i=1}^N \frac{1}{\sqrt{2\pi}\sigma_c} \left(1 - \exp\left(-\frac{(e[i])^2}{2\sigma_c^2}\right) \right) \quad (5.31)$$

$$= \min_{\Theta} \text{CIM}(E, 0) \quad (5.32)$$

$$= \max_{\Theta} \hat{\mathbf{V}}(E, 0). \quad (5.33)$$

Thus estimating the filter parameters by minimizing CIM of the error sequence corresponds to M-estimation with the function $\rho(e[i]) = \frac{1}{\sqrt{2\pi}\sigma_c} \left(1 - \exp\left(-\frac{(e[i])^2}{2\sigma_c^2}\right) \right)$. The kernel size σ_c controls the robustness to outliers in the estimation problem.

5.4.2 Zero-Order Statistics (ZOS)

L_2 norm is the widely accepted notion of *power* of a second-order random process [140]. For Gaussian random process, this is accurate as the L_2 directly relates to the variance of the process. For non-Gaussian random processes, however, the L_2 norm falls short of being an accurate measure for the signal strength. To this end, ZOS was proposed as a measure of power that is well defined over all distributions with algebraic or lighter tails [3].

Let \mathbf{X} be a logarithmic order random variable with algebraic or lighter tails, such that $\mathbb{E}\{\log|\mathbf{X}|\} < \infty$. Then the ZOS or geometric power of \mathbf{X} is defined as [3]

$$\text{ZOS}(\mathbf{X}) = e^{\mathbb{E}\{\log|\mathbf{X}|\}}. \quad (5.34)$$

When the probability density function of \mathbf{X} is not known and only finite sample instantiations of $X = \{x_i, i = 1, \dots, N\}$ are available, a sample estimator for

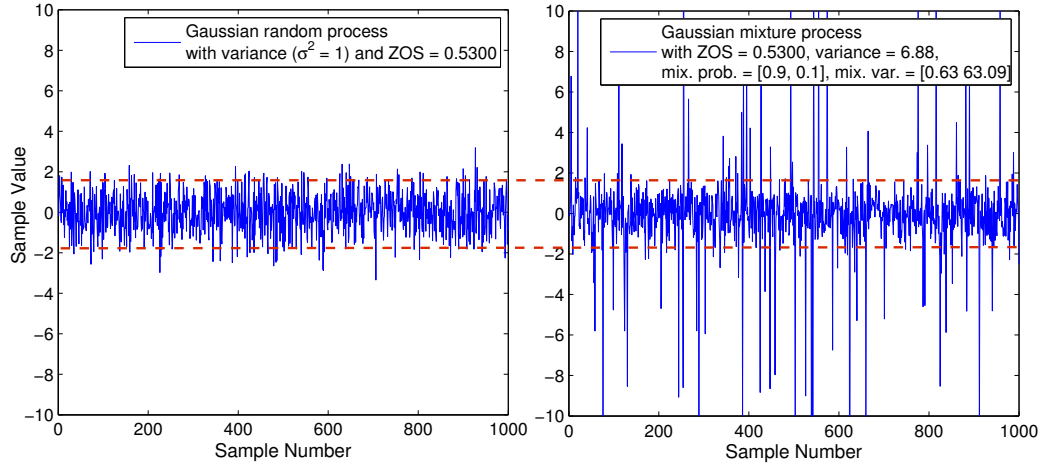


Figure 5.4: Sample snapshot of a Gaussian and Gaussian mixture random process with the same zero-order statistic(ZOS) power. With the same ZOS = 0.5300, smaller variations in the Gaussian mixture random process are indistinguishable from a Gaussian process, as indicated by the dotted lines. A similar illustration is presented in [3] for a symmetric alpha stable random process.

the ZOS can be expressed as

$$\text{ZOS}(X) = \exp\left(\frac{1}{N} \sum_{i=1}^N \log(|x_i|)\right) \quad (5.35)$$

$$= \left(\prod_{i=1}^N |x_i|\right)^{\frac{1}{N}} \quad (5.36)$$

When \mathbf{X}_G is Gaussian distributed with variance σ^2 , $\text{ZOS}(\mathbf{X}_G) = \frac{\sigma}{\sqrt{2C_g}}$, where $C_g \approx 1.78$ is the exponential of the Euler constant [3]. When \mathbf{X}_{GMM} follows a Gaussian mixture distribution with mixture probabilities p_i and mixture variances σ_i^2 for $i = 1, \dots, N$, $\text{ZOS}(\mathbf{X}_{GMM}) = \frac{\prod_{i=1}^N \sigma_i^{p_i}}{\sqrt{2C_g}}$.

Benefit of using ZOS as an estimate of power in very impulsive random variable has been argued in prior work [3]. Intuitively, this is due to the pres-

ence of $\log(\cdot)$ function in (5.34) that causes the lower values of \mathbf{X} to impact the ZOS much more than the higher values. To further illustrate this, Fig. 5.4 compares sample snapshot of two random processes with the same sample estimate of ZOS. With the same ZOS, smaller variations in the Gaussian mixture random process are indistinguishable from a Gaussian process. Thus ZOS can be intuitively argued to capture the strength of the “Gaussian part” in a non-Gaussian random process.

5.4.3 Using CIM and ZOS in pre-filter design

I propose to use CIM as a distance measure to design pre-filters in the presence of Gaussian mixture distributed interference. The distance between two complex sample points $X_1^{(I)} + jX_1^{(Q)}$ and $X_2^{(I)} + jX_2^{(Q)}$ is measured in the CIM space as $\text{CIM}\left(\left[X_2^{(I)} - X_1^{(I)}, X_2^{(Q)} - X_1^{(Q)}\right], [0, 0]\right)$. Further, to reduce the computational complexity, only $\hat{\mathbf{v}}\left(\left[X_2^{(I)} - X_1^{(I)}, X_2^{(Q)} - X_1^{(Q)}\right], [0, 0]\right)$ is required as it has a one-to-one correspondence to $\text{CIM}(\cdot, \cdot)$. $\hat{\mathbf{v}}(\cdot, \cdot)$ and $\text{CIM}(\cdot, \cdot)$ are inversely related and thus a larger $\hat{\mathbf{v}}(\cdot, \cdot)$ between two points indicates smaller distance between them in the CIM space. CIM has the advantage of behaving as L_2 norm for “Gaussian part” of the interference, while being robust to outliers through the use of lower order norms based on the intensity of the interference. In comparison, pre-filters design based on a fixed norm, e.g. L_1 norm, results in degradation in the presence of Gaussian distributed interference due to extra robustness and/or not be robust enough when interference is highly impulsive. Further, from (5.29), the additional complexity in

computing $\hat{V}(\cdot, \cdot)$ over L_2 norm is marginal (one multiplication and table look up for evaluating the exponential).

The choice of the Gaussian kernel size σ_c is central to the flexibility of CIM space. Intuitively, σ_c should be chosen such that the signal and the “Gaussian part” of the interference lies in the L_2 norm region in the CIM space. This motivates the following choice of σ_c :

$$\sigma_c = \frac{1}{\alpha_3} \left(\alpha_1 \sqrt{E_s} + \alpha_2 \sqrt{\sigma_{\text{Th}}^2 + 2C_g (\text{ZOS}(\mathbf{I}))^2} \right). \quad (5.37)$$

Here $2C_g (\text{ZOS}(\mathbf{I}))^2$ is the variance of a Gaussian distribution that has the same ZOS as the interference. From Fig. 5.3, the CIM space switches in behavior from L_2 to L_1 norm when the Euclidean distance between the points is $\alpha_3 \approx 1.5$ for a Gaussian kernel size $\sigma_c = 1$. Equation (5.37) attempts to maintain the same ratio based on maximum variation expected between two sample points. In a local neighborhood, two received samples can be apart by $\alpha_1 \sqrt{E_s}$ due to signal variations, where α_1 depends on the transmit waveform structure. For example, as $\frac{T_a}{T_d}$ increases, the signal variations in consecutive sample decreases. In addition to signal variations, the pre-filter should allow for variations due to thermal noise and the “Gaussian part” of the interference. This is accounted for in the term $\alpha_2 \sqrt{\sigma_{\text{Th}}^2 + 2C_g (\text{ZOS}(\mathbf{I}))^2}$. Thus $\alpha_2 = 2$ may be chosen so that variations up to twice the standard deviation of the Gaussian noise lie within the L_2 norm behavior region of CIM. Variations higher than those expected in (5.37) are most likely due to the impulsive behavior of interference, and the CIM space chooses an appropriate norm behavior to measure the distance.

The CIM space along with the novel choice of Gaussian kernel bandwidth in (5.37) enables use of non-parametric ZOS to adapt to the varying impulsive behavior of the interference environment.

5.4.4 Lower Bound on Error Probability

I propose an approximate lower bound on error probability using ZOS of interference. Lower bound on error probability is derived by assuming that the pre-filter removes all “impulses” from the interference, such that only residual “Gaussian part” of the interference is present at the output. The approximate lower bound can thus be expressed as

$$\text{Pe}^{\text{LB}} \triangleq \text{Pe}^{\text{G}} (\sigma_{\text{Th}}^2 + 2C_g (\text{ZOS}(\mathbf{I}))^2) \quad (5.38)$$

where $\text{Pe}^{\text{G}}(\sigma^2)$ is the error probability of the receiver, that is designed assuming Gaussian noise, in the presence of Gaussian distributed noise with variance σ^2 .

Even through the lower bound proposed in (5.38) is approximate, it provides a useful reference point. Since the lower bound is non-parametric, it is particularly useful when comparing performance of receivers in the presence of different interference statistics.

5.5 Pre-filter Design to Mitigate RFI

Using the design criterion discussed in the previous section, I now consider the design of selection and combination pre-filters. While I propose the use of CIM as a distance measure, comparison with pre-filters designed using

Table 5.2: Distance cost function corresponding to L₂ norm, L₁ norm, and CIM as a distance measure in a S pre-filter.

Distance Measure	Cost Function $J(x_1, x_2)$
L ₂ norm	$\ x_2^{(I)} - x_1^{(I)}\ ^2 + \ x_2^{(Q)} - x_1^{(Q)}\ ^2$
L ₁ norm	$ x_2^{(I)} - x_1^{(I)} + x_2^{(Q)} - x_1^{(Q)} $
CIM	$-\exp\left(-\frac{\ x_2^{(I)} - x_1^{(I)}\ ^2}{2\sigma_c^2}\right) - \exp\left(-\frac{\ x_2^{(Q)} - x_1^{(Q)}\ ^2}{2\sigma_c^2}\right)$

L₂ norm and L₁ norm as a distance measure is also provided.

For notational simplicity, an odd valued window size W in the sliding-window pre-filters is assumed. Let $\mathcal{X}_W(n) = \{x[n - \frac{W-1}{2}], \dots, x[n], \dots, x[n + \frac{W-1}{2}]\}$ denote the set of input samples in a window of size W used for calculating the n^{th} output sample. The output sequence $x_{\text{PF}}[\cdot]$ can then be expressed as

$$x_{\text{PF}}[n] = \text{PF}(\mathcal{X}_W(n)). \quad (5.39)$$

5.5.1 Selection Pre-filter (S pre-filter)

S pre-filter chooses one of the input samples in $\mathcal{X}_W(n)$ as the n^{th} output sample such that

$$x_{S\text{-PF}}[n] = \arg \min_{x_i \in \mathcal{X}_W(n)} \sum_{x_k \in \mathcal{X}_W(n), x_k \neq x_i} J(x_i, x_k) \quad (5.40)$$

where $J(\cdot, \cdot)$ is the cost function. Table 5.2 lists the cost function corresponding to the L₂ norm, L₁ norm, and CIM as a distance measure.

5.5.2 Combination Pre-filter ($L\ell$ pre-filter) with Impulse Masking

A drawback of S pre-filter is that it ignores the temporal order of input samples. This degrades the performance of the pre-filter, particularly when operating at moderate-to-high SIR values. $L\ell$ pre-filter performs a weighted combination of the samples in the windows such that the weights are dependent on the temporal and rank order of the samples.

Classical formulation of $L\ell$ filters assumes real samples [101]. I first extend the $L\ell$ pre-filter formulation to account for dependence in the in-phase and quadrature phase components of the interference, and hence the received samples. Further, due to the combination form of $L\ell$ pre-filter, the output of the filter is sensitive to very large variations in the input sample. Even though outliers get mapped to a small weight during combination, a large value of the outlier may still cause significant deviation to the pre-filter output. To this end, I propose a modification of the $L\ell$ pre-filter to mask out the high valued outliers. Identifying the high valued outliers in the set $\mathcal{X}_W(n)$ is done using ZOS framework.

The in-phase or quadrature phase component of a received sample are weighted individually. The weights of the in-phase or quadrature phase are expressed as a function of the temporal order of the sample, rank of the in-phase component among $\Re\{\mathcal{X}_W(n)\}$, and rank of the quadrature phase component among $\Im\{\mathcal{X}_W(n)\}$. High sample values are masked out prior to weighted com-

bination. The output of $L\ell$ pre-filter is expressed as [101]

$$x_{L\ell\text{-PF}}[n] = \overline{W}_{L\ell}^T \overline{X}_{L\ell}(n) \quad (5.41)$$

where $\overline{X}_{L\ell}(n)$ is the $2W^3$ long vector that combines the temporal information and rank information in in-phase and quadrature phase components. $\overline{X}_{L\ell}(n)$ is defined as

$$\overline{X}_{L\ell}(n) = \left[\left(\overline{X}_{L\ell}^{(I)}(n) \right)^T \left(\overline{X}_{L\ell}^{(Q)}(n) \right)^T \right]^T \quad (5.42)$$

where

$$\overline{X}_{L\ell}^{(I)}(n) = \left[x_{1(1,1)}^{(I)}, \dots, x_{1(1,W)}^{(I)} \mid x_{1(2,1)}^{(I)}, \dots, x_{1(2,W)}^{(I)} \mid \dots, x_{i(k^{(I)}, k^{(Q)})}^{(I)}, \dots \mid \right. \\ \left. x_{W-1(W-1,1)}^{(I)}, \dots, x_{W-1(W-1,W)}^{(I)} \mid x_{W(W,1)}^{(I)}, \dots, x_{W(W,W)}^{(I)} \right]^T \quad (5.43)$$

$$\overline{X}_{L\ell}^{(Q)}(n) = \left[x_{1(1,1)}^{(Q)}, \dots, x_{1(1,W)}^{(Q)} \mid x_{1(2,1)}^{(Q)}, \dots, x_{1(2,W)}^{(Q)} \mid \dots, x_{i(k^{(I)}, k^{(Q)})}^{(Q)}, \dots \mid \right. \\ \left. x_{W-1(W-1,1)}^{(Q)}, \dots, x_{W-1(W-1,W)}^{(Q)} \mid x_{W(W,1)}^{(Q)}, \dots, x_{W(W,W)}^{(Q)} \right]^T \quad (5.44)$$

where

$$x_{i(k^{(I)}, k^{(Q)})} = \begin{cases} m_i x_i & \text{if } x_i^{(I)}, x_i^{(Q)} \text{ has a rank of } k^{(I)}, k^{(Q)} \text{ in the set} \\ & \Re \{ \mathcal{X}_W(n) \}, \Im \{ \mathcal{X}_W(n) \}, \text{ respectively,} \\ 0 & \text{otherwise,} \end{cases} \quad (5.45)$$

and

$$m_i = \begin{cases} 0 & \text{if } \|x_i - x_{S\text{-PF}}[n]\| > \mathbf{M}_{\text{Thres}} \\ 1 & \text{otherwise.} \end{cases} \quad (5.46)$$

Here x_i is the i^{th} element of the set $\mathcal{X}_W(n)$, $x_{S\text{-PF}}[n]$ is the selection pre-filter output defined in (5.40), and $\mathbf{M}_{\text{Thres}}$ is the threshold value indicating a highly corrupted sample value.

The weight vector can be expressed as $\bar{W}_{L\ell} = [\bar{W}_{L\ell}^{(I)}, \bar{W}_{L\ell}^{(Q)}]$, where $\bar{W}_{L\ell}^{(I)} = \left[(\bar{W}_1^{(I)})^T \mid (\bar{W}_2^{(I)})^T \mid \cdots \mid (\bar{W}_W^{(I)})^T \right]^T$ and $\bar{W}_i^{(I)} = [w_{i(1,1)}^{(I)}, \dots, w_{i(1,W)}^{(I)}, \dots, w_{i(W,1)}^{(I)}, \dots, w_{i(W,W)}^{(I)}]^T$ is the W^2 long tap vector associated with the in-phase component of the i^{th} input sample in $\mathcal{X}_W(n)$. Weights of the quadrature phase components $\bar{W}_{L\ell}^{(Q)}$ are defined similarly. Note that even though the length of the vectors $\bar{X}_{L\ell}$ and $\bar{W}_{L\ell}$ is large, the weighted combination in (5.41) involves only $2W$ multiplications since $\bar{X}_{L\ell}$ has only $2W$ non-zero terms.

The threshold M_{Thres} is chosen using the ZOS framework. Let us assume that the CIM space gracefully morphs into L_0 norm behavior at an Euclidean distance of $\alpha_4\sigma_c$ away from the origin. From Fig. 5.3, $\alpha_4 \approx 2$. This motivates choosing M_{Thres} as

$$M_{\text{Thres}} = \alpha_4\sigma_c \quad (5.47)$$

$$= \frac{\alpha_4}{\alpha_3} \left(\alpha_1\sqrt{E_s} + \alpha_2\sqrt{\sigma_{\text{Th}}^2 + 2C_g(\text{ZOS}(\mathbf{I}))^2} \right). \quad (5.48)$$

Using 5.41, the filter weights can be derived similar to the Wiener solution as

$$\bar{W}_{L\ell, \text{opt}} = \arg \min_{\bar{W}_{L\ell}} \mathbb{E} \left\{ J \left(x_{\text{Tx}}[n] - \bar{W}_{L\ell}^T \bar{X}_{L\ell}(n), 0 \right) \right\} \quad (5.49)$$

where $x_{\text{Tx}}[n] = \sum_k \sqrt{E_s} s[k] g_{\text{Tx}} \left[n - k \frac{T_s}{T_d} \right]$ is the transmitted training samples known at the receiver, and $J(\cdot, \cdot)$ is the cost function corresponding to the chosen distance measure as listed in Table 5.2. For CIM distance, exact evaluation of the Wiener-type solution for filter weights is complicated. In the presence

Table 5.3: Weight update factor $\frac{\partial J(e^{(I)}[n],0)}{\partial \bar{W}_{L\ell,n}^{(I)}}$ for weights corresponding to in-phase sample values using L₂ norm, L₁ norm, and CIM as a distance measure in a adaptive $L\ell$ pre-filter. Here $e[n] = x_{\text{Tx}}[n] - \bar{W}_{L\ell}^T \bar{X}_{L\ell}(n)$ is the error in the estimate of the n^{th} training sample. Weight update factor for weights corresponding to quadrature phase sample values $\frac{\partial J(e^{(Q)}[n],0)}{\partial \bar{W}_{L\ell,n}^{(Q)}}$ follow similarly with (I) replaced by (Q) .

Distance Measure	$\frac{\partial J(e^{(I)}[n],0)}{\partial \bar{W}_{L\ell,n}^{(I)}}$
L ₂ norm	$2e^{(I)}[n] \bar{X}_{L\ell}^{(I)}(n)$
L ₁ norm	$\text{sign}(e^{(I)}[n]) \bar{X}_{L\ell}^{(I)}(n)$
CIM	$\frac{1}{\sqrt{2\pi\sigma_c^2}} \exp\left(\frac{-\ e^{(I)}[n]\ ^2}{2\sigma_c^2}\right) 2e^{(I)}[n] \bar{X}_{L\ell}^{(I)}(n)$

of training data, a computationally attractive adaptive update of the filter weights can be expressed as [101]

$$\bar{W}_{L\ell,n+1}^{(I)} = \bar{W}_{L\ell,n}^{(I)} + \frac{\mu}{\left(\sum_{x_i \in \mathcal{X}_W(n)} \|x_i^{(I)}\|^2 + \epsilon\right)} \frac{\partial J(e^{(I)}[n],0)}{\partial \bar{W}_{L\ell}^{(I)}(n)} \quad (5.50)$$

$$\bar{W}_{L\ell,n+1}^{(Q)} = \bar{W}_{L\ell,n}^{(Q)} + \frac{\mu}{\left(\sum_{x_i \in \mathcal{X}_W(n)} \|x_i^{(Q)}\|^2 + \epsilon\right)} \frac{\partial J(e^{(Q)}[n],0)}{\partial \bar{W}_{L\ell}^{(Q)}(n)} \quad (5.51)$$

where μ is the step size, ϵ is a small positive number to avoid error amplification when the energy of the received samples is near zero, $e[n] = x_{\text{Tx}}[n] - \bar{W}_{L\ell}^T \bar{X}_{L\ell}(n)$ is the error in estimating the n^{th} sample value. Note that $e^{(I)}[n] = x_{\text{Tx}}^{(I)}[n] - \left(\bar{W}_{L\ell,n}^{(I)}\right)^{(T)} \bar{X}_{L\ell}^{(I)}(n)$ and $e^{(Q)}[n] = x_{\text{Tx}}^{(Q)}[n] - \left(\bar{W}_{L\ell,n}^{(Q)}\right)^{(T)} \bar{X}_{L\ell}^{(Q)}(n)$. Closed-form expressions for $\frac{\partial J(e^{(I)}[n],0)}{\partial \bar{W}_{L\ell,n}^{(I)}}$, $\frac{\partial J(e^{(I)}[n],0)}{\partial \bar{W}_{L\ell,n}^{(I)}}$ are listed in Table 5.3 corresponding to L₂, L₁, and CIM distance measures [138].

Initial value of the weight vector $\bar{W}_{L\ell,0}$ may be chosen such that it

corresponds to a pass-through filter. A pass-through filter can be enforced by using $w_{\frac{W+1}{2}(\cdot,\cdot)}^{(I)} = w_{\frac{W+1}{2}(\cdot,\cdot)}^{(Q)} = 1$, and $w_{i(\cdot,\cdot)}^{(I)} = w_{i(\cdot,\cdot)}^{(Q)} = 0$ for $i \neq \frac{W+1}{2}$. When interference plus thermal noise follows a Gaussian distribution, a pass-through filter is BER optimal. When interference is non-Gaussian, the filter weights adapt to mitigate the impulsive nature of interference.

5.5.3 Extensions to include temporal dependence in RFI ($L^J\ell$ pre-filter)

Both S and $L\ell$ pre-filter do not account for the temporal dependence in interference [101]. The design of $L\ell$ pre-filters discussed in the previous subsection is directly applicable to a broader class of $L^J\ell$ pre-filters. In $L^J\ell$ filters, each sample weights is dependent on its temporal order, its own rank, and the rank of next $J - 1$ neighboring samples. Thus $L^1\ell$ is simply an $L\ell$ filter. Simulations reveal that the additional benefit of $L^J\ell$ filters with $J > 1$ are insignificant (less than 0.5 dB SNR gain at a BER of 10^{-3}) with respect to $L\ell$ filters for the system model and interference considered in this chapter. The improvement in BER performance is at the cost of increased number of filter weights ($2W^{2J+1}$) that require more computations (e.g. sorting) and training data.

5.5.4 Computational Complexity Analysis

Table 5.4 compares the computational complexity of S and $L\ell$ pre-filters (PF) of length W designed using different distance measure. Compared to L_2 norm, using CIM as a distance measure in pre-filter design requires

Table 5.4: Comparison of computation complexity of S and $L\ell$ pre-filters (PF) of length W that use L_2 , L_1 , or CIM as a distance measure. The computations are reported per output sample in the runtime phase (**RN**), and per training sample in the training phase (**TR**). T training samples are assumed to be available in the training phase. Computational complexity is reported with respect to the number of real multiplications or inverse operations ($\times, (\cdot)^{-1}$), additions or subtractions ($+, -$), comparisons ($>, <, =$), and exponential evaluations ($e^{(\cdot)}$) required. Reported numbers are accurate only up to $O(1)$. Other $O(\frac{1}{T})$ and $O(\frac{1}{W})$ operations, such as $\log(\cdot)$ and $\sqrt{(\cdot)}$ required in certain pre-filters, are not reported.

PF	Distance Measure	TR/ RN	$\times, (\cdot)^{-1}$	$+, -$	$>, <, =$	$e^{(\cdot)}$
S	L_2 norm		$W(W-1)$	$\frac{3W(W-1)}{2}$	W	0
	L_1 norm		0	$\frac{3W(W-1)}{2}$	W	0
	CIM	TR	1	$O(\frac{1}{T})$	0	$O(\frac{1}{T})$
		RN		$\frac{3W(W-1)}{2}$	$\frac{3W(W-1)}{2}$	W
$L\ell$	L_2 norm	TR	$W(W+5)$	$\frac{W(3W+5)}{2}$	$2W(1+\log(W))$	0
		RN	$W(W+1)$	$\frac{W(3W+1)}{2}$	$2W(1+\log(W))$	0
	L_1 norm	TR	$6W$	$\frac{W(3W+5)}{2}$	$2W(1+\log(W))$	0
		RN	$2W$	$\frac{W(3W+1)}{2}$	$2W(1+\log(W))$	0
	CIM	TR	$\frac{3W(W+3)}{2}$	$\frac{W(3W+5)}{2}$	$2W(1+\log(W))$	$W(W-1)$
		RN	$\frac{W(3W+1)}{2}$	$\frac{W(3W+1)}{2}$	$2W(1+\log(W))$	$W(W-1)$

marginal increase in multiplications, and $O(W^2)$ additional exponential evaluations. The improvement in communication performance offered by the CIM distance measure at this marginal increase in computational complexity motivates the use of CIM (and ZOS to aid the scaling of CIM space) in receiver design.

5.6 Simulation Results

Using the network model discussed in Section 5.2.2, I apply Monte-Carlo numerical techniques to simulate the interference observed at a typical

receiver in the network. The joint interference statistics derived in Section 4.3 are first validated by comparing the simulated joint tail probability of interference against the estimated tail probability derived from the statistical model. Closed-form joint tail probability of multivariate Gaussian mixture distributed interference is derived in Appendix B. Baseband communication between a transmitter-receiver pair in the presence of interference is then simulated based on the transmission model described in Section 5.2.1. Communication performance of various pre-filter based receivers is compared against the conventional matched receiver for 16-QAM modulated baseband transmissions.

The network model parameters used in the numerical simulations are

$$\gamma = 4, \mathbf{h} \sim \text{Rayleigh} \left(\frac{1}{\sqrt{2}} \right), \mathbf{B} = 10,$$

and the lifetime (\mathbf{L}) of a typical node is assumed be distributed in $[1, 3]$ such that

$$\mathbb{P}(\mathbf{L} = i) = \begin{cases} 0.4706 & i = 1, \\ 0.3529 & i = 2, \\ 0.1765 & i = 3, \\ 0 & \text{otherwise.} \end{cases}$$

Mean lifetime of typical node is 1.7059 time slots.

5.6.1 Joint Statistics of Interference

Fig. 5.5 compares the simulated and estimated joint tail probability of interference observed over $n = 1, 2, 3$ time slots. The simulated tail probability is empirically estimated using 200000 time samples of the received interference. The estimated tail probability match closely with the simulated joint

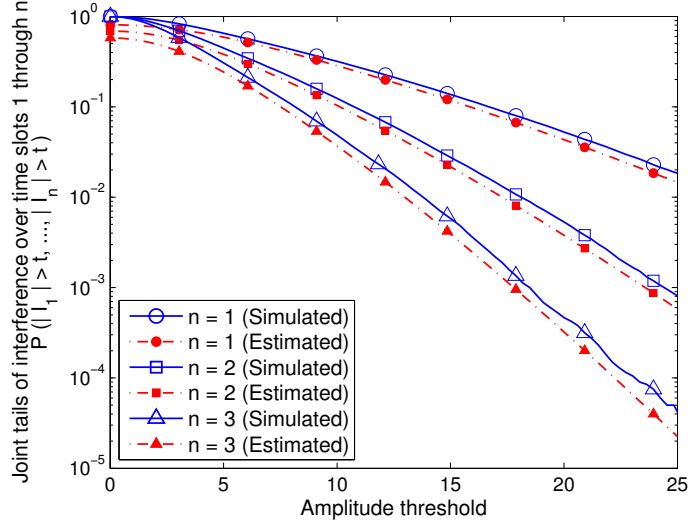


Figure 5.5: Joint tail probability of interference amplitude over $n = 1, 2, 3$ time slots with the intensity of emerging interferers $\lambda = 0.1$. A bounded pathloss function $l(r) = \min(1, r^{-\frac{\gamma}{2}})$ is assumed, where r is the propagation distance and $\gamma = 4$ is the power pathloss exponent. The number of mixture terms N_T for each contributing component was chosen as 4, that results in a total number of mixture terms $(N_T)^{2n!} = 4^2, 4^4, 4^6$ for $n = 1, 2,$ and 3 , respectively.

tail probability, thereby validating the closed-form joint interference statistics in (5.22).

5.6.2 Communication Performance of Pre-filter Based Receivers

Baseband communication between a typical transmitter-receiver pair in the network is simulated using (5.1). Thermal noise present in the system is assumed to be 30 dB below the interference power. Transmit filter is assumed to be a square-root raised cosine filter with rolloff factor 0.1, filter group delay of 8 input symbols, and $\frac{T_s}{T_d} = 14$ samples per symbol. Communication performance of various pre-filter based receivers is studied for both simulated network in-

interference and Gaussian distributed interference. Receivers are simulated for 100000 16-QAM modulated transmit symbols that includes $T = 5000$ training symbols in the beginning. Estimation of ZOS of interference, and adaptation of $L\ell$ filters is performed in the training phase.

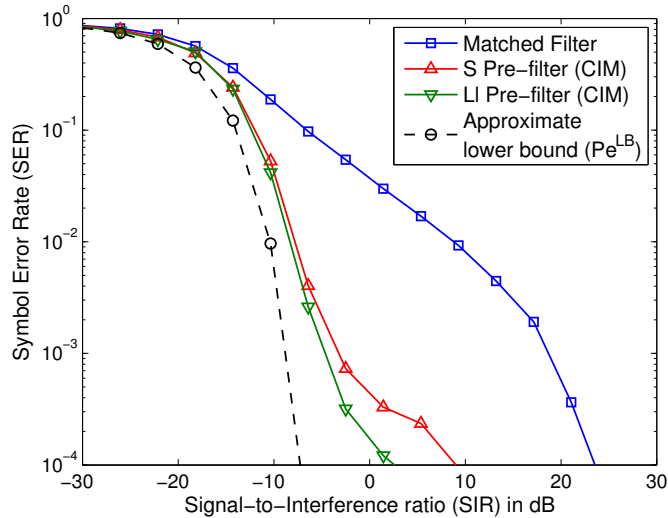


Figure 5.6: Communication performance of correntropy induced metric (CIM) based pre-filters in the presence of the simulated network interference. Intensity of emerging interferers $\lambda = 0.0001$ results in non-Gaussian impulsive interference. Interference-to-noise ratio is fixed at 30 dB. While $L\ell$ pre-filter outperform S pre-filter, the latter provides a good tradeoff between communication performance and computational complexity in the presence of impulsive non-Gaussian interference. Both pre-filters provide around 15–20 dB improvement over conventional matched receiver at a symbol-error-rate (SER) of 10^{-3} .

Pre-filter length $W = 5$ is chosen because the maximum lifetime of an interferer is set to 3 sampling time instants. Thus interference may exhibit strong dependence over 3 consecutive samples. A pre-filter length of 5 will generally result in less than half highly corrupted samples. The dependence in interference can be easily estimated in realtime implementation by listening

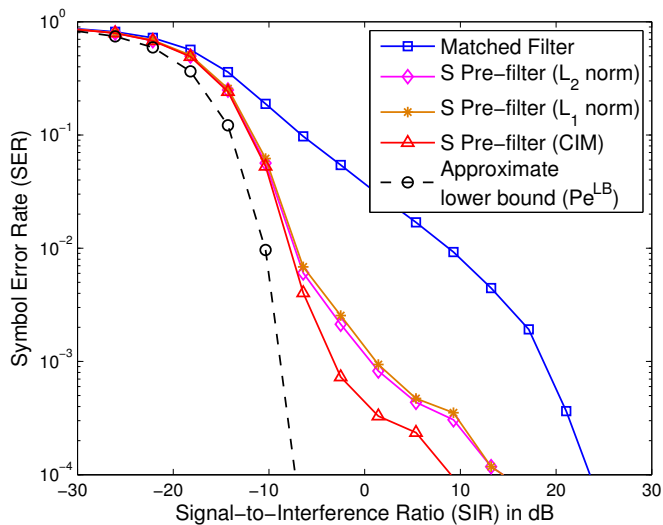


Figure 5.7: Communication performance of S pre-filters in the presence of the simulated network interference. Intensity of emerging interferers $\lambda = 0.0001$ results in non-Gaussian impulsive interference. Interference-to-noise ratio is fixed at 30 dB. CIM based S pre-filter outperforms its counterparts that use L_2 or L_1 norm as a distance measure.

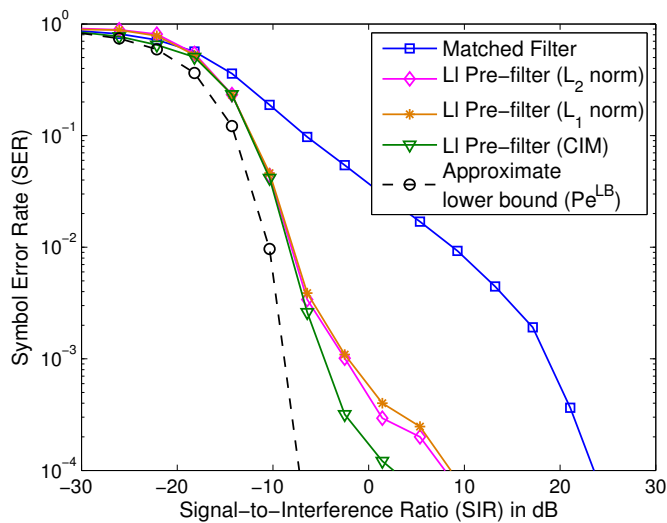


Figure 5.8: Communication performance of Ll pre-filters in the presence of the simulated network interference. Intensity of emerging interferers $\lambda = 0.0001$ results in non-Gaussian impulsive interference. Interference-to-noise ratio is fixed at 30 dB. CIM based Ll pre-filter outperforms its counterparts that use L_2 or L_1 norm as a distance measure.

to the RFI environment prior to active transmissions. For CIM based pre-filters, $\alpha_1 = 0.3$, $\alpha_2 = 2$, $\alpha_3 = \frac{1}{0.6}$, and $\alpha_4 = 2$ are used in (5.37) and (5.48). These values are consistent with the discussion provided in Section 5.4.3. $L\ell$ pre-filters are initialized as pass-through filters and adapted using a step size $\mu = 0.01$. Further, $\epsilon = 0.001$ is chosen to avoid instability in (5.50) and (5.51) during weight updates.

Simulated network interference: Interference is simulated using the network parameters listed in Section 5.6 with the intensity of emerging interferers $\lambda = 0.0001$. The low density of users causes the interference to be non-Gaussian. Fig. 5.6 compares the symbol error rate of CIM based pre-filters in the presence of the simulated interference with varying SIR. $L\ell$ pre-filter outperforms the S pre-filter by around 4–5 dB at a symbol error rate of 10^{-4} . S pre-filters, however, provides a good tradeoff between communication performance and computational complexity, particularly at low SIR. Both S and $L\ell$ pre-filters provide significant improvement over the conventional matched filter even at a very low SIR. This motivates using pre-filter based receiver structure to mitigate non-Gaussian distributed interference.

Figs. 5.7 and 5.8 compare the communication performance of S and $L\ell$ pre-filters, respectively, designed using L_2 norm, L_1 norm, and CIM distance measure. Pre-filters designed using CIM outperform their counterparts that are designed using L_2 or L_1 norm as a distance measure.

Gaussian distributed interference: Fig. 5.9 compares the communication performance of correntropy induced metric (CIM) based S and

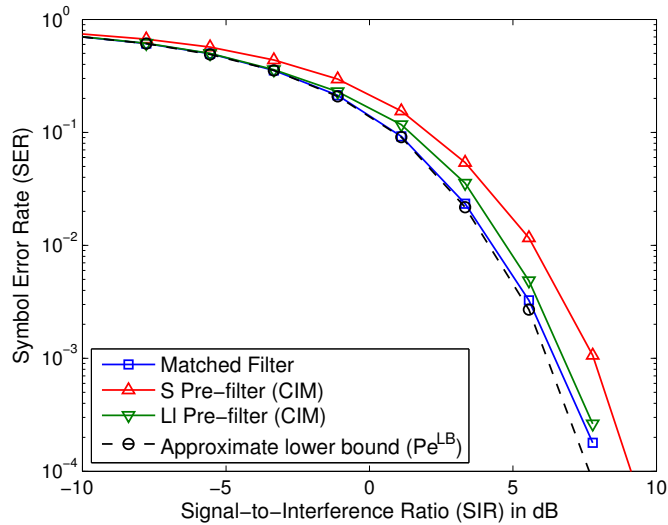


Figure 5.9: Communication performance of correntropy induced metric (CIM) based pre-filters in the presence of Gaussian distributed interference. Interference-to-noise ratio is fixed at 30 dB. Matched filter receiver is BER optimal in the presence of Gaussian distributed interference. At a symbol-error-rate (SER) of 10^{-3} , degradation in communication performance due to $L\ell$ and S pre-filters is approximately 0.3 dB and 1 dB, respectively.

$L\ell$ pre-filters in the presence of Gaussian distributed interference. In presence of Gaussian distributed thermal noise and interference, the matched filter is BER optimal. S pre-filter introduces some unwanted smoothing in the received signal, thereby degrading the receiver performance a little. $L\ell$ pre-filter, ideally, should be able to pass the received signal unaltered in the presence of Gaussian noise. Due to the adaptive weight updates, deviations from the ideal $L\ell$ pre-filter weights may cause a little degradation in communication performance. Fig. 5.9 shows that the degradation in communication performance at a symbol-error-rate (SER) of 10^{-3} is approximately 0.3 dB and 1 dB for $L\ell$ and S pre-filter, respectively, in the presence of Gaussian distributed interference.

5.7 Conclusions

This chapter demonstrates the advantage of pre-filter based receiver, where a filtering stage is placed prior to the conventional receiver with the task of removing the “impulsive component” of RFI. At a SER of 10^{-3} , a SNR gain of 15–20 dB is observed in for uncoded 16-QAM modulated transmissions. This translates to an improved link spectral efficiency by an additional 5–7 bits/sec/Hz for a desired SER of 10^{-3} for uncoded QAM transmissions. Even at low SER of 10^{-1} , an improved link spectral efficiency by an additional 1–2 bits/sec/Hz is attainable using pre-filtering methods. A disadvantage of pre-filter based receiver, however, is that it operates at the sample rate (T_s/T_a times the symbol rate) and significantly increases the computational complexity of the receiver. RFI mitigation methods that operate on the matched filter output at the symbol rate, however, yield reduced gains in communication performance compared to pre-filtering methods. [141, 142].

The chapter uses CIM as a distance measure and proposes using ZOS of non-Gaussian RFI to scale the CIM space. This framework can be used for a wide range of signal processing techniques to mitigate RFI in wireless receivers. For example, the ZOS scaled CIM space can be used as a robust metric for likelihood evaluation in Turbo decoders [142]. Further, the non-parametric nature of CIM and ZOS render the framework applicable for a wide range of non-Gaussian RFI statistics.

Chapter 6

Conclusions

6.1 Summary

In this dissertation, I show the benefit of using closed-form interference statistics to analyze and improve the communication performance of interference-limited wireless networks. Prior work has been limited in pursuing this approach since exact closed-form interference statistics are known only in a few interference scenarios. For interference-limited wireless networks, however, only accurate modeling of the tail probability of interference is required. Chapter 3 proposes a framework to derive closed-form instantaneous statistics of interference that accurately model the tail probability of interference in a wide variety of wireless networks. Focusing on decentralized wireless networks, Chapters 4 and 5 extend the framework to include temporal dependence in interference under the assumption of unbounded and bounded pathloss function, respectively. Chapter 4 uses the joint temporal interference statistics to study the throughput, delay, and reliability of single-hop transmission in a decentralized wireless network, unveiling $2\times$ improvement in network throughput by optimizing a MAC parameter to control the temporal dependence in interference. Chapter 5 uses the knowledge of joint interference statistics to derive pre-filtering methods to mitigate RFI, yielding improved

link spectral efficiency, e.g., by an additional 1–6 bits/sec/Hz for uncoded QAM modulated transmission per communication link in the network.

Table 6.1 compares the contributions of this dissertation to the prior work summarized in Table 2.2. Comparison is presented with respect to contributions in (i) statistical modeling of RFI, (ii) use of RFI statistics for communication performance analysis of wireless networks, and (iii) use of RFI statistics for receiver design to mitigate RFI. As seen from Table 6.1, the approach used in this dissertation leads to closed-form interference statistics in a wide range of interference scenarios. The benefit of closed-form statistics in communication performance analysis of wireless networks, and receiver design to mitigate RFI is also evident.

The specific contributions of this dissertation are built on the following novel approaches that can be utilized to analyze and improve the communication performance of wireless networks:

1. Chapter 3 proposes a framework to derive closed-form interference statistics that accurately model the tail probability of interference. The assumption of narrowband emissions and fading, using the Middleton’s identity given by (3.19), and using approximations such as (3.31), are the central ideas that enable expressing the statistics in closed-form. The framework enables establishing the applicability of symmetric alpha stable and Gaussian mixture distributions in a wide variety of wireless networks. While this framework works well for Poisson-based interferer

distributions (e.g., Poisson and Poisson-Poisson cluster), extension to general non-Poisson interferer distributions is not straightforward.

2. Chapter 4 uses a novel approach of utilizing the tail probability of interference to derive closed-form communication performance measures in wireless networks. This approach is particularly helpful when the exact statistics of interference are not known in closed-form. Formulating the problem at the amplitude and phase abstraction of the interference enables using additional assumptions on the user emissions and fading that help in deriving closed-form tail probability of interference.
3. Chapter 5 proposes the use of CIM as a distance measure, with ZOS of interference to scale the CIM space, to design receivers that are robust to the non-Gaussian impulsive statistics of residual interference. While the potential of CIM as a distance measure in non-Gaussian environments has been shown in prior work [2, 138], using the ZOS of the interference to scale the CIM space enables practical applicability of CIM space to varying non-Gaussian interference environments.

Practical applications of this work include the design of MAC layer protocols and robust transceivers to mitigate residual RFI in wireless networks. This dissertation proposes direct contributions in robust transceiver design and identifies the potential improvement in network throughput via optimization of MAC layer channel access protocols.

Table 6.1: Contributions of this dissertation compared to prior work in (i) statistical modeling of RFI, (ii) use of RFI statistics for network performance analysis, and (iii) use of RFI statistics for receiver design to mitigate RFI. SAS, MCA, and GMM are defined in Section 1.6. BPL/UBPL refer to the assumption of bounded/unbounded pathloss function. Unless specified, statistics are derived assuming an UBPL function. CIM and ZOS stand for correntropy induced metric and zero-order statistics, respectively.

Statistical Modeling of RFI	Instantaneous Statistics of RFI			
	Interferer Distribution	Spatial Topology	Prior Work	Chapter 3
	Poisson	Entire Plane	SAS [70–72]	SAS (UBPL) GMM (BPL)
		Finite Area	MCA [12, 13]	MCA
		Guard Zone	Not known	MCA
	Poisson-Poisson Cluster	Entire Plane	Not known	SAS
		Finite Area	Not known	GMM
		Guard Zone	Not known	GMM
	Joint Temporal Statistics of RFI			
	Interferer Distribution	Spatial Topology	Prior Work	Chapters 4, 5
Poisson	Entire Plane	Limited [71, 72]	SAS (UBPL) GMM (BPL)	
Network Performance Analysis	Throughput, Delay, and Reliability of Decentralized Wireless Networks			
		Prior Work	Chapter 4	
	Networks with temporal correlation	Limited [92–94]	Spans temporal independence to full correlation	
Receiver Design to Mitigate RFI	Pre-filter Design to Mitigate RFI			
		Prior Work	Chapter 5	
	Motivated by RFI statistics	Limited	Yes	
	Can include thermal noise	Limited [29, 112, 113]	Yes	
	Distance measure	L_2, L_1 norm, LD^a [101]	CIM (ZOS scaled)	

^aLogarithmic Deviation

6.2 Future Work

In this section, I outline several interesting research directions that this dissertation can be extended to.

Closed-form statistics in non-Poisson field of interferers: The assumption of Poisson distributed interferer locations is commonly made for analytical tractability [56, 68, 74, 76]. Many MAC protocols, such as CSMA, break this Poisson assumption. While various mathematical tools exist for Poisson distributed interferers, analysis of communication performance in wireless networks with non-Poisson distributed interferer locations is non-trivial [143]. If closed-form statistics that accurately model the tail probability of interference can be derived, then the analysis of communication performance will be significantly simplified. The framework used in Chapter 3 to derive closed-form interference, however, works only for Poisson-based interferer distributions (e.g. Poisson and Poisson-Poisson cluster). While the applicability of Gaussian mixture distributions can be intuitively argued under the assumption of bounded pathloss model in any interferer distribution, explicit mathematical characterization for communication performance analysis is required.

Applications to cognitive networks: The problem of modeling interference from secondary users in a cognitive network resembles closely to the network model used in this dissertation [66, 144]. In cognitive radios, time-domain spectrum sensing algorithm formulate the detection problem as a hypothesis test, and are sensitive to the assumption on interference statistics. The results of this dissertation on statistical modeling can be directly extended

to derive closed-form statistics of interference from the secondary users in the network. Secondary users in a cognitive network can be considered to be distributed according to a Poisson point process [66]. A secondary user is active if the received power of the uplink signal transmitted by a primary user falls below the detection threshold, thereby creating a Guard zone around the primary user [66]. The sum interference from secondary users can be modeled as *Case III* in Chapter 3, and shown to follow a Gaussian mixture distribution. The knowledge of closed-form interference statistics can be used to apply spectrum sensing algorithms with improved detection performance [145]. Prior work on signal detection in the presence of Gaussian mixture interference shows 15–38dB improvement in detection performance at a false detection probability of 0.1% over Gaussian detectors [145].

Applications to powerline communication networks (PCN):

The framework used in this dissertation can be adapted to model asynchronous noise in the last mile PLC network (from the customer power meters to the command and control center of the local utility) [146]. The last mile PLC network is a shared medium between several subscribers (as in the US) to hundreds of subscribers (as in Europe) [147]. The switching activity in these large number of subscribers connected to the PLC network results in temporally correlated non-Gaussian interference. Modeling the switching activity as a Poisson process, the results of this dissertation can be applied to model, analyze, and improve the communication performance of PLC networks.

Multi-hop communication performance of decentralized wire-

less networks: Chapter 4 used the joint temporal statistics of interference to characterize the single-hop communication performance in a decentralized wireless network. Extensions to analyze the multi-hop communication performance would require the knowledge of joint spatio-temporal statistics – deriving which is nontrivial in multi-hop networks. Nonetheless, if joint spatio-temporal statistics can be derived, then multi-hop communication performance of decentralized wireless can be analyzed using techniques similar to those used in Chapter 4.

Decentralized optimization of MAC parameters to mitigate RFI: Certain parameters of the MAC protocols, such as the channel access probability in slotted-ALOHA, can be optimized using the knowledge of interference statistics for improved network performance. In Chapter 4, $2\times$ improvement in the network throughput was shown by optimizing the number of physical packets that are transmitted in a burst by the users. The optimization required centralized knowledge of the network parameters such as the user density. To the best of my understanding, decentralized optimization of the MAC parameters at each user is nontrivial due to limited information available from acknowledgment packets. Certain network parameters, such as temporal correlation, may be partially characterized by observing the interference at user. MAC parameters can thus be optimized at any user using the additional information from the observed interference at that user.

Using CIM and ZOS based framework for robust receiver design: Many of the common receiver algorithms, such as time and frequency

synchronization, channel estimation, channel equalization, and turbo decoding, exhibit severe degradation in communication performance in the presence of non-Gaussian impulsive noise [39, 40, 96, 148]. The ZOS scaled CIM space proposed in Chapter 5 provides a useful distance measure in the presence of non-Gaussian interference, and can be applied to design robust receiver algorithms. For example, in turbo decoders robust distance metrics, such as limiting nonlinearities and Huber’s metric, are employed in likelihood calculations to provide robustness against outliers. Adapting these metrics to the changing interference environment is not straightforward. Using ZOS of interference to scale the CIM space provides a non-parametric framework to adapt to the changing RFI environment.

Impact of mismatch in RFI distribution on receiver performance: Simulations results presented in Chapter 3 and 5 show that receiver algorithms, such as pre-filters, to mitigate RFI are generally robust to mismatch in the assumed RFI distribution and parameter estimation errors [99, 145]. In particular, the robustness of the Gaussian mixture distribution to model RFI was argued. Analytical characterization of the impact of model mismatch on the BER performance of the receiver, however, is not studied in this dissertation. Such characterization, though hard, can further motivate the choice of a particular RFI distribution based on its robustness to estimation errors in practical receivers.

Appendices

Appendix A

Statistical Properties of Symmetric Alpha Stable Random Vectors

This appendix presents a brief review of the statistical properties of symmetric alpha stable vectors used extensively throughout this dissertation. I also prove some important theorems which are integral to the derivation of communication performance measures presented in Chapter 4. This appendix borrows heavily from the notation, theorems, and proofs used in [125], while still being consistent with the notation used in this dissertation.

The following two theorems are stated without without proof. Theorem A.1 concerns the representation of general symmetric alpha stable vectors, while Theorem A.2 concerns the representation of an *isotropic* symmetric alpha stable vector.

Theorem A.1. *[Theorem 2.4.3 in [125]] \mathbf{X} is a symmetric alpha stable vector in \mathbb{R}^d with $0 < \alpha < 2$ if and only if there exists a unique symmetric finite measure $\bar{\Gamma}$ on the unit sphere S_d such that*

$$\mathbb{E} \left\{ \exp \left(j \sum_{i=1}^d \omega_i \mathbf{X}_i \right) \right\} = \exp \left(- \int_{S_d} \left(\sqrt{\sum_{i=1}^d \omega_i \mathbf{s}_i} \right)^\alpha \bar{\Gamma}(d\mathbf{s}) \right). \quad (\text{A.1})$$

$\bar{\Gamma}$ is the spectral measure of the symmetric alpha stable vector \mathbf{X} .

Theorem A.2. [Adapted from Proposition 2.5.5 in [125]] Let \mathbf{X} be an isotropic symmetric alpha stable vector in \mathbb{R}^d with $0 < \alpha < 2$. Then the following three statements are equivalent:

(a) The characteristic function of X is of the form

$$\mathbb{E} \left\{ \exp \left(j \sum_{i=1}^d \omega_i \mathbf{X}_i \right) \right\} = \exp \left(-\sigma \left(\sqrt{\sum_{i=1}^d \omega_i^2} \right)^\alpha \right). \quad (\text{A.2})$$

(b) The spectral measure of \mathbf{X} is uniformly distributed over the d -dimensional unit sphere S_d .

(c) \mathbf{X} is sub-Gaussian such that

$$\mathbf{X} \stackrel{d}{=} \left\{ \mathbf{A}^{\frac{1}{2}} \mathbf{G}_1, \dots, \mathbf{A}^{\frac{1}{2}} \mathbf{G}_d \right\}. \quad (\text{A.3})$$

Here \mathbf{A} is a positive stable random variable with characteristic exponent $\frac{\alpha}{2}$, skewness parameter 1, and dispersion parameter $2^{\frac{\alpha}{2}} \sigma \cos \left(\frac{\pi\alpha}{4} \right)$ [125]. $\mathbf{G}_1, \dots, \mathbf{G}_d$ are mutually independent, zero mean, unit variance Gaussian random variables and independent of \mathbf{A} .

Using Theorem A.2, I derive the following corollary regarding the joint amplitude tails of an isotropic symmetric alpha stable vector.

Corollary A.3. Let $\mathbf{X} = (\mathbf{X}_{1,I}, \mathbf{X}_{1,Q}, \dots, \mathbf{X}_{d,I}, \mathbf{X}_{d,Q})$ be an isotropic symmetric alpha stable vector in \mathbb{R}^{2d} with $0 < \alpha < 2$ and dispersion parameter σ as defined by Theorem A.2. Then the joint tail probability of $\|\mathbf{X}_1\|, \dots, \|\mathbf{X}_d\|$ can be expressed as

$$\lim_{\beta \rightarrow \infty} \beta^\alpha \mathbf{P} (\|\mathbf{X}_1\| > \beta_1, \dots, \|\mathbf{X}_d\| > \beta_d) = 2^\alpha \sigma C_{\frac{\alpha}{2}} \cos \left(\frac{\pi\alpha}{4} \right) \Gamma \left(1 + \frac{\alpha}{2} \right) \quad (\text{A.4})$$

where $\beta = \sqrt{\sum_{i=1}^d \beta_i^2}$, $\|\mathbf{X}_i\| = \sqrt{\mathbf{X}_{i,I}^2 + \mathbf{X}_{i,Q}^2}$, and

$$C_\alpha = \begin{cases} \frac{2}{\pi} & \text{when } \alpha = 1, \\ \frac{1-\alpha}{\Gamma(2-\alpha) \cos(\frac{\pi\alpha}{2})} & \text{otherwise.} \end{cases} \quad (\text{A.5})$$

Proof. Using the sub-Gaussian representation of an isotropic symmetric alpha stable vector given in (A.3), $\mathbf{X} \stackrel{d}{=} \left\{ \mathbf{A}^{\frac{1}{2}} \mathbf{G}_{1,I}, \mathbf{A}^{\frac{1}{2}} \mathbf{G}_{1,Q}, \dots, \mathbf{A}^{\frac{1}{2}} \mathbf{G}_{d,I}, \mathbf{A}^{\frac{1}{2}} \mathbf{G}_{d,Q} \right\}$ where \mathbf{A} is a positive stable random variable and $\mathbf{G}_{1,I}, \mathbf{G}_{1,Q}, \dots, \mathbf{G}_{d,I}, \mathbf{G}_{d,Q}$ are *i.i.d.* Gaussian random variables as defined in Theorem A.2, gives

$$\begin{aligned} & \lim_{\beta \rightarrow \infty} \beta^\alpha \mathbf{P} (\|\mathbf{X}_1\| > \beta_1, \dots, \|\mathbf{X}_d\| > \beta_d) \\ &= \lim_{\beta \rightarrow \infty} \beta^\alpha \mathbf{P} (\mathbf{A} (\mathbf{G}_{1,I}^2 + \mathbf{G}_{1,Q}^2) > \beta_1^2, \dots, \mathbf{A} (\mathbf{G}_{d,I}^2 + \mathbf{G}_{d,Q}^2) > \beta_d^2) \quad (\text{A.6}) \end{aligned}$$

$$= \lim_{\beta \rightarrow \infty} \beta^\alpha \mathbf{P} \left(\mathbf{A} \frac{\beta^2}{\beta_1^2} (\mathbf{G}_{1,I}^2 + \mathbf{G}_{1,Q}^2) > \beta^2, \dots, \mathbf{A} \frac{\beta^2}{\beta_d^2} (\mathbf{G}_{d,I}^2 + \mathbf{G}_{d,Q}^2) > \beta^2 \right) \quad (\text{A.7})$$

$$= \lim_{\beta \rightarrow \infty} \beta^\alpha \mathbf{P} \left(\mathbf{A} \min_{i=1, \dots, d} \frac{\beta^2}{\beta_i^2} (\mathbf{G}_{i,I}^2 + \mathbf{G}_{i,Q}^2) > \beta^2 \right) \quad (\text{A.8})$$

$$= \lim_{\beta \rightarrow \infty} \beta^\alpha \int_0^\infty \mathbf{P} \left(\mathbf{A} > \frac{\beta^2}{x} \right) \frac{1}{2} e^{-\frac{x}{2}} dx \quad (\text{A.9})$$

$$= 2^\alpha \sigma C_{\frac{\alpha}{2}} \cos \left(\frac{\pi\alpha}{4} \right) \Gamma \left(1 + \frac{\alpha}{2} \right) \quad (\text{A.10})$$

where (A.9) is expressed by noting that for all i , $\frac{\beta_i^2}{\beta^2} (\mathbf{G}_{i,I}^2 + \mathbf{G}_{i,Q}^2)$ are independent and exponentially distributed with mean $\frac{2\beta_i^2}{\beta^2}$. Thus $\min_{i=1, \dots, d} \frac{\beta_i^2}{\beta^2} (\mathbf{G}_{i,I}^2 + \mathbf{G}_{i,Q}^2)$ is also exponentially distributed with mean $\left(\frac{\sum_{i=1}^d \beta_i^2}{2\beta^2} \right)^{-1} = 2$. Equation (A.10) follows from the dominated convergence theorem, and noting that \mathbf{A} is a positive $\frac{\alpha}{2}$ -stable random variable with tails $\lim_{t \rightarrow \infty} t^{\frac{\alpha}{2}} \mathbf{P} (\mathbf{A} > t) = 2^{\frac{\alpha}{2}} \sigma C_{\frac{\alpha}{2}} \cos \left(\frac{\pi\alpha}{4} \right)$. \square

Deriving the joint amplitude tail probability of a general symmetric alpha stable vector is more involved as compared to the specialized case of *isotropic* symmetric alpha stable vector dealt in Corollary A.3. I now state a Lemma without proof and then prove a theorem which relates the joint amplitude tail probability of a general symmetric alpha stable vector to its spectral measure.

Lemma A.4. [*Lemma 4.4.2 in [125]*] *Suppose that \mathbf{X} is a random variable with a regularly varying tail, i.e. , there is a number $\theta > 0$ such that for every number $a > 1$,*

$$\lim_{x \rightarrow \infty} \frac{\mathbb{P}(\mathbf{X} > ax)}{\mathbb{P}(\mathbf{X} > x)} = a^{-\theta}. \quad (\text{A.11})$$

Suppose also that the tail of \mathbf{X} dominates the tail of a positive random variable \mathbf{Y} in the sense that

$$\lim_{x \rightarrow \infty} \frac{\mathbb{P}(\mathbf{Y} > x)}{\mathbb{P}(\mathbf{X} > x)} = 0. \quad (\text{A.12})$$

Then

$$\lim_{x \rightarrow \infty} \frac{\mathbb{P}(\mathbf{X} + \mathbf{Y} > x)}{\mathbb{P}(\mathbf{X} > x)} = \frac{\mathbb{P}(\mathbf{X} - \mathbf{Y} > x)}{\mathbb{P}(\mathbf{X} > x)} = 1. \quad (\text{A.13})$$

Theorem A.5. *Let $\mathbf{X} = (\mathbf{X}_{1,I}, \mathbf{X}_{1,Q}, \dots, \mathbf{X}_{d,I}, \mathbf{X}_{d,Q})$ be a symmetric alpha stable vector in \mathbb{R}^{2d} with $0 < \alpha < 2$ and a unique symmetric finite measure $\bar{\Gamma}$ on the unit sphere S_{2d} . If $\beta_i = \beta \eta_i$ such that $0 < \eta_i < \infty$ for $i = 1, \dots, d$, then*

$$\lim_{\beta \rightarrow \infty} \beta^\alpha \mathbb{P}(\|\mathbf{X}_1\| > \beta_1, \dots, \|\mathbf{X}_d\| > \beta_d) = C_\alpha \int_{S_{2d}} \min_{i=1, \dots, d} \left(\frac{\sqrt{s_{2i-1}^2 + s_{2i}^2}}{\eta_i} \right)^\alpha \bar{\Gamma}(ds) \quad (\text{A.14})$$

where C_α is defined in (A.5).

Proof. This proof adopts the approach used in the proof of Theorem 4.4.1 in [125]. Using Theorems 3.5.6 and 3.10.1, and Corollary 3.10.4 in [125],

$$(\mathbf{X}_{1,I}, \mathbf{X}_{1,Q}, \dots, \mathbf{X}_{d,I}, \mathbf{X}_{d,Q}) \stackrel{d}{=} (\mathbf{Y}_1, \dots, \mathbf{Y}_{2d}) \quad (\text{A.15})$$

such that \mathbf{Y}_k have a Le-Page series representation

$$\mathbf{Y}_k = \left(C_\alpha \tilde{\Gamma}(S_{2d}) \right)^{\frac{1}{\alpha}} \sum_{i=1}^{\infty} \epsilon_i \Gamma_i^{-\frac{1}{\alpha}} \frac{f_k(\mathbf{V}_i)}{f^*(\mathbf{V}_i)} \quad (\text{A.16})$$

$$= \underbrace{\left(C_\alpha \tilde{\Gamma}(S_{2d}) \right)^{\frac{1}{\alpha}} \epsilon_1 \Gamma_1^{-\frac{1}{\alpha}} \frac{f_k(\mathbf{V}_1)}{f^*(\mathbf{V}_1)}}_{=\mathbf{U}_k} + \underbrace{\left(C_\alpha \tilde{\Gamma}(S_{2d}) \right)^{\frac{1}{\alpha}} \sum_{i=2}^{\infty} \epsilon_i \Gamma_i^{-\frac{1}{\alpha}} \frac{f_k(\mathbf{V}_i)}{f^*(\mathbf{V}_i)}}_{=\mathbf{W}_k} \quad (\text{A.17})$$

Here $f_k : S_{2d} \rightarrow \mathbb{R}$ is defined as $f_k(s) = s_k$ for $k = 1, \dots, 2d$ and $s \in S_{2d}$, $f^* : S_{2d} \rightarrow \mathbb{R}$ is defined as $f^*(s) = \max_{k=1, \dots, 2d} |f_k(s)|$ for $s \in S_{2d}$, $\tilde{\Gamma}(ds) = (f^*(s))^\alpha \bar{\Gamma}(ds)$ is a finite measure on $(S_{2d}, \text{Borel } \sigma\text{-algebra on } S_{2d})$, $\{\Gamma_1, \Gamma_2, \dots\}$ is the sequence of arrival times of a Poisson process with unit arrival rate, $\{\mathbf{V}_1, \mathbf{V}_2, \dots\}$ is the sequence independent of $\{\Gamma_1, \Gamma_2, \dots\}$ such that \mathbf{V}_i has a distribution $\frac{\tilde{\Gamma}}{\tilde{\Gamma}(S_{2d})}$ on S_{2d} , and $\{\epsilon_1, \epsilon_2, \dots\}$ is the sequence independent of $\{\Gamma_1, \Gamma_2, \dots\}$ and $\{\mathbf{V}_1, \mathbf{V}_2, \dots\}$ such that $\mathbb{P}(\epsilon_i = 1) = \mathbb{P}(\epsilon_i = -1) = \frac{1}{2}$.

Using (A.17), and the triangle inequality, gives

$$\begin{aligned} \min_{i=1, \dots, d} \frac{\sqrt{\mathbf{U}_{2i-1}^2 + \mathbf{U}_{2i}^2}}{\eta_i} - 2 \left(\frac{\max_{i=1, \dots, 2d} |\mathbf{W}_i|}{\min_{i=1, \dots, d} \eta_i} \right) &\leq \min_{i=1, \dots, d} \frac{\sqrt{\mathbf{Y}_{2i-1}^2 + \mathbf{Y}_{2i}^2}}{\eta_i} \\ &\leq \min_{i=1, \dots, d} \frac{\sqrt{\mathbf{U}_{2i-1}^2 + \mathbf{U}_{2i}^2}}{\eta_i} + 2 \left(\frac{\max_{i=1, \dots, 2d} |\mathbf{W}_i|}{\min_{i=1, \dots, d} \eta_i} \right). \end{aligned} \quad (\text{A.18})$$

Tails of the random variable $\min_{i=1,\dots,d} \frac{\sqrt{\mathbf{U}_{2i-1}^2 + \mathbf{U}_{2i}^2}}{\eta_i}$ can be expressed as

$$\begin{aligned} & \lim_{\beta \rightarrow \infty} \beta^\alpha \mathbb{P} \left(\min_{i=1,\dots,d} \frac{\sqrt{\mathbf{U}_{2i-1}^2 + \mathbf{U}_{2i}^2}}{\eta_i} > \beta \right) \\ &= \lim_{\beta \rightarrow \infty} \beta^\alpha \mathbb{P} \left(\left(C_\alpha \tilde{\Gamma}(S_{2d}) \right)^{\frac{1}{\alpha}} \Gamma_1^{-\frac{1}{\alpha}} \min_{i=1,\dots,d} \frac{\sqrt{f_{2i-1}^2(\mathbf{V}_1) + f_{2i}^2(\mathbf{V}_1)}}{\eta_i f^*(\mathbf{V}_1)} > \beta \right) \end{aligned} \quad (\text{A.19})$$

$$\begin{aligned} &= \lim_{\beta \rightarrow \infty} \beta^\alpha \int_{S_{2d}} \mathbb{P} \left(\left(C_\alpha \tilde{\Gamma}(S_{2d}) \right)^{\frac{1}{\alpha}} \Gamma_1^{-\frac{1}{\alpha}} \min_{i=1,\dots,d} \frac{\sqrt{f_{2i-1}^2(s) + f_{2i}^2(s)}}{\eta_i f^*(s)} > \beta \right) \frac{\tilde{\Gamma}(ds)}{\tilde{\Gamma}(S_{2d})} \\ & \hspace{20em} (\text{A.20}) \end{aligned}$$

$$\begin{aligned} &= \lim_{\beta \rightarrow \infty} \beta^\alpha \int_{S_{2d}} \left(1 - \exp \left(-C_\alpha \tilde{\Gamma}(S_{2d}) \beta^{-\alpha} \left(\min_{i=1,\dots,d} \frac{\sqrt{s_{2i-1}^2 + s_{2i}^2}}{\eta_i f^*(s)} \right)^\alpha \right) \right) \frac{\tilde{\Gamma}(ds)}{\tilde{\Gamma}(S_{2d})} \\ & \hspace{20em} (\text{A.21}) \end{aligned}$$

$$\begin{aligned} &= C_\alpha \int_{S_{2d}} \min_{i=1,\dots,d} \left(\frac{\sqrt{s_{2i-1}^2 + s_{2i}^2}}{\eta_i} \right)^\alpha \bar{\Gamma}(ds) \\ & \hspace{20em} (\text{A.22}) \end{aligned}$$

where (A.20) involves integrating over the distribution of \mathbf{V}_1 , and (A.22) is derived using the dominated convergence theorem and transforming the finite measure over which the integral is expressed. From (A.22), it can be noted that the random variable $\min_{i=1,\dots,d} \frac{\sqrt{\mathbf{U}_{2i-1}^2 + \mathbf{U}_{2i}^2}}{\eta_i}$ is regularly varying (as defined by (A.11)). Furthermore, $\frac{\max_{i=1,\dots,2d} |\mathbf{W}_i|}{\min_{i=1,\dots,d} \eta_i}$ is a positive random variable and the relation

$$\lim_{\beta \rightarrow \infty} \beta^\alpha \mathbb{P} \left(\max_{i=1,\dots,2d} |\mathbf{W}_i| > \beta \right) = 0 \quad (\text{A.23})$$

was proved as an intermediate step in the proof of Theorem 4.4.1 in [125]. Thus according to Lemma A.4, the tails of $\min_{i=1,\dots,d} \frac{\sqrt{\mathbf{U}_{2i-1}^2 + \mathbf{U}_{2i}^2}}{\eta_i} \pm 2 \left(\frac{\max_{i=1,\dots,2d} |\mathbf{W}_i|}{\min_{i=1,\dots,d} \eta_i} \right)$ are dominated by the tails of $\min_{i=1,\dots,d} \frac{\sqrt{\mathbf{U}_{2i-1}^2 + \mathbf{U}_{2i}^2}}{\eta_i}$. Using (A.14), (A.18), and Lemma

A.4,

$$\begin{aligned} & \lim_{\beta \rightarrow \infty} \beta^\alpha \mathbb{P}(\|\mathbf{X}_1\| > \beta_1, \dots, \|\mathbf{X}_d\| > \beta_d) \\ &= \lim_{\beta \rightarrow \infty} \beta^\alpha \mathbb{P}\left(\min_{i=1, \dots, d} \frac{\sqrt{\mathbf{Y}_{2i-1}^2 + \mathbf{Y}_{2i}^2}}{\eta_i} > \beta\right) \end{aligned} \quad (\text{A.24})$$

$$= \lim_{\beta \rightarrow \infty} \beta^\alpha \mathbb{P}\left(\min_{i=1, \dots, d} \frac{\sqrt{\mathbf{U}_{2i-1}^2 + \mathbf{U}_{2i}^2}}{\eta_i} > \beta\right) \quad (\text{A.25})$$

$$= C_\alpha \int_{S_{2d}} \min_{i=1, \dots, d} \left(\frac{\sqrt{s_{2i-1}^2 + s_{2i}^2}}{\eta_i}\right)^\alpha \bar{\Gamma}(ds). \quad (\text{A.26})$$

This concludes the proof of the theorem. \square

Using Theorem A.5, I now prove a result which is relevant for the particular form of the symmetric alpha stable vectors derived in Chapter 4.

Corollary A.6. *Let $\mathbf{X} = (\mathbf{X}_{1,I}, \mathbf{X}_{1,Q}, \dots, \mathbf{X}_{d,I}, \mathbf{X}_{d,Q})$ be a symmetric alpha stable vector in \mathbb{R}^{2d} with $0 < \alpha < 2$ and a spectral measure $\bar{\Gamma}$ on the unit sphere S_{2d} . Consider the case when the spectral measure is a sum of independent spectral measures of the form*

$$\bar{\Gamma} = \bar{\Gamma}_0 + \sum_{k=1}^{|\mathcal{X}|} \bar{\Gamma}_k \delta\left(\bigcup_{j \in \mathcal{X}(k)} \{s_{2j-1}, s_{2j}\}\right) \quad (\text{A.27})$$

where \mathcal{X} is an arbitrary collection of non-empty proper subsets of $\{1, 2, \dots, n\}$, $|\mathcal{X}|$ denotes the cardinality of \mathcal{X} , $\mathcal{X}(k)$ denotes the k^{th} set contained in \mathcal{X} , $\delta(\dots)$ denotes the dirac delta functional, $\bar{\Gamma}_0$ is a spectral measure distributed over the unit sphere S_{2n} , and $\bar{\Gamma}_k$ is a spectral measure distributed over $S_{2(n-|\mathcal{X}(k)|)}$ formed from the dimensions $\cup_{j=1, \dots, 2n; j \notin \mathcal{X}(k)} \{2j-1, 2j\}$. If $\beta_i = \beta \eta_i$ such that

$0 < \eta_i < \infty$ for $i = 1, \dots, d$, then the joint tail probability are dominated by the spectral measure $\bar{\Gamma}_0$ such that

$$\lim_{\beta \rightarrow \infty} \beta^\alpha \mathbb{P}(\|\mathbf{X}_1\| > \beta_1, \dots, \|\mathbf{X}_d\| > \beta_d) = C_\alpha \int_{S_{2d}} \min_{i=1, \dots, d} \left(\frac{\sqrt{s_{2i-1}^2 + s_{2i}^2}}{\eta_i} \right)^\alpha \bar{\Gamma}_0(d\mathbf{s}). \quad (\text{A.28})$$

Proof.

$$\begin{aligned} & \lim_{\beta \rightarrow \infty} \beta^\alpha \mathbb{P}(\|\mathbf{X}_1\| > \beta_1, \dots, \|\mathbf{X}_d\| > \beta_d) \\ &= C_\alpha \int_{S_{2d}} \min_{i=1, \dots, d} \left(\frac{\sqrt{s_{2i-1}^2 + s_{2i}^2}}{\eta_i} \right)^\alpha \bar{\Gamma}(d\mathbf{s}) \end{aligned} \quad (\text{A.29})$$

$$\begin{aligned} &= C_\alpha \left[\int_{S_{2d}} \min_{i=1, \dots, d} \left(\frac{\sqrt{s_{2i-1}^2 + s_{2i}^2}}{\eta_i} \right)^\alpha \bar{\Gamma}_0(d\mathbf{s}) \right. \\ & \quad \left. + \sum_{k=1}^{|\mathcal{X}|} \int_{S_{2d}} \min_{i=1, \dots, d} \left(\frac{\sqrt{s_{2i-1}^2 + s_{2i}^2}}{\eta_i} \right)^\alpha \delta \left(\bigcup_{j \in \mathcal{X}(k)} \{s_{2j-1}, s_{2j}\} \right) \bar{\Gamma}_k(d\mathbf{s}) \right] \end{aligned} \quad (\text{A.30})$$

$$= C_\alpha \int_{S_{2d}} \min_{i=1, \dots, d} \left(\frac{\sqrt{s_{2i-1}^2 + s_{2i}^2}}{\eta_i} \right)^\alpha \bar{\Gamma}_0(d\mathbf{s}) \quad (\text{A.31})$$

since $\min_{i=1, \dots, d} \left(\frac{\sqrt{s_{2i-1}^2 + s_{2i}^2}}{\eta_i} \right)^\alpha \delta \left(\bigcup_{j \in \mathcal{X}(k)} \{s_{2j-1}, s_{2j}\} \right) = 0$ as \mathcal{X}_k is a non-empty set. \square

Interpretation of Corollary A.6: A spectral measure of the form (A.27) arises when the alpha stable vector $\mathbf{X} = (\mathbf{X}_{1,I}, \mathbf{X}_{1,Q}, \dots, \mathbf{X}_{d,I}, \mathbf{X}_{d,Q})$ can be represented as a sum of independent stable random vectors such that $\mathbf{X} = \mathbf{Y}^{(0)} + \sum_i \mathbf{Y}^{(i)}$ where $\mathbf{Y}^{(0)}$ has all components $\left\{ \mathbf{Y}_{k,I}^{(0)}, \mathbf{Y}_{k,Q}^{(0)} \right\} \stackrel{p}{\neq} 0, k =$

$1, \dots, d$ and $\mathbf{Y}^{(i)}$ have at least one $\{\mathbf{Y}_{k,I}^{(i)}, \mathbf{Y}_{k,Q}^{(i)}\} \stackrel{p}{=} 0, k \in \{1, \dots, d\}$. Here $\stackrel{p}{=}$ and $\stackrel{p}{\neq}$ denote equality and non-equality in probability, respectively. Then Corollary A.6 states that joint tail probability of the random vector \mathbf{X} of the form $\mathbb{P}(\|\mathbf{X}_1\| > \beta_1, \dots, \|\mathbf{X}_d\| > \beta_d)$ is dominated by the tails of the random vector \mathbf{Y}_0 alone, when $\beta_1, \dots, \beta_d \rightarrow \infty$ at the same rate.

Appendix B

Statistical Properties of Gaussian Mixture Random Vectors

This appendix presents a brief review of the statistical properties of zero-mean Gaussian mixture random vectors. Let $\mathbf{X} = \{\mathbf{X}_{1,I}, \mathbf{X}_{1,Q}, \dots, \mathbf{X}_{d,I}, \mathbf{X}_{d,Q}\}$ be a $2d$ -dimensional Gaussian mixture random vector in \mathbb{R}^{2d} . This appendix assumes a particular case when $\{\mathbf{X}_{i,I}, \mathbf{X}_{i,Q}\}$ is isotropic for $i = 1, \dots, d$. The joint characteristic function of \mathbf{X} can be expressed as

$$\Phi_{\mathbf{X}}(\bar{\omega}) = \sum_{l=0}^{\infty} p_l e^{-\frac{|\omega_1|^2(\sigma_1(l))^2 + \dots + |\omega_d|^2(\sigma_d(l))^2}{2}}. \quad (\text{B.1})$$

where $\bar{\omega} = \{\omega_{1,I}, \omega_{1,Q}, \dots, \omega_{d,I}, \omega_{d,Q}\}$ is the set of frequency variables and $|\omega_i| = \sqrt{\omega_{i,I}^2 + \omega_{i,Q}^2}$. Here p_l are the mixture probabilities such that $p_l \geq 0$ and $\sum_{l=0}^{\infty} p_l = 1$, $(\sigma_i(l))^2$ is the variance of corresponding to $\{\mathbf{X}_{i,I}, \mathbf{X}_{i,Q}\}$ in the l^{th} mixture component.

Using (B.1), the joint probability density function can be expressed as

$$f_{\mathbf{X}}(X) = \sum_{l=0}^{\infty} p_l \prod_{m \in [1,d], \sigma_m(l)=0} \delta(X_{m,I}, X_{m,Q}) \prod_{m \in [1,d], \sigma_m(l) \neq 0} \frac{1}{\sqrt{2\pi}\sigma_m(l)} e^{-\frac{X_{m,I}^2 + X_{m,Q}^2}{2(\sigma_m(l))^2}} \quad (\text{B.2})$$

where $\delta(\cdot, \cdot)$ represents the two dimensional Dirac delta functional.

Using (B.2), the tail probability of the random envelope for the Gaussian mixture distribution with parameters p_l and $(\sigma_m(l))^2$ for $y \geq 0$ can be expressed as

$$\mathbb{P}_{GMM}(\|\mathbf{X}_1\| > \beta_1, \dots, \|\mathbf{X}_d\| > \beta_d) = \sum_{l=0}^{\infty} p_l \prod_{m \in [1, d], \sigma_m(l) \neq 0} e^{-\frac{\beta_m^2}{2(\sigma_m(l))^2}} \quad (\text{B.3})$$

where $\|\mathbf{X}_m\| = \sqrt{\mathbf{X}_{m,I}^2 + \mathbf{X}_{m,Q}^2}$ and $\beta_m \geq 0$ for $m \in [1, d]$.

Appendix C

Statistical Properties of Middleton Class A Complex Random Variables

The Middleton Class A distribution is a particular form of the Gaussian mixture distribution. The joint probability density function of a isotropic complex random variable $\mathbf{X} = \mathbf{X}_I + j\mathbf{X}_Q$ distributed according to Middleton Class A model (without an additive Gaussian component) can be expressed as [13]

$$f_{\mathbf{X}_I, \mathbf{X}_Q}(X_I, X_Q) = e^{-A} \delta(X_I, X_Q) + \sum_{m=1}^{\infty} \frac{e^{-A} A^m}{m!} e^{-\frac{X_I^2 + X_Q^2}{2m\Omega_{2A}}} \quad (\text{C.1})$$

where A is the overlap index and Ω_{2A} is the mean intensity of the random variable.

From (C.1), the joint characteristic function of the in-phase and quadrature phase components of the complex random variable can be expressed as

$$\Phi_{\mathbf{X}_I, \mathbf{X}_Q}(\omega_I, \omega_Q) = e^{A \left(e^{-\frac{(\omega_I^2 + \omega_Q^2)\Omega_{2A}}{2A}} - 1 \right)}. \quad (\text{C.2})$$

Note that as $A \rightarrow \infty$ while Ω_{2A} is finite, the Middleton Class A model converges to a Gaussian distribution with variance Ω_{2A} .

Using (C.1), the tail probability for the Middleton Class A distribution with parameters A and Ω_{2A} corresponding to an amplitude threshold $y \geq 0$

can be expressed as

$$\mathbb{P}_{MCA}(\|\mathbf{X}\| > \beta) = \sum_{m=1}^{\infty} \frac{e^{-A} A^m}{m!} e^{-\frac{\beta^2}{A}}. \quad (\text{C.3})$$

Bibliography

- [1] R. Baldick, *Applied Optimization: Formulation and Algorithms for Engineering Systems*. Cambridge University Press, 2006.
- [2] W. Liu, P. P. Pokharel, and J. C. Principe, “Correntropy: Properties and applications in non-Gaussian signal processing,” *IEEE Transactions on Signal Processing*, vol. 55, no. 11, pp. 5286–5298, 2007.
- [3] J. G. Gonzalez, J. L. Paredes, and G. R. Arce, “Zero-order statistics: A mathematical framework for the processing and characterization of very impulsive signals,” *IEEE Transactions on Signal Processing*, vol. 54, no. 10, pp. 3839–3851, Oct. 2006.
- [4] L. . Cohen, “The history of noise,” *IEEE Signal Processing Magazine*, vol. 22, no. 6, pp. 20–45, Nov. 2005.
- [5] M. Schwartz, “Improving the noise performance of communication systems: radio and telephony developments of the 1920s,” *IEEE Communications Magazine*, vol. 47, no. 12, pp. 16–20, Dec. 2009.
- [6] W. Schottky, “Über spontane stromschwankungen in verschiedenen elektrizitätsleitern,” *Annalen der Physik*, vol. 362, no. 23, pp. 541–567, 1918.

- [7] S. O. Rice, “Mathematical analysis of random noise,” *Bell Systems Technical Journal*, vol. 23, pp. 282–332, 1944.
- [8] J. B. Johnson, “Electronic noise: the first two decades,” *IEEE Spectrum*, vol. 8, no. 2, pp. 42–46, Feb. 1971.
- [9] P. Gupta and P. R. Kumar, “The capacity of wireless networks,” *IEEE Transactions on Information Theory*, vol. 46, no. 2, pp. 388–404, Mar. 2000.
- [10] A. Kamerman and N. Erkocevic, “Microwave oven interference on wireless LANs operating in the 2.4 GHz ISM band,” in *Proc. IEEE International Symposium on Personal, Indoor and Mobile Radio Communications*, vol. 3, Helsinki , Finland, Sep. 1–4 1997, pp. 1221–1227.
- [11] K. Slattery and H. Skinner, *Platform Interference in Wireless Systems: Models, Measurement, and Mitigation*. Newnes (Elsevier) Publishing, 2008.
- [12] D. Middleton, “Statistical–physical models of man–made and natural radio noise part II: First order probability models of the envelope and phase,” U.S. Department of Commerce, Office of Telecommunications, Tech. Rep., Apr. 1976.
- [13] ———, “Non-Gaussian noise models in signal processing for telecommunications: New methods and results for class A and class B noise models,”

- IEEE Transactions on Information Theory*, vol. 45, no. 4, pp. 1129–1149, May 1999.
- [14] A. Goldsmith, *Wireless Communications*. Cambridge University Press, 2005.
- [15] M. S. Alouini and A. J. Goldsmith, “Area spectral efficiency of cellular mobile radio systems,” *IEEE Transactions on Vehicular Technology*, vol. 48, no. 4, pp. 1047–1065, July 1999.
- [16] 3rd Generation Partnership Project (3GPP), *Technical Specification Group Radio Access Network; Physical layer aspects for evolved Universal Terrestrial Radio Access (E-UTRA)*, 3rd ed., March 2011.
- [17] J. M. Peha, “Wireless communications and coexistence for smart environments,” *IEEE Personal Communications*, vol. 7, no. 5, pp. 66–68, Oct. 2000.
- [18] IEEE ComSoc LAN MAN Standards Committee, *Wireless LAN Medium Access Control (MAC) and Physical Layer (PHY) Specifications: IEEE Standard 802.11*, The Institute of Electrical and Electronics Engineers, 1997.
- [19] Bluetooth SIG, *Core Specification of the Bluetooth System*, v2.1 + edr ed., Jul. 2007.
- [20] IEEE 802.15.4 Standard, *Wireless medium access control (MAC) and physical layer (PHY) specifications for low-rate Wireless Personal Area*

Networks (LR-WPANs), The Institute of Electrical and Electronics Engineers, 2003.

- [21] ZigBee Alliance, *Zigbee Specification Document 053474*, revision 14 ed., Nov. 2006.
- [22] C. F. Chiasserini and R. R. Rao, “Coexistence mechanisms for interference mitigation between IEEE 802.11 WLANs and Bluetooth,” in *Proc. IEEE International Conference on Computer Communications*, vol. 2, Nov. 2002, pp. 590–598.
- [23] IEEE ComSoc LAN MAN Standards Committee, *IEEE Standard for Local and metropolitan area networks - Part 16: Air Interface for Broadband Wireless Access Systems*, IEEE Std 802.16-2009 ed., The Institute of Electrical and Electronics Engineers, May 2009.
- [24] J. Zhu and H. Yin, “Enabling collocated coexistence in IEEE 802.16 networks via perceived concurrency,” *IEEE Communications Magazine*, vol. 47, no. 6, pp. 108–114, Jun. 2009.
- [25] Federal Communications Commission, *Code of Federal Regulations - Part 15 : Radio Frequency Device*, 47th ed., Oct 2009.
- [26] K. Blackard, T. Rappaport, and C. Bostian, “Measurements and models of radio frequency impulsive noise for indoor wireless communications,” *IEEE Journal on Selected Areas in Communications*, vol. 11, no. 7, pp. 991–1001, Sep. 1993.

- [27] Y. Zhao, B. Agee, and J. Reed, "Simulation and measurement of microwave oven leakage for 802.11 WLAN interference management," in *Proc. IEEE International Symposium on Microwave, Antenna, Propagation and EMC Technologies for Wireless Communications*, vol. 2, Beijing, Aug. 2005, pp. 1580–1583.
- [28] J. Shi, A. Bettner, G. Chinn, K. Slattery, and X. Dong, "A study of platform EMI from LCD panels - impact on wireless, root causes and mitigation methods," in *IEEE International Symposium on Electromagnetic Compatibility*, vol. 3, Portland, Oregon, Aug. 2006, pp. 626–631.
- [29] A. Spaulding and D. Middleton, "Optimum reception in an impulsive interference environment-part I: Coherent detection," *IEEE Transactions on Communications*, vol. 25, no. 9, pp. 910–923, 1977.
- [30] J. G. Andrews, "Interference cancellation for cellular systems: A contemporary overview," *IEEE Wireless Communications Magazine*, vol. 12, no. 2, pp. 19–29, Apr. 2005.
- [31] J. G. Andrews, N. Jindal, M. Haenggi, R. Berry, S. Jafar, D. Guo, S. Shakkottai, R. W. Heath, M. Neely, S. Weber, and A. Yener, "Rethinking information theory for mobile ad hoc networks," *IEEE Communications Magazine*, vol. 46, no. 12, pp. 94–101, Dec. 2008.
- [32] V. Chandrasekhar, J. G. Andrews, and A. Gatherer, "Femtocell networks: a survey," *IEEE Communications Magazine*, vol. 46, no. 9, pp. 59–67, Sep. 2008.

- [33] V. MacDonald, "The cellular concept," *Bell Systems Technical Journal*, vol. 58, no. 1, pp. 15–41, Jan. 1979.
- [34] Nokia Siemens Networks, *LTE Performance for initial deployments*, 2009. [Online]. Available: www.nokiasiemensnetworks.com/sites/default/files/document/LTE_measurement_A4.1302.0.pdf
- [35] D. Cox, "Cochannel interference considerations in frequency reuse small-coverage-area radio systems," *IEEE Transactions on Communications*, vol. 30, no. 1, pp. 135–142, Jan 1982.
- [36] P. S. Jha, "Frequency reuse scheme with reduced co-channel interference for fixed cellular systems," in *Proc. IEEE Electronic Letters*, vol. 34, no. 3, Feb 1998, pp. 237–238.
- [37] E. Kuruoglu, "Signal processing in alpha stable environments: A least lp approach," Ph.D. dissertation, University of Cambridge, 1998.
- [38] R. S. Blum, R. J. Kozick, and B. Sadler, "An adaptive spatial diversity receiver for non-Gaussian interference and noise," *IEEE Transactions on Signal Processing*, vol. 47, no. 8, pp. 2100–2111, Aug. 1999.
- [39] J. Haring and A. J. H. Vinck, "Iterative decoding of codes over complex numbers for impulsive noise channels," *IEEE Transactions on Information Theory*, vol. 49, no. 5, pp. 1251–1260, May 2003.

- [40] ———, “Coding and signal space diversity for a class of fading and impulsive noise channels,” *IEEE Transactions on Information Theory*, vol. 50, no. 5, pp. 887–895, May 2004.
- [41] P. Gao and C. Tepedelenlioglu, “Space-time coding over fading channels with impulsive noise,” *IEEE Transactions on Wireless Communications*, vol. 6, no. 1, pp. 220–229, Jan 2007.
- [42] M. A. Maddah-Ali, A. S. Motahari, and A. K. Khandani, “Signaling over MIMO multi-base systems: Combination of multi-access and broadcast,” in *Proc. IEEE International Symposium on Information Theory*, Jul. 9–14 2006, pp. 2104–2108.
- [43] V. R. Cadambe and S. A. Jafar, “Interference alignment and degrees of freedom of the k-user interference channel,” *IEEE Transactions on Information Theory*, vol. 54, no. 8, pp. 3425–3441, Aug. 2008.
- [44] C. Suh and D. Tse, “Interference alignment for cellular networks,” in *Proc. Allerton Conference on Communication, Control, and Computing*, Sep. 23–26 2008, pp. 1037–1044.
- [45] U. Niesen, “Interference alignment in dense wireless networks,” in *Proc. IEEE Information Theory Workshop*, Cairo, Jan. 6–8 2010, pp. 1–5.
- [46] R. Tresch and M. Guillaud, “Performance of interference alignment in clustered wireless ad hoc networks,” in *Proc. IEEE International Symposium on Information Theory*, Jun. 13–18 2010, pp. 1703–1707.

- [47] H. Zhou and T. Ratnarajah, “A novel interference draining scheme for cognitive radio based on interference alignment,” in *Proc. IEEE Symposium on New Frontiers in Dynamic Spectrum*, Apr. 6–9 2010, pp. 1–6.
- [48] R. Tresch, M. Guillaud, and E. Riegler, “On the achievability of interference alignment in the k-user constant MIMO interference channel,” in *Proc. IEEE Workshop on Statistical Signal Processing*, Aug. 31 – Sep. 3 2009, pp. 277–280.
- [49] O. El Ayach, S. Peters, and R. W. Heath, “The feasibility of interference alignment over measured MIMO-OFDM channels,” *IEEE Transactions on Vehicular Technology*, vol. 59, no. 9, pp. 4309–4321, Nov. 2010.
- [50] R. T. Krishnamachari and M. K. Varanasi, “Interference alignment under limited feedback for MIMO interference channels,” in *Proc. IEEE International Symposium on Information Theory*, Jun. 13–18 2010, pp. 619–623.
- [51] G. J. Foschini, “Layered space-time architecture for wireless communication in a fading environment when using multi-element antennas,” *Bell Labs Technical Journal*, vol. 1, no. 2, pp. 41–59, 1996.
- [52] S. Verdú, *Multuser Detection*. Cambridge University Press, 1998.
- [53] S. Weber, J. G. Andrews, X. Yang, and G. de Veciana, “Transmission capacity of wireless ad hoc networks with successive interference cancel-

- lation,” *IEEE Transactions on Information Theory*, vol. 53, no. 8, pp. 2799–2814, Aug. 2007.
- [54] K. Huang, J. G. Andrews, R. W. Heath Jr., D. Guo, and R. Berry, “Spatial interference cancellation for multi-antenna mobile ad hoc networks,” *IEEE Transactions on Information Theory*, Jul. 2008, submitted. [Online]. Available: arxiv.org/pdf/0807.1773
- [55] F. Baccelli, B. Błaszczyszyn, and P. Muhlethaler, “An Aloha protocol for multihop mobile wireless networks,” *IEEE Transaction on Information Theory*, vol. 52, no. 2, pp. 412–436, Sep. 2006.
- [56] A. Hasan, “Interference suppression in wireless ad hoc networks,” Ph.D. dissertation, The University of Texas at Austin, May 2006.
- [57] M. Kaynia, G. E. Oien, and N. Jindal, “Joint transmitter and receiver sensing capability of CSMA in MANETs,” in *Proc. IEEE International Conference on Wireless Communications and Signal Processing*, Nanjing, China, Nov. 2009.
- [58] I. C. Wong, “A unified framework for optimal resource allocation in multiuser multicarrier wireless systems,” Ph.D. dissertation, The University of Texas at Austin, May 2007.
- [59] J. G. Andrews and A. Hasan, “Old standard new use,” *IEE Communications Engineer*, vol. 2, no. 1, pp. 22–26, Feb. 2004.

- [60] A. Hasan and J. G. Andrews, “The guard zone in wireless ad hoc networks,” *IEEE Transactions on Wireless Communications*, vol. 4, no. 3, pp. 897–906, Mar. 2007.
- [61] H. Inaltekin, S. B. Wicker, M. Chiang, and H. V. Poor, “On unbounded path-loss models: effects of singularity on wireless network performance,” *IEEE Journal on Selected Areas in Communications*, vol. 27, no. 7, pp. 1078–1092, Sep. 2009.
- [62] F. Baccelli, M. Klein, M. Lebourges, and S. Zuyev, “Stochastic geometry and architecture of communication networks,” *Journal of Telecommunication Systems*, vol. 7, pp. 209–227, Jun. 1997.
- [63] M. Haenggi and R. K. Ganti, “Interference in large wireless networks,” in *Foundations and Trends in Networking*. Now Publishers Inc., Dec. 2008, vol. 3, no. 2, pp. 127–248.
- [64] M. Z. Win, P. C. Pinto, and L. A. Shepp, “A mathematical theory of network interference and its applications,” *Proceedings of the IEEE*, vol. 97, no. 2, pp. 205–230, Feb. 2009.
- [65] E. Salbaroli and A. Zanella, “Interference analysis in a Poisson field of nodes of finite area,” *IEEE Transactions on Vehicular Technology*, vol. 58, no. 4, pp. 1776–1783, May 2009.
- [66] A. Rabbachin, T. Q. Quek, H. Shin, and M. Z. Win, “Cognitive network interference,” *IEEE Transactions on Selected Areas in Communications*,

- vol. 29, no. 2, pp. 480–493, Feb. 2011.
- [67] F. Baccelli and B. Błaszczyszyn, “Stochastic geometry and wireless networks, volume 1 — theory,” in *Foundations and Trends in Networking*. Now Publishers Inc., March 2009, vol. 3, no. 3–4, pp. 249–449.
- [68] —, “Stochastic geometry and wireless networks, volume 2— applications,” in *Foundations and Trends in Networking*. Now Publishers Inc., March 2009, vol. 4, no. 1–2, pp. 1–312.
- [69] F. Baccelli, M. Klein, M. Lebourges, and S. Zuyev, “Stochastic geometry and architecture of communication networks,” *Telecommunication Systems*, vol. 7, no. 1, pp. 209–227, 1997.
- [70] E. S. Sousa, “Performance of a spread spectrum packet radio network link in a Poisson field of interferers,” *IEEE Transactions on Information Theory*, vol. 38, no. 6, pp. 1743–1754, Nov. 1992.
- [71] J. Ilow and D. Hatzinakos, “Analytic alpha-stable noise modeling in a Poisson field of interferers or scatterers,” *IEEE Transactions on Signal Processing*, vol. 46, no. 6, pp. 1601–1611, Jun. 1998.
- [72] X. Yang and A. Petropulu, “Co-channel interference modeling and analysis in a Poisson field of interferers in wireless communications,” *IEEE Transactions on Signal Processing*, vol. 51, no. 1, pp. 64–76, Jan. 2003.

- [73] K. F. McDonald and R. S. Blum, “A statistical and physical mechanisms-based interference and noise model for array observations,” *IEEE Transactions on Signal Processing*, vol. 48, pp. 2044–2056, Jul. 2000.
- [74] M. Haenggi, J. G. Andrews, F. Baccelli, O. Dousse, and M. Franceschetti, “Stochastic geometry and random graphs for the analysis and design of wireless networks,” *IEEE Journal on Selected Areas of Communications*, vol. 27, no. 7, pp. 1029–1046, Sep. 2009.
- [75] R. Ganti and M. Haenggi, “Interference and outage in clustered wireless ad hoc networks,” *IEEE Transactions on Information Theory*, vol. 55, no. 9, pp. 4067–4086, Sep. 2009.
- [76] S. Weber, J. G. Andrews, and N. Jindal, “An overview of the transmission capacity of wireless networks,” *IEEE Transactions on Communications*, vol. 58, no. 12, pp. 3593–3604, Dec. 2010.
- [77] X. Yang and G. de Veciana, “Inducing multiscale spatial clustering using multistage MAC contention in spread spectrum ad hoc networks,” *IEEE/ACM Transactions on Networking*, vol. 15, no. 6, pp. 1387–1400, Dec. 2007.
- [78] M. Haenggi, “Outage, local throughput, and capacity of random wireless networks,” *IEEE Transactions on Wireless Communications*, vol. 8, no. 8, pp. 4350–4359, Aug. 2009.

- [79] R. K. Ganti and J. G. Andrews, “A new method for computing the transmission capacity of non-Poisson wireless networks,” in *Proc. IEEE International Symposium on Information Theory*, Austin, TX, Jun. 13–18 2010, pp. 1693–1697.
- [80] M. Franceschetti, M. D. Migliore, and P. Minero, “The capacity of wireless networks: Information-theoretic and physical limits,” *IEEE Transactions on Information Theory*, vol. 55, no. 8, pp. 3413–3424, Aug. 2009.
- [81] M. Franceschetti, O. Dousse, D. Tse, and P. Thiran, “Closing the gap in the capacity of wireless networks via percolation theory,” *IEEE Transactions on Information Theory*, vol. 53, no. 3, pp. 1009–1018, Mar. 2007.
- [82] R. Negi and A. Rajeswaran, “Capacity of power constrained ad-hoc networks,” in *Proc. IEEE Conference on Computer Communications*, Hong Kong, May 2004, pp. 443–453.
- [83] M. Grossglauser and D. Tse, “Mobility increases the capacity of adhoc wireless networks,” *IEEE/ACM Transactions on Networking*, vol. 10, no. 4, pp. 477–486, Aug. 2002.
- [84] J. G. Andrews, S. Weber, M. Kountouris, and M. Haenggi, “Random access transport capacity,” *IEEE Transactions On Wireless Communications*, vol. 9, no. 6, pp. 2101–2111, Jun. 2010.

- [85] U. Niesen, P. Gupta, and D. Shah, “The balanced unicast and multi-cast capacity region of large wireless networks,” *IEEE Transactions on Information Theory*, vol. 56, no. 5, pp. 2249–2271, May 2010.
- [86] L. Xie and P. R. Kumar, “A network information theory for wireless communication: Scaling laws and optimal operation,” *IEEE Transactions on Information Theory*, vol. 50, no. 5, pp. 748–767, May 2004.
- [87] S. Weber, X. Yang, J. G. Andrews, and G. de Veciana, “Transmission capacity of wireless ad hoc networks with outage constraints,” *IEEE Transactions on Information Theory*, vol. 51, no. 12, pp. 4091–4102, Dec. 2005.
- [88] S. Weber, J. G. Andrews, and N. Jindal, “The effect of fading, channel inversion, and threshold scheduling on ad hoc networks,” *IEEE Transactions on Information Theory*, vol. 53, no. 11, pp. 4127–4149, Nov. 2007.
- [89] A. M. Hunter, J. G. Andrews, and S. P. Weber, “Transmission capacity of ad hoc networks with spatial diversity,” *IEEE Transactions on Wireless Communications*, vol. 7, no. 12, pp. 5058–5071, Dec. 2008.
- [90] R. Vaze and J. R. W. Heath, “Transmission capacity of multiple antenna ad-hoc networks without channel state information at the transmitter and interference cancelation at the receiver,” in *Proc. IEEE Asilomar Conference on Signals, Systems, and Computers*, Pacific Grove, CA, Nov. 1–4 2009.

- [91] R. Vaze, “Throughput-delay-reliability tradeoff in ad hoc networks,” in *Workshop on Spatial Stochastic Models for Wireless Networks*, Jun. 2010.
- [92] M. Haenggi, “Local delay in static and highly mobile Poisson networks with ALOHA,” in *Proc. IEEE International Conference on Communications*, Cape Town, South Africa, May 2010.
- [93] —, “Local delay in Poisson networks with and without interference,” in *Proc. Allerton Conference on Communication, Control, and Computing*, Sep. 29 – Oct. 1 2010.
- [94] F. Baccelli and B. Błaszczyszyn, “A new phase transition for local delays in MANETs,” in *Proc. IEEE International Conference on Computer Communications*, San Diego, CA, Mar. 14–19 2010, pp. 1–9.
- [95] G. Alfano, R. Tresch, and M. Guillaud, “Spatial diversity impact on the local delay of homogeneous and clustered wireless networks,” in *Proc. IEEE International Workshop on Smart Antennas*, Aachen, Germany, Feb. 24–25 2011, pp. 1–6.
- [96] J. Haring and A. J. H. Vinck, “Performance bounds for optimum and suboptimum reception under class-A impulsive noise,” *IEEE Transactions for Communications*, vol. 50, no. 7, pp. 1130–1136, Jul. 2002.
- [97] S. V. Zhidkov, “Analysis and comparison of several simple impulsive noise mitigation schemes for OFDM receivers,” *IEEE Transactions on*

Communications, vol. 56, no. 1, pp. 5–9, Jan. 2008.

- [98] K. Gulati, A. Chopra, R. W. Heath, B. L. Evans, K. R. Tinsley, and X. E. Lin, “MIMO receiver design in the presence of radio frequency interference,” in *Proc. IEEE Global Communications Conference*, New Orleans, LA, Nov. 30–Dec. 4 2008.
- [99] M. Nassar, K. Gulati, M. DeYoung, B. L. Evans, and K. R. Tinsley, “Mitigating near-field interference in laptop embedded wireless transceivers,” *Journal of Signal Processing Systems*, Mar. 2009. [Online]. Available: <http://dx.doi.org/10.1007/s11265-009-0350-7>
- [100] P. J. Huber, *Robust Statistics*. John Wiley & Sons, 1981.
- [101] G. R. Arce, *Nonlinear Signal Processing: A Statistical Approach*. John Wiley & Sons, 2005.
- [102] S. Ambike, J. Ilow, and D. Hatzinakos, “Detection for binary transmission in a mixture of Gaussian noise and impulsive noise modeled as an alpha-stable process,” *IEEE Signal Processing Letters*, vol. 1, no. 3, pp. 55–57, Mar. 1994.
- [103] H. Vikalo, B. Hassibi, and T. Kailath, “On robust multiuser detection,” in *Proc. Asilomar Conference on Signals, Systems and Computers*, no. Nov., 29 Oct.–1 Nov. 2000, pp. 1168–1172.
- [104] K. Gulati, B. L. Evans, J. G. Andrews, and K. R. Tinsley, “Statistics of co-channel interference in a field of Poisson and Poisson-Poisson

- clustered interferers,” *IEEE Transactions on Signal Processing*, vol. 58, no. 12, pp. 6207–6222, Dec. 2010.
- [105] J. Gonzalez, D. Griffith, and G. Arce, “Matched myriad filtering for robust communications,” in *Proc. Conference on Information Sciences and Systems*, 1996.
- [106] J. G. Gonzalez, “Robust techniques for wireless communications in non-Gaussian environments,” Ph.D. dissertation, University of Delaware, Newark, 1997.
- [107] J. G. Gonzalez and G. Arce, “Optimality of the myriad filter in practical impulsive-noise environments,” *IEEE Transactions on Signal Processing*, vol. 49, no. 2, pp. 438–441, Feb. 2001.
- [108] C. L. Nikias and M. Shao, *Signal Processing with Alpha-Stable Distributions and Applications*. John Wiley & Sons, 1995.
- [109] H. Ong and A. Zoubir, “Estimation and detection in a mixture of symmetric alpha stable and Gaussian interference,” in *Proc. IEEE Signal Processing Workshop on High-Order Statistics*, Madison, Wisconsin, Jun. 14–16 1999.
- [110] H. W. Sorenson and D. L. Alspach, “Recursive Bayesian estimation using Gaussian sums,” *Automatica*, vol. 7, pp. 465–479, 1971.

- [111] D. L. Alspach and H. W. Sorenson, "Nonlinear Bayesian estimation using Gaussian sum approximation," *IEEE Transactions on Automatic Control*, vol. 17, no. 4, pp. 439–448, Apr. 1972.
- [112] Y. Eldar and A. Yeredor, "Finite-memory denoising in impulsive noise using Gaussian mixture models," *IEEE Transactions on Circuits and Systems II: Analog and Digital Signal Processing*, vol. 48, no. 11, pp. 1069–1077, Nov. 2001.
- [113] J. H. Kotecha and P. M. Djuric, "Gaussian sum particle filtering," *IEEE Transactions on Signal Processing*, vol. 51, no. 10, pp. 2602–2612, Oct. 2003.
- [114] J. H. Miller and J. B. Thomas, "Detectors for discrete-time signals in non-Gaussian noise," *IEEE Transactions on Information Theory*, vol. 18, pp. 241–250, Mar. 1972.
- [115] J. Astola and Y. Neuvo, "Nonlinear median based receiver for QAM signals," in *Proc. IEEE Global Telecommunications Conference*, vol. 3, San Diego, CA, Dec. 2–5 1990, pp. 2030–2034.
- [116] N. C. Beaulieu and S. Niranjayan, "New UWB receiver designs based on a Gaussian-Laplacian noise-plus-MAI model," in *Proc. IEEE International Conference on Communications*, Glasgow, Jun. 24–28 2007, pp. 4128–4133.

- [117] V. J. Mathews and G. L. Sicuranza, *Polynomial Signal Processing*. Wiley-Interscience, 2000.
- [118] V. Milosevic and B. Ristic, “Effect of impulse noise rejection with median filter on binary digital receiver performance,” *IEEE Electronic Letters*, vol. 25, no. 6, pp. 392–394, Mar. 1989.
- [119] C. Nikias and A. P. Petropulu, *Higher Order Spectra Analysis: A Non-Linear Signal Processing Framework*. Prentice Hall, 1993.
- [120] B. M. Sadler, G. B. Giannakis, and K.-S. Lii, “Estimation and detection in non-Gaussian noise using higher order statistics,” *IEEE Transactions on Signal Processing*, vol. 42, no. 10, pp. 2729–2741, Oct. 1994.
- [121] M. Janzura and T. Koski, “Minimum entropy of error principle in estimation,” *Information Sciences*, vol. 79, no. 1–2, pp. 123–144, Jul. 1994.
- [122] K. Gulati, A. Chopra, B. L. Evans, and K. R. Tinsley, “Statistical modeling of co-channel interference,” in *Proc. IEEE Global Communications Conference*, Honolulu, Hawaii, Nov. 30–Dec. 4 2009.
- [123] K. Gulati, B. L. Evans, and K. R. Tinsley, “Statistical modeling of co-channel interference in a field of Poisson distributed interferers,” in *Proc. IEEE International Conference on Acoustics, Speech, and Signal Processing*, Dallas, TX, Mar. 14–19 2010, pp. 3490–3493.

- [124] V. Chandrasekhar and J. G. Andrews, “Uplink capacity and interference avoidance for two-tier femtocell networks,” *IEEE Transactions on Wireless Communications*, vol. 8, no. 7, pp. 3498–3509, Jul. 2009.
- [125] G. Samorodnitsky and M. S. Taqqu, *Stable Non-Gaussian Random Processes: Stochastic Models with Infinite Variance*. Chapman and Hall, New York, 1994.
- [126] M. Westcott, “On the existence of a generalized shot-noise process,” in *Studies in Probability and Statistics: Papers in Honour of Edwin J. G. Pitman*, Amsterdam, 1976, pp. 73–88.
- [127] S. B. Lowen and M. C. Teich, “Power-law shot noise,” *IEEE Transactions on Information Theory*, vol. 36, no. 6, pp. 1302–1318, Nov. 1990.
- [128] J. Venkataraman, M. Haenggi, and O. Collins, “Shot noise models for outage and throughput analysis in wireless ad hoc networks,” in *Proc. Military Communications Conference*, Oct. 2006, pp. 1–7.
- [129] D. J. Daley and D. Vere-Jones, *An Introduction to the Theory of Point Processes*, 1st ed. Springer, New York, 1988.
- [130] Z. I. Botev, “A novel nonparametric density estimator,” The University of Queensland, Australia, Tech. Rep., Nov. 2006.
- [131] T. M. Cover and J. A. Thomas, *Elements of Information Theory*, 2nd ed. Wiley & Sons, New York, 2006.

- [132] R. K. Ganti and M. Haenggi, “Spatial and temporal correlation of the interference in ALOHA ad hoc networks,” *IEEE Communications Letters*, vol. 13, no. 9, pp. 631–633, Sep. 2009.
- [133] S. Srinivasa and M. Haenggi, “Throughput-delay-reliability tradeoffs in multihop networks with random access,” in *Allerton Conference on Communication, Control and Computing*, Monticello, IL, Sep. 2010.
- [134] S. S. Rappaport and L. Kurz, “An optimal nonlinear detector for digital data transmission through non-Gaussian channels,” *IEEE Transactions on Communications Technology*, vol. 14, no. 3, pp. 266–274, Jun. 1966.
- [135] J. J. Sheehy, “Optimum detection of signals in non-Gaussian noise,” *Journal of Acoustical Society of America*, vol. 63, no. 1, pp. 81–90, Jan. 1978.
- [136] W. Liu, P. P. Pokharel, and J. C. Principe, “Error entropy, correntropy and M-estimation,” in *Proc. IEEE Workshop on Machine Learning for Signal Processing*, Arlington, VA, Sep. 6–8 2006, pp. 179–184.
- [137] P. P. Pokharel, R. Agrawal, and J. C. Principe, “Correntropy based matched filtering,” in *Proc. IEEE Workshop on Machine Learning for Signal Processing*, 28 Sep. 2005, pp. 341–346.
- [138] A. Singh and J. C. Principe, “Using correntropy as a cost function in linear adaptive filters,” in *Proc. IEEE International Joint Conference on Neural Networks*, Atlanta, GA, Jun. 14–19 2009, pp. 2950–2955.

- [139] A. Kenarsari-Anhari and L. H. J. Lampe, “Performance analysis for BICM transmission over Gaussian mixture noise fading channels,” *IEEE Transactions on Communications*, vol. 58, no. 7, pp. 1962–1972, Jul. 2010.
- [140] M. H. Hayes, *Statistical Digital Signal Processing and Modeling*. John Wiley & Sons, 2006.
- [141] D. Umehara, H. Yamaguchi, and Y. Morihoro, “Turbo decoding in impulsive noise environment,” in *Proc. IEEE Global Telecommunications Conference*, 29 Nov. – 3 Dec. 2004, pp. 194–198.
- [142] D. Fertonani and G. Colavolpe, “A robust metric for soft-output detection in the presence of class-A noise,” *IEEE Transactions on Communications*, vol. 57, no. 1, pp. 36–40, Jan. 2009.
- [143] R. K. Ganti, F. Baccelli, and J. G. Andrews, “Series expansion for interference in wireless networks,” *IEEE Transactions on Information Theory*, Jan. 2011, submitted. [Online]. Available: <http://arxiv.org/abs/1101.3824>
- [144] C. Lee and M. Haenggi, “Interference and outage in doubly Poisson cognitive networks,” in *Proc. IEEE International Conference on Computer Communications and Networks*, Aug. 2–5 2010.
- [145] D. W. J. Stein, “Detection of random signals in Gaussian mixture noise,”

IEEE Transactions on Information Theory, vol. 41, no. 6, pp. 1788–1801, Nov. 1995.

- [146] M. Nassar, K. Gulati, Y. Mortazavi, and B. L. Evans, “Statistical modeling of asynchronous impulsive noise in powerline communication networks,” in *Proc. IEEE Global Communications Conference*, Houston, TX, Dec. 5–9 2011, submitted.
- [147] J. Lin, M. Nassar, Y. Mortazavi, and B. L. Evans, “Combating channel impairments and impulsive noise in local utility powerline communications,” *IEEE Signal Processing Magazine*, Apr. 2011, submitted.
- [148] F. Abdelkefi, P. Duhamel, and F. Alberge, “Impulsive noise cancellation in multicarrier transmission,” *IEEE Transactions on Communications*, vol. 53, no. 1, pp. 94–106, Jan. 2005.

Vita

Kapil Gulati received the B.Tech. degree in Electronics and Communications Engineering from the Indian Institute of Technology, Guwahati in May 2004 and the M.S. degree in Electrical Engineering from The University of Texas at Austin in May 2008. From 2004 to 2006, he was employed as a Hardware Design Engineer at Texas Instruments, India. He enrolled at The University of Texas at Austin in Fall 2006. In Fall 2006, he was a teaching assistant for the senior design projects course. Since Spring 2007, he has been a research assistant at the Embedded Signal Processing Laboratory. In summer 2007 and 2008, he was a intern at Intel Labs in Santa Clara, California. He co-authored a paper on his work at Intel Labs that won the best paper award at the 2009 IEEE Computer Society Annual Symposium on VLSI, Tampa, Florida. In summer 2010, he was a intern at Qualcomm Inc. in San Diego, California. His research interests include mathematical modeling of wireless networks and signal processing in the presence of non-Gaussian noise.

Permanent address: 1100 E 32 Street
Austin, Texas 78722

This dissertation was typeset with L^AT_EX[†] by the author.

[†]L^AT_EX is a document preparation system developed by Leslie Lamport as a special version of Donald Knuth's T_EX Program.